

# **Exploring brain structure and blood metabolic profiles using Alzheimer's pathway specific polygenic risk scores**

**Dr Judith Rose Harrison**



**School of Psychology**

**Cardiff University**

**2021**

Thesis submitted in fulfilment of the requirements for the degree of  
Doctor of Philosophy

## **ACKNOWLEDGEMENTS**

I have benefitted from the help and support of many people through the course of this PhD, from developing the project proposal, securing funding, training in the necessary techniques, processing and analysing the data, as well as writing this thesis.

Particular thanks must be given to my supervisors Prof Derek Jones, Prof Valentina Escott-Price and Dr Evie Stergiakouli whose guidance has been invaluable; to Prof David Linden who helped to develop the ideas for this project; to Xavier Caseras, Sonya Foley-Bozorgzard, Tom Lancaster, Chantal Tax and my other CUBRIC colleagues for their assistance with neuroimaging data processing and analysis; to Emily Baker, Katherine Tansey and Leon Hubbard for their assistance with polygenic scoring; to Panagiota Pagoni from Bristol University for assistance with generating principal components; to my friends and colleagues in Cardiff and Bristol Universities, particularly Joanne Doherty, Miriam Cooper, Olga Eyre, Kim Kendall, Sarah Clarke, Chantelle Wiseman and others for their kindness and support; to Profs Jeremy Hall, Mike Owen, Mick O'Donovan and Ian Jones for their advice and encouragement; to the Wellcome Trust GW4-CAT for funding my fellowship; to Dr Jayne Bailey and Ms Tracey Jarvis for their sympathy, care and reinforcement; and most importantly to all the participants who took part in this research.

To my parents, Bruce and Pauline, thank you for giving me the confidence and encouragement to pursue this, and thank you Dad for taking time to proof-read this thesis. To my husband Brad, thank you for being my perpetual cheerleader, and also for your expertise with Microsoft Excel and Microsoft Word. To my son Peter, you have little idea what I have been doing on my laptop all this time, but you bring me ceaseless joy. This thesis is dedicated to my wonderful family. I hope it makes you proud.

## CONTRIBUTIONS

I obtained funding for the work presented in this thesis from the Wellcome Trust, through a GW4 Clinical Academic Training Fellowship. In preparation for this work, I attended modules on the Cardiff University Masters programmes in Biostatistics and Neuroimaging. I also attended external training courses on Genetic Epidemiology, at the University of Bristol, and on Diffusion MRI, at the University of Utrecht. I received specific in-house training on volumetric and diffusion MRI processing and quality control, and polygenic scoring methodology. I also attended external and internal training on the statistical computing software R.

I carried out the background literature review and summarised all the background information in this thesis. For the systematic reviews, I determined the question each review addressed, generated the search criteria, reviewed every paper against the search criteria, assigned quality scores, extracted data into tables, and wrote the narrative synthesis of studies. Following standard systematic review protocol, my colleagues also reviewed papers against the search criteria and disagreements were resolved by my supervisors.

All of the data presented in this thesis was gathered by two large population cohort studies, the Avon Longitudinal Study of Parents and Children (ALSPAC) and UK Biobank. Both datasets were also being used for other projects in the department, therefore parts of the pre-processing were collaborative. For example, for ALSPAC I assisted with the pre-processing of the raw imaging data. Dr Xavier Caseras ran Freesurfer and I assisted again with quality control of the output. I conducted all of the white matter tractography, including performing manual tractography to train automated tractography models, and extracting all the diffusion metrics. Dr Katherine Tansey assisted with genotyping quality control in ALSPAC and I computed the polygenic scores in ALSPAC. In UK Biobank, again Dr Caseras ran Freesurfer. I used the diffusion Imaging Derived Phenotypes (IDPs) published by UK Biobank. Dr Emily Baker computed the UK Biobank polygenic scores. Before analysis, I checked and cleaned the data. I analysed and summarised all of the data presented in the experimental chapters and interpreted the results. Details of others who contributed to each experiment are given at the start of each chapter. This thesis was written by me with the guidance and support of my supervisors.

## PUBLICATIONS RELATED TO THIS PHD

**Harrison, JR**, Mistry S, Muskett N, Escott-Price V. 2020. From polygenic scores to precision medicine in Alzheimer's Disease: A systematic review. *Journal of Alzheimer's Disease* 74(4), pp. 1271-1283.

**Harrison J**, Caseras X, Foley S, Baker E, Williams J, Linden D, Holmans P, Escott-Price V, Jones D. Pathway-specific polygenic scores for Alzheimer's disease are associated with multi-modal structural brain imaging markers in young adults. *Proceedings of the 28th ISMRM Annual Scientific Meeting & Exhibition*, 2020 August.

**Harrison JR**, Bhatia S, Tan ZX, Mirza-Davies A, Benkert H, Tax CMW, Jones DK. 2020. Imaging Alzheimer's genetic risk using Diffusion MRI: a systematic review. *NeuroImage: Clinical* 27, article number:102359. (10.1016/j.nicl.2020.102359)

**Harrison J**, Caseras X, Foley S, Baker E, Tansey K, Williams J, Linden D, Holmans P, Jones D, Escott-Price V. Structural magnetic resonance imaging markers are associated with Alzheimer's disease pathway-specific polygenic scores. *European Neuropsychopharmacology* 2019, DOI: 10.1016/j.euroneuro.2019.01.086

Mirza-Davies, A. and **Harrison, J**. 2019. Extending the frontiers of neuroimaging: an introduction to Diffusion Tensor Imaging Tractography. *The British Student Doctor Journal* 3(2), pp. 34-39. (10.18573/bsdj.80)

Caseras X, Foley S, Bracher-Smith M, **Harrison J**, Tansey K. Fractional anisotropy of the uncinate fasciculus and cingulum in bipolar disorder type I, type II, their unaffected siblings and healthy controls. *BJPsych*. Volume 213, Issue 3, September 2018, pp. 548-554.

Mistry S, **Harrison JR**, Smith DJ, Escott-Price V, Zammit S. The use of polygenic risk scores to identify phenotypes associated with genetic risk of bipolar disorder and depression: a systematic review. *J Affect Disord* . 2018;234:148-155. DOI: <https://doi.org/10.1016/j.jad.2018.02.005>

Mistry S, **Harrison JR**, Smith DJ, Escott-Price V, Zammit S. The use of polygenic risk scores to identify phenotypes associated with genetic risk of schizophrenia: Systematic review. *Schizophr Res.* 2017 Nov 9. pii:S0920-9964(17)30665-5. doi: 10.1016/j.schres.2017.10.037.

**Harrison J.** & Mistry S. The use of polygenic risk scores to inform aetiology of mood and psychotic disorders. *European Psychiatry.* DOI: <http://dx.doi.org/10.1016/j.eurpsy.2017.01.2051>

**Harrison J**, Baker E, Hubbard L, Linden D, Williams J, Escott-Price V, Holmans P. Identification of biological pathways to Alzheimer's disease using polygenic scores. *European Psychiatry* DOI: <http://dx.doi.org/10.1016/j.eurpsy.2017.01.2052>

**Harrison J**, Owen M. Alzheimer's Disease: The Amyloid Hypothesis on Trial. *BJPsych* Jan 2016, 208 (1) 1-3; DOI: 10.1192/bjp.bp.115.167569

## SUMMARY

Alzheimer's disease (AD) is a progressive neurodegenerative disorder that affects older people. It is common, affecting around one in ten people over 65 years old. In addition to the autosomal dominant AD genes and Apolipoprotein E (*APOE*), genome wide association studies (GWAS) have identified a number of small risk loci. These can be combined into polygenic risk scores (PRS) which can predict AD relatively accurately and are associated with a number of neurodegeneration phenotypes. Pathway analyses of GWAS data have implicated a number of biological processes, including the immune response and lipid metabolism. How AD pathway specific genetic burden manifests in brain structure or serum metabolic profiles is not well understood.

In this thesis, volumetric and diffusion MRI and serum lipid and inflammatory markers were used to investigate manifestations of AD polygenic risk in two large population cohorts. Specifically, these analyses sought to determine 1) whether AD polygenic risk scores were associated with neuroimaging and blood marker phenotypes linked to neurodegeneration in younger and older adult cohorts; and 2) whether PRS informed by disease pathways were associated with different patterns of alteration in brain structure, serum lipids or inflammatory markers. The relationships between PRS and phenotypes were explored using linear regression.

There were significant associations between pathway specific PRS, grey matter volumes and white matter microstructure. Although some of these attenuated when the *APOE* region was excluded from the score, some were maintained, in particular cortical thickness in mature adults, which appeared to be independent of *APOE*. Increased pathway specific polygenic risk for AD was also associated with serum markers such as increased blood lipids, particularly low density lipoprotein (LDL) cholesterol and total cholesterol, and decreased C-Reactive Protein (CRP). However, these effects seemed to be driven by the *APOE* locus. Further longitudinal studies, combining advanced MRI techniques with cerebrospinal fluid and neuroradiology biomarkers, will be required to confirm these findings and assess their biological significance.

## CONTENTS

<b>CHAPTER 1: INTRODUCTION</b> .....	<b>1</b>
1.1 WHAT IS ALZHEIMER'S DISEASE?.....	1
1.2 THE PATHOLOGY OF ALZHEIMER'S DISEASE.....	1
1.3 GENETICS.....	2
1.4 BIOMARKERS.....	3
1.5 THE AMYLOID HYPOTHESIS .....	4
1.6 ALTERNATIVE DISEASE PATHWAYS .....	6
1.7 NEUROIMAGING.....	6
1.7.1 <i>Why use neuroimaging to study genetic risk?</i> .....	6
1.7.2 <i>Structural Magnetic Resonance Imaging tools for AD</i> .....	7
1.7.3 <i>What have neuroimaging studies revealed about brain structure in AD?</i> ..	8
1.8 METABOLOMICS.....	9
1.8.1 <i>What are metabolic markers &amp; how are they measured?</i> .....	9
1.8.2 <i>How do metabolic markers relate to Alzheimer's disease?</i> .....	10
1.9 AIMS AND THESIS OUTLINE.....	11
<b>CHAPTER 2: FROM POLYGENIC SCORES TO PRECISION MEDICINE IN ALZHEIMER'S DISEASE: A SYSTEMATIC REVIEW</b> .....	<b>13</b>
2.1 SUMMARY .....	13
2.2 INTRODUCTION .....	14
2.3 METHODS .....	15
2.3.1 <i>Search strategy</i> .....	15
2.3.2 <i>Article selection</i> .....	15
2.3.3 <i>Data extraction</i> .....	16
2.4 RESULTS .....	16
2.4.1 <i>Search results</i> .....	16
2.4.2 <i>Study characteristics</i> .....	17
2.4.3 <i>PRS Calculation</i> .....	18
2.4.4 <i>Prediction of AD Case/Control Status</i> .....	19
2.4.5 <i>Mild Cognitive Impairment to AD conversion</i> .....	20
2.4.6 <i>Cognitive Measures</i> .....	20
2.4.7 <i>MRI phenotypes</i> .....	21
2.4.8 <i>Amyloid and Tau Biomarkers</i> .....	22
2.4.9 <i>Other diseases and syndromes</i> .....	23
2.4.10 <i>Disease pathways</i> .....	24
2.4.11 <i>Study quality</i> .....	25
2.5 DISCUSSION.....	25

2.5.1	<i>PRS in disease prediction</i> .....	26
2.5.2	<i>Associations between AD PRS, phenotypes and biomarkers</i> .....	26
2.5.3	<i>PRS in disease pathways</i> .....	27
2.5.4	<i>Strengths and limitations</i> .....	28
2.5.5	<i>Conclusion</i> .....	30

**CHAPTER 3: IMAGING ALZHEIMER'S GENETIC RISK USING DIFFUSION MRI:  
A SYSTEMATIC REVIEW.....31**

3.1	SUMMARY.....	31
3.2	INTRODUCTION.....	32
3.2.1	<i>Alzheimer's Disease genetic risk</i> .....	32
3.2.2	<i>Diffusion MRI</i> .....	32
3.2.3	<i>Structural changes observed in Alzheimer's Disease</i> .....	33
3.2.4	<i>Current review</i> .....	34
3.3	METHODS.....	35
3.3.1	<i>Study selection</i> .....	35
3.3.2	<i>Article Selection</i> .....	35
3.3.3	<i>Data Extraction</i> .....	36
3.3.4	<i>Quality assessment</i> .....	36
3.4	RESULTS.....	36
3.4.1	<i>Search results</i> .....	36
3.4.2	<i>Study characteristics: study design, sample, Alzheimer's genetic risks</i> ... 37	37
3.4.3	<i>Genotypes</i> .....	38
3.4.4	<i>dMRI pre-processing and analysis methods</i> .....	38
3.4.5	<i>Studies of white matter structure and APOE status</i> .....	40
3.4.6	<i>Studies of white matter and autosomal-dominant AD genes</i> .....	45
3.4.7	<i>Studies of white matter and AD risk loci from GWAS</i> .....	48
3.4.8	<i>Study quality overview</i> .....	49
3.5	DISCUSSION.....	49
3.5.1	<i>White matter changes associated with AD risk genes</i> .....	49
3.5.2	<i>Methodological considerations</i> .....	52
3.5.3	<i>Interpretation of dMRI signal change in AD</i> .....	53
3.5.4	<i>Strengths and limitations of this review</i> .....	54
3.5.5	<i>Potential clinical applications</i> .....	55
3.5.6	<i>Conclusions</i> .....	56

**CHAPTER 4: GENERAL METHODOLOGY.....57**

4.1	PARTICIPANTS AND PROCEDURES.....	57
4.1.1	<i>The Avon Longitudinal Study of Parents and Children (ALSPAC)</i> .....	57
4.1.2	<i>UK Biobank</i> .....	58
4.2	BRAIN IMAGING.....	59

4.2.1	<i>MRI data in ALSPAC</i> .....	59
4.2.2	<i>MRI data in UK Biobank</i> .....	61
4.3	GENOTYPING.....	61
4.4	METABOLOMICS.....	62
4.4.1	<i>Metabolomic data in ALSPAC</i> .....	62
4.5	DATA ANALYSIS.....	62
4.5.1	<i>Data cleaning and pre-processing in ALSPAC</i> .....	62
4.5.2	<i>Data cleaning and pre-processing in UK Biobank</i> .....	63
4.5.3	<i>Polygenic score calculation</i> .....	63
4.5.4	<i>Statistical analyses</i> .....	67

## **CHAPTER 5: ALZHEIMER’S POLYGENIC RISK SCORES & GRAY MATTER**

<b>VOLUMES</b> .....	<b>68</b>	
5.1	SUMMARY.....	68
5.2	INTRODUCTION.....	69
5.2.1	<i>Rationale and Aims</i> .....	74
5.2.2	<i>Hypothesis</i> .....	75
5.3	METHODS.....	75
5.3.1	<i>Participants</i> .....	75
5.3.2	<i>MRI Acquisition</i> .....	76
5.3.3	<i>Analysis Pipeline</i> .....	77
5.3.4	<i>Genotyping</i> .....	77
5.3.5	<i>Polygenic Score (PRS) Calculations</i> .....	78
5.3.6	<i>Statistical Analysis</i> .....	79
5.4	RESULTS.....	79
5.4.1	<i>Subcortical Volumes in ALSPAC</i> .....	79
5.4.2	<i>Subcortical Volumes in UK Biobank</i> .....	87
5.4.3	<i>Cortical Thickness in ALSPAC</i> .....	95
5.4.4	<i>Cortical thickness in UK Biobank</i> .....	107
5.4.5	<i>Cortical Surface Area in ALSPAC</i> .....	118
5.4.6	<i>Cortical Surface Area in UK Biobank</i> .....	128
5.5	DISCUSSION.....	139
5.5.1	<i>Strength and limitations</i> .....	143
5.5.2	<i>Conclusion</i> .....	144

## **CHAPTER 6: ALZHEIMER’S POLYGENIC RISK SCORES & WHITE MATTER**

<b>MICROSTRUCTURE</b> .....	<b>145</b>	
6.1	SUMMARY.....	145
6.2	INTRODUCTION.....	147
6.2.1	<i>Rationale and Aims</i> .....	150

6.2.2	<i>Hypothesis</i> .....	151
6.3	METHODS .....	151
6.3.1	<i>Participants</i> .....	151
6.3.2	<i>MRI Acquisition</i> .....	152
6.3.3	<i>Analysis Pipeline</i> .....	153
6.3.4	<i>Genotyping</i> .....	155
6.3.5	<i>Polygenic Score (PRS) Calculations</i> .....	156
6.3.6	<i>Statistical Analysis</i> .....	156
6.4	RESULTS .....	157
6.4.1	<i>Fornix dMRI metrics</i> .....	157
6.4.2	<i>Cingulum dMRI metrics</i> .....	158
6.4.3	<i>Parahippocampal dMRI metrics</i> .....	159
6.5	DISCUSSION.....	175
6.5.1	<i>Strength and limitations</i> .....	178
6.5.2	<i>Conclusion</i> .....	179
<b>CHAPTER 7: ALZHEIMER’S POLYGENIC RISK SCORES, BLOOD LIPID &amp; INFLAMMATORY MARKERS .....</b>		<b>180</b>
7.1	SUMMARY .....	180
7.2	INTRODUCTION .....	181
7.2.1	<i>Rationale and Aims</i> .....	184
7.2.2	<i>Hypothesis</i> .....	185
7.3	METHODS .....	185
7.3.1	<i>Participants</i> .....	185
7.3.2	<i>Blood marker processing</i> .....	185
7.3.3	<i>Genotyping</i> .....	186
7.3.4	<i>Polygenic Score Calculations</i> .....	187
7.3.5	<i>Statistical Analysis</i> .....	187
7.4	RESULTS .....	188
7.4.1	<i>C-Reactive Protein</i> .....	188
7.4.2	<i>Blood Lipids</i> .....	188
7.5	DISCUSSION.....	196
7.5.1	<i>Strengths and limitations</i> .....	200
7.5.2	<i>Conclusion</i> .....	201
<b>CHAPTER 8: DISCUSSION.....</b>		<b>202</b>
8.1	SUMMARY OF FINDINGS .....	202
8.2	IMPLICATIONS OF THIS RESEARCH .....	205
8.2.1	<i>How should we use AD polygenic scores?</i> .....	205

8.2.2	<i>The role of AD biomarkers in translational research and clinical practice</i>	208
8.2.3	<i>Value of the pathway PRS approach in AD</i>	211
8.3	METHODOLOGICAL CONSIDERATIONS	211
8.3.1	<i>Participant selection and sample size</i>	211
8.3.2	<i>Imaging considerations</i>	213
8.3.3	<i>Genetic considerations</i>	214
8.3.4	<i>Summary of strengths and limitations</i>	216
8.4	FUTURE RESEARCH DIRECTIONS	217
8.4.1	<i>AD polygenic risk and brain function</i>	217
8.4.2	<i>Longitudinal studies</i>	219
8.4.3	<i>Improving and augmenting pathways analyses</i>	220
8.5	CONCLUSIONS	220
	<b>REFERENCES</b>	<b>222</b>
	<b>APPENDIX A</b>	<b>263</b>
	<b>APPENDIX B</b>	<b>265</b>

## LIST OF FIGURES

FIGURE 1.1 BIOMARKERS OF THE AD PATHOLOGICAL CASCADE.....	4
FIGURE 2.1 PRISMA FLOW CHART, AD PRS STUDIES.....	17
FIGURE 3.1 PRISMA FLOW CHART, DMRI STUDIES.....	37
FIGURE 3.2 THE CHANGE IN THE DIFFUSION SIGNAL (ISOTROPIC TO ANISOTROPIC DIFFUSION) CAN RESULT FROM MULTIPLE DIFFERENT PATHOLOGIES .....	53
FIGURE 5.1 ASSOCIATIONS BETWEEN GENOME-WIDE PRS AND SUBCORTICAL VOLUMES IN ALSPAC.....	85
FIGURE 5.2 ASSOCIATIONS BETWEEN PROTEIN-LIPID COMPLEX PRS AND SUBCORTICAL VOLUMES IN ALSPAC.....	86
FIGURE 5.3 SCATTERPLOT SHOWING NORMALISED GENOME WIDE PRS AND NORMALISED LEFT CAUDATE VOLUME IN ALSPAC.....	86
FIGURE 5.4 ASSOCIATIONS BETWEEN GENOME-WIDE PRS AND SUBCORTICAL VOLUMES IN UK BIOBANK.....	93
FIGURE 5.5 ASSOCIATIONS BETWEEN GENOME-WIDE PRS AND SUBCORTICAL VOLUMES IN UK BIOBANK.....	94
FIGURE 5.6 SCATTERPLOT SHOWING NORMALISED GENOME-WIDE PRS AND NORMALISED LEFT ACCUMBENS VOLUME.....	94
FIGURE 5.7. ASSOCIATIONS BETWEEN PRS ( $P^T = 0.001$ ) AND THICKNESS IN CORTICAL AND TEMPORAL REGIONS OF CORTEX IN ALSPAC, $P < 0.05$ .....	105
FIGURE 5.9. ASSOCIATIONS BETWEEN PRS ( $P^T = 0.001$ ) AND THICKNESS IN CORTICAL AND TEMPORAL REGIONS OF CORTEX IN UK BIOBANK, $P < 0.05$ .....	116
FIGURE 5.10. ASSOCIATIONS BETWEEN PRS ( $P^T = 0.001$ ) EXCLUDING <i>APOE</i> AND THICKNESS IN CORTICAL AND TEMPORAL REGIONS OF CORTEX IN UK BIOBANK, $P < 0.05$ .....	117
FIGURE 5.11. ASSOCIATIONS BETWEEN PRS ( $P^T = 0.001$ ) EXCLUDING <i>APOE</i> AND SURFACE AREA IN CORTICAL AND TEMPORAL REGIONS OF CORTEX IN ALSPAC, $P < 0.05$ .....	127
FIGURE 5.12. ASSOCIATIONS BETWEEN PRS ( $P^T = 0.001$ ) AND SURFACE AREA IN CORTICAL AND TEMPORAL REGIONS OF CORTEX IN UK BIOBANK, $P < 0.05$ .....	137
FIGURE 5.13. ASSOCIATIONS BETWEEN PRS ( $P^T = 0.001$ ) EXCLUDING <i>APOE</i> AND SURFACE AREA IN CORTICAL AND TEMPORAL REGIONS OF CORTEX IN UK BIOBANK, $P < 0.05$ . .....	138
FIGURE 6.1 SHOWING THE DMRI REGIONS OF INTEREST DEFINED FOR ALSPAC. LEFT IMAGE: THE FORNIX; CENTRE IMAGE: THE CINGULUM; RIGHT IMAGE: THE PARAHIPPOCAMPAL CINGULUM.....	155

FIGURE 6.2 ALSPAC GENOME-WIDE PRS AND DMRI METRICS, SHOWING NO SIGNIFICANT RESULTS. ....	161
FIGURE 6.3 ALSPAC TAU PROTEIN BINDING PRS (EXCLUDING THE APOE REGION) AND DIFFUSION METRICS, SHOWING TRENDS TOWARDS SIGNIFICANCE IN MORE LIBERAL PT IN THE CINGULUM.....	162
FIGURE 6.4 SCATTER PLOT SHOWING ALSPAC NON-SIGNIFICANT ASSOCIATION BETWEEN NORMALISED GENOME-WIDE PRS AND NORMALISED MD IN THE LEFT CINGULUM. ....	163
FIGURE 6.5 UK BIOBANK GENOME-WIDE PRS AND DMRI METRICS, SHOWING ASSOCIATIONS WITH REDUCED FA AND INCREASED MD .....	168
FIGURE 6.6 UK BIOBANK PROTEIN LIPID COMPLEX SUBUNIT PRS AND DMRI METRICS, SHOWING ASSOCIATIONS WITH DECREASED FA AND INCREASED MD.....	169
FIGURE 6.7 SCATTER PLOT SHOWING UK BIOBANK ASSOCIATION BETWEEN NORMALISED GENOME-WIDE PRS AND NORMALISED MD IN THE RIGHT PARAHIPPOCAMPAL CINGULUM .....	170
FIGURE 7.1 ASSOCIATIONS BETWEEN GENOME-WIDE PRS, CRP AND BLOOD LIPIDS ACROSS P VALUE THRESHOLDS .....	189
FIGURE 7.2 ASSOCIATIONS BETWEEN GENOME WIDE PRS EXCLUDING APOE, CRP AND BLOOD LIPIDS ACROSS P VALUE THRESHOLDS .....	190
FIGURE 7.3 ASSOCIATIONS BETWEEN APOE REGION SNPS ONLY, CRP AND BLOOD LIPIDS ACROSS P VALUE THRESHOLDS .....	191
FIGURE 7.4. ASSOCIATIONS BETWEEN TAU PROTEIN-BINDING PRS, CRP AND BLOOD LIPIDS ACROSS P VALUE THRESHOLDS .....	192
FIGURE 7.5. ASSOCIATIONS BETWEEN TAU PROTEIN-BINDING PRS EXCLUDING THE APOE REGION, CRP AND BLOOD LIPIDS ACROSS P VALUE THRESHOLDS.....	193
FIGURE 7.6 A SCATTER PLOT SHOWING THE CORRELATION BETWEEN NORMALISED GENOME-WIDE PRS AND NORMALISED CRP .....	193
FIGURE 8.1 EXAMPLES OF PRS APPLICATIONS IN HEART DISEASE AND BREAST CANCER. ....	207

## LIST OF TABLES

Table 2.1 Summary of included studies by type of PRS.....	18
Table 3.1 Summary of sample characteristics, methodology and main findings for APOE studies ....	43
Table 3.2 Summary of sample characteristics, methodology and main findings for studies of FAD genes .....	47
Table 3.3 Summary of key findings for the most commonly implicated tracts by gene risk (APOE or FAD).....	51
Table 4.1 Sample demographics by neuroimaging sub-study.....	60
Table 4.2 Significant pathways ( $q$ values $\leq 0.05$ ) from MAGMA pathway analysis for common and rare variant subsets.....	66
Table 5.1 Results for ALSPAC subcortical volumes and PRS including APOE at $P^T$ 0.001 .....	81
Table 5.2 Results for ALSPAC subcortical volumes and PRS excluding APOE at $P^T$ 0.001 .....	82
Table 5.3 Results for ALSPAC subcortical volumes and PRS including APOE at $P^T$ 0.001 .....	83
Table 5.4 Results for ALSPAC subcortical volumes and PRS excluding APOE at $P^T$ 0.001 .....	84
Table 5.5 Results for UK Biobank subcortical volumes and PRS including APOE at $P^T$ 0.001.....	89
Table 5.6 Results for UK Biobank subcortical volumes and PRS excluding APOE at $P^T$ 0.001.....	90
Table 5.7 Results for UK Biobank subcortical volumes and PRS including APOE at $P^T$ 0.001.....	91
Table 5.8 Results for UK Biobank subcortical volumes and PRS excluding APOE at $P^T$ 0.001.....	92
Table 5.9 Results for ALSPAC cortical thickness in left parietal regions and PRS including APOE at $P^T$ 0.001 .....	97
Table 5.10 Results for ALSPAC cortical thickness in left temporal regions and PRS including APOE at $P^T$ 0.001 .....	98
Table 5.11 Results for ALSPAC cortical thickness in left parietal regions and PRS excluding APOE at $P^T$ 0.001 .....	99
Table 5.12 Results for ALSPAC cortical thickness in left temporal regions and PRS excluding APOE at $P^T$ 0.001 .....	100
Table 5.13 Results for ALSPAC cortical thickness in right parietal regions and PRS including APOE at $P^T$ 0.001 .....	101
Table 5.14 Results for ALSPAC cortical thickness in right temporal regions and PRS including APOE at $P^T$ 0.001 .....	102
Table 5.15 Results for ALSPAC cortical thickness in right parietal regions and PRS excluding APOE at $P^T$ 0.001 .....	103

Table 5.16 Results for ALSPAC cortical thickness in right temporal regions and PRS including APOE at $P^T$ 0.001 .....	104
Table 5.17 Results for UK Biobank cortical thickness in left parietal regions and PRS including APOE at $P^T$ 0.001 .....	108
Table 5.18 Results for UK Biobank cortical thickness in left temporal regions and PRS including APOE at $P^T$ 0.001 .....	109
Table 5.19 Results for UK Biobank cortical thickness in left parietal regions and PRS including APOE at $P^T$ 0.001 .....	110
Table 5.20 Results for UK Biobank cortical thickness in left temporal regions and PRS excluding APOE at $P^T$ 0.001 .....	111
Table 5.21 Results for UK Biobank cortical thickness in right parietal regions and PRS including APOE at $P^T$ 0.001 .....	112
Table 5.22 Results for UK Biobank cortical thickness in right temporal regions and PRS including APOE at $P^T$ 0.001 .....	113
Table 5.23 Results for UK Biobank cortical thickness in right parietal regions and PRS excluding APOE at $P^T$ 0.001 .....	114
Table 5.24 Results for UK Biobank cortical thickness in right temporal regions and PRS excluding APOE at $P^T$ 0.001 .....	115
Table 5.25 Results for ALSPAC cortical surface area in left parietal regions and PRS including APOE at $P^T$ 0.001 .....	119
Table 5.26 Results for ALSPAC cortical surface area in left temporal regions and PRS including APOE at $P^T$ 0.001 .....	120
Table 5.27 Results for ALSPAC cortical surface area in left parietal regions and PRS excluding APOE at $P^T$ 0.001 .....	121
Table 5.28 Results for ALSPAC cortical surface area in left temporal regions and PRS excluding APOE at $P^T$ 0.001 .....	122
Table 5.29 Results for ALSPAC cortical surface area in right parietal regions and PRS including APOE at $P^T$ 0.001 .....	123
Table 5.30 Results for ALSPAC cortical surface area in right temporal regions and PRS including APOE at $P^T$ 0.001 .....	124
Table 5.31 Results for ALSPAC cortical surface area in right parietal regions and PRS excluding APOE at $P^T$ 0.001 .....	125
Table 5.32 Results for ALSPAC cortical surface area in right temporal regions and PRS excluding APOE at $P^T$ 0.001 .....	126

Table 5.33 Results for UK Biobank cortical surface area in left parietal regions and PRS including APOE at $P^T$ 0.001 .....	129
Table 5.34 Results for UK Biobank cortical surface area in left temporal regions and PRS including APOE at $P^T$ 0.001 .....	130
Table 5.35 Results for UK Biobank cortical surface area in left parietal regions and PRS excluding APOE at $P^T$ 0.001 .....	131
Table 5.36 Results for UK Biobank cortical surface area in left temporal regions and PRS excluding APOE at $P^T$ 0.001 .....	132
Table 5.37 Results for UK Biobank cortical surface area in right parietal regions and PRS including APOE at $P^T$ 0.001 .....	133
Table 5.38 Results for UK Biobank cortical surface area in right temporal regions and PRS including APOE at $P^T$ 0.001 .....	134
Table 5.39 Results for UK Biobank cortical surface area in right parietal regions and PRS excluding APOE at $P^T$ 0.001 .....	135
Table 5.40 Results for UK Biobank cortical surface area in right temporal regions and PRS excluding APOE at $P^T$ 0.001 .....	136
Table 6.1 Results for ALSPAC fractional anisotropy area and PRS including APOE at $P^T$ 0.001.....	164
Table 6.2 Results for ALSPAC fractional anisotropy area and PRS excluding APOE at $P^T$ 0.001....	165
Table 6.3 Results for ALSPAC mean diffusivity and PRS including APOE at $P^T$ 0.001 .....	166
Table 6.4 Results for ALSPAC mean diffusivity and PRS excluding APOE at $P^T$ 0.001 .....	167
Table 6.5 Results for UK Biobank fractional anisotropy and PRS including APOE at $P^T$ 0.001 .....	171
Table 6.6 Results for UK Biobank fractional anisotropy and PRS excluding APOE at $P^T$ 0.001 .....	172
Table 6.7 Results for UK Biobank mean diffusivity and PRS including APOE at $P^T$ 0.001 .....	173
Table 6.8 Results for UK Biobank mean diffusivity and PRS excluding APOE at $P^T$ 0.001 .....	174
Table 7.1 Results for maternal blood marker phenotypes and PRS including APOE at $P^T$ 0.001.....	194
Table 7.2 Results for maternal blood marker phenotypes and PRS excluding APOE at $P^T$ 0.001....	195
Table 8.1 Council of Europe, Committee of Ministers, Recommendation No. R (94) 11 on Screening as a Tool of Preventive Medicine (Oct. 10, 1994).....	208

## CHAPTER 1: INTRODUCTION

*This chapter includes some material that was previously published in Harrison JR & Owen MJ. Alzheimer's disease: the amyloid hypothesis on trial. British J Psychiatry. 2016 Jan;208(1):1-3. doi: 10.1192/bjp.bp.115.167569.*

### 1.1 What is Alzheimer's Disease?

Alzheimer's disease (AD) is a progressive neurodegenerative disorder that affects older adults. It affects around one in ten people over the age of 65 (Alzheimer's Association, 2019).

### 1.2 The pathology of Alzheimer's Disease

The classical histological features of AD are a triad of amyloid- $\beta$  ( $A\beta$ ) plaques, neurofibrillary tangles and neuronal cell loss (Selkoe, 1991). The first of these are insoluble extracellular plaques consisting of  $A\beta$ , which accumulates in very high levels in the brains of those with AD.  $A\beta$  is derived from a larger molecule, amyloid precursor protein (*APP*), which is a trans-membrane protein, with a long extracellular N-terminal and a shorter intracellular C-terminal. The  $A\beta$  sequence consists of some of the extracellular portion of *APP* and part of the trans-membrane domain and is 39–42 amino acids in length. The protein has a  $\beta$ -pleated sheet structure and demonstrates Congo red birefringence and resistance to proteolysis (Hardy and Allsop, 1991). In AD,  $A\beta$  is deposited in abundant extracellular plaques typically composed of straight fibrils, 6–10 nm in diameter. These structures are also found in normal ageing but in less profusion and are sometimes referred to as senile plaques. They are associated with dystrophic neurites and changes in microglia and astrocytes (Selkoe, 1991). Non-fibrillar, diffuse  $A\beta$  deposits, which are not associated with dystrophic neurites or reactive glial cells, are also found in AD and these may represent an early stage of plaque formation. In AD these diffuse plaques are found throughout the central nervous system, whereas typical  $A\beta$  plaques are not present in regions such as the spinal cord and cerebellum (Hardy and Allsop, 1991).

The second pathological structure found in AD is the neurofibrillary tangle, which consist of dystrophic neurites containing paired helical filaments, 10 nm in diameter. These paired helical filaments in turn consist of a phosphorylated microtubule-associated protein, tau (MAPT) (Selkoe, 1991). In the 1980s there was much debate as to which one of these is the primary driver of AD pathogenesis.

### 1.3 Genetics

Early molecular genetic studies of AD focused on rare families where the disorder occurs exceptionally early and follows an autosomal dominant mode of inheritance. It was discovered that autosomal-dominant AD is caused by mutations either in the *APP* gene itself, or in presenilin 1 and 2 (*PS1* and *PS2*) that are involved in cleaving A $\beta$  from *APP* (Tanzi, 2012). In addition, AD frequently affects those with trisomy 21, who have a triplication of the *APP* gene (Tanzi, 2012).

Sporadic AD, also known as late-onset AD, is common, affecting around 10% of all those over 65 (Alzheimer's Association, 2019). The heritability of sporadic AD is estimated to be almost 75% (Gatz *et al.*, 1997). Genome-wide association studies (GWAS) have identified a number of loci associated with sporadic AD. The largest genome-wide association study (GWAS) of clinically confirmed AD has identified 25 loci that are associated with increased risk of sporadic AD (Kunkle *et al.*, 2019). These are common genetic variants, known as single nucleotide polymorphisms (SNPs). The largest of these genetic risks are SNPs in the Apolipoprotein E (*APOE*) region. Carriers of two copies of the *APOE* Epsilon 4 (*APOE* E4) allele have an eight-fold increase in risk compared to non-carriers (Corder *et al.*, 1993). In comparison to *APOE*, other common risk loci have only a modest effect on disease risk. However, their combined effect can be studied using polygenic risk scores. These are calculated from the weighted sum of allelic dosages across the genome, and have proven particularly effective in predicting AD (Escott-Price, Sims, Bannister, *et al.*, 2015). They have allowed the exploration of how genetic risk for AD is manifest in different populations (Wray *et al.*, 2014). However, genetic score methodology varies greatly between

studies. The methodology and application of PRS in AD is described in more detail in Chapter 2.

In addition to common genetic risk captured by GWAS, advances in sequencing techniques have assessed entire exomes and genomes, identifying rare mutations with moderate-to-strong effects. For example, *TREM2* is a variant that encodes the trigger receptor expressed on myeloid cells 2 (Guerreiro, Wojtas, Bras, Carrasquillo, Rogaeva, Majounie, Cruchaga, Sassi, John S K Kauwe, *et al.*, 2013). Other novel variants are involved in immune response and transcriptional regulation (Bis *et al.*, 2018).

#### **1.4 Biomarkers**

Brain A $\beta$  deposition in AD can be demonstrated *in vivo* using biomarkers such as cerebrospinal fluid (CSF) A $\beta$ 42 and A $\beta$  positron emission tomography (PET) imaging (Jack Jr. *et al.*, 2010). Clinical diagnoses of AD and A $\beta$  pathology at autopsy correlate with low concentrations of CSF A $\beta$ 42. Most patients with a diagnosis of AD have increased retention of radioligands for A $\beta$  on PET. Moreover, low CSF A $\beta$  and positive A $\beta$  PET show nearly 100% concordance (Jack Jr. *et al.*, 2010).

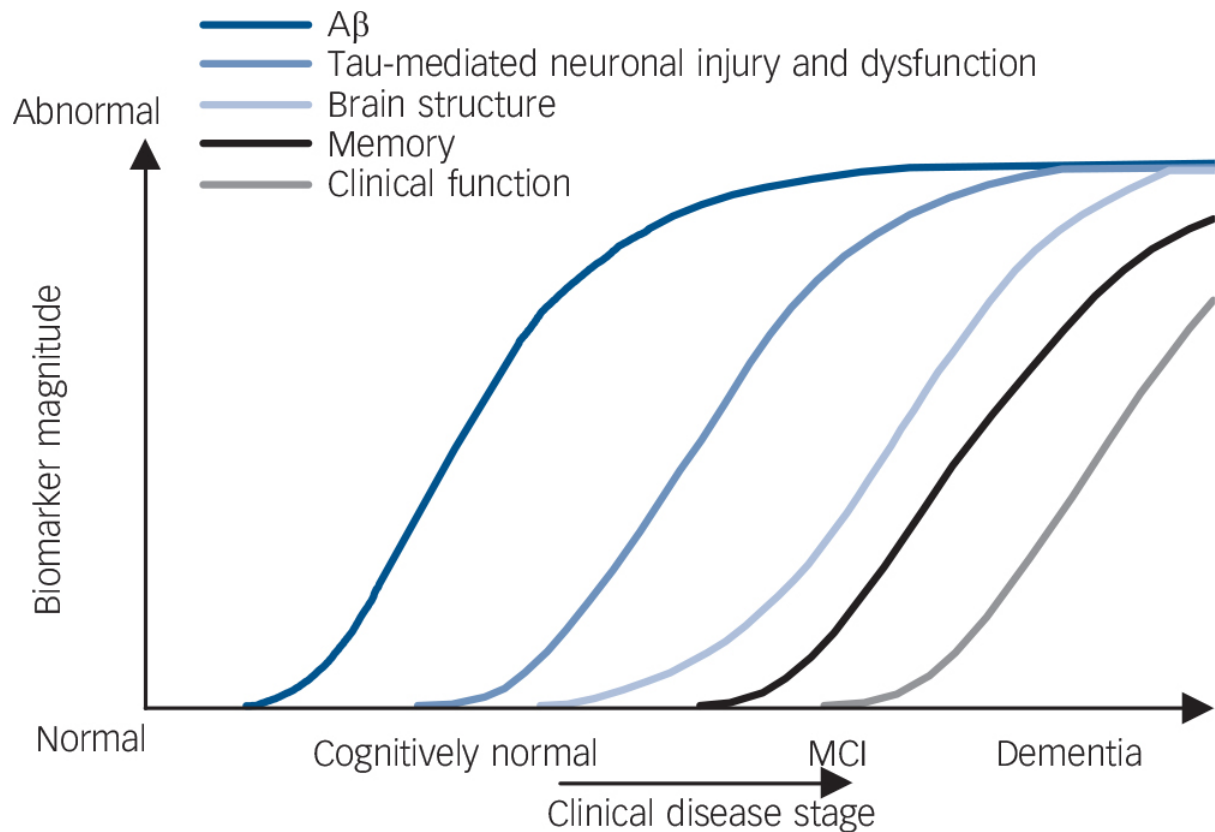


**Figure. 1.1 Biomarkers of the AD pathological cascade.**

Beta-amyloid (A $\beta$ ) is indicated by low cerebrospinal fluid (CSF) A $\beta$ 42 or positron emission tomography (PET) A $\beta$  imaging. Tau neuronal injury and dysfunction is shown by CSF tau or fluorodeoxyglucose-PET. Cerebral atrophy is measured with structural magnetic resonance imaging. Acronyms: MCI = mild cognitive impairment. Reprinted with permission from Elsevier Limited. Jack CR, Knopman DS, Jagust WJ, Shaw LM, Aisen PS, Weiner MW, et al. Hypothetical model of dynamic biomarkers of the Alzheimer's pathological cascade. *Lancet Neurol* 2010; **9**: 119–28.

### 1.5 The Amyloid Hypothesis

Hardy & Allsop (Hardy and Allsop, 1991) postulated that *APP* mismetabolism and A $\beta$  deposition are the primary events in the disease process with tau phosphorylation and neurofibrillary tangle formation occurring downstream. This became known as the amyloid hypothesis. It later transpired that the autosomal-dominant AD genes increase levels of 42 amino acid A $\beta$  (A $\beta$ 42) relative to the shorter 40 amino acid protein, and this form of A $\beta$  aggregates more readily into plaques (Wurth, Guimard and Hecht,

2002). Thus, a substantial body of evidence appears to support a causative, pathogenic link between A $\beta$  and AD. However, there are a few pieces of the AD jigsaw that do not quite fit.

AD is not an all-or-none phenomenon even at the neuropathological level. Moreover, autopsy studies find sufficient numbers of A $\beta$  plaques and neurofibrillary tangles to meet criteria for a diagnosis of AD in around a third of cognitively intact elderly people (Rodrigue *et al.*, 2012). This is corroborated by biomarker studies, which suggest that 20–40% of elderly people without cognitive impairment show significant brain A $\beta$  load, either on A $\beta$  PET or CSF A $\beta$ 42 concentrations (Rodrigue *et al.*, 2012).

The topographic distribution of A $\beta$  plaques differs from neurofibrillary tangle deposition and neurodegenerative changes. In early AD, neural loss occurs predominantly in the hippocampus and entorhinal cortex, whereas plaques are first found in frontal regions, basal ganglia or elsewhere (Heiko Braak and Braak, 1997; Jack Jr. *et al.*, 2010). Clinical symptoms are more closely associated with neurofibrillary tangles than A $\beta$  burden. However, cerebral atrophy, representing neuron and synapse loss, corresponds best with cognitive impairment (Jack *et al.*, 2013).

How distant A $\beta$  plaques might induce neurofibrillary tangles or damage neurons is unclear. It has been proposed that soluble oligomers of A $\beta$  could be neurotoxic. Although soluble oligomers cannot be seen *in vivo* or post-mortem, they have been found to interfere with postsynaptic potentiation in tissue culture studies. However, the concentration of A $\beta$  oligomers shown to have this effect is greater than usual physiological levels (Karran, Mercken and De Strooper, 2011). Another suggestion is that A $\beta$  plaques could act as a ‘reservoir’ eluting soluble A $\beta$ , but A $\beta$  has a strong tendency to polymerise and fix fragments to plaques, which makes this less likely (Karran, Mercken and De Strooper, 2011). Furthermore, many animal models based on *APP* and *PS1* mutations have not shown progression to synaptic loss, neurofibrillary tangle formation and neurodegeneration (Sambamurti *et al.*, 2012).

Critics of the amyloid hypothesis also point out that autosomal dominant AD, where the aetiological link with *APP* is strong, is rare and might be an atypical form of the disorder. They point to recent GWAS which have implicated many novel genes as

containing risk factors for typical AD but not *APP* or its metabolising enzymes. In defence of the amyloid hypothesis, GWAS only assess common genetic variation and failure to find association does not exclude an important role for a protein in disease. Moreover, some of the genes implicated by GWAS may be involved in A $\beta$  processing. For example, *CLU* encodes clusterin, which binds soluble A $\beta$  in animal models, forming complexes that can cross the blood–brain barrier, and *PICALM* encodes phosphatidylinositol binding clathrin assembly protein, which has been postulated to increase AD risk through *APP* processing via endocytic pathways, resulting in changes in A $\beta$  levels (Harold *et al.*, 2009). The biggest challenge to the amyloid hypothesis has come from the failure of phase III trials of anti-A $\beta$  therapies despite promising results in animal models (Sambamurti *et al.*, 2012; Drachman, 2014).

## **1.6 Alternative Disease Pathways**

As GWAS allows all variants in the genome to be tested for association simultaneously without any *a priori* hypothesis, they have implicated a number of biological processes previously unconnected to AD. Pathway analyses of genome-wide association data have shown that the disease processes that underpin AD are highly complex, involving a number of biological processes, including immunity, lipid metabolism, tau binding proteins, and amyloid precursor protein metabolism (Jones *et al.*, 2010; Kunkle *et al.*, 2019).

## **1.7 Neuroimaging**

### **1.1.7 Why use neuroimaging to study genetic risk?**

The brain is a comparatively inaccessible organ, making it difficult to study the impact of genetic risks on its structure and function. Neuroimaging technologies provide an intermediate phenotype in AD and have an established role in AD diagnosis and monitoring. It is likely that disease-modifying therapies, when available, will only be effective if administered early in the disease process, long before the onset of symptoms. Therefore, it is imperative that advanced imaging techniques are developed to enable early detection of differences in brain structure and function. Such

information could be combined with genetic profiling, using risk profile scores based on panels of SNPs that are associated with increased risk (Harold *et al.*, 2009).

### **1.2.7 Structural Magnetic Resonance Imaging tools for AD**

Magnetic resonance imaging (MRI) is a non-invasive neuroimaging method that can be used to investigate brain structure and function. MRI involves a powerful static magnetic field, magnetic field gradients and radiofrequency pulses. The spin of the protons in the tissue interacts with the magnetic field. A receiver coil detects signals released by protons as they return to their equilibrium state. Detailed information about brain morphology, microstructure, neurochemical composition and blood flow can be inferred using different sequences.

Structural MRI relies on the differing relaxation times of protons in different tissues. This signal encodes spatial and contrast information. Structural MRI uses T1-weighted images to a) investigate discrete brain structure abnormalities; b) measure the volume of a collection of voxels within specific areas, known as region-of-interest (ROI) studies; c) quantify surface structures such as cortical folds and thickness, using software such as Freesurfer (Fischl, 2012); d) measure volume and density of each voxel in the entire brain, as in voxel-based morphometry (VBM) (Ashburner and Friston, 2000).

Diffusion MRI (dMRI) probes the movement of water molecules to assess the microstructural configuration of tissue (Jones, 2011; Winston, 2012). dMRI measures indicate how readily water molecules can diffuse in and around structures such as white matter fibres or cell bodies (Strijkers, Drost and Nicolay, 2011; Johansen-Berg and Behrens, 2013). In white matter, the rate of diffusion is modulated by multiple microstructural features including axon diameter, axon density and myelination (Jones, 2011). In highly ordered white matter, the rate of diffusion is anisotropic, i.e., it is strongly dependent on the direction in which it is measured.

### 1.3.7 What have neuroimaging studies revealed about brain structure in AD?

Conventional MRI measures of atrophy, such as Voxel-Based Morphometry (VBM), are established markers for AD diagnosis and measurement of progression (Frisoni *et al.*, 2010). Longitudinal imaging studies of cognitively normal people have demonstrated that those with smaller brain structures at baseline are more likely to show cognitive decline. Atrophy in the hippocampal formation and temporoparietal cortical regions are particularly likely to herald dementia symptoms (Kaye *et al.*, 1997; Den Heijer *et al.*, 2006; C. D. Smith *et al.*, 2007; Apostolova *et al.*, 2010; Martin *et al.*, 2010). Indeed, subtle changes are often present years before the onset of cognitive problems (Fox *et al.*, 1996, 2001; Schott *et al.*, 2003). Cortical thickness has also been shown to be an early marker of AD. Regionally specific cortical thinning relates to symptom severity in very mild to mild AD dementia and is detectable in asymptomatic amyloid-positive individuals (Dickerson, Bakkour, *et al.*, 2009; Desikan *et al.*, 2010; Becker *et al.*, 2011).

More recently, diffusion MRI (dMRI) has allowed the exploration of AD white matter microstructure, finding extensive changes. A detailed introduction to dMRI methodology is provided in Chapter 3. To summarise, dMRI uses the movement of water molecules to provide contrast. Where no structures limit the movement of water molecules, the rate of diffusion is equal in all directions, known as isotropic diffusion. The inverse, where diffusion occurs predominantly along one axis, for example in a dense bundle of axons, is known as anisotropic diffusion (Beaulieu and Allen, 1994; Pierpaoli and Basser, 1996; Beaulieu, 2009; Winston, 2012). These are often indexed by fractional anisotropy (FA) (Basser and Pierpaoli, 1996) and mean diffusivity (MD). An FA of 0 represents diffusion occurring equally in all directions (isotropic diffusion), and 1 represents diffusion occurring exclusively in one direction (anisotropic diffusion) (Beaulieu and Allen, 1994; Pierpaoli and Basser, 1996; Beaulieu, 2009; Winston, 2012). Mean diffusivity (MD) represents the rate of diffusion orientationally-averaged. A meta-analysis of 41 studies found reduced FA and increased MD in AD brains compared to controls. Differences were marked in frontal and temporal lobes, and the posterior cingulum, corpus callosum, superior longitudinal fasciculi and uncinate fasciculi (Sexton *et al.*, 2011). Late-myelinating tracts may be affected primarily by AD neurodegeneration (Benitez *et al.*, 2014). This has given rise to a 'last in, first out'

theory of white matter condition across the life course (Davis *et al.*, 2009). Longitudinal studies suggest that the pattern of decreased FA and increased MD becomes more distinct as the disease progresses (Mayo *et al.*, 2017). Changes in the parahippocampal cingulum have been shown to discriminate between AD and healthy controls (Mayo *et al.*, 2017). Diffusion measurements in the fornix are another possible biomarker (Ringman *et al.*, 2007). Perea and colleagues found that AD preferentially degraded the crus and body of the fornix. The diffusion differences remained after controlling for fornix volume (Perea *et al.*, 2018). Chapter 3 contains a systematic review of dMRI changes in relation to AD genetic risk.

## **1.8 Metabolomics**

### **1.4.8 What are metabolic markers & how are they measured?**

As analysis of DNA is genomics and analysis of RNA and differences in mRNA expression is transcriptomics, the investigation of biologically active molecules, commonly known as metabolites, is metabolomics.

Metabolites are small molecules, typically with a mass range from 50 to 1500 Daltons. They can be sampled from cells, blood fluids such as serum, or tissues. Together, these metabolites and their relationship with a biological system, such as the human body, are referred to as the metabolome. There are an estimated 3,000 common metabolites that are endogenous in humans (*The Metabolomics Innovation Centre*, 2020). The metabolome is altered by genetic and environmental factors. Metabolomics represents the substrates and products of metabolism. It reveals the biochemical activity within cells and tissues and is considered the molecular phenotype.

Metabolomic tests on serum are high throughput processes, involving the collection of the sample from the participant, sample preparation using solvents, concentrating or purifying the sample, and analysis using analytical platforms such as mass spectrometry. Biochemical tests used in clinical practice measure individual metabolite concentrations to identify disorders. However, analytical techniques only provide a snapshot of metabolite concentrations in specific conditions. Some reactions occur

continuously, therefore levels of individual molecules change significantly depending on the time of measurement.

### 1.5.8 How do metabolic markers relate to Alzheimer's disease?

Metabolic degeneration on fluorodeoxyglucose positron emission tomography (FDG-PET) is one of the earliest detectable markers in MCI and early AD (Pagani *et al.*, 2017). Hypometabolism in the brain appears around two decades before the onset of symptoms suggesting that metabolic perturbation is strongly linked with AD pathology (Toledo *et al.*, 2017).

AD genetic risk is also linked to metabolic changes. Young mice with *APP/PS1* show metabolic changes in the liver, kidney, and heart (Zheng *et al.*, 2019). These are evident even before the accumulation of A $\beta$  in the brain (Trushina *et al.*, 2012). The *APOE* alleles, Epsilon 2, 3 and 4, encode protein isoforms with different lipid interactions in serum (Liu *et al.*, 2013). *APOE* E4 is associated with higher low density lipoprotein (LDL) cholesterol (Lahoz *et al.*, 2001). Genome-wide association studies have also implicated lipid metabolism in AD pathophysiology (Kunkle *et al.*, 2019).

Epidemiological studies exploring the effect of serum cholesterol levels on AD risk have reported contradictory findings. AD risk was reportedly associated with both low and high cholesterol (Li *et al.*, 2005; Reitz *et al.*, 2010; Tynkkynen *et al.*, 2018; Wagner *et al.*, 2018; Ferguson *et al.*, 2020), although divergence could be attributed in part to the smaller sample sizes used in older studies.

Metabolomics and lipidomics provide further evidence that lipid metabolites are involved in AD pathology (Wilkins and Trushina, 2018). For example, changes in levels of sphingomyelin, a key element of lipid rafts, are associated with preclinical AD determined by CSF profile (Koal *et al.*, 2015). Plasma and brain tissue from humans and mice revealed that bile acids, which are important for lipid metabolism, are perturbed in AD (Pan *et al.*, 2017).

Taken together, genomic and epidemiological studies along with metabolomics and lipidomics provide convincing evidence that lipid homeostasis is an important component of the AD pathological processes.

## 1.9 Aims and Thesis Outline

This thesis is divided into three parts. The first objective is to examine the current literature using AD PRS and the current literature examining the effect of AD risk on white matter microstructure. The aims are to:

1. Systematically review studies using a PRS approach to investigate phenotypes associated with AD, summarise PRS methodology and provide a narrative synthesis of findings (Chapter 2)
2. Systematically review studies that apply dMRI techniques to investigate genetic risk for AD, discuss dMRI techniques and provide a narrative synthesis of findings (Chapter 3)

The second objective is to determine whether genetic burden for AD, represented by PRS, is associated with relevant neuroimaging phenotypes in healthy general population samples. The specific aims are to:

1. Determine whether AD PRS are associated with volumetric changes suggestive of AD pathology in healthy younger and older adults from the general population (Chapter 5)
2. Determine whether AD PRS are associated with changes in white matter microstructure suggestive of AD pathology in healthy younger and older adults from the general population (Chapter 6)
3. Determine whether pathway-specific PRS for AD are associated with distinct patterns of changes in the above phenotypes (Chapters 5 and 6)

The third objective is to determine whether AD polygenic risk is associated with changes in levels of blood lipids and inflammatory markers in a healthy population sample. The aims are to:

1. Determine whether AD PRS are associated with increased or decreased levels of blood lipids and inflammatory markers in healthy adults (Chapter 7)
2. Determine whether pathway-specific PRS for AD are associated with distinct patterns of changes in the metabolic phenotype (Chapter 7)

Chapters 2 to 7 begin with a summary section, which condenses the relevant background and key findings without references, akin to an abstract.

Chapters 2 and 3 comprise the systematic reviews. Chapter 4 will provide a general description of the two population cohorts used for addressing the above aims. Chapters 5 and 6 will address the second objective and Chapter 7 will address the third objective. Chapter 8 concludes the thesis with a discussion of the implications of the findings, methodological considerations, strengths and limitations and suggestions for further areas of work.

## **CHAPTER 2: FROM POLYGENIC SCORES TO PRECISION MEDICINE IN ALZHEIMER'S DISEASE: A SYSTEMATIC REVIEW**

*The chapter includes some material that was previously published Harrison, J. R. et al. 2020. From polygenic scores to precision medicine in Alzheimer's Disease: A systematic review. Journal of Alzheimer's Disease 74(4), pp. 1271-1283. (10.3233/JAD-191233). Dr Sum Mistry and Ms Natalie Muskett assisted with the assessment of selected studies.*

*Some information from Chapter 1 is repeated here for convenience.*

### **2.1 Summary**

As described in Chapter 1, many common genetic variants, known as single nucleotide polymorphisms (SNPs), confer risk for AD. These variants are clustered in areas of biology, notably immunity and inflammation, cholesterol metabolism, endocytosis and ubiquitination. Polygenic scores (PRS), which weight the sum of an individual's risk alleles, have been used to draw inferences about the pathological processes underpinning AD.

This Chapter systematically reviews how AD PRS are being used to study a range of outcomes and phenotypes related to neurodegeneration. The literature was searched from July 2008-July 2018 following Preferred Reporting Items for Systematic Reviews and Meta-Analyses (PRISMA) guidelines. 57 studies met criteria. There was evidence that the AD PRS can distinguish AD cases from controls. The ability of AD PRS to predict conversion from Mild Cognitive Impairment (MCI) to AD was less clear. There is strong evidence of association between AD PRS and cognitive impairment. AD PRS are correlated with a number of biological phenotypes associated with AD pathology, such as neuroimaging changes and amyloid and tau measures. Pathway-specific polygenic scores are also associated with AD-related biologically relevant phenotypes.

The evidence suggests PRS can predict AD and are associated with other phenotypes relevant to neurodegeneration, particularly cognitive impairment. The associations between pathway specific polygenic scores and phenotypic changes may allow us to define the biology of the disease in individuals and indicate who may benefit from specific treatments. Longitudinal cohort studies are required to test the ability of PRS to delineate pathway-specific disease activity.

## 2.2 Introduction

As discussed in Chapter 1, the heritability of late-onset AD is estimated to be almost 75% (Gatz *et al.*, 1997). Genome-wide association studies (GWAS) have identified a number of loci associated with AD. The largest meta-analysis to date reported 25 loci associated with increased risk for AD at genome-wide significant level (Kunkle *et al.*, 2019). These common genetic variants, known as single nucleotide polymorphisms (SNPs), have only a small effect on disease risk.

Polygenic risk scores (PRS) sum the weighted allelic dosages across the genome, and have allowed the exploration of how genetic risk for AD is manifest in different populations (Wray *et al.*, 2014). However, genetic score methodology varies greatly between studies. For example, Escott-Price *et al.* analysed over 200,000 SNPs, including *APOE* and reported an area under the curve (AUC) value of 0.84 (Escott-Price, Sims, Bannister, *et al.*, 2015) whereas Tosto *et al.* used only 21 SNPs excluding *APOE* resulting in an AUC of 0.57 (Tosto *et al.*, 2017).

As GWAS test all variants in the genome for association with disease without any *a priori* hypothesis, they have implicated a number of biological systems previously unconnected to AD. Pathway analyses of GWAS data have shown that the disease processes that underpin AD are highly complex, involving a number of biological processes, including immunity, lipid metabolism, tau binding proteins, and amyloid precursor protein metabolism (Jones *et al.*, 2010; Kunkle *et al.*, 2019).

Since the PRS approach was first described, many studies have investigated whether AD PRS are associated with a wide variety of phenotypes. This Chapter presents

a systematic review of studies that have used a PRS to investigate phenotypes associated with AD and summarises their results.

## **2.3 Methods**

The review was conducted in accordance with the PRISMA guidelines for systematic reviews (Moher *et al.*, 2009).

### **2.3.1 Search strategy**

MEDLINE, PSYCHINFO and EMBASE were searched from July 2008-July 2018 using a list of predetermined search terms listed in Supplementary Materials Table 1. Reference lists of relevant articles were also manually searched.

Inclusion criteria:

- Longitudinal, cross-sectional or case-control studies including genotyped data
- Validated risk loci for AD identified and combined into a PRS
- Reported associations with AD case/control status or another phenotype

Exclusion criteria:

- Studies reporting associations with family history only
- Studies reporting on genetic risk for other conditions or loci that have not been previously shown to increase risk of AD
- Studies reporting the effect of only one locus or gene (e.g. *APOE*), or *APOE* combined with non-genetic risk factors
- Non-English publications (in the absence of an existing translation or resources to make one).

### **2.3.2 Article selection**

All articles selected for inclusion were original research reports written in English. The design of the studies was cross-sectional, longitudinal or observational. The initial

search was conducted by NM. Based on the eligibility criteria, two reviewers (JH and SM) independently selected studies. Any discrepancies were resolved by a third reviewer (VEP).

### **2.3.3 Data extraction**

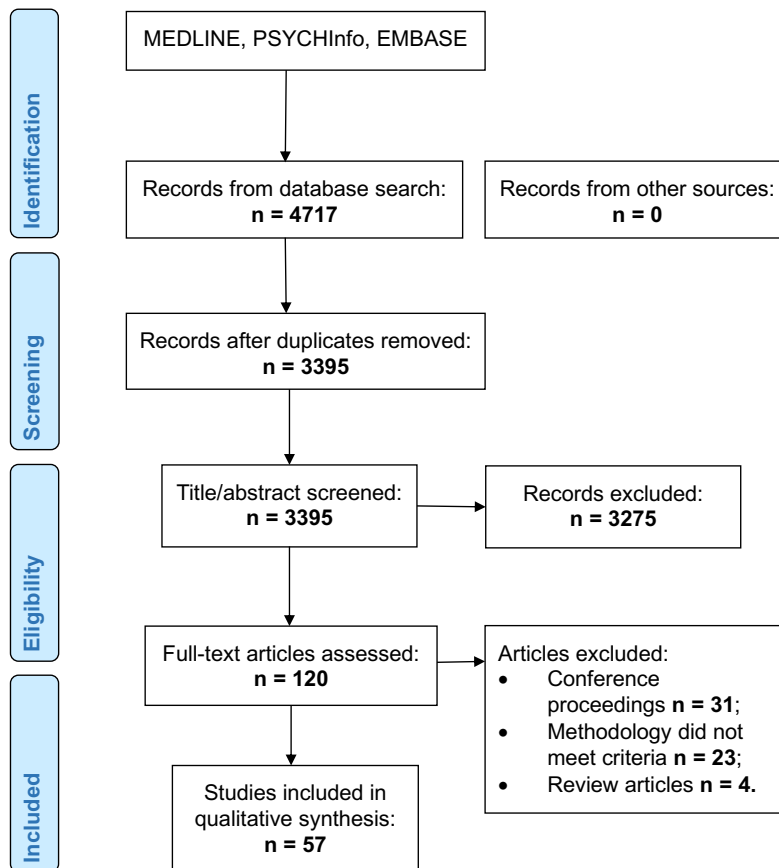
The reviewers (JH and SM) extracted data from the studies independently and in duplicate. The extracts included: 1) the type of study, 2) the discovery sample (study name, sample size and number of cases), 3) the target sample (study name, sample size, and case number), 4) the number of SNPs included in the PRS (see data extraction form in Supplementary Material). Results that were reported in separate papers were only included once.

## **2.4 Results**

### **2.4.1 Search results**

The initial search produced 4717 articles (see PRISMA flow chart in Figure 1). 1322 were removed as duplicates. A further 3275 were excluded based on their title and abstract. The reviewers (JH and SM) reviewed the full text of the remaining 120 articles and applied strict inclusion criteria, excluding a further 63. 57 articles were eligible for inclusion. The review followed PRISMA systematic review guidelines.

**Figure 2.1 PRISMA flow chart, AD PRS studies**



## 2.4.2 Study characteristics

There was a variety of study designs. Please see Tables 3 and 4 in Appendix 1 for further details on the included studies. Most were case-control studies, comparing those with AD or Mild Cognitive Impairment (MCI) to healthy controls (Rodríguez-Rodríguez *et al.*, 2013; Dubé *et al.*, 2013; Chouraki *et al.*, 2014; Adams *et al.*, 2015; Martiskainen *et al.*, 2015; Slegers *et al.*, 2015; Xiao *et al.*, 2015; Yokoyama, Lee, *et al.*, 2015; Escott-Price, Sims, Bannister, *et al.*, 2015; Escott-Price, Sims, Harold, *et al.*, 2015; Laiterä *et al.*, 2016; Louwersheimer *et al.*, 2016; Hohman *et al.*, 2017; Lacour *et al.*, 2017; Polimanti *et al.*, 2017; Su *et al.*, 2017; Tosto *et al.*, 2017; Voyle *et al.*, 2017; Escott-Price *et al.*, 2017; Ahmad *et al.*, 2018; Patel *et al.*, 2018; Chaudhury *et al.*, 2018; Cruchaga *et al.*, 2018; Del-Aguila *et al.*, 2018). Others were cross-sectional (Sabuncu *et al.*, 2012; Verhaaren *et al.*, 2013; Marden *et al.*, 2014, 2016; Papenberg

*et al.*, 2015; Wollam *et al.*, 2015; Andrews *et al.*, 2016; Hagenaars, Harris, Davies, Hill, *et al.*, 2016; Hagenaars, Harris, Davies, Marioni, *et al.*, 2016; Lupton *et al.*, 2016; Mormino *et al.*, 2016; Pilling *et al.*, 2016, 2017; Foley *et al.*, 2016; Habes *et al.*, 2016; Andrews, Das, *et al.*, 2017; Hayes *et al.*, 2017; Marioni *et al.*, 2017; Morgan *et al.*, 2017; Andrews, Eramudugolla, *et al.*, 2017; Polimanti *et al.*, 2017; Schultz *et al.*, 2017; Voyle *et al.*, 2017; Bressler *et al.*, 2017; Darst *et al.*, 2017; Gibson *et al.*, 2017; Li *et al.*, 2018; Tan *et al.*, 2018; Axelrud *et al.*, 2018; Corlier *et al.*, 2018; Logue *et al.*, 2019) and some were longitudinal (Harris *et al.*, 2014; Carrasquillo *et al.*, 2015; Hayden *et al.*, 2015; Harrison and Bookheimer, 2016; Felsky *et al.*, 2018; Sapkota and Dixon, 2018). The majority included participants of European ancestry from Europe, the US or Australia, although some included Black African American (Marden *et al.*, 2014, 2016; Bressler *et al.*, 2017), Hispanic (Tosto *et al.*, 2017; Axelrud *et al.*, 2018), Caribbean (Tosto *et al.*, 2017), or Han Chinese participants (Xiao *et al.*, 2015; Su *et al.*, 2017; Li *et al.*, 2018). Sample size ranged from 66 (Harrison *et al.*, 2016) to over 100,000 (Pilling *et al.*, 2016). The articles examined associations with several phenotypes. See Table 2.1 for a summary of study characteristics.

**Table 2.1 Summary of included studies by type of PRS**

<b>Correlates/Outcomes</b>	<b>N Studies</b>	<b>N Threshold PRS Studies</b>	<b>N GWAS Significant PRS Studies</b>
AD risk prediction	15	5	10
MCI risk prediction or MCI conversion	4	2	2
MRI phenotypes	12	7	5
Cognition	21	5	16
CSF biomarkers	8	3	5
Other diseases/syndromes	4	2	2
Disease pathways	3	1	2

Acronyms: AD = Alzheimer's Disease; MCI = Mild Cognitive Impairment; MRI = Magnetic Resonance Imaging; CSF = Cerebrospinal Fluid; GWAS = Genome-wide Association Study.

### 2.4.3 PRS Calculation

All studies computed PRS using SNPs that have been associated with AD in large meta-analyses. Most used the International Genomics of Alzheimer's Project (IGAP) (Lambert *et al.*, 2013) or another recent GWAS. There were two approaches to identifying SNPs for inclusion: 1) selecting SNPs that reached genome-wide

significance in meta-analysis, or 2) using p-value thresholds, including a greater number of nominally associated SNPs (please see Tables 3 and 4 in Appendix 1 for a summary of PRS calculation). Two of the studies in Han Chinese populations chose to verify that the SNPs were associated with AD in their population before computing PRS (Xiao *et al.*, 2015; Su *et al.*, 2017). Most studies weighted PRS by effect size, specifically the logarithm of the odds ratio or beta-coefficient from the regression analysis model, as described by Purcell and colleagues (Purcell *et al.*, 2009). There were five exceptions: one study weighted by explained variance (Andrews, Eramudugolla, *et al.*, 2017); four studies created unweighted scores by summing the number of risk loci (Dubé *et al.*, 2013; Wollam *et al.*, 2015; Bressler *et al.*, 2017; Papenberg *et al.*, 2017). *APOE* was either included as a co-variate, included in the PRS or excluded (see Tables 3 and 4 in Appendix A).

#### **2.4.4 Prediction of AD Case/Control Status**

15 studies used PRS to predict AD case/control status with various statistical approaches. Some studies used the area under the receiver operating characteristic (ROC) curve, whereas others used time-to-event analysis, Odds Ratios (OR) or a combination of methods. All found that PRS was able to discriminate cases from controls, although prediction accuracy varied.

Of those studies reporting Area Under the Curve (AUC), five included *APOE* and achieved AUC ranging from 0.62–0.84 (Escott-Price, Sims, Harold, *et al.*, 2015; Sleegers *et al.*, 2015; Xiao *et al.*, 2015; Yokoyama, Bonham, *et al.*, 2015; Escott-Price *et al.*, 2017; Chaudhury *et al.*, 2018). Four studies excluded *APOE* and achieved AUC ranging from 0.57–0.75 (Sleegers *et al.*, 2015; Lupton *et al.*, 2016; Tosto *et al.*, 2017; Cruchaga *et al.*, 2018). Of those studies using time-to-event analysis, all four excluded *APOE* and reported Hazard Ratios (HR) ranging from 1.11 – 2.36 (Chouraki *et al.*, 2016; Ahmad *et al.*, 2018; Tan *et al.*, 2018). Of those studies using ORs, two included *APOE* in their PRS and reported OR ranging from 2.06– 2.32 (Sabuncu *et al.*, 2012; Sleegers *et al.*, 2015). Four studies excluded *APOE* and reported OR ranging from 1.14–2.85 (Biffi *et al.*, 2010; Lupton *et al.*, 2016; Tosto *et al.*, 2017; Cruchaga *et al.*, 2018). More detailed information, including the details of the samples

and outcome measures used by each study, is contained in Tables 3 and 4 in Appendix A.

#### **2.4.5 Mild Cognitive Impairment to AD conversion**

Eight studies assessed the ability of PRS to predict MCI to AD conversion. Three studies did not report statistically significant results (Rodríguez-Rodríguez *et al.*, 2013; Andrews, Eramudugolla, *et al.*, 2017; Lacour *et al.*, 2017). Rodríguez-Rodríguez *et al.* compared those in the 1<sup>st</sup> and 3<sup>rd</sup> tertile of PRS (OR: 1.32, 95% CI: 0.57–3.06). Neither of the hazard models used by Lacour *et al.* and Andrews *et al.* produced significant results (Lacour HR: 1.18, 95% CI: 0.37–2.0; Andrews HR: 1.05, 95% CI: 0.86–1.29)(Andrews, Eramudugolla, *et al.*, 2017; Lacour *et al.*, 2017). However, Andrews *et al.* found their PRS was associated with an increased risk of transitioning from normal cognition to dementia (HR = 4.19, 95% CI: 1.72–10.20) (Andrews, Eramudugolla, *et al.*, 2017). Five studies reported statistically significant results (Adams *et al.*, 2015; Carrasquillo *et al.*, 2015; Mormino *et al.*, 2016; Tan *et al.*, 2018; Logue *et al.*, 2019). However, when *APOE* was removed, only one study remained significant (Logue *et al.*, 2019). An additional study evaluated genetic contributors to the Diagnostic and Statistical Manual IV (DSM-IV) diagnosis of Cognitive Impairment, No Dementia (CIND), which is similar to MCI. They found no significant difference in the frequency of risk alleles between cases and controls ( $p = 0.710$ ) (Dubé *et al.*, 2013).

#### **2.4.6 Cognitive Measures**

Cognition and PRS were examined in 21 studies (Rodríguez-Rodríguez *et al.*, 2013; Verhaaren *et al.*, 2013; Marden *et al.*, 2014, 2016; Harris *et al.*, 2014; Wollam *et al.*, 2015; Carrasquillo *et al.*, 2015; Hayden *et al.*, 2015; Mormino *et al.*, 2016; Foley *et al.*, 2016; Hagenaars, Harris, Davies, Hill, *et al.*, 2016; Andrews, Das, *et al.*, 2017; Hayes *et al.*, 2017; Marioni *et al.*, 2017; Papenberg *et al.*, 2017; Bressler *et al.*, 2017; Axelrud *et al.*, 2018; Li *et al.*, 2018; Sapkota and Dixon, 2018; Del-Aguila *et al.*, 2018; Felsky *et al.*, 2018). Whilst a variety of cognitive measures were used, all but four studies reported some significant associations with PRS. Most studies were in healthy older adults, although two studies included participants with established AD/MCI (Rodríguez-Rodríguez *et al.*, 2013; Del-Aguila *et al.*, 2018), two studies had young

adult participants (Foley *et al.*, 2016; Li *et al.*, 2018), one study had adolescent participants (Axelrud *et al.*, 2018) and one included longitudinal data from children aged 11 (Harris *et al.*, 2014). There were some cross-sectional studies that only reported associations with AD polygenic risk and cognition at one timepoint (Verhaaren *et al.*, 2013; Wollam *et al.*, 2015; Foley *et al.*, 2016; Hagenaars, Harris, Davies, Hill, *et al.*, 2016; Hagenaars, Harris, Davies, Marioni, *et al.*, 2016; Papenberg *et al.*, 2017; Axelrud *et al.*, 2018; Li *et al.*, 2018), whereas longitudinal studies were able to report the correlations with change in cognition over time (Rodríguez-Rodríguez *et al.*, 2013; Marden *et al.*, 2014, 2016; Carrasquillo *et al.*, 2015; Hayden *et al.*, 2015; Mormino *et al.*, 2016; Andrews, Das, *et al.*, 2017; Hayes *et al.*, 2017; Marioni *et al.*, 2017; Sapkota and Dixon, 2018; Del-Aguila *et al.*, 2018; Felsky *et al.*, 2018). As expected, most studies reported that the effects attenuated or were no longer significant when *APOE* was excluded from the PRS. Please see Appendix A Tables 3 and 4 for full details of cohorts and measures used.

#### **2.4.7 MRI phenotypes**

12 studies explored correlations between AD PRS and MRI phenotypes. Most studies looked at subcortical volumes (Foley *et al.*, 2016; Lupton *et al.*, 2016; Mormino *et al.*, 2016; Su *et al.*, 2017; Axelrud *et al.*, 2018). Some also explored cortical thickness (Sabuncu *et al.*, 2012; Hayes *et al.*, 2017; Corlier *et al.*, 2018), white matter metrics (Foley *et al.*, 2016), and functional MRI (Su *et al.*, 2017). One study used a high dimensional pattern classification algorithm trained to assess the spatial atrophy patterns in normal aging and in AD (Habes *et al.*, 2016). Most studies sampled healthy older adults, although some included younger adults (Foley *et al.*, 2016; Li *et al.*, 2018), adolescents (Axelrud *et al.*, 2018), or a range of age groups (Lupton *et al.*, 2016). Some studies included some participants with MCI or AD (Lupton *et al.*, 2016; Mormino *et al.*, 2016; Su *et al.*, 2017) and one study sampled military veterans with head injuries (Hayes *et al.*, 2017).

Of the six studies that explored subcortical volumes, all reported significant negative correlations between PRS and hippocampal volume (Hohman, Koran and Thornton-Wells, 2014; Foley *et al.*, 2016; Harrison and Bookheimer, 2016; Lupton *et al.*, 2016;

Mormino *et al.*, 2016; Axelrud *et al.*, 2018). One study only found a significant association in participants who were negative for amyloid on PET (Hohman *et al.*, 2017). One study reported a significant negative association with amygdala volume (Lupton *et al.*, 2016) but only in participants with diagnoses of MCI or AD. A separate study used an algorithm to detect the spatial patterns of healthy brain aging and atrophy in AD. They found a significant association between AD PRS and the spatial pattern for AD but not for normal aging (Habes *et al.*, 2016).

Of those studies looking at cortical thickness (Sabuncu *et al.*, 2012; Harrison and Bookheimer, 2016; Hayes *et al.*, 2017; Corlier *et al.*, 2018; Li *et al.*, 2018), all but one (Harrison and Bookheimer, 2016) reported significant associations between increased PRS and cortical thinning. Studies either reported associations with cortical thinning across multiple regions that are susceptible to AD pathology (Sabuncu *et al.*, 2012; Hayes *et al.*, 2017; Corlier *et al.*, 2018), or with cortical thinning in specific regions such as the precuneus (Li *et al.*, 2018).

One study assessed white matter, and identified reduced fractional anisotropy in the right cingulum with increasing PRS (Foley *et al.*, 2016). Another study explored changes in the Default Mode Network and reported changes in functional connectivity in the left medial temporal gyrus and the right hippocampal/parahippocampal gyrus in those with MCI. However, there were no significant associations in healthy controls (Su *et al.*, 2017).

#### **2.4.8 Amyloid and Tau Biomarkers**

Nine studies explored associations between PRS and amyloid and tau biomarkers (Martiskainen *et al.*, 2015; Laiterä *et al.*, 2016; Louwersheimer *et al.*, 2016; Mormino *et al.*, 2016; Schultz *et al.*, 2017; Voyle *et al.*, 2017; Cruchaga *et al.*, 2018; Felsky *et al.*, 2018; Tan *et al.*, 2018). They were all case/control studies. One study sampled those with autosomal dominant and sporadic AD (Cruchaga *et al.*, 2018). Another included participants with normal pressure hydrocephalus (Laiterä *et al.*, 2016). The phenotypes included: CSF amyloid and tau measures (Martiskainen *et al.*, 2015; Mormino *et al.*, 2016; Schultz *et al.*, 2017; Voyle *et al.*, 2017; Cruchaga *et al.*, 2018;

Tan *et al.*, 2018); post-mortem biomarkers or histology (Martiskainen *et al.*, 2015; Laiterä *et al.*, 2016; Tan *et al.*, 2018); amyloid PET (Mormino *et al.*, 2016; Tan *et al.*, 2018). A variety of analysis approaches were taken. Some studies assessed each tau and amyloid biomarker independently (Martiskainen *et al.*, 2015; Louwersheimer *et al.*, 2016), whereas others created composite variables using CSF, PET or histology biomarkers (Schultz *et al.*, 2017; Voyle *et al.*, 2017; Cruchaga *et al.*, 2018; Tan *et al.*, 2018).

There were significant associations reported between AD PRS and the following: increased CSF tau and phosphorylated tau (Louwersheimer *et al.*, 2016); CSF A $\beta$  (Martiskainen *et al.*, 2015); lower A $\beta$ 42/A $\beta$ 40 (Schultz *et al.*, 2017); higher t-tau/A $\beta$ 42 and higher p-tau/A $\beta$ 42 ratio (Schultz *et al.*, 2017; Cruchaga *et al.*, 2018); positive A $\beta$  PET (Mormino *et al.*, 2016); total PET/CSF amyloid load and tau load (Tan *et al.*, 2018); post-mortem soluble A $\beta$ 42 and  $\beta$ -secretase activity (Martiskainen *et al.*, 2015); post-mortem amyloid plaques and neurofibrillary tangles (Felsky *et al.*, 2018). Some studies did not report significant associations between AD PRS and CSF tau (Martiskainen *et al.*, 2015; Mormino *et al.*, 2016) or CSF A $\beta$  (Louwersheimer *et al.*, 2016; Mormino *et al.*, 2016). There was also no association with microglial density on post-mortem histology (Felsky *et al.*, 2018) or amyloid deposition in brain biopsies of Normal Pressure Hydrocephalus patients (Laiterä *et al.*, 2016). One study combined CSF biomarkers with PRS to predict AD, but the PRS did not improve prediction over and above the CSF amyloid and tau (Voyle *et al.*, 2017).

#### **2.4.9 Other diseases and syndromes**

Other studies have explored associations between AD PRS and other disorders or syndromes. Pilling and colleagues reported significant negative correlations with longevity (Pilling *et al.*, 2016), and red cell volume, a measure of anaemia (Pilling *et al.*, 2017). However there were no significant associations reported with depression (Gibson *et al.*, 2017) or post-concussive syndrome (Polimanti *et al.*, 2017).

#### 2.4.10 Disease pathways

Four studies explored patterns associations between AD pathway PRS and disease-related phenotypes. Each study used sets of SNPs based on previous pathway analyses in AD (Jones *et al.*, 2010; Holmans and Jones, 2012). Some used only Bonferroni-significant loci (Darst *et al.*, 2017; Ahmad *et al.*, 2018; Corlier *et al.*, 2018), whereas others used a threshold-based PRS (Morgan *et al.*, 2017). Various phenotypes were assessed including: MCI risk (Ahmad *et al.*, 2018), MRI phenotypes (Ahmad *et al.*, 2018; Corlier *et al.*, 2018), cognition (Darst *et al.*, 2017), CSF A $\beta$  and tau (Darst *et al.*, 2017), A $\beta$  PET (Darst *et al.*, 2017) and complement markers (Morgan *et al.*, 2017).

Using PRS for the immune response, endocytosis, cholesterol transport, hematopoietic cell lineage, protein ubiquitination, haemostasis, clathrin/AP2 adaptor complex, and protein folding pathway, Ahmad et al reported the immune response and clathrin/AP2 adaptor complex pathways showed nominal associations with white matter lesions, but this did not withstand correction for multiple testing. The endocytosis risk score was significantly associated with risk of MCI (Ahmad *et al.*, 2018). Darst et al used PRS for amyloid  $\beta$  clearance, cholesterol metabolism, and the immune response. They found no association between cognition and any PRS, even when *APOE* was included (Darst *et al.*, 2017). A higher A $\beta$  clearance PRS and cholesterol PRS was associated with lower CSF A $\beta_{42}$ , a narrower A $\beta_{42}$ /A $\beta_{40}$  ratio, and greater A $\beta$  PET deposition. With *APOE* excluded, the only significant associations were between the cholesterol PRS and CSF A $\beta_{42}$ /A $\beta_{40}$  and the immune response PRS and CSF tau, though not when corrected for multiple comparisons (Darst *et al.*, 2017).

Two studies focused on the immune response PRS. Corlier et al found that the immune response PRS was significantly associated with an overall measure of cortical thinning (Corlier *et al.*, 2018). Morgan et al reported that clusterin, C1 inhibitor, and C-Reactive Protein all showed nominal association with the inflammation-specific PRS. Plasma clusterin levels were associated with the overall AD PRS (Morgan *et al.*, 2017).

### 2.4.11 Study quality

Overall, the articles had clear research questions and used adequate methodology. Some studies used small sample sizes (Wollam *et al.*, 2015; Harrison *et al.*, 2016; Morgan *et al.*, 2017; Schultz *et al.*, 2017) and many studies failed to describe sample ascertainment clearly. They used standard outcome measures. Of those looking at AD prediction, all but two (Xiao *et al.*, 2015; Yokoyama, Lee, *et al.*, 2015) used NINDS-ADRDA diagnostic criteria for AD. Most studies weighted PRS by effect size or odds ratio, although in some studies this was not clearly described (Xiao *et al.*, 2015; Yokoyama, Lee, *et al.*, 2015). Some studies had some overlap between training and validation datasets which may have inflated their results. Most studies attempted to assess the contribution of *APOE* by either excluding it from the PRS or including it as a co-variate. Some studies included cohorts of non-European ancestry (Marden *et al.*, 2014, 2016; Xiao *et al.*, 2015; Bressler *et al.*, 2017; Tosto *et al.*, 2017). These studies acknowledged that: i) they may have had insufficient power in their non-European samples or ii) PRS based on GWAS conducted in European populations may not capture AD genetic risk among those of non-European descent.

## 2.5 Discussion

This Chapter systematically reviews how AD PRS are associated with a range of phenotypes and outcomes. Previous papers have covered PRS methodology (Wray *et al.*, 2014) and some have reviewed the use of PRS in AD prediction alone (Stocker *et al.*, 2018).

Since the advent of large-scale genetics consortia such as the International Genomics of Alzheimer's Project (IGAP), our understanding of the genetic underpinnings of AD has rapidly expanded. GWAS have resulted in the identification of over 20 novel genetic risk loci in addition to *APOE*  $\epsilon$ 4 (Lambert *et al.*, 2013; Kunkle *et al.*, 2019). Most of these SNPs only increase AD risk incrementally. Therefore, combining SNPs into PRS has proved an important strategy for studying their effects. Some of the studies included in this review used only the most significant loci in their PRS. However, more recent studies used liberal threshold-based PRS computed from thousands of AD risk loci.

### 2.5.1 PRS in disease prediction

AD PRS have demonstrated strong predictive ability. Conservative PRS, including only genome-wide significant SNPs, have achieved reasonable prediction accuracy (AUC range: 57–72%) (Escott-Price, Sims, Bannister, *et al.*, 2015; Sleegers *et al.*, 2015; Yokoyama, Bonham, *et al.*, 2015; Tosto *et al.*, 2017; Cruchaga *et al.*, 2018). Threshold-based PRS, including many more SNPs, have proved superior to both conservative PRS and to *APOE* alone (AUC 75%)(Escott-Price, Sims, Bannister, *et al.*, 2015). Prediction accuracy is even greater using a threshold-based PRS in histologically confirmed cases and controls (AUC 84%) (Escott-Price *et al.*, 2017). The findings for MCI conversion prediction are more mixed. Of the three studies reporting negative results, two had relatively low power (Rodríguez-Rodríguez *et al.*, 2013; Lacour *et al.*, 2017). Almost all the studies exploring PRS prediction accuracy report that there is some overlap between cases and controls at high polygenic risk. Moreover, in the absence of therapeutic consequences, the clinical utility of these findings remains limited.

### 2.5.2 Associations between AD PRS, phenotypes and biomarkers

Overall, the evidence from cross-sectional, case-control and longitudinal cohort studies pointed towards an association between PRS and a range of AD-related phenotypes. Of these, cognition has been the most widely investigated. Whilst the methodology and samples were diverse, the vast majority of studies reported significant associations (Rodríguez-Rodríguez *et al.*, 2013; Verhaaren *et al.*, 2013; Marden *et al.*, 2014, 2016; Wollam *et al.*, 2015; Yokoyama, Bonham, *et al.*, 2015; Carrasquillo *et al.*, 2015; Mormino *et al.*, 2016; Hagenaars, Harris, Davies, Hill, *et al.*, 2016; Andrews, Das, *et al.*, 2017; Papenberg *et al.*, 2017; Hayes *et al.*, 2017; Marioni *et al.*, 2017; Axelrud *et al.*, 2018; Sapkota and Dixon, 2018; Del-Aguila *et al.*, 2018; Felsky *et al.*, 2018). Of the negative studies, one used a threshold-based PRS (Harris *et al.*, 2014) and another used a PRS including 15 Bonferroni-significant risk SNPs (Bressler *et al.*, 2017) but both excluded *APOE* entirely. The other two negative studies both used samples of young adults (Foley *et al.*, 2016; Li *et al.*, 2018), suggesting that cognitive changes related to AD genetic risk may not manifest until later in life.

There was consistent evidence to support an association between AD PRS and changes in brain structure, particularly in decreased hippocampal volume (Hohman, Koran and Thornton-Wells, 2014; Foley *et al.*, 2016; Harrison and Bookheimer, 2016; Lupton *et al.*, 2016; Mormino *et al.*, 2016; Axelrud *et al.*, 2018) and reduced cortical thickness (Sabuncu *et al.*, 2012; Harrison and Bookheimer, 2016; Hayes *et al.*, 2017; Corlier *et al.*, 2018; Li *et al.*, 2018). This was reported even in samples of young adults,(Foley *et al.*, 2016; Axelrud *et al.*, 2018) suggesting that AD risk may manifest in brain structure decades before the onset of disease. These studies also found that the threshold based PRS yielded better results. For example, Mormino *et al.* found an association between a threshold PRS and hippocampal volume that was not present when only genome-wide significant SNPs were used (Mormino *et al.*, 2016).

There were mixed findings for amyloid and tau biomarkers. Of those studies exploring CSF, PET or histology biomarkers, all but one reported statistically significant associations. However, findings were not consistent across biomarkers. For example, one study reported an association between CSF tau and phosphorylated tau but not A $\beta$  (Louwersheimer *et al.*, 2016), whereas a different study found the reverse (Martiskainen *et al.*, 2015). Another study reported a significant association with A $\beta$  PET but not with CSF A $\beta$  or tau (Mormino *et al.*, 2016). However, studies with post-mortem samples did find evidence of association between AD PRS and soluble A $\beta$ 42 levels,  $\beta$ -secretase activity (Martiskainen *et al.*, 2015), neuritic amyloid plaques and neurofibrillary tangles (Felsky *et al.*, 2018). PRS for other neuropsychiatric disorders were not associated (Felsky *et al.*, 2018). Moreover, AD PRS was not associated with amyloid accumulation in Normal Pressure Hydrocephalus (Laiterä *et al.*, 2016). This suggests that the genetic foundations of amyloid deposition in other conditions may be distinct from those in AD. In addition, there was no evidence for pleiotropy between AD and depression (Gibson *et al.*, 2017).

### **2.5.3 PRS in disease pathways**

GWAS have resulted in the identification of novel genetic risk loci in addition to *APOE4* (Lambert *et al.*, 2013; Kunkle *et al.*, 2019) which have been associated with a range of biological pathways including lipid metabolism, immune response, and synaptic

processes (Jones *et al.*, 2010; Holmans and Jones, 2012). AD is heterogeneous and multifactorial. Polygenic profiling can allow individual molecular sub-classification, by identifying the pathways enriched for risk alleles for an individual. Four of the most recent studies included in this review took this approach, suggesting that the field is moving in this direction. They found some evidence for association between pathway-specific polygenic scores and MCI risk (Ahmad *et al.*, 2018), cognition (Darst *et al.*, 2017), brain structure (Ahmad *et al.*, 2018; Corlier *et al.*, 2018), CSF biomarkers (Darst *et al.*, 2017), A $\beta$  PET (Darst *et al.*, 2017) and serum complement markers (Morgan *et al.*, 2017). The variance that each of these pathways explains is small (Darst *et al.*, 2017). This will probably increase as discovery sample sizes increase (Dudbridge, 2013), but will be restricted as PRS do not capture the contributions of copy number variant or rare SNPs.

Pathway-specific polygenic profiling could enable personalised treatment of each individual with AD. This could allow entrants to clinical trials and biomarker studies to be stratified based on evidence of involvement of specific disease pathways. Moreover, if polygenic risk profiles can give prognostic information, they may aid decision making for individuals and clinicians. For example, a high PRS has been associated with a more accelerated progression from MCI to AD (Rodríguez-Rodríguez *et al.*, 2013).

#### **2.5.4 Strengths and limitations**

We used a systematic and comprehensive search strategy to avoid missing eligible studies. Articles were not limited to a particular sampling framework or research design (e.g. longitudinal studies or clinical samples), or to European ancestry samples. We also included studies investigating broad ranges of outcomes which enhanced our ability to assess how AD polygenic risk is manifest. However, results were not reported consistently across studies, meaning only a narrative review was feasible, and we were not able to assess for publication bias. In addition, we were not able to include studies that were not in English-language journals.

We identified a number of limitations in the studies included in this review. In order to conduct a polygenic score analysis, two completely independent datasets are required. Any overlap in the datasets will inflate the associations found. Some studies appeared to use sub-samples of the discovery sample as target samples and not all attempted to account for this. Some studies also appeared to be underpowered. Authors often did not provide a clear description of sample ascertainment, making it harder to put their findings into the context of the wider literature. Standardized effect estimates or confidence intervals were also often omitted, which are required to compare effect sizes across studies. We have previously proposed a reporting framework for studies which might assist future researchers who synthesize data across such studies (Mistry *et al.*, 2017).

A number of studies explored similar phenotypes in comparable samples but reported different results. Heterogeneity may stem from the PRS or the study design. Regarding the PRS, the exact list of SNPs is likely to differ between studies. Some researchers selected SNPs that reached genome-wide significance, and others used a p-value threshold approach, a key distinction. With threshold based PRS, experimenters exclude SNPs with low imputation quality scores. These vary depending on the array, imputation platform and pre- and post- imputation quality control steps. In addition, even small differences in population genetics may lead to distinctive linkage disequilibrium (LD) structure and allele frequencies (Moskvina *et al.*, 2010). Pruning, an essential part of PRS calculation, relies on LD structure to retain SNPs that are most associated with a trait whilst removing others that are closely linked. Where LD structure diverges, alternative SNPs will be selected. Furthermore, in disease pathway PRS, the gene sets are determined by the databases used to define the pathways. Regarding study design, there are other potential causes of heterogeneity. There may be discrepancies in how phenotypes are defined or measured, and different approaches to data analysis. Finally, there are possible sources of bias. For example, disease prediction studies using PRS can be affected by selection bias. If the target dataset is enriched for AD or MCI cases, this will affect the prediction accuracy.

### **2.5.5 Conclusion**

The PRS approach is an important method for capturing the contribution of genome wide common variation of complex diseases. This is the first review attempting to collate information on how the use of the PRS approach has informed our understanding of a variety of phenotypes associated with AD genetic risk. PRS can predict AD and are associated with cognitive impairment. There is also evidence of association between AD PRS and other phenotypes relevant to neurodegeneration. The associations between pathway specific PRS and phenotypic changes may allow us to define the pathophysiology of the disease in individuals, heralding precision medicine in AD. However, longitudinal cohort studies are required to test the ability of PRS to delineate pathway-specific disease activity. In the absence of therapeutic consequences, the clinical utility of PRS is limited.

### **Appendix A: Supplementary Material**

Table 1.1. Search strategy terms used for searching Embase, Medline via Ovid and PsychINFO.

Table 1.2. List of data extracted from all studies

Table 1.3. Studies examining associations with threshold-based PRS, principle results

Table 1.4. Studies examining associations with Bonferroni-significant SNP PRS, principal results

## **CHAPTER 3: IMAGING ALZHEIMER'S GENETIC RISK USING DIFFUSION MRI: A SYSTEMATIC REVIEW**

*The chapter includes some material that was previously published in Harrison, J. R. et al. 2020. Imaging Alzheimer's genetic risk using Diffusion MRI: a systematic review. NeuroImage: Clinical 27, article number: 102359. (10.1016/j.nicl.2020.102359). Dr Zhao Xuan Tan, Ms Sanchita Bhatia, Ms Anastasia Mirza-Davies and Ms Hannah Benkert assisted with the assessment of selected studies.*

*Some information from Chapters 1 and 2 is repeated here for convenience.*

### **3.1 Summary**

Diffusion magnetic resonance imaging (dMRI) is an imaging technique which probes the random motion of water molecules in tissues and has been widely applied to investigate changes in white matter microstructure in AD. This chapter aims to systematically review studies that examined the effect of Alzheimer's risk genes on white matter microstructure. The findings from 37 studies were assimilated and their diffusion pre-processing and analysis methods were reviewed. Most studies estimate the diffusion tensor and compare derived quantitative measures such as fractional anisotropy and mean diffusivity between groups. Those with increased AD genetic risk are associated with reduced anisotropy and increased diffusivity across the brain, most notably the temporal and frontal lobes, cingulum and corpus callosum. Structural abnormalities are most evident amongst those with established AD. Recent studies employ signal representations and analysis frameworks beyond diffusion tensor MRI but show that dMRI overall lacks specificity to disease pathology. However, as the field advances, these techniques may prove useful in pre-symptomatic diagnosis or staging of Alzheimer's disease.

## 3.2 Introduction

AD is characterised by amyloid plaques, hyperphosphorylated tau and atrophy (Braak and Braak, 1995), and histopathological studies have also identified AD pathology in white matter (Englund, Brun and Alling, 1988). In recent years, diffusion Magnetic Resonance Imaging (dMRI) has been used to examine white matter microstructure in AD and to study the effect of AD genetic risk on white matter microstructure.

### 3.2.1 Alzheimer's Disease genetic risk

As discussed in previous chapters, GWAS of clinically confirmed AD has identified over 25 loci that are associated with increased risk for sporadic AD (Kunkle *et al.*, 2019), with the largest in single nucleotide polymorphisms (SNPs) in the Apolipoprotein E (*APOE*) region (Corder *et al.*, 1993). As described in Chapter 2, loci of smaller effect can be combined using polygenic risk scores. These are calculated from the weighted sum of weighted allelic dosages across the genome, and have proven particularly effective in predicting AD (Escott-Price, Sims, Bannister, *et al.*, 2015). Whole exome sequencing techniques have also identified additional rare mutations with moderate-to-strong effects such as *TREM2*, a variant that encodes the trigger receptor expressed on myeloid cells 2 (Guerreiro, Wojtas, Bras, Carrasquillo, Rogaeva, Majounie, Cruchaga, Sassi, John S K Kauwe, *et al.*, 2013). In contrast to sporadic AD, autosomal dominant AD is caused by rare mutations either in the amyloid precursor protein (*APP*) gene, or in presenilin 1 and 2 (*PS1* and *PS2*) that are involved in cleaving amyloid  $\beta$  and *APP*. The disease onset is often predictable, depending on the specific mutation (Tanzi, 2012).

### 3.2.2 Diffusion MRI

dMRI is a non-invasive imaging method that probes the movement of water molecules to assess the microstructural configuration of tissue, including white matter tracts (Jones, 2011; Winston, 2012). dMRI measures indicate how readily water molecules can diffuse in and around structures such as white matter fibres or cell bodies (Stejskal and Tanner, 1965; Bihan, 1995; Strijkers, Drost and Nicolay, 2011; Johansen-Berg

and Behrens, 2013). In white matter, the rate of diffusion is modulated by multiple microstructural features including axon diameter, axon density and myelination (Jones, 2011). In highly ordered white matter, the rate of diffusion is anisotropic, i.e., it is strongly dependent on the direction in which it is measured. As mentioned in Chapter 1, the most commonly used index of anisotropy is the fractional anisotropy (FA) introduced by Basser and Pierpaoli (Basser and Pierpaoli, 1996). An FA of 0 indicates that the rate of diffusion is the same in all directions (isotropic diffusion), and 1 represents the extreme case where diffusion can only occur along one axis (anisotropic diffusion) (Beaulieu and Allen, 1994; Pierpaoli and Basser, 1996; Beaulieu, 2009; Winston, 2012). Clinical studies often employ this as a measure of tissue integrity (Thomason and Thompson, 2011), although at best this interpretation is an oversimplification (Jones, Knösche and Turner, 2013). Another widely used metric is mean diffusivity (MD), which represents the orientationally-averaged rate of diffusion. Additional commonly used metrics from diffusion tensor imaging are the 'longitudinal diffusivity' (LD) and 'radial diffusivity' (RD), which in turn represent the highest and lowest rates of diffusion. In the case of perfectly aligned axonal bundles, these would represent diffusivity parallel and perpendicular to the main axis of the bundle, respectively. However, given the ubiquity of multiple fibre populations within an image voxel, this interpretation carries some risk (see: (Wheeler-Kingshott and Cercignani, 2009) but also see (Wheeler-Kingshott *et al.*, 2012)). Collectively, FA, MD, LD and RD can help to characterise changes in diffusion resulting from differences in white matter microstructure.

### **3.2.3 Structural changes observed in Alzheimer's Disease**

MRI measures of atrophy, such as Voxel-Based Morphometry (VBM), are routinely used for AD diagnosis and measurement of disease progression (Frisoni *et al.*, 2010). dMRI have reported widespread changes in white matter microstructure in AD. A meta-analysis of 41 studies found reduced FA and increased MD in AD brains compared to controls. Differences were marked in frontal and temporal lobes, and the posterior cingulum, corpus callosum, superior longitudinal fasciculi and uncinate fasciculi (Sexton *et al.*, 2011). Late-myelinating tracts may be affected primarily by AD neurodegeneration (Benitez *et al.*, 2014). Longitudinal studies suggest that the pattern

of decreased FA and increased MD becomes more distinct as the disease progresses (Mayo *et al.*, 2017). Changes in the parahippocampal cingulum have been shown to discriminate between AD and healthy controls (Mayo *et al.*, 2017). Diffusion measurements in the fornix are another possible biomarker (Ringman *et al.*, 2007). Perea and colleagues found that AD preferentially degraded the crus and body of the fornix. The diffusion differences remained after controlling for fornix volume (Perea *et al.*, 2018).

Mild Cognitive Impairment (MCI) describes a degree of cognitive problems that do not affect day-to-day living, and are considered to be an AD prodrome (Petersen and Morris, 2005). A meta-analysis of 41 studies found that compared to healthy controls, patients with MCI had lower FA in all white matter areas except parietal and occipital regions, and higher MD except in occipital and frontal regions (Sexton *et al.*, 2011). More recently, whole brain white matter histogram analysis found that RD, LD and MD were able to discriminate between AD and controls and between MCI and controls in the Alzheimer's Disease Neuroimaging Initiative (ADNI) cohort. LD appeared to be the most sensitive marker (Giulietti *et al.*, 2018).

dMRI metrics in the fornix are markers of cognitive problems, and can distinguish MCI from AD (Egli *et al.*, 2015; Tang *et al.*, 2017). The volume of the body of the fornix and LD in the fornix are correlated with decline from normal cognition (Fletcher *et al.*, 2013). Reduced FA in the fornix can predict conversion both from healthy cognition to MCI and from MCI to AD with high specificity and >90% accuracy (Mielke *et al.*, 2012; Oishi *et al.*, 2012). Reduced FA and increased MD in the fornix might even precede hippocampal atrophy (Zhuang *et al.*, 2012).

#### **3.2.4 Current review**

This systematic review aimed to collate studies applying dMRI techniques to investigate genetic risk for AD. In the narrative synthesis, the goal of this chapter is to assess the evidence for manifestations of Alzheimer's genetic risk in white matter microstructure. The studies were also reviewed in terms of their study design and diffusion methodology, including pre-processing and analysis.

### **3.3 Methods**

This systematic review was conducted in accordance with PRISMA guidelines (Moher *et al.*, 2009).

#### **3.3.1 Study selection**

Search terms were defined at the outset (listed in Table 1, Appendix B). MEDLINE, PSYCHINFO and EMBASE were searched from January 2000-July 2019, and the reference lists of related articles were hand-searched.

Inclusion criteria:

- Case-control, cross-sectional or longitudinal studies
- Genotyped participants
- Imaged with dMRI sequences
- Associations reported between AD risk genes/SNPs and measures derived from dMRI

Exclusion criteria:

- Publications in non-English language journals
- Conference proceedings
- Studies of non-Alzheimer's dementia or unspecified dementia
- Studies using family history and genotype as a composite variable
- Studies using MRI but not including dMRI
- Studies investigating genes/SNPs that are not associated with AD risk
- Studies that co-vary for AD genes (e.g. *APOE*) but that do not report associations with AD risk genes/SNPs

#### **3.3.2 Article Selection**

The articles included in this review are all English language original research papers. Study designs included case-control, cross-sectional and longitudinal studies. The primary search was conducted by SB. Five reviewers (JH, SB, HB, AMD, ZXT) all

independently selected studies based on the eligibility criteria. Disagreements were resolved by consensus.

### **3.3.3 Data Extraction**

Reviewers (JH, SB, HB, AMD, ZXT) extracted information from papers independently. Data were extracted from each study in duplicate to ensure consistency. Key data included: study design; the number of participants; the AD genetic risk measured; MRI acquisition parameters; dMRI pre-processing; dMRI analysis techniques; reported findings. A complete list of the data extracted can be found in Appendix B Table 2.

### **3.3.4 Quality assessment**

The quality of each included study was assessed independently by two reviewers using the appropriate version of the Newcastle-Ottawa Scale (Stang, 2010) for the study design (case/control, cross-sectional or cohort study). The NOS assesses the quality of non-randomized studies in three main areas: the selection of study groups; the comparability of the groups; and the ascertainment of the exposure or outcome of interest. This tool was chosen because of the type of studies included. A consensus meeting between all reviewers established a manual to ensure this was applied consistently. The assessment tool was adapted to fit the included studies, where the exposure was defined as genetic risk, and important covariates were age, sex and *APOE4* status. A point was awarded in each category.

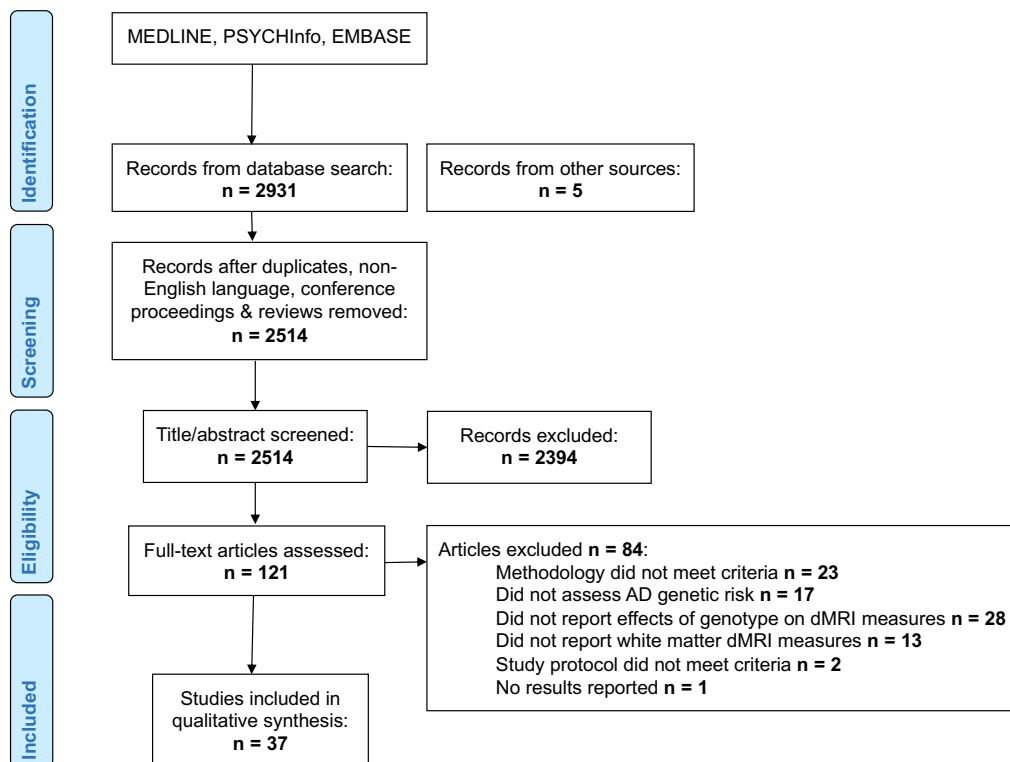
## **3.4 Results**

### **3.4.1 Search results**

2931 articles were identified in the initial search (see PRISMA flow diagram in Figure 1). Duplicates, non-English language studies, non-human studies and conference proceedings were excluded. 2514 articles were screened based on their titles and abstracts and a further 2394 were excluded. The reviewers (JH, SB, HB, AMD, ZXT) reviewed the full text of 120 articles and applied the inclusion criteria. 32 studies met

the criteria for inclusion. A further 4 studies were identified through hand-searches of reference lists.

**Figure 3.1 PRISMA flow chart, dMRI studies**



### 3.4.2 Study characteristics: study design, sample, Alzheimer’s genetic risks

The majority of the studies were case/control design, although some were cross-sectional (Foley *et al.*, 2016) and some longitudinal cohort studies (Lyall *et al.*, 2014). Some studies were conducted using the same cohorts: three used data from the Beijing Aging Brain Rejuvenation Initiative (BABRI); two used the Wisconsin Registry for Alzheimer’s Prevention (WRAP); two used the European Diffusion Tensor Imaging Study on Dementia (EDSA) and the DZNE database, Rostock, Germany. Only one article reported data from the Alzheimer’s Disease Neuroimaging Initiative (ADNI). Most studies included participants who were pre-symptomatic. Only ten included those with established AD or MCI.

### 3.4.3 Genotypes

Two approaches were used to assess genetic risk for AD. Most studies tested participants for specific mutations (APP, PS1/2 mutations or APOE alleles). One study used an array to genotype participants and calculate polygenic risk scores based on sporadic AD GWAS (Foley *et al.*, 2016).

### 3.4.4 dMRI pre-processing and analysis methods

Prior to modelling or statistical analysis, it is essential to pre-process the dMRI data, correcting for artefacts, motion and eddy-current induced distortions (Jones, Knösche and Turner, 2013). Once pre-processed, different approaches can be applied to represent the dMRI signal. Beyond the diffusion tensor framework, two common ways to represent the orientation dependence of the signal in dMRI are the diffusion orientation density function (dODF) (Wedeen *et al.*, 2005) and the fibre orientation density function (fODF) (Dell'Acqua and Tournier, 2019). The dODF is a spherical function which characterises the probability of diffusion along a unit direction. On the other hand, the fODF is a function that characterises the probability of finding a fibre oriented along a particular axis (Jones, Knösche and Turner, 2013).

An additional method, known as neurite orientation dispersion and density imaging (NODDI), aims to provide more specific microstructural information (Zhang *et al.*, 2012). NODDI assumes there are three biophysical compartments in white matter, intra-cellular, extra-cellular and cerebrospinal fluid, in a single voxel. By imposing constraints on some of the parameters that describe these compartments, NODDI aims to estimate proxies of intracellular volume fraction (IVF), neurite density index (NDI), orientational dispersion index (ODI) and increased free isotropic water fraction (FISO) (Zhang *et al.*, 2012).

Quantitative dMRI measures, such as FA, MD, RD and LD (all derived from the diffusion tensor), can be analysed using tractography or whole-brain voxel-wise analysis. Tractography involves reconstructing the trajectory of fibres and connection patterns, using either the principal eigenvector of the diffusion tensor, or peaks in the dODF or fODF, within successive adjacent voxels (Tournier, Mori and Leemans, 2011;

Jones, Knösche and Turner, 2013). These local orientations are used to infer total fibre trajectories (Jeurissen *et al.*, 2019). Commonly used methods include deterministic and probabilistic tractography. In deterministic tracking, a path is propagated along local maxima of the ODF (or, in the case of diffusion tensor imaging, along the principal eigenvector). However, imaging noise and artifacts can make estimates of local maxima imprecise and adds some local orientational uncertainty. Probabilistic tractography techniques illustrate these uncertainties by assigning an uncertainty, or conversely, a probability to the orientational estimates. As such, each local maximum in an ODF can generate a collection of possible trajectories (Jeurissen *et al.*, 2019).

A tractography-based region-of-interest (ROI) approach allows the researcher to define 'seeds' to begin fibre tracking, or to define 'way-points' that prescribe regions through which a reconstructed tract must pass in order to be retained for analysis (Conturo *et al.*, 1999). These can be drawn manually or automatically. Alternatively, whole-brain tractography places seeds throughout the whole brain (Soares *et al.*, 2013), again using 'way-point' ROIs to filter out target pathways. In tractography, each tract is segmented in the native space of the individual (rather than requiring that the individual's data are co-registered to some standardised template space, providing a representation of tract anatomy for each individual (Bastin *et al.*, 2013)). It is important to recognise that the reconstructed tracts do not represent nerve fibres or fibre bundles directly. Rather, they represent pathways or trajectories through the signal, and we assume that the nerve fibres run approximately in parallel. These pathways can be translated into qualitative information, e.g., on the tract shape, and into quantitative information, as measures averaged along the tract (Jones and Pierpaoli, 2005) or in assessing the extent of connections between brain regions (Kaden, Knösche and Anwender, 2007).

Whole brain voxel-based techniques, such as Tract Based Spatial Statistics (TBSS) (Smith *et al.*, 2006; S. M. Smith *et al.*, 2007) or Voxel-Based Analysis (VBA) (Büchel *et al.*, 2004; Van Hecke *et al.*, 2009), are an alternative approach to tractography. They typically involve the nonlinear registration of quantitative diffusion tensor imaging maps, (e.g. FA), from each individual to a standard template space. The aligned FA images are then averaged, and a skeletonised mean FA structure is created.

Thresholds are applied to suppress areas of low mean FA or high inter-subject variation. Each subject's FA image is then projected onto the skeleton, and voxel-wise statistics can be carried out across subjects. For comprehensive descriptions of these different dMRI methods and possible pitfalls, please see (Smith *et al.*, 2006; Jones, Knösche and Turner, 2013; Soares *et al.*, 2013; Bach *et al.*, 2014)).

Inter-regional connectivity can be assessed by constructing networks of the human brain using diffusion signals and tractography (Yeh *et al.*, 2020). The resultant networks can be characterised using graph theoretical approaches. Graph theory is a mathematical framework for representing complex networks. The brain can be illustrated using nodes, representing regions or voxels, and edges, representing connections between nodes (E. Bullmore and Sporns, 2009). A number of network metrics can be produced such as small-world and network efficiency. Please see (Boccaletti *et al.*, 2006) for a detailed summary of graph theory.

The studies that met the inclusion criteria used a range of dMRI analysis methods. 15 used TBSS, seven used a tractography-based ROI approach, eight used VBA, three combined TBSS and VBA, one combined TBSS and ROI, and three calculated structural connectivity matrices.

### **3.4.5 Studies of white matter structure and *APOE* status**

The majority of the papers which met our inclusion criteria explored the effects of *APOE* (27 articles). Most used a case-control design, although some were longitudinal studies. There was a wide range of sample sizes (N range = 14 - 885). The literature predominantly examined samples of cognitively healthy older adults (age > 60). Five studies included participants with diagnoses of AD or MCI (Bagepally *et al.*, 2012; Kljajevic *et al.*, 2014; Wai *et al.*, 2014; Ma *et al.*, 2017; Slattery *et al.*, 2017). Studies of younger age groups included adolescents (Dell'Acqua *et al.*, 2015), adults in their 20's (Heise *et al.*, 2011; O'Dwyer, Lamberton, Matura, Scheibe, *et al.*, 2012; Dowell *et al.*, 2013), 40's and 50's (Westlye *et al.*, 2012; Operto *et al.*, 2018). Some studies were able to compare groups with different combinations of *APOE* alleles (Lyll *et al.*, 2014), although most simply compared *APOE* E4 carriers (homozygotes and heterozygotes)

to those without an E4 allele. Diffusion methodology included: TBSS (12 studies); tractography-based ROI (6 studies); VBA (4 studies); TBSS and VBA (3 studies); TBSS and ROI (1 study); structural connectivity (3 studies). Table 3.1 provides a summary of studies exploring white matter metrics and *APOE* genotype.

Five studies reported no significant differences in white matter microstructure between carriers and non-carriers (Honea *et al.*, 2009; Bendlin *et al.*, 2012; Nyberg and Salami, 2014; Dell'Acqua *et al.*, 2015; R. Wang *et al.*, 2015). All other studies reported some significant changes in diffusion metrics associated with *APOE4*. The pattern of alteration in affected tracts or regions was similar to studies of autosomal-dominant AD genes: reduced FA was commonly reported, often in tandem with increased MD, RD or LD. Reduced neurite density index (NDI) and increased free isotropic water fraction (FISO) are also reported. The white matter regions found to be associated with *APOE* status (summarised in Table 3.1) included: the genu (Newlander *et al.*, 2014; Zhang *et al.*, 2015; Cai *et al.*, 2017; Cavedo *et al.*, 2017), body (Persson *et al.*, 2006; Zhang *et al.*, 2015) and splenium of the corpus callosum (Ryan *et al.*, 2011; Slattery *et al.*, 2017) and the corpus callosum overall (Heise *et al.*, 2011; Westlye *et al.*, 2012; Cavedo *et al.*, 2017); the parahippocampal cingulum (Nierenberg *et al.*, 2005; Bagepally *et al.*, 2012; Kljajevic *et al.*, 2014; Zhang *et al.*, 2015) and the cingulum overall (Adluru *et al.*, 2014; Lyall *et al.*, 2014; Cavedo *et al.*, 2017); the intracalcarine sulcus (Bagepally *et al.*, 2012; Westlye *et al.*, 2012); the brain stem (Westlye *et al.*, 2012; Newlander *et al.*, 2014); the corona radiata (Heise *et al.*, 2011; Smith *et al.*, 2016; Cai *et al.*, 2017; Cavedo *et al.*, 2017; Slattery *et al.*, 2017; Operto *et al.*, 2018); the external capsule (Heise *et al.*, 2011; Cavedo *et al.*, 2017) and internal capsule (Heise *et al.*, 2011; Westlye *et al.*, 2012; Smith *et al.*, 2016; Cavedo *et al.*, 2017); the superior longitudinal fasciculus (Adluru *et al.*, 2014; Lyall *et al.*, 2014; Cavedo *et al.*, 2017; Operto *et al.*, 2018) and inferior longitudinal fasciculus (Dowell *et al.*, 2013; Cavedo *et al.*, 2017); the fronto-occipital fasciculus (Cavedo *et al.*, 2017; Operto *et al.*, 2018); the fornix (Zhang *et al.*, 2015); the cerebral peduncles (Zhang *et al.*, 2015); the cortico-spinal tract (Laukka *et al.*, 2015); the uncinate fasciculus (Salminen *et al.*, 2013); the forceps major (Laukka *et al.*, 2015) and forceps minor (Operto *et al.*, 2018).

Three papers used measures of structural connectivity based on graph theory. Brown et al found that *APOE4* carriers had age-related loss of mean local interconnectivity and regional local interconnectivity in the precuneus, medial orbitofrontal cortex, and lateral parietal cortex (Brown *et al.*, 2011). Ma et al studied participants with MCI and with normal cognition. They found that healthy *APOE E4* carriers had increased clustering coefficient and local efficiency compared to healthy non-carriers. In those with MCI, carriers showed decreased clustering coefficient and local efficiency relative to MCI non-carriers. When all carriers were compared to all non-carriers, they showed decreased nodal efficiency in the inferior frontal gyrus, the left superior frontal gyrus, and the left middle occipital gyrus. Carriers also showed increased nodal efficiency in the left cuneus, the left inferior parietal, supramarginal and angular gyri (Ma *et al.*, 2017). A further study reported that E4 carriers had lower global efficiency but no significant differences in local efficiency. Decreased nodal efficiency in left anterior cingulate, left paracingulate gyrus, right dorsolateral superior frontal gyrus, and left inferior occipital gyrus was reported in carriers relative to non-carriers. In addition, they used structural connectivity measures to predict AD with Receiver-Operator Curves (ROC). Using global efficiency, they produced an Area Under Curve (AUC) of 0.74. Using mean nodal efficiency of significant decreasing regions, this improved to 0.81 (Chen *et al.*, 2015).

**Table 3.1 Summary of sample characteristics, methodology and main findings for APOE studies**

Study	N (E4 carriers; non-carriers)	Age (SD)	dMRI Method	Field Strength (T)	B value (s/mm <sup>2</sup> )	Acquisition Voxel Size (mm)	N Directions	NEX	Regions of Interest	Results
Adluru et al, 2014	343 (123; 220)	61.03 (6.72)	ROI	3	0, 1300	2.5 x 2.5 x 2.5	40	1	Fomix, splenium & genu of corpus callosum, cingulum, uncinate, superior longitudinal fasciculus.	<ul style="list-style-type: none"> <li>• Older (&gt;65) carriers vs. non-carriers: ↑ MD in SLF &amp; cingulum bundle</li> </ul>
Bagepally et al, 2012	32 (19; 13)	69.3 (5.7)	TBSS	3	0, 1000	Not reported	32	1	Whole brain	<ul style="list-style-type: none"> <li>• AD carriers vs. AD non-carriers: ↓ FA in left medial temporal areas, parahippocampal cingulum, bilateral intracalcarine sulcus, precuneus, lingual area</li> <li>• Healthy carriers vs. healthy non-carriers: ↓ FA bilateral medial temporal areas, scattered regions in frontal &amp; parietal lobes &amp; cerebellum</li> </ul>
Bendlin et al, 2010	136 (56; 80)	69.2 (10.2)	VBA	3	0	2 x 2 x 3	12	1	Whole brain	<ul style="list-style-type: none"> <li>• Carriers vs. non-carriers: no significant differences</li> </ul>
Brown et al, 2011	55 (25; 30)	62.3 (9.0)	Structural connectivity	3	800 or 1000	2.5 x 2.5 x 2.5	30	1	Global & regional connectivity	<ul style="list-style-type: none"> <li>• Carriers vs. non-carriers: age-related loss of mean local interconnectivity, &amp; regional local interconnectivity decreases in the precuneus, medial orbitofrontal cortex, &amp; lateral parietal cortex.</li> </ul>
Cai et al, 2017	309 (116; 193)	73.9 (4.6)	VBA	3	Not reported	1.02 x 1.02 x 1.02	Not reported	1	Superior corona radiata, genu of corpus callosum	<ul style="list-style-type: none"> <li>• Carriers vs. non-carriers: ↑ MD in superior corona radiata, genu of corpus callosum. No significant associations with FA or RD</li> </ul>
Cavedo et al, 2017	74 (31; 43) across 4 centres	68.9 (6.9)	TBSS, VBA	1.5 or 3	0, 1000 or 0, 800	2 x 2 x 2 or 1 x 1 x 2.4	12, 15, 20 or 60	1	Whole brain	<ul style="list-style-type: none"> <li>• Carriers vs. non-carriers: ↓ FA globally, and in genu, body &amp; splenium of corpus callosum, internal capsule, external capsule, inferior fronto-occipital &amp; inferior longitudinal fasciculi, cingulum (left &amp; right), ↑ MD in right hemisphere, in genu of corpus callosum, right internal capsule, right corona radiata, right superior longitudinal fasciculus. ↑ RD globally, &amp; bilaterally in genu &amp; splenium of corpus callosum, internal capsule, inferior fronto-occipital &amp; inferior longitudinal fasciculi, cingulum, external capsule</li> </ul>
Chen et al, 2016	75 (35; 40)	65.8 (7.5)	Structural connectivity	3	0, 1000	Not reported	30	3	Whole brain structural network	<ul style="list-style-type: none"> <li>• Carriers vs. controls: lower global efficiency, no significant differences in local efficiency. Decreased nodal efficiency in left anterior cingulate, left paracingulate gyrus, right dorsolateral superior frontal gyrus, left inferior occipital gyrus</li> <li>• Case/control prediction: ROC AUC for global efficiency 0.74; decreasing region 0.81</li> </ul>
Dell'Acqua et al, 2015	575 (119; 374)	14.4 (0.5)	TBSS	3	0, 1300	2.4 x 2.4 x 2.4	60	1	Whole brain	<ul style="list-style-type: none"> <li>• Carriers vs. non-carriers: no significant differences</li> </ul>
Dowell et al, 2013	41 (20; 21)	20.0 (2.0)	TBSS	1.5	0, 1000	2.5 x 2.5 x 2.5	30	1	Whole brain	<ul style="list-style-type: none"> <li>• Carriers vs. controls: ↑ RD in carriers, particularly in inferior longitudinal fasciculus. No significant differences in FA or MD.</li> </ul>
Heise et al, 2010	71 (33; 38)	Young cohort 28.6 (4.2); Older cohort: 64.9 (7.2)	TBSS		1000	1.1 x 0.9 x 3		1	Whole brain	<ul style="list-style-type: none"> <li>• Young carriers vs. non-carriers: ↓ FA in cingulum, corona radiata, corpus callosum, external capsule, internal capsule, superior longitudinal fasciculus</li> <li>• Older carriers vs. non-carriers: ↑ MD in cingulum, corona radiata, corpus callosum, external capsule, internal capsule, superior longitudinal fasciculus</li> </ul>
Honea et al, 2009	53 (14; 39)	73.4 (6.3)	TBSS	3	0, 1000	1 x 1 x 1	12	1	Whole brain	<ul style="list-style-type: none"> <li>• Carriers vs. non-carriers: no significant differences</li> </ul>
Kljajevic et al, 2014	126 (63; 63) across 5 centres	67.7 (5.9)	VBA	1.5 + 3	0, 800 or 0, 1000	2 x 2 x 2, 2 x 2 x 2.5 or 2 x 2 x 3	6 or 20	1	Whole brain	<ul style="list-style-type: none"> <li>• Healthy carriers vs. healthy non-carriers: ↑ MD in left lentiform nucleus</li> <li>• AD carriers &amp; AD non-carriers: ↓ FA in middle frontal areas, insular white matter, superior temporal areas</li> </ul>
Laukka et al, 2015	89 (23; 66)	81.4 (3.0)	TBSS	1.5	600	1 x 1 x 1	6	1	Cingulate gyrus part of cingulum, parahippocampal cingulum, corticospinal tract, forceps major & minor, inferior fronto-occipital fasciculus, superior longitudinal fasciculus	<ul style="list-style-type: none"> <li>• Carriers vs. non-carriers: ↓ FA in forceps major, ↑ MD in corticospinal tract</li> </ul>
Lyall et al, 2014	645 (187; 423)	72.7 (0.7)	ROI	1.5	0, 1000	1.8 x 1.8 x 1.8	64	1	Genu & splenium of corpus callosum, bilateral anterior thalamic radiations, ventral & rostral cingulum bundles, & arcuate, uncinate, & inferior longitudinal fasciculi.	<ul style="list-style-type: none"> <li>• Carriers vs. non-carriers: ↓ FA in right ventral cingulum &amp; left inferior longitudinal fasciculus</li> </ul>

Author	Year	n	Age (M)	SD (M)	Structural connectivity	3T	1000	Not reported	30	1	Whole brain structural network	Findings
Ma et al.	2017	885	(145; 729)	65.3 (7.4)	Structural connectivity	3T	1000	Not reported	30	1	Whole brain structural network	<ul style="list-style-type: none"> <li>Healthy carriers vs healthy non-carriers: ↑ clustering coefficient &amp; local efficiency</li> <li>MCI carriers vs. non-carriers: ↓ clustering coefficient &amp; local efficiency</li> <li>All carriers vs. non-carriers: ↓ nodal efficiency in: inferior frontal gyrus, orbital part; left superior frontal gyrus, orbital part; left middle occipital gyrus. ↑ nodal efficiency in: left cuneus; left inferior parietal but supramarginal and angular gyri</li> <li>Carriers vs. non-carriers: ↓ FA in genu of corpus callosum &amp; brain stem</li> <li>Carriers vs. non-carriers: ↓ FA &amp; ↑ RD in parahippocampal cingulum</li> <li>Carriers vs. controls: no significant difference for whole brain metrics or specific subregion metrics in TBSS. ↓ FA in five anterior and posterior midline regions on VBA</li> <li>Carrier vs. non-carrier: no significant differences in diffusion indices</li> <li>Carrier/non-carrier prediction accuracy: sensitivity &amp; specificity range 93-100% using a feature selection algorithm, support vector machines &amp; FA data</li> <li>Carriers vs. non-carriers: ↑ MD, RD &amp; LD in corona radiata, superior longitudinal fasciculus, inferior longitudinal fasciculus, inferior fronto-occipital fasciculus, corticospinal tract</li> <li>Carriers vs. non-carriers: ↓ FA in occipito-frontal fasciculus, body of corpus callosum</li> <li>Carriers vs. non-carriers: no significant difference in LD. ↓ FA in frontal white matter &amp; splenium</li> </ul>
Newländer et al.	2014	14	(7; 7)	72.7 (6.1)	VBA	1.5	0, 800	1 x 1 x 1	12	1	Whole brain	
Nierenberg et al.	2005	29	(14; 15)	67.1 (6.5)	ROI	1.5	0, 1000	Not reported	20	1	Parahippocampal cingulum	
Nyberg et al.	2014	273	(69; 204)	67.01 (8.0)	TBSS, VBA	3	1000	0.98 x 0.98 x 2	32	1	Whole brain	
O'Dwyer et al.	2012	44	(22; 22)	26.7 (4.0)	TBSS	3	1000	2 x 2 x 2	60	1	Whole brain	
Operto et al.	2018	532	(275; 257)	58.1 (7.5)	TBSS	3	0, 1000	2 x 2 x 2	64	1	Whole brain	
Persson et al.	2006	60	(30; 30)	66.3 (7.7)	ROI	Not reported	1000	Not reported	6	1	Whole brain analysis; genu, splenium, body of corpus callosum	
Ryan et al.	2011	126	(36; 88)	69.2 (10.2)	ROI	3	0, 1000	2.6 x 2.6 x 2.6	25	2	Frontal white matter, lateral parietal white corpus callosum, splenium of the corpus callosum, temporal stem white matter.	
Salmänen et al.	2013	64	(23; 41)	61.75 (7.6)	ROI	3	0, 996	2 x 2 x 2	31	1	Left uncinata fasciculus, right uncinata fasciculus, temporal lobe	
Slattery et al.	2017	37	(22; 15)	61.7 (5.0)	TBSS, ROI	3	1000	2.5 x 2.5 x 2.5	64	1	Quadrants (anterior, posterior, left & right)	
Smith et al.	2016	88	(34; 53)	74.1 (4.5)	TBSS	3	0, 1000	1 x 1 x 1	25	2	Longitudinal fasciculus, sagittal stratum, uncinata fasciculus, cingulate gyrus, parahippocampal cingulum, genu, body, genuum & splenium of corpus callosum, internal capsule, corona radiata	<ul style="list-style-type: none"> <li>AD carriers vs. AD non-carriers: ↓ FA in splenium of corpus callosum &amp; anterior corona radiata. ↑ RD in white-matter projections from frontal lobes. More widespread ↓ NDI in parieto-occipital white-matter projections. ↑ FISO in corpus callosum</li> <li>Healthy carriers vs. non-carriers: no significant differences</li> <li>Carriers vs. non-carriers: no significant effects on FA, LD or MD. ↓ RD in right anterior internal capsule, bilateral posterior corona radiata, left superior corona radiata.</li> </ul>
Wai et al.	2014	120	(22; 98)	68.9 (7.7)	TBSS	3	1000	2 x 2 x 2	64	1	Whole brain	
Wang et al.	2015	241	(73; 126)	72.0 (9.0)	TBSS	1.5	0, 600	1 x 1 x 1	6	1	Whole brain	
Westlye et al.	2012	203	(60; 143)	47.6 (14.9)	TBSS	1.5	1000	2 x 2 x 2	60	1	Whole brain	<ul style="list-style-type: none"> <li>Amnesic MCI carriers vs. controls: ↓ FA &amp; ↑ MD</li> <li>Carriers vs. non-carriers: no significant differences</li> <li>Carriers vs. non-carriers: increased RD brainstem, basal temporal lobe, internal capsule, anterior parts of the corpus callosum, forceps minor, superior longitudinal fasciculus, occipital &amp; corticospinal pathways.</li> </ul>
Zhang et al.	2015	75	(35; 40)	65.9 (7.5)	TBSS, VBA	3	0, 1000	2 x 2 x 2	30	1	Genu, body, splenium of corpus callosum, anterior & posterior corona radiata, fornix, cerebral peduncles, parahippocampal cingulum	<ul style="list-style-type: none"> <li>Carriers vs. non-carriers: ↓ FA &amp; ↑ MD in genu &amp; body of corpus callosum, anterior &amp; posterior corona radiata bilaterally with TBSS. ↓ FA in genu and body of corpus callosum &amp; right fornix stria terminalis. ↑ MD in genu &amp; splenium of corpus callosum, right cerebral peduncle &amp; right parahippocampal cingulum with VBA</li> </ul>

Please note that we report findings from the most rigorous analyses conducted by studies, including models controlling for multiple comparisons. When not otherwise reported, NEX was assumed to be 1. Acronyms: dMRI = diffusion Magnetic Resonance Imaging, E4 = APOE Epsilon 4; TBSS = Tract-Based Spatial Statistics; VBA = Voxel-Based Analysis; ROI = Region of Interest; FA = Fractional Anisotropy; MD = Mean Diffusivity; RD = Radial Diffusivity; LD = Longitudinal Diffusivity; NDI = Neurite Dispersion Index; FISO = Free Isotropic Water Fraction; ROC = Receiver Operating Characteristic; AUC = Area Under Curve.

### 3.4.6 Studies of white matter and autosomal-dominant AD genes

Six studies explored white matter metrics in participants with autosomal-dominant AD genes: three studied *PS1* carriers, two studied *APP* and *PS1* carriers and one studied *PS1*, *PS2* and *APP* carriers. All used a case/control design. They compared pre-symptomatic and symptomatic gene carriers to non-carriers. Sample sizes reflect the rarity of the genes (N range = 20-109, of which 10-64 were carriers). Three studies used VBA, three used TBSS.

Of the three studies of *PS1* carriers, one study identified reduced MD and LD in the right cingulum among pre-symptomatic carriers (Ryan *et al.*, 2013), and the other two studies reported no significant differences between pre-symptomatic *PS1* and non-carriers (Parra *et al.*, 2015; Sanchez-Valle *et al.*, 2016). In symptomatic *PS1* carriers, changes included: increased MD, RD and LD and reduced FA in all the fornix, cingulum and corpus callosum (Ryan *et al.*, 2013); higher MD in the left inferolateral frontal white matter, right parahippocampal cingulum bundle, splenium left of the mid-line and genu symmetrically around the mid-line of the callosum (Parra *et al.*, 2015); decreased FA in the genu and body of corpus callosum and corona radiata bilaterally and increased MD, LD, and RD in the splenium of corpus callosum relative to age (Sanchez-Valle *et al.*, 2016).

Two studies with mixed cohorts of *PS1* or *APP* carriers reported a number of changes in pre-symptomatic carriers: reduced FA in the fornix and frontal white matter (Ringman *et al.* 2007); increased MD in the left inferior longitudinal fasciculus, left forceps major, left cingulum and bilateral superior longitudinal fasciculus (X Li *et al.*, 2015). In the same *PS1/APP* studies, symptomatic carriers showed: decreased mean FA across the whole brain, especially in the left frontal white matter, and right and left perforant paths (Ringman *et al.* 2007); increased MD in the inferior longitudinal fasciculus, forceps major, cingulum and bilateral superior longitudinal fasciculus (X Li *et al.*, 2015). The effects seen in the symptomatic *APP/PS1* carriers were greater and more widespread than in pre-symptomatic carriers (Ringman *et al.*, 2007; X Li *et al.*, 2015). Caballero *et al.* studied a large mixed cohort of *PS1/2* and *APP* carriers. They found increased MD in the forceps minor, forceps major and long projecting fibres 5-

10 years before the estimated onset of symptoms (Caballero *et al.*, 2018). See Table 3.2 for a summary of these studies.

**Table 3.2 Summary of sample characteristics, methodology and main findings for studies of FAD genes**

Study	Gene	N (FAD carriers; non-carriers)	Mean Age (SD)	dMRI Method	Field Strength (T)	B value (s/mm <sup>2</sup> )	Acquisition Voxel Size (mm)	N	Directions	NEX	Region of Interest	Results
Caballero et al, 2018	PS1, PS2, APP	109 (64; 45)	Symptomatic & pre-symptomatic 38.8 (10.6); Non-carriers 36.0 (11.2)	TBSS	3	0, 1000	0.9 x 0.9 x 5.0	64	1	1	Whole brain	<ul style="list-style-type: none"> <li>Symptomatic &amp; pre-symptomatic carriers: ↑ MD in posterior parietal &amp; medial frontal regions</li> </ul>
Li et al, 2015	APP, PS1	30 (10; 20)	Symptomatic 46.5 (9.3); Pre-symptomatic 42.7 (8.4); Non-carriers 48.4 (15.1)	TBSS	3	0, 1000	1 x 1 x 1	30	1	1	Cingulum, superior longitudinal fasciculus, inferior longitudinal fasciculus	<ul style="list-style-type: none"> <li>Pre-symptomatic carriers vs controls: ↑ MD left inferior longitudinal fasciculus, left forceps major, right &amp; left superior longitudinal fasciculus, left cingulum</li> <li>Symptomatic &amp; pre-symptomatic vs controls: pattern as above, differences ↑</li> </ul>
Parra et al, 2015	PS1	58 (22; 14)	Symptomatic 47.5 (6.4); Pre-symptomatic 35.1 (5.5); Non-carriers 39.3 (8.3)	VBA	1.5	0, 1000	1.72 x 1.72 x 3	12	1	1	Parahippocampal cingulum, genu & splenium of corpus callosum, frontal white matter, parahippocampal cingulum, centrum semiovale	<ul style="list-style-type: none"> <li>Pre-symptomatic carriers vs controls: no significant differences</li> <li>Symptomatic carriers vs controls: ↑ MD in parahippocampal cingulum, left splenium, genu bilaterally, left inferior lateral frontal white matter</li> </ul>
Ringman et al, 2007	APP, PS1	20 (12; 8)	Symptomatic [age not reported]; Pre-symptomatic 32 (6.4); Non-carriers 36 (6.2)	VBA	1.5	0, 1000	3 x 3 x 3	6	1	1	Genu & splenium of corpus callosum, frontal white matter, fornix, cingulum, perforant path, corticospinal tract, whole brain	<ul style="list-style-type: none"> <li>Pre-symptomatic carriers vs controls: ↓ FA fornix &amp; frontal white matter</li> <li>Symptomatic &amp; pre-symptomatic carriers vs controls: ↓ mean FA whole brain, ↓ FA left frontal white matter, right &amp; left perforant path</li> </ul>
Ryan et al, 2013	PS1	40 (20; 20)	Symptomatic 49.0 (9.4); Presymptomatic 37.8 (4.7); Non-carriers 44.3 (12.7)	TBSS	3	1000	1.1 x 1.1 x 1.1	64	1	1	Fornix, cingulum, corpus callosum	<ul style="list-style-type: none"> <li>Pre-symptomatic carriers vs. controls: ↓ MD &amp; RD in right cingulum</li> </ul>
Sanchez-Valle et al, 2016	PS1	36 (22; 14)	Symptomatic 46.63 (9.1); Pre-symptomatic 39.2 (10.4); Non-carriers 39.0 (9.5)	VBA	3	0	2 x 2 x 2	30	1	1	Whole brain	<ul style="list-style-type: none"> <li>Symptomatic carriers vs controls: ↓ FA, ↑ MD &amp; LD in all tracts</li> <li>Pre-symptomatic carriers vs controls: no significant differences</li> <li>Symptomatic carriers vs controls: ↓ FA with ↑ relative age ratio in genu &amp; body of corpus callosum &amp; corona radiate; ↑ MD, LD, RD with ↑ relative age ratio in splenium</li> </ul>

Please note that we report findings from the most rigorous analyses conducted by studies, including models controlling for multiple comparisons. When not otherwise reported, NEX was assumed to be 1. Acronyms: dMRI = diffusion Magnetic Resonance Imaging; PS1 = Presinilin 1; APP = Amyloid Precursor Protein; TBSS = Tract-Based Spatial Statistics; VBA = Voxel-Based Analysis; ROI = Region of Interest; FA = Fractional Anisotropy; MD = Mean Diffusivity; RD = Radial Diffusivity; LD = Longitudinal Diffusivity.

### 3.4.7 Studies of white matter and AD risk loci from GWAS

Three studies correlated white matter metrics with AD risk loci identified through GWAS. One was cross-sectional and two were case/control studies. They all included healthy participants (Mean age range 23.6 - 72.7; N range 197 - 645). Two studies used an ROI approach, one used VBA.

Braskie et al. imaged healthy young adults and found that each C allele copy of the *CLU* allele was associated with lower FA in the splenium of the corpus callosum, the fornix, cingulum, and superior and inferior longitudinal fasciculi bilaterally (Braskie *et al.*, 2011). The Lothian Birth cohort study identified lower FA associated with different length genotypes of the poly-T repeat in *TOMM40*. Shorter genotypes were significantly associated with lower FA in the right rostral cingulum and left ventral cingulum. This effect was independent of *APOE* genotype (Lyll *et al.*, 2014). Foley et al used an Alzheimer's polygenic score, the weighted sum of the risk loci from GWAS, as a continuous variable. They identified an association between increased AD polygenic score and decreased FA in the right cingulum in young adults (Foley *et al.*, 2016).

Elliot et al undertook a GWAS of brain imaging phenotypes in the UK Biobank cohort (Elliott *et al.*, 2018). They used imaging data from around 15,000 participants. All results are available on the Oxford Brain Imaging Genetics (BIG) web browser (<http://big.stats.ox.ac.uk/>). The BIG website can be browsed for associations by phenotype, gene or SNP. The associations between AD risk loci identified in the Kunkle et al GWAS (Kunkle *et al.*, 2019) and FA/MD derived from TBSS in UK Biobank were explored and Appendix B Table 4 summarises these results. Broadly, the results corroborate the findings of other studies included in this review. *APOE* and *CR1* showed particular evidence of association with reduced fractional anisotropy and increased mean diffusivity. However, these results are not corrected for multiple comparisons.

### **3.4.8 Study quality overview**

Most studies scored highly on the Newcastle Ottawa Scale. Generally, the comparability of the groups was clearly explained. As the exposure was gene status, there was little possibility of ascertainment bias. Some studies had one point deducted for failing to describe the selection of study groups, particularly of control subjects. The outcomes of interest (white matter metrics) were defined, although the methodology employed to measure these was variable. It was often difficult to assess the quality of the diffusion methodology, as authors often did not provide sufficient information. Most studies gave some details of their pre-processing, although one acknowledged they had not corrected for Gibbs ringing, a common artefact (Gibbs, 1898). The papers generally did not give details of their model estimation technique (for example nonlinear least squares (NLLS), weighted linear least squares (WLLS) or ordinary least squares (OLS)), which can lead to different outcomes (Koay *et al.*, 2006). The majority of studies, 27 of 37, used TBSS or VBA. Of those papers that used tractography, only some described or referenced the specific methods (such as deterministic or probabilistic).

## **3.5 Discussion**

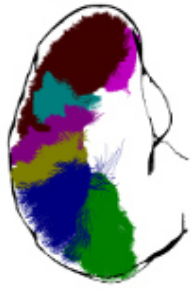
This chapter establishes that the literature reports AD genetic risk is related to altered white matter microstructure, as indexed by increased diffusivity and decreased anisotropy. By synthesising results across studies, this review demonstrates that AD risk genes were associated with widespread white matter changes, rather than discrete microstructural abnormalities in medial temporal structures such as the fornix. This review also found evidence of changes related to AD risk even in studies of young, healthy adults.

### **3.5.1 White matter changes associated with AD risk genes**

AD genetic risk is associated with reduced anisotropy and increased diffusivity across the brain, most notably in temporal and frontal lobes, cingulum and corpus callosum. Table 3.3 contains a summary of the five tracts that were implicated in the most

studies. Although some studies reported no differences between pre-symptomatic gene carriers and non-carriers, many of these studies were limited by small sample sizes. Differences between symptomatic carriers and non-carriers frequently paralleled the differences between pre-symptomatic carriers and non-carriers, but in the pre-symptomatic group often fewer regions reached statistical significance or effect sizes were smaller.

**Table 3.3 Summary of key findings for the most commonly implicated tracts by gene risk (APOE or FAD)**

Tract	Diagram	Summary of APOE Findings	Summary of FAD Findings
<p><b>Corpus Callosum:</b> Connects the left and right cerebral hemispheres</p> 		<p>E4 carriers vs. non-carriers: ↓FA (Persson et al, 2006, Newlander et al, 2014, Heise et al, 2010, Cavedo et al, 2017, Zhang et al, 2015, Ryan et al, 2011, Slattery et al, 2017) ↑MD (Heise et al, 2010, Cavedo et al, 2017, Cai et al, 2017, Zhang et al, 2015) ↑RD (Cavedo et al, 2017, Westlye et al, 2012)</p>	<p>Pre-symptomatic carriers vs. controls: ↓FA (Sanchez-Valle et al, 2016)  Symptomatic carriers vs. controls: ↑MD (Sanchez-Valle et al, 2016, Para et al, 2015) ↑LD (Sanchez-Valle et al, 2016) ↑RD (Sanchez-Valle et al, 2016)</p>
<p><b>Cingulum:</b> Connects the temporal and frontal lobes, cingulate and medial gyri of frontal, occipital, parietal and temporal lobes</p> 		<p>E4 carriers vs. controls: ↓FA (Lyall et al, 2014, Bagepally et al, 2012, Heise et al, 2010, Cavedo et al, 2017, Nierenberg et al, 2005) ↑MD (Li et al, 2012, Zhang et al, 2015, Cavedo et al, 2017, Adluru et al, 2014) ↑RD (Cavedo et al, 2017, Nierenberg et al, 2005)</p>	<p>Pre-symptomatic carriers vs. controls: ↓MD (Ryan et al, 2013) ↑MD (Li et al, 2012) ↓LD (Ryan et al, 2013)  Symptomatic carriers vs. controls: ↓FA (Ryan et al, 2013) ↑MD (Ryan et al, 2013, Para et al, 2015, Li et al, 2012) ↑LD (Ryan et al, 2013)  No significant findings</p>
<p><b>Inferior Occipito-Frontal Fascicle:</b> Connects the medial temporal lobe and the inferior frontal lobe</p> 		<p>E4 carriers vs. non-carriers: ↓FA (Persson et al, 2006, Cavedo et al, 2017) ↑MD (Operto et al, 2018) ↑LD (Operto et al, 2018) ↑RD (Cavedo et al, 2017, Westlye et al, 2012, Operto et al, 2018)</p>	
<p><b>Superior Longitudinal Fascicle:</b> Connects the frontal, parietal, occipital and temporal lobes</p> 		<p>E4 carriers vs non-carriers: ↓FA (Heise et al, 2010) ↑MD (Adluru et al, 2014, Operto et al, 2018, Cavedo et al, 2017, Heise et al, 2010) ↑RD (Operto et al, 2018, Westlye et al, 2012) ↑LD (Operto et al, 2018)</p>	<p>Pre-symptomatic carriers vs non-carriers: ↑MD (Li et al, 2012)  Symptomatic carriers vs non-carriers: ↑MD (Li et al, 2012)</p>
<p><b>Inferior Longitudinal Fascicle:</b> Connects the occipital pole and temporal pole</p> 		<p>E4 carriers vs non-carriers: ↓FA (Lyall et al, 2014, Cavedo et al, 2017) ↑MD (Operto et al, 2018) ↑RD (Operto et al, 2018, Dowell et al, 2013, Cavedo et al, 2017) ↑LD (Operto et al, 2018)</p>	<p>Pre-symptomatic carriers vs non-carriers: ↑MD (Para et al, 2015, Li et al, 2012)  Symptomatic carriers vs non-carriers: ↑MD (Li et al, 2012)</p>

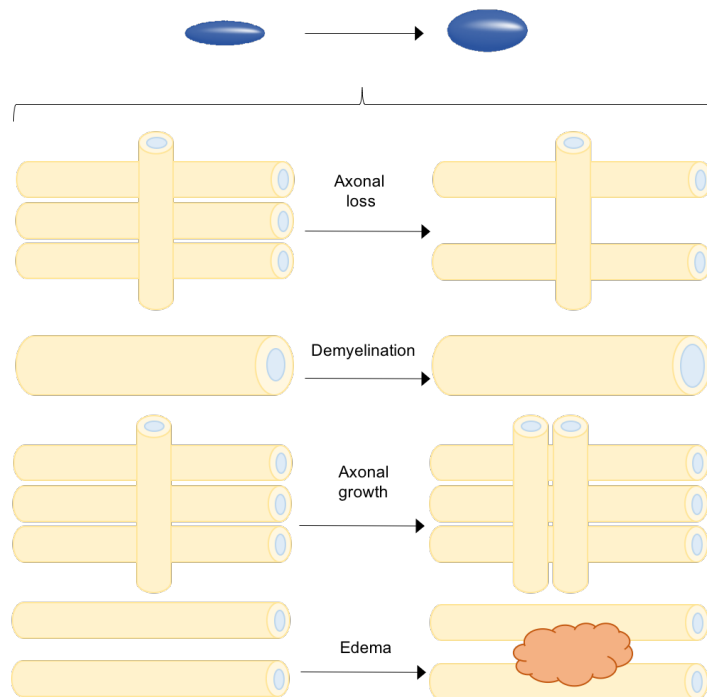
Acronyms: E4 = APOE Epsilon 4; FAD = Familial Alzheimer's Disease; FA = Fractional Anisotropy; MD = Mean Diffusivity; RD = Radial Diffusivity; LD = Longitudinal Diffusivity. Tract images were generated using FiberNavigator (Chamberland et al., 2014) and TractSeg (Wasserthal et al., 2018).

The literature included in this review reported widespread increasing diffusivity and decreased anisotropy and changes in global structural connectivity. These reflect the changes across regions and hemispheres that underpin emergent AD. There was significant overlap between the regions implicated by studies of *APOE*, autosomal-dominant AD genes and GWAS loci. This suggests that although these genes are involved in different biological processes, these pathways may converge on a common final pathway resulting in a corresponding pattern of neurodegeneration. This is in keeping with the literature on AD pathology (Naj and Schellenberg, 2017). However, there was no evidence that microstructural changes were related to any individual microstructure component, as abnormalities were evident across white matter metrics.

### **3.5.2 Methodological considerations**

The field has some key limitations (Jones and Cercignani, 2010; Jones, Knösche and Turner, 2013). Firstly, water diffusion is not a direct measure of neuroanatomy. Secondly, dMRI is an intrinsically noise-sensitive and low-resolution technique (Jones, Knösche and Turner, 2013). Several dMRI models assume fibre bundles to run parallel in a tract. However, fibres cross within voxels in many brain regions, which reduces the FA. The percentage of voxels containing crossing fibres is estimated to be ~90% (Jeurissen *et al.*, 2013). It is also difficult to separate tracts that are closely aligned and then diverge (Tournier, Mori and Leemans, 2011). DTI also demonstrates 'degeneracy': the same change in the diffusion tensor can be explained by multiple processes e.g., differently oriented fibre populations ('crossing fibres'), or the ratio intra/extra-axonal space (see Figure 2). Therefore dMRI is sensitive but lacks specificity (Jelescu, Veraart, *et al.*, 2016) and cannot provide an interpretable marker other than a vague concept of 'tissue integrity' (Wheeler-Kingshott and Cercignani, 2009).

**Figure 3.2** The change in the diffusion signal (isotropic to anisotropic diffusion) can result from multiple different pathologies. States that can produce the same signal change include axonal loss, demyelination, axonal growth or oedema.



### 3.5.3 Interpretation of dMRI signal change in AD

In addition to neurodegeneration, a number of different pathological processes can result in the same changes in diffusion signals. However, the presence of abnormal dMRI measures in AD correlates with other AD biomarkers, such as amyloid PET (Kantarci *et al.*, 2014), CSF amyloid-beta and phosphorylated tau (Amlien *et al.*, 2013; Gold *et al.*, 2014; X Li *et al.*, 2015). Among those with AD, lower Mini-Mental State (MMSE) scores are associated with a greater effect size for FA in several brain areas, particularly the parietal region.

There is still much debate about the pathophysiology underpinning white matter changes in AD. For example, it is not clear whether white matter alterations are related to, or independent of, gray matter degeneration in AD. One hypothesis is that changes in white matter microstructure result from Wallerian degeneration (Coleman, 2005). According to this hypothesis, patterns of white matter alterations should correspond to grey matter pathology, occurring first in the hippocampal and entorhinal areas, before

extending to wider temporal and parietal regions (Braak & Braak, 1997). Conversely, the theory of retrogenesis suggests that those tracts which are last to myelinate are the first to degenerate (Reisberg *et al.*, 2002; Bartzokis, 2004). In this case, late-myelinating tracts would be affected first. It was striking that in the results of this systematic review there were no longitudinal dMRI studies comparing those at high and low genetic risk at different time points. Such debates cannot be resolved without serial imaging to assess dynamic changes in white matter signal.

Caution is required when interpreting diffusion metrics in AD. Some AD dMRI studies have concluded their findings showed disruption of myelin rather than axon damage based on the effect on LD relative to RD (Operto *et al.* 2018). Indeed, authors of *ex-vivo* studies in rats (Nevo *et al.*, 2001) and mice (Song *et al.*, 2002) as well as a small study of cervical spondylosis patients (Ries *et al.*, 2000) have suggested that a decrease in LD and increase in RD could potentially be used to differentiate demyelination from axonal injury. However, it may not be safe to generalize findings from controlled animal experiments and spinal cord studies to the human brain, which has complex white matter architecture. Microstructural dMRI models (Assaf and Basser, 2005; Panagiotaki *et al.*, 2012; Zhang *et al.*, 2012), which aim to be more specific than dMRI by describing the signal as arising from a sum of tissue compartments, hold great promise, but the nonlinear fitting suffers from poor precision (Jelescu, Veraart, *et al.*, 2016). Furthermore, microstructural dMRI models do not account for water in myelin because it cannot be detected with common dMRI acquisitions. Measuring myelin content is relevant for monitoring pathologies where demyelination, dysmyelination and remyelination are implicated. Thus, despite dMRI signals being modulated by changes in myelin content through changes in intra/extra-axonal space (Jelescu, Zurek, *et al.*, 2016), it can only reveal 'part of the picture'.

#### **3.5.4 Strengths and limitations of this review**

We followed PRISMA guidelines and used a comprehensive systematic search strategy to avoid missing relevant studies. We did not narrow our eligibility criteria to studies using particular research designs (e.g. case/control studies), samples (e.g. only clinical or healthy) or only young or older participants. We also included studies

using any dMRI technique (e.g. TBSS, VBA or tractography-based ROI) or analysis (e.g. structural connectivity) to enhance our ability to evaluate how AD genetic risk is manifest in white matter. Unfortunately, any eligible studies in non-English language journals would have been overlooked. The methodology was heterogeneous, and even when the same techniques are applied there can be differences between scanners (Vollmar *et al.*, 2010). Furthermore, although some standardisation exists for dMRI acquisition, other designs are largely ad hoc and can vary between centres. This meant that we were unable to perform a meta-analysis, could not establish the magnitude of effect sizes or assess for publication bias. The studies included in this review had a number of limitations. Some of the studies were probably underpowered. Authors often failed to describe sample ascertainment, making it more difficult to contextualise their results. The majority of studies included used either TBSS or VBA, which have a number of limitations, such as the requirement for spatial smoothing in VBA (Jones *et al.*, 2005; Jones and Cercignani, 2010; Edden and Jones, 2011).

### **3.5.5 Potential clinical applications**

As this review demonstrates, there is evidence that dMRI markers can detect changes in white matter microstructure in those with increased genetic risk of AD. The evidence suggests that some white matter tracts may be more sensitive than others, offering a possible marker of incipient disease. dMRI may also prove to be a useful tool for monitoring disease progression. However, dMRI presents a number of methodological challenges, and the biological changes that underpin alterations in dMRI signal are uncertain. However, with continuous improvements in imaging technology (McNab *et al.*, 2013; Jones *et al.*, 2018), and biophysical modelling (Novikov, Kiselev and Jespersen, 2018), we are likely to deepen our understanding of those biological underpinnings. Conventional T1- and T2- weighted images give established diagnostic markers and are widely used in clinical practice (Frisoni *et al.*, 2010). The utility of dMRI as an adjunct to traditional structural assessment is as yet unproven. Beyond that, there are also practical challenges, such as the length of acquisition protocols, and a lack of standardisation of models, acquisition and analysis.

### **3.5.6 Conclusions**

Despite some methodological limitations, the majority of the studies presented in this review demonstrate significant associations between AD genetic risk and diffusivity in white matter tracts. Specifically, lower FA and increased MD, RD and LD were found in a number of white matter tracts. This review emphasises the need for longitudinal studies of AD genetic risk to fully characterise white matter changes related to neurodegeneration across the lifespan. It is probable that very early pathology will be more amenable to therapeutic intervention. Therefore, early detection and pre-symptomatic treatment are vital. As acquisition and analysis techniques develop, dMRI is able to provide increasingly detailed information about the structure of white matter and brain connections and may develop useful biomarkers for AD pathology in future.

### **Appendix B. Supplementary Material**

Table 1. List of pre-defined search terms

Table 2. List of data extracted

Table 3. PRISMA checklist

Table 4. Associations with TBSS phenotypes in UK Biobank

## CHAPTER 4: GENERAL METHODOLOGY

*An overview of the methods relevant to the subsequent experimental chapters is outlined in this section. Detailed information about the neuroimaging analysis pipelines and the subsets of participants included in each analysis are described separately in each experimental chapter.*

### 4.1 Participants and procedures

#### 4.1.1 The Avon Longitudinal Study of Parents and Children (ALSPAC)

The Avon Longitudinal Study of Parents and Children (ALSPAC) also known as 'Children of the 90's', is a transgenerational prospective observational study. It explores influences on development and health throughout life. It investigates numerous exposures including genetic, epigenetic, biological, psychological, social and other environmental factors. The outcomes include a broad spectrum of health, social and developmental states (A. Fraser *et al.*, 2013; Boyd *et al.*, 2013). Initially conceived to investigate modifiable factors affecting child health and development, ALSPAC recruited N = 14,541 pregnant women living in the Avon area of South-west England in 1990–92. All the women were expected to deliver between the 1<sup>st</sup> of April 1991, and the 31<sup>st</sup> of December 1992. Of these pregnant women, N = 13,988 had babies alive at one year of age. 713 additional children who were not enrolled during pregnancy but who were eligible were included at the age of seven. This resulted in a total sample of N = 14,701 children. A sub-sample of 10% of the original offspring cohort, the Children in Focus (CiF) groups, attended research clinics at intervals between 4 and 61 months of age. The CiF cohort were randomly selected from the last six months of births. 1432 families attended at least one follow-up clinic. All of the mothers were invited to attend follow-up clinics, known as Follow-up Mothers or FOM. 4834 attended the first assessment, FOM1. Mothers were excluded if they had moved away from the area or were lost to follow-up, and those taking part in another local study of child development.

Participants provided rich phenotypic data. For the children, follow-up included 59 questionnaires (4 weeks–18 years old) and nine clinic assessment visits (7–17 years old). The resource comprises a wide range of environmental measures in addition to biological samples and genetic data (genome-wide data for >8000 children; complete genome sequencing on 2000 children) (Abigail Fraser *et al.*, 2013). The mothers have completed up to 20 questionnaires and have had comprehensive information linked from medical records including data on any cancer diagnoses and deaths. Follow-up assessments were completed 17–18 years after the birth of their children. These included anthropometry, blood pressure, fat measurements, bone mass, carotid intima media thickness, and a fasting blood sample. Further follow-up clinics also measured cognitive function, physical fitness, physical activity and wrist bone architecture. A comprehensive biobank contains DNA (genome-wide data available on >10 000 participants) and repeat samples of serum and plasma that have been stored. MRI data was also obtained for subsets of participants (A. Fraser *et al.*, 2013). Details of all the data available through ALSPAC can be found on the data dictionary on the study website (<http://www.bris.ac.uk/alspac/researchers/data-access/data-dictionary/>). Ethical approval for the research was granted by the ALSPAC Ethics and Law Committee and the local Research Ethics Committees. The analyses reported in this thesis were permitted by the ALSPAC Executive Committee (project reference B2399).

The 1991 census was used to compare the population of mothers with infants in ALSPAC to the average British population and the Avon population. Whilst ALSPAC mothers were more likely to be homeowners and car owners than other mothers in Avon or Britain, they were also more likely to be in overcrowded accommodation (Abigail Fraser *et al.*, 2013).

#### **4.1.2 UK Biobank**

UK Biobank was established to improve the prevention, diagnosis and treatment of serious diseases that occur in later life such as cancers, heart disease, stroke, diabetes, arthritis, osteoporosis, eye disorders, depression and forms of dementia (Sudlow *et al.*, 2015).

It is a national cohort that has recruited 500,000 participants in midlife. Participants were aged 40-69 at recruitment between 2006 and 2010. At baseline assessment, detailed information was gathered about health status including cognitive health, physical condition, physical activity, and environmental exposures including diet and lifestyle. Venesection was also performed. A subset of 100,000 participants wore an activity monitor 24 hours-a-day for a week, and 20,000 provided repeated measures of a number of variables. A series of online questionnaires has provided further information on phenotypes and exposures such as diet, cognitive function and work history. 100,000 participants are being scanned using MRI. The acquisition includes brain, heart, abdomen, bones & carotid artery imaging. Blood and serum samples have been analysed to provide rich biochemistry data. Genotyping has been undertaken on all 500,000 participants.

Participants also agreed to have their health followed through their medical records for cancer, death and general practice. Hospital Episodes Statistics and data from repeat assessment is also available for 20,000 participants in the North West of England. Details of the data available from UK Biobank can be found on the data dictionary on the project website <http://biobank.ndph.ox.ac.uk/showcase/>. UK Biobank had independent ethical approval from a number of bodies (UK Biobank, 2007). UK Biobank granted approval for the analyses reported in this thesis (UK Biobank Application 15175).

Of note, the UK Biobank sample is not representative of the general population. There is evidence of 'healthy volunteer' selection bias. Sociodemographic information, lifestyle and health-related characteristics are particularly divergent from the general population (Fry *et al.*, 2017).

## **4.2 Brain imaging**

### **4.2.1 MRI data in ALSPAC**

A number of studies have recalled sub-samples of ALSPAC offspring for further assessments, some of which undertook brain imaging (Sharp *et al.*, 2020). This thesis uses data from two of these sub-studies, summarised in Table 4.1. The first explored the effects of testosterone on brain structure (ALSPAC project ID B648) and the second investigated psychotic experiences (ALSPAC project ID B709). Ethical

approval for the neuroimaging sub-studies was given by the ALSPAC Ethics and Law Committee and Local Research Ethics Committees (North Somerset and South Bristol Research Ethics Committee: 08/H0106/96). Participants provided written informed consent.

The ALSPAC Testosterone study recruited 513 male participants. The inclusion criteria were the availability of multiple blood samples collected during puberty and proximity to Cardiff, Wales, the scanning centre. Those participants who responded to the invitation first were included. The ALSPAC psychotic experience study was based on a subset of 4,323 ALSPAC participants who were assessed for psychotic-like experiences using a semi-structured interview. Of these, 152 agreed to undergo scanning.

The same acquisition protocol was used for both studies, further details of which are given in each experimental chapter. Both scanned participants when they were approximately 20 years old. The present study excluded participants if they did not report white British and Irish descent or if they had asked to have their data removed from ALSPAC.

**Table 4.1 Sample demographics by neuroimaging sub-study**

		Testosterone Study		Psychotic Experiences Study		Core ALSPAC Sample			
<b>Sample size</b>		513		252		14220			
<b>Selection criteria (N, %)</b>		Healthy males (513, 100%)		Subjects with PE (126, 50%), healthy controls (126, 50%)		Pregnant women in Avon, due 1991/1992			
				<b>No PE</b>	<b>PE</b>				
<b>Age: years</b>	Mean (SD)	19.62	(0.04)	20.1	(0.002)	20.05	(0.002)		
<b>Sex: N (%)</b>	Male	513	(100)	49	(38.89)	39	(30.95)	7356	(51.73)
	Female	0	(0)	77	(61.11)	87	(69.05)	6864	(48.27)
<b>Ethnicity: N (%)</b>	White	456	(96.41)	109	(95.61)	107	(97.27)	11186	(94.19)
	Non-white	17	(3.59)	5	(4.39)	3	(2.73)	690	(5.81)
<b>Handedness: N (%)</b>	Right	295	(63.17)	75	(68.18)	81	(71.68)	6507	(65.23)
	Left	54	(11.56)	11	(10)	5	(4.42)	1102	(11.05)
	Mixed	118	(25.27)	24	(21.82)	27	(23.89)	2367	(23.73)
<b>IQ score</b>	Mean (SD)	98.8	(0.56)	99.51	(1.1)	95.12	(1.18)	94.36	(0.18)

Adapted from Sharp, Tamsin H et al. "Population neuroimaging: generation of a comprehensive data resource within the ALSPAC pregnancy and birth cohort." Wellcome open research vol. 5 203. 28 Aug. 2020, doi:10.12688/wellcomeopenres.16060.1.

Acronyms: PE = psychotic experiences; IQ = Intelligence Quotient.

### 4.2.2 MRI data in UK Biobank

UK Biobank is currently imaging 100,000 participants for brain imaging. Data from those who have already been imaged is released in batches. The analyses presented in this thesis include the first 20,000 datasets that were released. Structural T1/2 weighted images, diffusion MRI (dMRI) and functional MRI (fMRI) data were acquired. As with ALSPAC, further details of the acquisition protocol and parameters are given in the experimental chapters. UK Biobank undertook some pre-processing of the MRI data, and has published Imaging Derived Phenotypes (IDPs) based on their analysis. Further information about the pre-processing is included in the experimental chapters.

### 4.3 Genotyping

Participants from the ALSPAC study were genotyped with the Illumina HumanHap550 quad genome-wide single nucleotide polymorphism (SNP) genotyping platform (Illumina Inc., San Diego, California, USA) by 23andMe, subcontracting the Wellcome Trust Sanger Institute (Cambridge, UK) and the Laboratory Corporation of America (Burlington, North Carolina, USA).

In UK Biobank, genome wide genotype data is available for all 500,000 participants. UK Biobank sample processing is described in their documentation ([https://biobank.ctsu.ox.ac.uk/crystal/docs/genotyping\\_sample\\_workflow.pdf](https://biobank.ctsu.ox.ac.uk/crystal/docs/genotyping_sample_workflow.pdf)). The first 50,000 participants were genotyped using the Affymetrix UK BiLEVE Axiom array. Subsequent participants were genotyped with the Affymetrix UK Biobank Axiom array, which genotyped around 850,000 variants. The two arrays have over 95% of their variants in common. A collaborative group, headed by the Wellcome Trust Centre for Human Genetics, performed quality control and imputation to more than 90 million SNPs, indels and large structural variants. Further details can be found on the UK Biobank website (<https://www.ukbiobank.ac.uk/scientists-3/genetic-data/>).

In ALSPAC, Dr Katherine Tansey assisted with the quality control of the genotype data. PLINK was used for quality control (Purcell *et al.*, 2007). Exclusions were made for the following in ALSPAC: i) ambiguous sex (phenotypic and genotypic sex discrepancy); ii) cryptic relatedness (first, second or third-degree relatives, ascertained

with identity-by-descent; iii) less than 97% genotyping completeness; and iv) non-British or Irish ethnicity. Ethnicity admixture outliers were identified using an EIGENSTRAT analysis of the dataset pruned for linkage disequilibrium (Price *et al.*, 2006). In UK Biobank, exclusions were made for i) less than 97% genotyping completeness; and ii) non-British or Irish ethnicity. For both datasets, SNPs were selected using the following criteria: i) imputed on the Haplotype Reference Consortium (McCarthy *et al.*, 2016); ii) minor allele frequency (MAF) > 1%; iii) SNP call rate > 98%; iv) INFO score  $\geq 0.4$ ; v) posterior probability  $\geq 0.4$ ; vi)  $\chi^2$  test for Hardy-Weinberg equilibrium  $p > 1 \times 10^{-6}$ . Imputation was performed using the prephasing/imputation approach in IMPUTE2/SHAPEIT (Howie, Marchini and Stephens, 2011; Delaneau, Marchini and Zagury, 2012) with 1000 Genomes (December 2013, release 1000 Genomes haplotypes Phase I integrated variant set) (1000 Genomes Project Consortium *et al.*, 2015) as the reference dataset.

## **4.4 Metabolomics**

### **4.4.1 Metabolomic data in ALSPAC**

ALSPAC has measured a wide range of biochemical markers from the blood and urine samples. ALSPAC developed a panel of biomarkers with a view to studying a wide range of diseases, established disease risk factors for disease, diagnostic measures, and biomarkers that characterise organ function such as renal profiles and liver function tests. Data is available for mothers and offspring for blood lipids (triglycerides, very Low Density Lipoprotein (vLDL), Low Density Lipoprotein (LDL), High Density Lipoprotein (HDL)) and inflammatory markers (C-Reactive Protein (CRP) and interleukin 6 (IL-6)).

## **4.5 Data analysis**

### **4.5.1 Data cleaning and pre-processing in ALSPAC**

Quality controlled genotype information and metabolomic data was supplied by Bristol University ALSPAC Team. Structural MRI data were downloaded from CUBRIC servers. Data were pre-processed using in-house MATLAB scripts (MATLAB and Statistics Toolbox Release 2012b, The MathWorks, Inc., Natick, Massachusetts,

United States; <https://www.mathworks.com/products/matlab.html>), and ExploreDTI\_4.8.3 (<http://www.exploredti.com/generalinfo.htm>) (Leemans *et al.*, 2009).

Neuroimaging data were cleaned and pre-processed with assistance from Ms Sonya Foley and Dr Xavier Caseras, who used the same data for a separate project (Foley *et al.*, 2018). A detailed description of ALSPAC MRI data pre-processing pipelines and analysis is provided in Chapters 5 and 6.

#### **4.5.2 Data cleaning and pre-processing in UK Biobank**

The UK Biobank team provided access to all variables through a secure portal. Quality controlled genotype data was supplied. For the imaging analysis, we received the raw DICOM files and UK Biobank's Imaging Derived Phenotypes (IDPs) for dMRI measures. Dr Xavier Caseras used Freesurfer v.5.3 (Fischl, 2012) (<https://surfer.nmr.mgh.harvard.edu>) running in UNIX to process T1-weighted brain images, as these data were being used for a separate analysis (Caseras *et al.*, 2020). Details of UK Biobank neuroimaging pre-processing pipelines and analysis is provided in Chapters 5 and 6.

Data pertaining to all chapters were cleaned, scored and exported to R Studio (version 1.1383 for Mac, [www.rstudio.com](http://www.rstudio.com)). Statistical analysis of genetic, metabolomic and neuroimaging data was performed in R Studio.

#### **4.5.3 Polygenic score calculation**

PRS computation was performed according to the International Schizophrenia Consortium procedure (Purcell *et al.*, 2009). The discovery sample, used to select SNPs relevant for polygenic analysis, was the summary statistics from the largest Genome-wide Association Study (GWAS) of late onset AD to date (Kunkle *et al.*, 2019). This meta-analysis of previous case-control studies comprised 63,926 individuals. This data is publicly available at <https://www.niagads.org/datasets/ng00075>. Although other recent AD GWAS exist (Marioni *et al.*, 2018; Jansen *et al.*, 2019), Kunkle and colleagues used clinically

diagnosed cases and controls, whereas the other GWAS used family history of AD as a proxy. First, SNPs with a low minor allele frequency ( $< .01$ ) were removed from the analysis. Secondly, the data was pruned for linkage disequilibrium. This was done in PLINK (Purcell *et al.*, 2007) using the clumping function (--clump). Parameters were set to remove SNPs within  $r^2 > 0.2$  (--clump-r2) and 500 kilobase (--clump-kb) of a SNP that was more significantly associated with AD. PRS were calculated using the --score command in PLINK (Purcell *et al.*, 2007). A  $P^T$  of 0.001 was used to select relevant SNPs for the primary analysis, as an AD PRS using this threshold was found to explain the most variance in neuroimaging phenotypes (Foley *et al.*, 2016). For the secondary analysis, we applied seven progressive thresholds ( $p = 0.5, 0.3, 0.1, 0.01, 0.0001, 0.00001, 0.000001$ ). The lower  $P^T$  conservatively selected only SNPs that were more significantly associated with AD case status in the discovery dataset. In contrast, the higher  $P^T$  liberally selected SNPs, including those only nominally associated with disease, thereby including a greater amount of genetic information. In AD, a liberal  $P^T$  of 0.5 has been shown to be the best predictor of case-control status (Escott-Price, Sims, Bannister, *et al.*, 2015).

In order to calculate pathway-specific PRS, relevant disease pathways were taken from the paper by Kunkle and colleagues (Kunkle *et al.*, 2019). They conducted a pathways analysis of AD GWAS data using MAGMA (Multi-marker Analysis of GenoMic Annotation) (de Leeuw *et al.*, 2015). MAGMA uses a multiple regression model, to perform gene analysis and gene-set analysis. They detected a number of functional clusters that were significantly enriched for common variants. These are summarised in Table 4.2. Each PRS was computed including and excluding SNPs in the *APOE* region (chromosome 19 between 44.4Mb and 46.5Mb). Non-coding variants within the *APOE* locus have been shown to contribute to AD risk (Zhou *et al.*, 2019), therefore this process was followed even for those pathways which did not include the *APOE* gene.

Polygenic score calculation was completed using the HAWK Linux supercomputer (<https://portal.supercomputing.wales/index.php/about-hawk/>) and PLINK version 1.07 (<https://www.cog-genomics.org/plink>) (Purcell *et al.*, 2007). Pathway specific polygenic scores were calculated using a list of SNPs based on the pathway analysis included in Kunkle *et al.* (Kunkle *et al.*, 2019).

In UK Biobank, the quality control of genetic data and computation of polygenic scores was performed by Dr Emily Baker using the Raven Linux supercomputer and PLINK version 1.07 (<https://www.cog-genomics.org/plink>) (Purcell *et al.*, 2007).

**Table 4.2 Significant pathways (q values ≤0.05) from MAGMA pathway analysis for common and rare variant subsets**

Geneset No.	Pathway	Pathway description	N genes in pathway in dataset	Pathway includes APOE (Y/N)	Common		Rare		N SNPs in summary stats, P <sup>†</sup> 0.001	
					variant P <sup>a</sup>	variant q value	variant P <sup>a</sup>	variant q value	summary stats, P <sup>†</sup> 0.001	summary stats, P <sup>†</sup> 0.001
1	GO:65005	Protein-lipid complex assembly	20	Y	1.4 × 10 <sup>-7a</sup>	9.5 × 10 <sup>-4</sup>	6.7 × 10 <sup>-2</sup>	8.4 × 10 <sup>-1</sup>	177	177
2	GO:1902003	Regulation of Aβ formation	10	Y	4.5 × 10 <sup>-7a</sup>	1.4 × 10 <sup>-3</sup>	4.9 × 10 <sup>-2</sup>	8.4 × 10 <sup>-1</sup>	189	189
3	GO:32994	Protein-lipid complex	39	Y	1.1 × 10 <sup>-6a</sup>	2.5 × 10 <sup>-3</sup>	1.7 × 10 <sup>-2</sup>	8.1 × 10 <sup>-1</sup>	211	211
4	GO:1902991	Regulation of amyloid precursor protein catabolic process	12	Y	3.5 × 10 <sup>-6a</sup>	5.8 × 10 <sup>-3</sup>	5.6 × 10 <sup>-2</sup>	8.4 × 10 <sup>-1</sup>	223	223
5	GO:48156	Tau protein binding	10	Y	3.1 × 10 <sup>-5a</sup>	2.6 × 10 <sup>-2</sup>	7.7 × 10 <sup>-1</sup>	8.5 × 10 <sup>-1</sup>	235	235
6	GO:43691	Reverse cholesterol transport	17	Y	5.5 × 10 <sup>-6a</sup>	6.7 × 10 <sup>-3</sup>	3.0 × 10 <sup>-2</sup>	8.1 × 10 <sup>-1</sup>	256	256
7	GO:71825	Protein-lipid complex subunit organization	35	Y	6.1 × 10 <sup>-6a</sup>	6.7 × 10 <sup>-3</sup>	1.2 × 10 <sup>-1</sup>	8.4 × 10 <sup>-1</sup>	266	266
8	GO:34377	Plasma lipoprotein particle assembly	18	Y	1.6 × 10 <sup>-5a</sup>	1.5 × 10 <sup>-2</sup>	1.8 × 10 <sup>-1</sup>	8.4 × 10 <sup>-1</sup>	148	148
9	GO:2253	Activation of immune response	382	N	6.3 × 10 <sup>-5a</sup>	4.6 × 10 <sup>-2</sup>	2.0 × 10 <sup>-1</sup>	8.4 × 10 <sup>-1</sup>	145	145

<sup>a</sup> Significant after FDR correction (q value ≤0.05). Acronyms: MAGMA = Multi-marker Analysis of GenoMic Annotation; GO = Gene Ontology. Table adapted from Kunkle, B.W., Grenier-Boley, B., Sims, R. et al. Genetic meta-analysis of diagnosed Alzheimer's disease identifies new risk loci and implicates Aβ, tau, immunity and lipid processing. Nat Genet 51, 414–430 (2019).

#### 4.5.4 Statistical analyses

The data distributions for each variable were checked for normality using Shapiro-Wilk normality test in R Studio. Differences for normally-distributed continuous data were analysed using parametric statistical tests e.g. Pearson correlation ( $r$ ). Non-normally-distributed data were analysed using non-parametric statistical tests e.g. Spearman correlation ( $\rho$ ).

Linear regression was used to explore the relationships between PRS, brain imaging measures and metabolomic measures and to investigate the effects of covariates. The regression models included brain imaging and metabolomic variables as dependent variables while PRS were included in the models as independent variables. The PRS were normalised before inclusion in the regression models. For the primary analysis, a p value threshold of 0.001 was used to select SNPs for the PRS. A further seven p value thresholds were also included in a secondary analysis to assess the effect of more or less conservative scores. The variables that were included as covariates were age, gender and ancestry principal components, and imaging variables where appropriate. Results which were significant after correction were re-analysed using polygenic risk scores which excluded *APOE* SNPs, thereby assessing whether *APOE* explained the signal. Further analysis of SNPs in the *APOE* region was performed to compare how much of the variance was explained by *APOE* compared to the PRS.

Correction for multiple comparisons of phenotype and PRS using the False Discovery Rate (FDR) in the R statistical computing package (R Development Core Team 3.0.1., 2013). This was applied for 21 scores (nine pathway polygenic scores and the genome-wide polygenic score including the *APOE* region, nine pathway polygenic scores excluding the *APOE* region and the genome-wide score excluding the *APOE* region plus the *APOE* region SNPs score) and for the number of phenotypes tested in each analysis.

## CHAPTER 5: ALZHEIMER'S POLYGENIC RISK SCORES & GREY MATTER VOLUMES

*The chapter includes some material that was previously published as an abstract Harrison J, Caseras X, Foley S, Baker E, Williams J, Linden D, Holmans P, Escott-Price V, Jones D. Pathway-specific polygenic scores for Alzheimer's disease are associated with multi-modal structural brain imaging markers in young adults. Proceedings of the 28th ISMRM Annual Scientific Meeting & Exhibition, 2020 August.*

*Dr Xavier Caseras, Ms Sonya Foley and Dr Matthew Bracher-Smith assisted with the initial curation of imaging data, pre-processing and quality control, as this data was also used for other projects. Dr Emily Baker provided the lists of SNPs in the Kunkle et al 2019 disease pathways and calculated the polygenic scores in the UK Biobank data, as they were used for separate analyses. Dr Katherine Tansey assisted with genotyping quality control in ALSPAC.*

*Some information from Chapters 1, 2 and 3 is repeated here for convenience.*

### 5.1 Summary

Grey matter atrophy, particularly in medial temporal areas, is an established diagnostic marker of AD pathology. It is evident in pre-symptomatic carriers of autosomal dominant AD genes and has also been associated with the AD risk gene APOE Epsilon 4 (*APOE4*).

Genome-wide association studies (GWAS) have identified multiple AD risk loci of small effect. As discussed in Chapter 2, these variants can be combined in polygenic risk scores (PRS) to quantify polygenic burden for AD. PRS have also been associated with changes in grey matter measurements. Previous studies have found significant negative correlations between PRS, hippocampal volume and cortical thickness in healthy participants. A few previous studies have used gene sets based on disease pathways to inform the PRS, however these have only used Bonferroni-significant loci, thereby excluding many variants likely to be involved in the disease.

The chapter explored associations between disease pathway specific PRS and grey matter volumes in areas preferentially affected by AD pathology in young and mature adults.

Data from two population cohorts were used, the Avon Longitudinal Study of Parents and Children (ALSPAC) and UK Biobank, with a combined n of over 18,000. PRS were computed in PLINK using the largest genome-wide association study (GWAS) of clinically assessed AD to date, published by Kunkle and colleagues. Pathway-specific polygenic scores were generated using lists of SNPs from a recent pathway analysis. T1-weighted MRI data were processed using the surface-based method Freesurfer to calculate subcortical volumes, cortical thickness and cortical surface area. Relationships between imaging phenotypes, genome-wide and pathway specific PRS were assessed with linear regression.

Increased PRS across pathway groups were associated with increased subcortical volume in the younger group, and decreased subcortical volumes in the older cohort, particularly in the left hemisphere. Increased pathway specific PRS were also associated with cortical thinning in younger and older cohorts. There was little evidence of association between cortical surface area and any PRS. The disease pathway PRS had broadly similar patterns of association but showed greater evidence of association with grey matter phenotypes than the genome-wide score, suggesting that this may be a helpful way to reduce noise inherent within polygenic scores.

## **5.2 Introduction**

Morphometric MRI is a safe, non-invasive and reliable method used in the diagnosis of AD and monitoring disease progression (McKhann *et al.*, 1984; Frisoni *et al.*, 2010). AD pathology is evident decades before symptoms are detectable (Jack *et al.*, 2013). Morphometric changes in the medial temporal lobe are widely reported in early AD (Busatto, Diniz and Zanetti, 2008). Atrophy in this region, particularly in the hippocampus, can predict progression from MCI, considered an AD prodrome, to dementia (Korf *et al.*, 2004; Jack *et al.*, 2005). Medial temporal atrophy is also associated with a number of pre-clinical risk groups (Mak *et al.*, 2017). However, grey

matter atrophy is also reported in other regions in early AD, particularly the cortex and subcortical volumes such as the amygdala (Busatto, Diniz and Zanetti, 2008).

The relationship of AD genetic risk to grey matter structure has been widely studied. Pre-symptomatic carriers of autosomal dominant AD genes have associated changes in brain structure. As discussed in previous chapters, autosomal-dominant AD is caused by mutations either in the amyloid precursor protein gene (*APP*), or in presenilin 1 and 2 (*PS1* and *PS2*) that are involved in cleaving amyloid  $\beta$  and APP (Tanzi, 2012). Cognitively normal *PS1* carriers have been found to have reduced cortical thickness (Reiman *et al.*, 2012; Quiroz *et al.*, 2013). Pre-symptomatic carriers also have hippocampal atrophy (Bateman *et al.*, 2012; Fleisher *et al.*, 2015). However, not all studies report significant findings (Mak *et al.*, 2017). One study only reported trends toward decreased volumes in regions such as the thalamus in those closer to the expected age of disease onset (Cash *et al.*, 2013). The discordance in findings may be partly explained by small sample sizes, reflecting the rarity of the autosomal dominant genes. Another study reported an increase in grey matter in the cortex and subcortical regions in children carrying autosomal dominant mutations (Fortea *et al.*, 2010; Quiroz *et al.*, 2015). These changes may result from gene effects on grey matter development. For example, in animal models it has been demonstrated that *PS1* is involved in neural and vascular development (Saura *et al.*, 2004; Xia *et al.*, 2015).

The most significant common genetic risk for AD, Apolipoprotein Epsilon 4 (*APOE4*), has been reported to be associated with decreased grey matter volume in a number of regions in pre-symptomatic individuals (Mak *et al.*, 2017). Several studies found generalised volume loss and reduced cortical thickness in *APOE4* carriers in later life (Lemaître *et al.*, 2005; Hashimoto *et al.*, 2009; Crivello *et al.*, 2010; Fan *et al.*, 2010) even among younger samples (Wishart *et al.*, 2006; Burggren *et al.*, 2008). In particular, studies report volume loss in the entorhinal cortex and medial temporal lobe in *APOE4* carriers compared to non-carriers (Wishart *et al.*, 2006; Burggren *et al.*, 2008; Fan *et al.*, 2010). Longitudinal studies have shown accelerated cortical thinning with age among *APOE* carriers (Espeseth *et al.*, 2008).

The literature on heterozygous *APOE4* carriers is more discrepant. A number of studies have found changes in subcortical and cortical volumes in homozygous but

not heterozygous carriers (Lemaître *et al.*, 2005; Chen *et al.*, 2007; Dufouil *et al.*, 2007). Some of this disagreement could be explained by lack of statistical power when participants are divided into sub-groups. However some studies that combined homozygous and heterozygous carriers also reported no significant differences (Cherbuin *et al.*, 2008). Studies of infant *APOE4* carriers have reported intriguing results. One study of babies (n = 162) found carriers had reduced grey matter volume in the precuneus, posterior and middle cingulate, lateral temporal, and medial occipitotemporal areas. However, it also reported carriers also had significantly greater frontal grey matter volumes (Dean *et al.*, 2014). A further study of neonates (n = 272) reported reduced cortical grey matter volumes in the temporal region of *APOE4* carriers (Knickmeyer *et al.*, 2014).

A variable poly-T length polymorphism in the translocase of the outer mitochondrial membrane (*TOMM40*) gene affects AD age of onset. Short poly-T length is associated with later onset and very long poly-T length with earlier onset (Roses *et al.*, 2010). A few studies have examined the effect of poly-T length in *TOMM40* on brain volumes in healthy individuals. Johnson *et al.* found that very long poly-T *TOMM40* polymorphism carriers have lower grey matter volume in the medial ventral precuneus and ventral posterior cingulate, regions affected early in AD (Johnson *et al.*, 2011). Burggren *et al.* also reported an association between very long poly-T and cortical thinning in healthy older people (Burggren *et al.*, 2011). However, Ferencz *et al.* reported no association between *TOMM40* polymorphisms and hippocampal volume (Ferencz *et al.*, 2013).

Brain-derived neurotrophic factor (BDNF) is a neurotrophin that is widely distributed throughout the central nervous system. It is involved in synaptic plasticity and neuronal survival (Diniz and Teixeira, 2011). The *BDNF* variant produces an amino acid substitution (valine to methionine, Val66Met) that affects *BDNF* intracellular packaging and activity-dependent secretion (Chen *et al.*, 2004). This is associated with changes in human memory function (Egan *et al.*, 2003) and hippocampal morphology (Bueller *et al.*, 2006). It is implicated in the pathogenesis of a number of neurodegenerative diseases (Zuccato and Cattaneo, 2009). In a longitudinal study, Met-*BDNF* carriers showed increased rate of atrophy in the bilateral posterior cingulate cortex and cingulate gyrus compared to homozygotes for Val-*BDNF* allele (Hashimoto *et al.*,

2009). Knickmeyer explored the effect of *BDNF* variants on brain structure in neonates. They found lower volume in the right occipital and temporal cortex among Met carriers, but also noted reduced volume in Val/Val homozygotes (Knickmeyer *et al.*, 2014). The inconsistency may result from differences in the effect of *BDNF* genotype at different ages.

As described in Chapter 2, genome-wide association studies (GWAS) have highlighted multiple AD risk loci of small effect in addition to *APOE* (Marioni *et al.*, 2018; Jansen *et al.*, 2019; Kunkle *et al.*, 2019) which can be combined in polygenic risk scores (PRS) (Wray *et al.*, 2014). PRS have been shown to be associated with changes in grey matter measurements. In particular, studies have reported significant negative correlations between PRS and hippocampal volume in healthy participants (Foley *et al.*, 2016; Harrison and Bookheimer, 2016; Mormino *et al.*, 2016; Axelrud *et al.*, 2018; Walhovd *et al.*, 2020), even in children (Walhovd *et al.*, 2020). Lupton *et al.* reported significant negative association with hippocampal volume (Lupton *et al.*, 2016) but only when participants with MCI or AD were included. Xiao *et al.* did not find any significant associations between PRS and subcortical volumes (Xiao *et al.*, 2017).

The effect of AD polygenic risk on cortical thickness has also been examined (Sabuncu *et al.*, 2012; Harrison and Bookheimer, 2016; Hayes *et al.*, 2017; Corlier *et al.*, 2018; Li *et al.*, 2018). All but two studies (Harrison and Bookheimer, 2016; Xiao *et al.*, 2017) reported significant associations between increased PRS and cortical thinning. Studies either reported associations with cortical thinning across multiple regions that are susceptible to AD pathology (Sabuncu *et al.*, 2012; Hayes *et al.*, 2017; Corlier *et al.*, 2018), or with cortical thinning in specific regions such as the precuneus (Li *et al.*, 2018).

Three studies used a gene set based on disease pathways to inform the PRS. However, their PRS comprised only Bonferroni significant SNPs identified in earlier GWAS (Lambert *et al.*, 2013), therefore relevant genetic information that was below the stringent threshold for genome-wide significance was excluded. Corlier *et al.* found that the immune response PRS (n SNPs = 11) was significantly associated with an overall measure of cortical thinning (Corlier *et al.*, 2018). Ahmad and colleagues found no significant associations between seven different pathway polygenic scores (n SNPs

= 20), hippocampal volume and whole brain volume (Ahmad *et al.*, 2018). The most recent study reported distinct patterns of cortical thinning associated with different pathway specific polygenic scores (n SNPs = 20) (Caspers *et al.*, 2020).

There are a number of methods to assess grey matter volume using MRI. The most frequently used techniques, beyond visual rating of regional atrophy, are voxel-based morphometry (VBM) (Ashburner and Friston, 2000) and surface-based analysis (SBA) (Greve, 2011; Fischl, 2012). For both methods, input is a high-resolution T1-weighted image, pre-processed to segment brain from non-brain tissue. Briefly, standard VBM analysis involves: 1) spatial normalisation of an individual's T1-weighted image to a group template, e.g. the Montreal Neurological Institute (MNI) International Consortium of Brain Mapping (ICBM) 152 template; 2) segmenting into grey matter, white matter, and cerebrospinal fluid (CSF)); next, the normalized data are smoothed using an 8-mm full-width at half-maximum (FWHM) isotropic Gaussian kernel to create a mean image (Good *et al.*, 2001; Greve, 2011). Spatial normalisation can cause some brain regions to expand, and others to become smaller. A modulation step has been added to maintain the volume of a particular region which involves multiplying the values of voxel in segmented images by the Jacobian determinants produced by the spatial normalization step (Good *et al.*, 2001).

SBA derives values from geometric models. SBA methods can be summarised as follows: 1) extraction of the grey matter surface, such as the cortex. The surface boundaries between white matter and grey matter, and between grey matter and CSF are delineated; 2) the grey matter is modelled using a mesh of triangles and the corners of the triangles, known as vertices, are assigned coordinates; 3) morphometric measures are computed based on the coordinates. In addition, the image can be manipulated to inflate the surface of the cortex to display grey matter normally hidden within sulci and 4) surface-based spatial normalization, by aligning the sulci and gyri between subjects using a non-linear registration. The results for each individual can be tabulated and compared, or volumetric data can be mapped to a common space, allowing volumes to be compared in homologous places between subjects (Greve, 2011). FreeSurfer, a free to use platform ([surfer.nmr.mgh.harvard.edu](http://surfer.nmr.mgh.harvard.edu)), is an example of SBA implementation (Fischl, 2012).

### 5.2.1 Rationale and Aims

Evidence from histological and MRI studies in humans demonstrates that grey matter atrophy is a core feature of AD neurodegeneration and a marker of progression (Busatto, Diniz and Zanetti, 2008; Harrison and Owen, 2016). The literature summarised above provides evidence of the effect of AD risk genes on grey matter volumes in healthy, pre-clinical individuals. Chapter 3 systematically reviewed and summarised literature that demonstrated significant associations between AD genetic risk and diffusivity in white matter tracts.

Chapter 2 comprises a systematic review that found evidence that AD PRS could predict AD case/control status and were associated with phenotypes relevant to neurodegeneration. As discussed in Chapter 2, GWAS have resulted in the identification of novel genetic risk loci in addition to *APOE*  $\epsilon$ 4 (*APOE4*) (Lambert *et al.*, 2013; Kunkle *et al.*, 2019) which have been associated with a range of biological pathways including lipid metabolism, immune response, and synaptic processes (Jones *et al.*, 2010; Holmans and Jones, 2012). Few studies have used AD pathway polygenic scores to assess brain structure. Those studies that did attempt it used only Bonferroni significant SNPs (Ahmad *et al.*, 2018; Corlier *et al.*, 2018), omitting potentially relevant SNPs that fell below the stringent threshold. The variance that each of these pathways explains is small (Darst *et al.*, 2017), therefore large discovery and target sample sizes are required (Dudbridge, 2013).

The primary aim of this chapter is to explore associations between disease pathway specific PRS and grey matter volumes in areas preferentially affected by AD pathology in healthy adults, both young and in mid-later life. This will be achieved using large population cohorts and the SBA method Freesurfer. The secondary aim is to compare the associations between phenotypes and PRS using more and less conservative thresholds to assess which p value cut off achieves the best correlation with the phenotype.

### **5.2.2 Hypothesis**

It is hypothesised that increasing genetic burden for AD, measured in increasing PRS, will be associated with i) decreasing volume in subcortical regions, particularly the hippocampus, ii) decreased cortical thickness in temporal and parietal regions of cortex. It is further hypothesised that different disease pathways will show different patterns of brain structure changes.

## **5.3 Methods**

### **5.3.1 Participants**

Participants were recruited by the Avon Longitudinal Study of Parents and Children (ALSPAC) and UK Biobank. Please see Chapter 4 for a detailed description of recruitment methods and sample characteristics.

To summarise, the ALSPAC data were gathered for two population neuroimaging studies (Sharp *et al.*, 2020). As described, the first explored the effects of testosterone on brain structure (ALSPAC project ID B648;  $n = 513$ ) and the second investigated psychotic experiences (ALSPAC project ID B709,  $n = 152$ ). Ethical approval for the neuroimaging sub-studies was given by the ALSPAC Ethics and Law Committee and Local Research Ethics Committees (North Somerset and South Bristol Research Ethics Committee: 08/H0106/96). Participants provided written informed consent. Please see Chapter 4 for a description of the inclusion criteria for these sub-studies.

A subset of 100,000 UK Biobank participants are being recalled for multimodal imaging (Sudlow *et al.*, 2015). As detailed in Chapter 4, the first 20,000 datasets released by UK Biobank are analysed here. UK Biobank granted approval for the analyses reported in this thesis (UK Biobank Application 15175). UK Biobank obtained approval from a number of external bodies (UK Biobank, 2007). All participants gave informed consent.

The present study excluded UK Biobank participants if they self-reported a history of neurological or major psychiatric disorders, such as dementia, cerebrovascular disease, intellectual disability, at an assessment visit or during online follow-up, or had

a hospital admission ICD-10 code for a relevant disorder. Participants were excluded from ALSPAC and UK Biobank if they did not report white British and Irish descent or if they had asked to have their data removed. Data was retained if it successfully reconstructed and passed quality control.

After genotyping and imaging data quality control procedures, 517 individuals with structural T1 data remained (19.3% female, 80.7% male) in ALSPAC and 18172 in UK Biobank (52.7% female, 47.3% male). At the time of inclusion, the average ages of ALSPAC and UK Biobank participants were 19.81 years (SD 0.02) and 64.2 (SD 7.75) respectively.

### **5.3.2 MRI Acquisition**

For ALSPAC, data were acquired on a 3 Tesla General Electric HDx (GE Medical Systems) at Cardiff University Brain Research Imaging Centre (CUBRIC) with an 8 channel head coil. As far as possible, acquisition parameters were harmonised between ALSPAC sub-studies. Coronal T1-weighted structural images were acquired using the following parameters: 3D fast spoiled gradient echo (FSPGR) using 168–182 oblique-axial anterior commissure-posterior commissure (AC-PC) slices; 1mm isotropic resolution; flip angle = 20°; repetition time (TR) = 7.9ms and 7.8ms in the Testosterone and psychotic experiences studies respectively; echo time (TE) = 3.0ms; inverse time (TI) = 450ms; voxel size = 1mm × 1mm x 1mm; slice thickness 1mm; field of view (FOV) 256mm × 192mm matrix; acquisition time approximately 6-10 minutes (Sharp *et al.*, 2020).

For UK Biobank, data was acquired using three identical Siemens Skyra 3T scanners at the UK Biobank recruitment centres in Stockport, Newcastle and Reading, UK, with a standard Siemens 32 channel head coil. Sagittal T1-weighted structural images were acquired using the following parameters: 3D Magnetization Prepared - RApid Gradient Echo (MPRAGE); R = 2, TI = 880ms; TR = 2000ms; voxel size 1 x 1 x 1mm; FOV 208 mm x 256mm x 256mm matrix; acquisition time approximately 5 minutes (Alfaro-Almagro *et al.*, 2018).

### 5.3.3 Analysis Pipeline

Subcortical volumes, cortical thickness in temporal and parietal regions, and intracranial volume (ICV) were assessed using the SBA tool FreeSurfer version 5.3 ([surfer.nmr.mgh.harvard.edu](http://surfer.nmr.mgh.harvard.edu)) (Fischl, 2012). FreeSurfer has been validated as an appropriate method to segment grey matter volumes in large samples (Cherbuin *et al.*, 2009). The output was quality controlled using a freely available protocol devised by ENIGMA (<http://enigma.ini.usc.edu/>). Briefly, this comprised: 1) Outlier detection, using an R statistical computing script (R Development Core Team 3.0.1., 2013) to identify participants with divergent values; 2) The internal surface method; and 3) The external surface method, which used a function in Matlab to generate a webpage showing \*.png external views of segmentation from different angles. When a region-of-interest was determined to be inadequately segmented, its value was designated as missing, excluding it from analysis.

For each subcortical ROI, the final numbers included in the ALSPAC analysis were: left and right thalamus, left and right caudate, left accumbens, left and right putamen, right pallidum: n = 516; left pallidum and right accumbens: n = 515; right amygdala: n = 509; right hippocampus: n = 504; left amygdala: n = 502; left hippocampus: n = 497. For the cortical ROI, final numbers in the ALSPAC analysis ranged from: the entorhinal cortex, n = 486, to the right superior parietal and right supramarginal, n = 517.

For subcortical ROIs in UK Biobank, the final number was n = 18172. For cortical ROI, final numbers in the ALSPAC analysis ranged from the left parahippocampal region, n = 18165, to the left superior parietal and other regions, n = 18171. Metrics were curated and stored in files compatible with R.

### 5.3.4 Genotyping

As described in Chapter 4, ALSPAC participants were genotyped with the Illumina HumanHap550 quad genome-wide SNP genotyping platform (Illumina Inc., San Diego, California, USA). In UK Biobank, the first 500 participants were genotyped using the Affymetrix UK BiLEVE Axiom array and the remainder on the Affymetrix UK Biobank Axiom array. Quality control was completed in PLINK (Purcell *et al.*, 2007).

As detailed, exclusions were made for: i) ambiguous sex; ii) cryptic relatedness; iii) < 97% genotyping completeness; and iv) non-British or Irish ancestry in ALSPAC and i) < 97% genotyping completeness and ii) non-British or Irish ancestry in UK Biobank. For both datasets, SNPs were further filtered by: i) minor allele frequency (MAF) < 1%; ii) SNP call rate < 98%; iii)  $\chi^2$  test for Hardy-Weinberg equilibrium  $p < 1 \times 10^{-4}$ . Please see Chapter 4 for further details of genotyping procedures.

### 5.3.5 Polygenic Risk Score Calculations

PRS computation was performed according to the International Schizophrenia Consortium procedure, described in Chapter 4 (Purcell *et al.*, 2009). Briefly, the discovery sample, used to select relevant SNPs, was the Genome-wide Association Study (GWAS) conducted by Kunkle *et al.* (Kunkle *et al.*, 2019). Although other recent AD GWAS exist (Marioni *et al.*, 2018; Jansen *et al.*, 2019), Kunkle and colleagues used clinically diagnosed cases and controls, whereas the other GWAS used family history of AD as a proxy. SNPs with a low minor allele frequency (< .01) were excluded. The data was pruned for linkage disequilibrium using the clumping function (--clump) in PLINK (Purcell *et al.*, 2007) (parameters were  $r^2 > 0.2$  (--clump-r2) and 500 kilobase (--clump-kb)). PRS were calculated using the PLINK --score command (Purcell *et al.*, 2007). A previous study (Foley *et al.*, 2016) found that a PRS computed with p-value threshold ( $P^T$ ) of 0.001 explained the most variance in structural neuroimaging phenotypes. Therefore, the primary analysis used  $P^T$  0.001 to select relevant SNPs from the discovery sample. Seven progressive thresholds were applied for the secondary analysis ( $p = 0.5, 0.3, 0.1, 0.01, 0.0001, 0.00001, 0.000001$ ).

Disease pathways implicated by Kunkle and colleagues were used to compute pathway specific PRS (Kunkle *et al.*, 2019). Pathway gene sets were used to create lists of SNPs that were matched to the discovery sample. Polygenic scores were then calculated using the method described above. Please see Chapter 4 for a more detailed description of the polygenic score calculations and disease pathways.

### 5.3.6 Statistical Analysis

Statistical analyses were conducted using R Studio version 1.1.383 for Mac, [www.rstudio.com](http://www.rstudio.com) (R Development Core Team 3.0.1., 2013). The relationships between T1-weighted phenotypes and PRS were tested using hierarchical linear multiple regression, co-varying for age, gender, intracranial volume, and for UK Biobank scanning site and genotyping array. Initially, analyses were performed on the overall genome-wide AD PRS and the pathway-specific PRS separately. As described in Chapter 4, the resulting p-values were corrected for multiple comparisons of phenotype and PRS using the False Discovery Rate (FDR) in the R statistical computing package (R Development Core Team 3.0.1., 2013). Results were re-analysed using a polygenic risk score which excluded *APOE* SNPs (chromosome 19 between 44.4Mb and 46.5Mb), thereby assessing whether *APOE* explained the signal. Further analysis of SNPs in the *APOE* region was performed to compare how much of the variance was explained by *APOE* compared to the PRS. Regression analyses adjusted for population structure using 10 principal components for ALSPAC and 15 for UK Biobank as covariates. Additional covariates were gender and intracranial volume in ALSPAC and gender, intracranial volume, age, scanning site and genotyping array in UK Biobank.

## 5.4 Results

P values reported correspond only to the PRS variable in the regression model. The primary analysis, reported below, used a  $P^T$  of 0.001.

### 5.4.1 Subcortical Volumes in ALSPAC

In the ALSPAC cohort, there were no significant associations between the genome wide PRS and any subcortical volumes ( $p > 0.05$ ). The direction of the effect suggested a trend towards a positive association between increased genome wide PRS and volume in subcortical regions.

There were significant positive associations between the protein-lipid complex subunit organisation PRS, the left amygdala ( $p = 0.007$ ,  $R^2 = 1.06 \times 10^{-2}$ ) and the left caudate

( $p = 0.007$ ,  $R^2 = 9.11 \times 10^{-3}$ ). There was also a significant positive association between the left caudate, the protein lipid complex PRS ( $p = 0.002$ ,  $R^2 = 1.19 \times 10^{-2}$ ) and reverse cholesterol transport PRS ( $p = 0.003$ ,  $R^2 = 1.09 \times 10^{-2}$ ). Similar trends toward association with the left amygdala and left caudate were observed in the PRS for protein–lipid complex assembly, regulation of A $\beta$  formation, regulation of amyloid precursor protein catabolic process, tau protein binding, and plasma lipoprotein particle assembly pathways. However, none of these associations withstood correction for multiple comparisons. There was also some evidence of association between some pathway PRS and increased left hippocampal volume, but again this was no longer significant when corrected for multiple testing using FDR. There were no significant association between the immune response pathway PRS and subcortical volume in any region. None of the PRS showed statistically significant associations with the *APOE* region excluded. SNPs in the *APOE* region alone were positively associated with volume in the left caudate ( $p = 0.002$ ,  $R^2 = 1.18 \times 10^{-2}$ ) and there was trend toward association with the right caudate, although not with FDR correction applied. See Tables 5.1-5.4 for a summary of results for each PRS.

Secondary analysis of ALSPAC subcortical volumes and PRS across a range of  $P^T$  showed that the association between AD PRS and increased grey matter volumes persisted, particularly with more inclusive  $P^T$ . Associations between subcortical grey matter and PRS at all thresholds is shown in Figure 5.1 and Figure 5.2.

**Table 5.1 Results for ALSPAC subcortical volumes and PRS including APOE at  $P^T$  0.001**

	L Accumbens	L Amygdala	L Caudate	L Hippocampus	L Pallidum	L Putamen	L Thalamus
	$R^2$ p (CI)	$R^2$ p (CI)	$R^2$ p (CI)	$R^2$ p (CI)	$R^2$ p (CI)	$R^2$ p (CI)	$R^2$ p (CI)
<b>Polygenic risk score</b>							
<b>Protein-lipid complex assembly</b>	4.92E-05 0.861 (-8.845,10.586)	9.96E-03 0.009 (5.603,37.889)*	9.84E-03 0.005 (16.118,89.558)*	6.90E-03 0.037 (3.384,101.603)*	4.53E-03 0.059 (-0.475,25.891)	3.35E-03 0.080 (-4.305,78.068)	2.79E-03 0.075 (-97.677,4.577)
<b>Regulation of A<math>\beta</math> formation</b>	2.39E-06 0.969 (-9.696,10.085)	7.63E-03 0.021 (2.898,35.642)*	6.15E-03 0.027 (5.034,80.016)*	3.81E-03 0.121 (-10.334,89.096)	5.85E-03 0.032 (1.299,28.149)*	3.09E-03 0.093 (-5.897,77.977)	2.59E-03 0.086 (-97.714,6.402)
<b>Protein-lipid complex</b>	9.17E-06 0.940 (-9.424,10.182)	8.45E-03 0.016 (3.893,36.438)*	1.19E-02 0.002 (21.602,95.578)**	7.75E-03 0.027 (6.593,105.482)*	3.28E-03 0.109 (-2.407,24.208)	3.33E-03 0.081 (-4.473,78.639)	2.16E-03 0.117 (-92.967,10.277)
<b>Regulation of amyloid precursor protein catabolism</b>	2.39E-06 0.969 (-9.696,10.085)	7.63E-03 0.021 (2.898,35.642)*	6.15E-03 0.027 (5.034,80.016)*	3.81E-03 0.121 (-10.334,89.096)	5.85E-03 0.032 (1.299,28.149)*	3.09E-03 0.093 (-5.897,77.977)	2.59E-03 0.086 (-97.714,6.402)
<b>Tau protein binding</b>	4.58E-06 0.957 (-9.555,10.092)	7.88E-03 0.019 (3.204,35.805)*	1.03E-02 0.004 (17.481,91.705)*	6.65E-03 0.040 (2.445,101.460)*	4.28E-03 0.067 (-0.840,25.813)	3.07E-03 0.093 (-5.934,77.369)	1.92E-03 0.140 (-90.768,12.717)
<b>Reverse cholesterol transport</b>	1.26E-04 0.779 (-8.349,11.141)	7.67E-03 0.021 (2.917,35.287)*	1.09E-02 0.003 (19.092,92.695)**	7.72E-03 0.027 (6.439,104.717)*	4.36E-03 0.064 (-0.719,25.712)	3.49E-03 0.074 (-3.517,79.101)	1.35E-03 0.216 (-83.814,18.925)
<b>Protein-lipid complex subunit organization</b>	3.98E-05 0.875 (-8.946,10.513)	1.06E-02 0.007 (6.278,38.571)**	9.11E-03 0.007 (14.113,87.700)**	6.04E-03 0.051 (-0.038,98.247)	5.87E-03 0.032 (1.307,27.693)*	3.40E-03 0.077 (-4.002,78.483)	3.07E-03 0.062 (-100.099,2.267)
<b>Plasma lipoprotein particle assembly</b>	2.08E-07 0.991 (-9.722,9.836)	8.50E-03 0.015 (3.952,36.499)*	9.29E-03 0.006 (14.695,88.646)*	6.56E-03 0.042 (2.056,100.954)*	3.98E-03 0.077 (-1.282,25.260)	3.98E-03 0.056 (-0.972,81.890)	3.95E-03 0.034 (-107.168,-4.383)*
<b>Activation of immune response</b>	5.94E-05 0.847 (-10.779,8.848)	4.55E-04 0.575 (-11.634,20.960)	2.28E-04 0.670 (-29.259,45.495)	4.54E-05 0.866 (-53.535,45.025)	2.76E-03 0.141 (-3.269,23.115)	1.36E-05 0.911 (-44.103,39.356)	1.17E-04 0.716 (-42.172,61.429)
<b>Genome-wide PRS</b>	2.56E-03 0.205 (-3.442,16.075)	2.10E-03 0.228 (-6.203,26.049)	1.27E-03 0.315 (-18.093,56.292)	1.34E-03 0.359 (-26.259,72.612)	1.46E-04 0.736 (-10.958,15.518)	2.28E-04 0.648 (-31.872,51.229)	1.40E-04 0.690 (-62.074,41.099)

$R^2$  and p values for subcortical volumes in the left hemisphere and each polygenic score at a  $P^T$  of 0.001. The column names show the region of interest, while the row names show the polygenic scores.

\* Nominally significant associations (p value < .05).

\*\* FDR corrected associations <0.05.

Acronyms: PRS = Polygenic Risk Score;  $P^T$  = polygenic threshold; APOE = Apolipoprotein E; L = left; R = right; FDR = false discovery rate.

**Table 5.2 Results for ALSPAC subcortical volumes and PRS excluding APOE at P<sup>T</sup> 0.001**

	L Accumbens	L Amygdala	L Caudate	L Hippocampus	L Pallidum	L Putamen	L Thalamus
Polygenic risk score	R <sup>2</sup> p (CI)	R <sup>2</sup> p (CI)	R <sup>2</sup> p (CI)	R <sup>2</sup> p (CI)	R <sup>2</sup> p (CI)	R <sup>2</sup> p (CI)	R <sup>2</sup> p (CI)
Protein-lipid complex assembly (-APOE)	1.04E-04 0.799 (-8.714,11.318)	8.37E-04 0.447 (-10.189,23.102)	1.86E-03 0.224 (-14.443,61.758)	3.72E-03 0.126 (-11.011,90.386)	4.61E-04 0.548 (-17.628,9.353)	1.79E-05 0.898 (-39.809,45.376)	2.30E-03 0.106 (-9.116,96.366)
Regulation of Aβ formation (-APOE)	1.57E-05 0.921 (-9.198,10.180)	4.56E-06 0.955 (-15.525,16.440)	1.23E-04 0.755 (-42.790,31.016)	1.55E-04 0.755 (-56.553,41.006)	4.03E-04 0.574 (-9.316,16.810)	2.96E-05 0.869 (-44.652,37.741)	4.22E-04 0.489 (-33.058,69.187)
Protein-lipid complex (-APOE)	9.09E-04 0.451 (-13.769,6.115)	1.08E-03 0.387 (-9.182,23.691)	1.77E-03 0.236 (-14.919,60.759)	3.00E-03 0.169 (-15.000,85.898)	3.91E-03 0.080 (-25.327,1.394)	5.07E-05 0.830 (-46.944,37.647)	2.12E-04 0.624 (-39.359,65.638)
Regulation of amyloid precursor protein catabolism (-APOE)	1.57E-05 0.921 (-9.198,10.180)	4.56E-06 0.955 (-15.525,16.440)	1.23E-04 0.755 (-42.790,31.016)	1.55E-04 0.755 (-56.553,41.006)	4.03E-04 0.574 (-9.316,16.810)	2.96E-05 0.869 (-44.652,37.741)	4.22E-04 0.489 (-33.058,69.187)
Tau protein binding (-APOE)	2.87E-03 0.180 (-16.724,3.134)	2.65E-04 0.669 (-12.937,20.157)	1.07E-04 0.770 (-43.527,32.243)	4.68E-04 0.587 (-36.319,64.182)	1.07E-03 0.361 (-19.638,7.142)	1.22E-03 0.290 (-65.056,19.436)	2.41E-03 0.098 (-8.080,96.647)
Reverse cholesterol transport (-APOE)	2.73E-04 0.680 (-7.859,12.060)	1.46E-04 0.751 (-13.875,19.239)	4.51E-04 0.549 (-26.334,49.529)	3.45E-03 0.140 (-12.400,88.365)	1.63E-04 0.721 (-15.862,10.974)	7.14E-06 0.936 (-40.610,44.103)	5.06E-03 0.016 (11.983,116.551)*
Protein-lipid complex subunit organization (-APOE)	8.96E-05 0.813 (-8.838,11.267)	4.78E-03 0.069 (-1.159,32.005)	6.36E-04 0.477 (-24.369,52.183)	1.76E-03 0.292 (-23.413,78.074)	2.35E-03 0.175 (-4.158,22.894)	3.60E-05 0.856 (-38.791,46.701)	3.67E-03 0.041 (2.427,108.127)*
Plasma lipoprotein particle assembly (-APOE)	1.87E-05 0.914 (-9.359,10.452)	2.18E-04 0.698 (-19.771,13.242)	1.22E-03 0.325 (-18.732,56.659)	1.98E-03 0.264 (-21.495,78.708)	3.87E-03 0.081 (-25.154,1.454)	1.63E-08 0.997 (-42.202,42.036)	2.33E-04 0.607 (-38.548,66.004)
Activation of immune response (-APOE)	2.43E-04 0.697 (-7.741,11.583)	9.04E-04 0.430 (-9.580,22.522)	4.76E-04 0.538 (-48.358,25.236)	1.48E-03 0.334 (-24.551,72.447)	1.13E-03 0.348 (-6.771,19.245)	1.05E-03 0.328 (-61.559,20.544)	9.53E-05 0.742 (-42.452,59.564)
Genome-wide PRS (-APOE)	7.16E-03 0.034 (0.828,20.394)*	2.21E-04 0.696 (-13.092,19.614)	6.04E-04 0.488 (-50.661,24.169)	8.12E-04 0.475 (-31.514,67.763)	2.67E-04 0.648 (-16.337,10.157)	6.32E-05 0.810 (-36.658,46.907)	3.96E-04 0.503 (-34.113,69.592)
APOE SNPs PRS	1.64E-03 0.310 (-14.782,4.693)	4.23E-03 0.087 (-2.052,30.633)	1.18E-02 0.002 (21.155,94.720)**	5.72E-04 0.548 (-34.505,65.012)	2.50E-03 0.161 (-3.760,22.687)	2.57E-04 0.628 (-31.191,51.684)	3.03E-03 0.063 (-99.992,2.567)

R<sup>2</sup> and p values for subcortical volumes in the left hemisphere and each polygenic score at a P<sup>T</sup> of 0.001. The column names shows the region of interest, while the row names show the polygenic scores.

\* Nominally significant associations (p value < .05).

\*\* FDR corrected associations <0.05.

Acronyms: PRS = Polygenic Risk Score; PT = polygenic threshold; APOE = Apolipoprotein E; L = left; R = right; FDR = false discovery rate.

**Table 5.3 Results for ALSPAC subcortical volumes and PRS including APOE at P<sup>T</sup> 0.001**

	R Accumbens	R Amygdala	R Caudate	R Hippocampus	R Pallidum	R Putamen	R Thalamus
	R <sup>2</sup> p (CI)						
Polygenic risk score							
Protein-lipid complex assembly	0.188 (-2.632,13.463)	0.128 (-3.169,25.263)	0.028 (4.476,78.109)*	0.190 (-12.686,64.014)	0.416 (-6.491,15.707)	0.403 (-22.475,56.017)	0.426 (-60.367,25.467)
Regulation of Aβ formation	0.454 (-5.075,11.354)	0.063 (-0.730,28.238)	0.050 (0.015,75.045)	0.179 (-12.248,65.903)	0.584 (-8.140,14.466)	0.195 (-13.473,66.352)	0.266 (-68.492,18.833)
Protein-lipid complex	1.86E-03	2.76E-03	7.38E-03	2.49E-03	4.33E-04	7.42E-04	2.98E-04
	0.273 (-3.574,12.681)	0.154 (-3.885,24.781)	0.017 (8.134,82.362)*	0.164 (-11.215,66.326)	0.531 (-7.616,14.787)	0.408 (-22.853,56.343)	0.551 (-56.485,30.142)
Regulation of amyloid precursor protein catabolism	0.454 (-5.075,11.354)	0.063 (-0.730,28.238)	0.050 (0.015,75.045)	0.179 (-12.248,65.903)	0.584 (-8.140,14.466)	0.195 (-13.473,66.352)	0.266 (-68.492,18.833)
	8.65E-04	4.67E-03	4.99E-03	2.33E-03	3.31E-04	1.82E-03	1.04E-03
Tau protein binding	1.55E-03	2.95E-03	6.33E-03	2.17E-03	7.71E-04	8.54E-04	1.34E-04
	0.317 (-3.982,12.311)	0.140 (-3.531,25.166)	0.027 (4.786,79.229)*	0.195 (-13.096,64.432)	0.403 (-6.425,16.018)	0.374 (-21.674,57.678)	0.690 (-52.248,34.575)
Reverse cholesterol transport	2.23E-03	2.45E-03	6.47E-03	2.47E-03	7.24E-04	7.70E-04	5.85E-05
	0.230 (-3.121,13.035)	0.179 (-4.460,24.062)	0.026 (5.211,79.061)*	0.167 (-11.281,65.649)	0.417 (-6.524,15.744)	0.399 (-22.408,56.327)	0.792 (-48.877,37.272)
Protein-lipid complex subunit organization	2.51E-03	3.74E-03	5.91E-03	2.06E-03	1.28E-03	8.72E-04	5.58E-04
	0.203 (-2.812,13.308)	0.097 (-2.145,26.315)	0.033 (3.297,77.055)*	0.206 (-13.605,63.170)	0.280 (-4.985,17.234)	0.369 (-21.285,57.310)	0.415 (-60.865,25.088)
Plasma lipoprotein particle assembly	2.81E-03	2.72E-03	6.31E-03	1.83E-03	2.37E-04	9.92E-04	8.95E-04
	0.177 (-2.519,13.681)	0.157 (-3.947,24.652)	0.028 (4.687,78.798)*	0.233 (-15.075,62.052)	0.643 (-8.530,13.824)	0.338 (-20.178,58.809)	0.302 (-65.947,20.410)
Activation of immune response	3.50E-06	7.10E-04	4.15E-05	1.77E-04	1.85E-06	7.77E-06	1.38E-05
	0.962 (-8.340,7.944)	0.469 (-19.530,8.995)	0.859 (-33.968,40.765)	0.711 (-31.025,45.477)	0.967 (-11.454,10.984)	0.933 (-41.385,37.955)	0.898 (-40.537,46.218)
Genome-wide PRS	2.36E-03	1.56E-03	1.57E-04	1.32E-03	6.18E-04	2.83E-05	1.14E-03
	0.216 (-2.984,13.207)	0.284 (-6.452,22.038)	0.729 (-30.638,43.782)	0.312 (-18.465,57.955)	0.454 (-15.439,6.894)	0.872 (-36.247,42.766)	0.244 (-68.805,17.479)

R<sup>2</sup> and p values for subcortical volumes in the right hemisphere and each polygenic score at a P<sup>T</sup> of 0.001. The column names shows the region of interest, while the row names show the polygenic scores.

\* Nominally significant associations (p value < .05).

\*\* FDR corrected associations <0.05.

Acronyms: PRS = Polygenic Risk Score; PT = polygenic threshold; APOE = Apolipoprotein E; L = left; R = right; FDR = false discovery rate.

**Table 5.4 Results for ALSPAC subcortical volumes and PRS excluding APOE at  $P^T$  0.001**

Polygenic risk score	R Accumbens		R Amygdala		R Caudate		R Hippocampus		R Pallidum		R Putamen		R Thalamus		
	R <sup>2</sup> p (CI)														
Protein-lipid complex assembly (-APOE)	0.888 (-7.712,8.902)	0.854 (-15.877,13.151)	0.479 (-24.327,51.915)	0.574 (-27.708,50.024)	0.703 (-13.678,9.221)	0.673 (-49.195,31.772)	0.462 (-27.619,60.883)								
Regulation of A $\beta$ formation (-APOE)	0.330 (-12.056,4.042)	0.353 (-7.398,20.733)	0.954 (-35.806,37.975)	0.496 (-24.568,50.701)	0.726 (-13.052,9.097)	0.423 (-23.120,55.159)	0.735 (-50.230,35.410)								
Protein-lipid complex (-APOE)	0.404 (-11.759,4.728)	0.851 (-13.039,15.797)	0.477 (-24.118,51.594)	0.618 (-28.939,48.717)	0.171 (-19.285,3.415)	0.730 (-47.288,33.121)	0.716 (-52.119,35.805)								
Regulation of amyloid precursor protein catabolism (-APOE)	0.330 (-12.056,4.042)	0.353 (-7.398,20.733)	0.954 (-35.806,37.975)	0.496 (-24.568,50.701)	0.726 (-13.052,9.097)	0.423 (-23.120,55.159)	0.735 (-50.230,35.410)								
Tau protein binding (-APOE)	0.029 (-17.367,-0.947)*	0.571 (-10.253,18.588)	0.545 (-49.543,26.174)	0.902 (-41.238,36.343)	0.706 (-13.557,9.181)	0.923 (-42.192,38.218)	0.249 (-18.067,69.744)								
Reverse cholesterol transport (-APOE)	0.817 (-9.237,7.284)	0.812 (-16.165,12.666)	0.945 (-39.265,36.592)	0.597 (-28.186,49.005)	0.738 (-13.329,9.443)	0.806 (-45.314,35.213)	0.123 (-9.272,78.578)								
Protein-lipid complex subunit organization (-APOE)	0.748 (-9.705,6.968)	0.360 (-7.776,21.415)	0.722 (-31.325,45.223)	0.706 (-31.572,46.632)	0.055 (-0.227,22.674)	0.845 (-44.691,36.581)	0.255 (-18.584,70.174)								
Plasma lipoprotein particle assembly (-APOE)	0.698 (-6.585,9.842)	0.385 (-20.669,7.969)	0.539 (-25.882,49.521)	0.677 (-30.211,46.537)	0.062 (-22.073,0.495)	0.692 (-48.140,31.927)	0.928 (-41.763,45.801)								
Activation of immune response (-APOE)	0.873 (-7.359,8.672)	0.740 (-16.375,11.631)	0.232 (-59.159,14.327)	0.666 (-29.330,45.902)	0.506 (-14.794,7.290)	0.465 (-53.603,24.481)	0.888 (-45.782,39.643)								
Genome-wide PRS (-APOE)	0.286 (-3.700,12.580)	0.474 (-9.016,19.418)	0.304 (-56.986,17.768)	0.478 (-24.308,51.953)	0.442 (-15.630,6.824)	0.666 (-30.971,48.459)	0.488 (-58.773,28.056)								
APOE SNPs PRS	0.527 (-5.477,10.702)	0.376 (-7.841,20.766)	0.019 (7.325,81.149)*	0.433 (-23.104,53.389)	0.851 (-32.209,10.076)	0.695 (-47.277,31.514)	0.269 (-67.344,18.719)								

R<sup>2</sup> and p values for subcortical volumes in the right hemisphere and each polygenic score at a  $P^T$  of 0.001. The column names shows the region of interest, while the row names show the polygenic scores.

\* Nominally significant associations (p value < .05).

\*\* FDR corrected associations <0.05.

Acronyms: PRS = Polygenic Risk Score; PT = polygenic threshold; APOE = Apolipoprotein E; L = left; R = right; FDR = false discovery rate.

**Figure 5.1** Associations between genome-wide PRS and subcortical volumes in ALSPAC. Imaging phenotypes are shown on the X axis, the beta coefficients (positive and negative) are shown on the Y axis. The heights of the bars indicate the amount of variance explained ( $R^2$ ), and any nominally significant results are labelled with their p value. Each bar represents a version of the polygenic risk score. The bars are colour coded by the p value threshold used in the training data, shown on the legend.

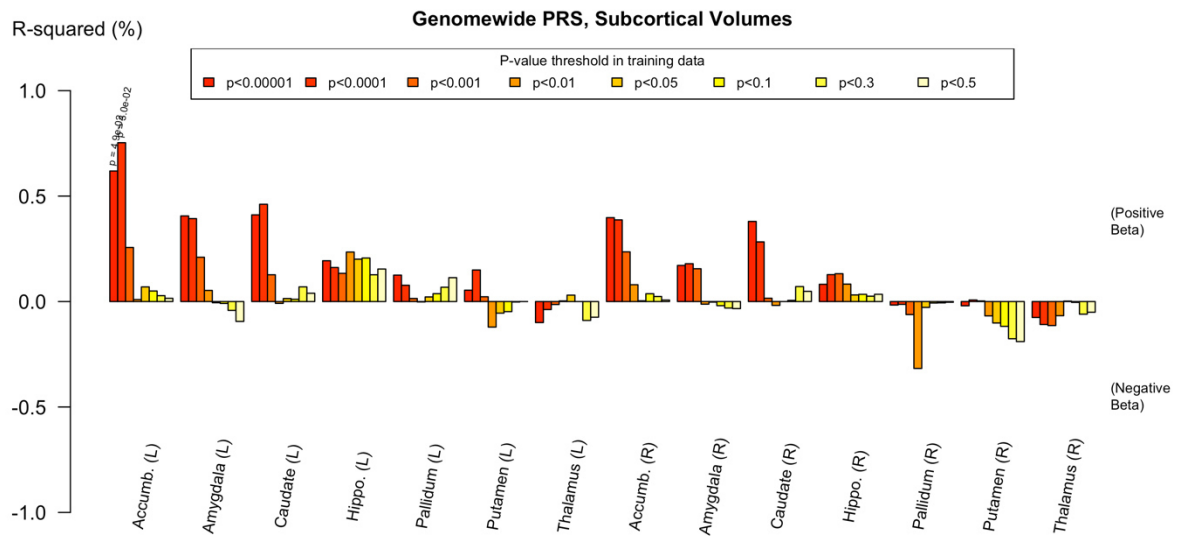


**Figure 5.2** Associations between protein-lipid complex PRS and subcortical volumes in ALSPAC. Imaging phenotypes are shown on the X axis, the beta coefficients (positive and negative) are shown on the Y axis. The heights of the bars indicate the amount of variance explained ( $R^2$ ), and any nominally significant results are labelled with their p value. Each bar represents a version of the PRS. The bars are colour coded by the p value threshold used in the training data, shown on the legend.

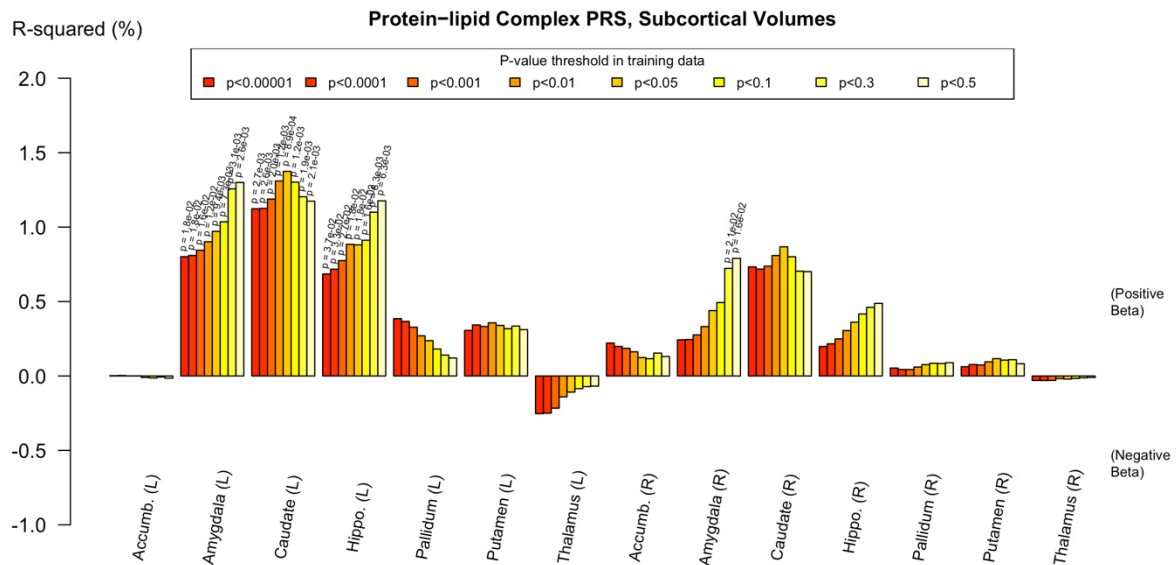
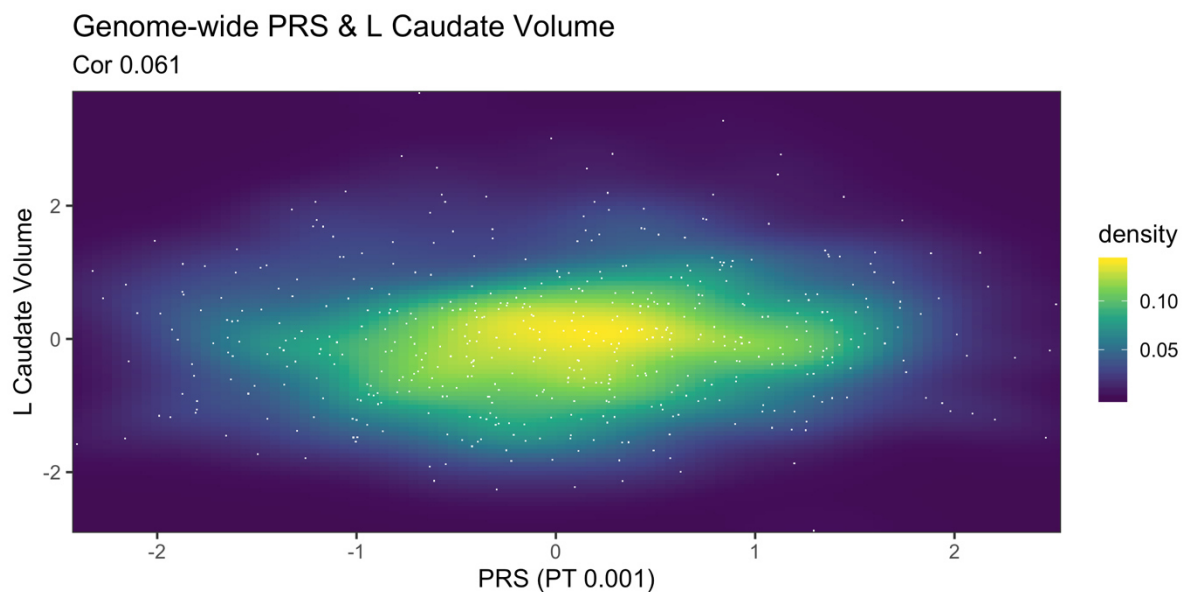


**Figure 5.3** Scatterplot showing normalised genome wide PRS and normalised left caudate volume in ALSPAC. White circles indicate individual data points. Density represents the number of data points in each area.



#### 5.4.2 Subcortical Volumes in UK Biobank

In UK Biobank, there were negative associations between genome-wide PRS and volume in the left and right nucleus accumbens ( $p = 4.31 \times 10^{-4}$ ,  $R^2 = 5.79 \times 10^{-4}$  and  $p = 0.001$ ,  $R^2 = 5.26 \times 10^{-4}$  respectively), and the left hippocampus ( $p = 3.57 \times 10^{-4}$ ,  $R^2 = 9.49 \times 10^{-5}$ ) which withstood FDR correction for multiple comparisons (see Tables 5.5 to 5.8). There was also a nominally significant association with the left and right thalamus ( $p = 0.021$ ,  $R^2 = 1.74 \times 10^{-4}$  and  $p = 0.046$ ,  $R^2 = 1.8 \times 10^{-4}$  respectively). There were no significant positive associations. However, all of these associations attenuated when the *APOE* region was removed from the PRS ( $p > 0.05$ ).

The protein–lipid complex assembly PRS had a similar pattern of association as the genome-wide PRS, with negative associations between pathway PRS and volume in the left and right accumbens ( $p = 6.64 \times 10^{-6}$ ,  $R^2 = 9.49 \times 10^{-4}$  and  $p = 0.01$ ,  $R^2 = 2.97 \times 10^{-4}$  respectively), the left and right hippocampus ( $p = 8.57 \times 10^{-5}$ ,  $R^2 = 5.93 \times 10^{-4}$  and  $p = 0.01$ ,  $R^2 = 2.44 \times 10^{-4}$  respectively) which remained after correction for multiple testing. Without the *APOE* region, the results remained significant in those regions with comparable  $p$  values (see Tables 5.6 and 5.8). Similar results were observed in the regulation of A $\beta$  formation, protein–lipid complex, regulation of amyloid precursor protein catabolic process, tau protein binding, protein–lipid complex subunit organization and plasma lipoprotein particle assembly pathways. There were significant negative associations in the left and right accumbens and left and right hippocampus ( $p$  range  $6.69 \times 10^{-6}$  to 0.001), even when the *APOE* region was removed. Slightly different results were observed for the immune response PRS, which was negatively associated with volume in the left hippocampus ( $p = 0.003$ ,  $R^2 = 3.32 \times 10^{-4}$ ) and right accumbens ( $p = 0.005$ ,  $R^2 = 3.64 \times 10^{-4}$ ). However, when the *APOE* region was excluded from the score, these results did not withstand correction for multiple testing.

SNPs in the *APOE* region were significantly negatively associated with the volume of the left and right accumbens ( $p = 4.91 \times 10^{-6}$ ,  $R^2 = 9.76 \times 10^{-4}$  and  $p = 4.6 \times 10^{-4}$ ,  $R^2 = 5.53 \times 10^{-4}$  respectively), left and right hippocampus ( $p = 4.78 \times 10^{-4}$ ,  $R^2 = 4.78 \times 10^{-4}$  and  $p = 0.011$ ,  $R^2 = 2.41 \times 10^{-4}$  respectively), left and right thalamus ( $p = 0.021$ ,  $R^2 = 1.73 \times 10^{-4}$  and  $p = 0.006$ ,  $R^2 = 1.73 \times 10^{-4}$  respectively) and right caudate ( $p = 0.012$ ,

$R^2 = 2.43 \times 10^{-4}$ ). There was also a trend towards a negative association in the left caudate although this did not survive correction for multiple testing. The results are summarised in Tables 5.5 to 5.8, and those surviving FDR correction for multiple comparisons of PRS and phenotype are indicated. Secondary analysis of subcortical volumes and PRS across a range of  $P^T$ , with and without the *APOE* region, showed that the association between AD PRS and decreased grey matter volumes persisted, particularly with more inclusive  $P^T$ . Associations between subcortical grey matter and genome wide PRS at all thresholds is shown in Figure 5.1.

**Table 5.5 Results for UK Biobank subcortical volumes and PRS including APOE at  $P^T$  0.001**

	L Accumbens		L Amygdala		L Caudate		L Hippocampus		L Pallidum		L Putamen		L Thalamus	
	$R^2$	p (CI)	$R^2$	p (CI)	$R^2$	p (CI)	$R^2$	p (CI)	$R^2$	p (CI)	$R^2$	p (CI)	$R^2$	p (CI)
<b>Polygenic risk score</b>														
<b>Protein-lipid complex assembly</b>	9.49E-04	6.64E-06 (-5.056,-1.991)**	9.42E-05	0.117 (-5.177,0.575)	8.22E-05	0.152 (-9.897,1.536)	5.93E-04	8.57E-05 (-17.048,-5.700)**	2.29E-05	0.489 (-2.186,4.574)	4.12E-07	0.921 (-9.294,8.403)	1.23E-04	0.052 (-24.365,0.129)
<b>Regulation of A<math>\beta</math> formation</b>	9.48E-04	6.69E-06 (-5.055,-1.990)**	9.43E-05	0.117 (-5.179,0.573)	8.25E-05	0.151 (-9.903,1.529)	5.93E-04	8.53E-05 (-17.051,-5.703)**	2.28E-05	0.490 (-2.190,4.570)	4.31E-07	0.920 (-9.304,8.393)	1.23E-04	0.052 (-24.365,0.129)
<b>Protein-lipid complex</b>	9.48E-04	6.69E-06 (-5.054,-1.989)**	9.44E-05	0.116 (-5.180,0.572)	8.27E-05	0.150 (-9.910,1.523)	5.94E-04	8.44E-05 (-17.059,-5.710)**	2.26E-05	0.482 (-2.195,4.566)	4.46E-07	0.918 (-9.312,8.385)	1.23E-04	0.053 (-24.361,0.133)
<b>Regulation of amyloid precursor protein catabolism</b>	9.47E-04	6.74E-06 (-5.053,-1.988)**	9.44E-05	0.116 (-5.180,0.572)	8.29E-05	0.150 (-9.915,1.518)	5.94E-04	8.41E-05 (-17.061,-5.713)**	2.25E-05	0.493 (-2.199,4.562)	4.60E-07	0.917 (-9.319,8.378)	1.23E-04	0.053 (-24.355,0.139)
<b>Tau protein binding</b>	9.47E-04	6.78E-06 (-5.052,-1.987)**	9.44E-05	0.116 (-5.180,0.572)	8.32E-05	0.149 (-9.921,1.511)	5.95E-04	8.35E-05 (-17.066,-5.718)**	2.23E-05	0.494 (-2.202,4.559)	4.74E-07	0.916 (-9.326,8.370)	1.23E-04	0.053 (-24.352,0.142)
<b>Reverse cholesterol transport</b>	9.46E-04	6.81E-06 (-5.052,-1.987)**	9.44E-05	0.116 (-5.180,0.572)	8.34E-05	0.149 (-9.927,1.505)	5.95E-04	8.32E-05 (-17.069,-5.721)**	2.23E-05	0.495 (-2.204,4.557)	4.85E-07	0.915 (-9.332,8.365)	1.23E-04	0.053 (-24.349,0.145)
<b>Protein-lipid complex subunit organization</b>	9.46E-04	6.83E-06 (-5.051,-1.986)**	9.44E-05	0.116 (-5.180,0.572)	8.36E-05	0.148 (-9.932,1.500)	5.95E-04	8.29E-05 (-17.071,-5.723)**	2.22E-05	0.495 (-2.205,4.556)	4.95E-07	0.914 (-9.337,8.360)	1.23E-04	0.053 (-24.348,0.146)
<b>Plasma lipoprotein particle assembly</b>	9.46E-04	6.87E-06 (-5.050,-1.985)**	9.43E-05	0.117 (-5.179,0.573)	8.38E-05	0.148 (-9.936,1.497)	5.95E-04	8.28E-05 (-17.072,-5.724)**	2.22E-05	0.496 (-2.205,4.555)	5.00E-07	0.913 (-9.339,8.358)	1.23E-04	0.053 (-24.350,0.144)
<b>Activation of immune response</b>	1.45E-04	0.079 (-2.908,0.158)	1.00E-05	0.609 (-3.625,2.126)	1.30E-04	0.071 (-10.971,0.459)	3.32E-04	0.003 (-14.183,-2.835)**	1.83E-04	0.051 (-6.747,0.011)	1.78E-04	0.040 (-18.100,-0.410)*	1.05E-04	0.073 (-23.449,1.039)
<b>Genome-wide PRS</b>	5.79E-04	4.31E-04 (-4.286,-1.221)**	1.30E-05	0.560 (-3.730,2.022)	1.61E-05	0.525 (-7.569,3.864)	3.57E-04	0.002 (-14.506,-3.156)**	7.04E-06	0.701 (-2.719,4.042)	3.20E-08	0.978 (-9.724,8.972)	1.74E-04	0.021 (-26.651,-2.159)*

R<sup>2</sup> and p values for subcortical volumes in the left hemisphere and each polygenic score at a  $P^T$  of 0.001. The column names shows the region of interest, while the row names show the polygenic scores.

\* Nominally significant associations (p value < .05).

\*\* FDR corrected associations <0.05.

Acronyms: PRS = Polygenic Risk Score;  $P^T$  = polygenic threshold; APOE = Apolipoprotein E; L = left; R = right; R<sup>2</sup> = false discovery rate.

**Table 5.6 Results for UK Biobank subcortical volumes and PRS excluding APOE at P<sup>T</sup> 0.001**

	L Accumbens		L Amygdala		L Caudate		L Hippocampus		L Pallidum		L Putamen		L Thalamus	
	R <sup>2</sup>	p (CI)	R <sup>2</sup>	p (CI)	R <sup>2</sup>	p (CI)	R <sup>2</sup>	p (CI)	R <sup>2</sup>	p (CI)	R <sup>2</sup>	p (CI)	R <sup>2</sup>	p (CI)
Polygenic risk score														
Protein-lipid complex assembly (-APOE)	9.49E-04	6.64E-06 (-5.056,-1.991)**	9.43E-05	0.117 (-5.179,0.573)	8.22E-05	0.152 (-9.896,1.537)	5.93E-04	8.55E-05 (-17.050,-5.701)**	2.29E-05	0.489 (-2.187,4.573)	4.18E-07	0.921 (-9.297,8.400)	1.23E-04	0.052 (-24.373,0.121)
Regulation of Aβ formation (-APOE)	9.48E-04	6.65E-06 (-5.056,-1.991)**	9.43E-05	0.116 (-5.179,0.573)	8.26E-05	0.151 (-9.905,1.527)	5.94E-04	8.49E-05 (-17.054,-5.706)**	2.28E-05	0.490 (-2.190,4.570)	4.33E-07	0.919 (-9.305,8.392)	1.23E-04	0.052 (-24.367,0.127)
Protein-lipid complex (-APOE)	9.48E-04	6.70E-06 (-5.054,-1.989)**	9.44E-05	0.116 (-5.180,0.572)	8.27E-05	0.151 (-9.909,1.524)	5.94E-04	8.44E-05 (-17.058,-5.710)**	2.26E-05	0.492 (-2.195,4.566)	4.47E-07	0.918 (-9.312,8.385)	1.23E-04	0.053 (-24.362,0.132)
Regulation of amyloid precursor protein catabolism (-APOE)	9.47E-04	6.72E-06 (-5.054,-1.989)**	9.44E-05	0.116 (-5.180,0.572)	8.30E-05	0.150 (-9.915,1.517)	5.94E-04	8.39E-05 (-17.063,-5.714)**	2.25E-05	0.493 (-2.199,4.562)	4.61E-07	0.917 (-9.320,8.377)	1.23E-04	0.053 (-24.356,0.138)
Tau protein binding (-APOE)	9.47E-04	6.77E-06 (-5.053,-1.988)**	9.44E-05	0.116 (-5.180,0.572)	8.32E-05	0.149 (-9.922,1.511)	5.95E-04	8.35E-05 (-17.066,-5.718)**	2.23E-05	0.494 (-2.202,4.559)	4.75E-07	0.916 (-9.327,8.370)	1.23E-04	0.053 (-24.352,0.142)
Reverse cholesterol transport (-APOE)	9.46E-04	6.81E-06 (-5.052,-1.987)**	9.44E-05	0.116 (-5.180,0.572)	8.34E-05	0.149 (-9.927,1.506)	5.95E-04	8.32E-05 (-17.069,-5.720)**	2.23E-05	0.495 (-2.204,4.557)	4.86E-07	0.915 (-9.332,8.365)	1.23E-04	0.053 (-24.350,0.144)
Protein-lipid complex subunit organization (-APOE)	9.46E-04	6.83E-06 (-5.051,-1.986)**	9.44E-05	0.116 (-5.180,0.572)	8.36E-05	0.148 (-9.932,1.500)	5.95E-04	8.29E-05 (-17.072,-5.723)**	2.22E-05	0.496 (-2.205,4.556)	4.96E-07	0.914 (-9.337,8.360)	1.23E-04	0.053 (-24.349,0.145)
Plasma lipoprotein particle assembly (-APOE)	9.46E-04	6.85E-06 (-5.050,-1.986)**	9.44E-05	0.116 (-5.180,0.572)	8.38E-05	0.148 (-9.936,1.496)	5.96E-04	8.27E-05 (-17.073,-5.725)**	2.22E-05	0.496 (-2.206,4.555)	5.03E-07	0.913 (-9.340,8.356)	1.23E-04	0.053 (-24.348,0.146)
Activation of immune response (-APOE)	5.73E-05	0.268 (-2.399,0.667)	5.49E-07	0.905 (-3.051,2.700)	1.22E-04	0.081 (-10.800,0.629)	2.04E-04	0.021 (-12.351,-1.003)*	1.59E-04	0.069 (-6.519,0.240)	1.31E-04	0.078 (-16.797,0.894)	6.91E-05	0.146 (-21.320,3.168)
Genome-wide PRS (-APOE)	4.54E-05	0.324 (-2.305,0.762)	1.67E-05	0.510 (-3.844,1.908)	2.08E-05	0.471 (-3.616,7.818)	5.35E-05	0.238 (-9.094,2.261)	1.86E-06	0.844 (-3.041,3.721)	2.88E-06	0.794 (-7.671,10.028)	4.44E-05	0.244 (-19.526,4.972)
APOE SNPs PRS	9.76E-04	4.91E-06 (-5.102,-2.039)**	3.48E-07	0.924 (-3.014,2.735)	1.63E-04	0.044 (-11.595,-0.170)*	4.78E-04	4.24E-04 (-15.872,-4.530)**	6.85E-06	0.705 (-2.726,4.030)	3.83E-06	0.763 (-10.201,7.485)	1.73E-04	0.021 (-26.614,-2.137)**

R2 and p values for subcortical volumes in the left hemisphere and each polygenic score at a P<sup>T</sup> of 0.001. The column names shows the region of interest, while the row names show the polygenic scores.

\* Nominally significant associations (p value < .05).

\*\* FDR corrected associations <0.05.

Acronyms: PRS = Polygenic Risk Score; PT = polygenic threshold; APOE = Apolipoprotein E; L = left; R = right; FDR = false discovery rate.

**Table 5.7 Results for UK Biobank subcortical volumes and PRS including APOE at P<sup>T</sup> 0.001**

	R Accumbens	R Amygdala	R Caudate	R Hippocampus	R Putamen	R Thalamus
	R <sup>2</sup> p (CI)	R <sup>2</sup> p (CI)	R <sup>2</sup> p (CI)	R <sup>2</sup> p (CI)	R <sup>2</sup> p (CI)	R <sup>2</sup> p (CI)
Polygenic risk score						
Protein-lipid complex assembly	2.97E-04 0.010 (-3.184,-0.427)**	6.13E-05 0.204 (-4.722,1.006)	1.76E-04 0.033 (-12.231,-0.527)*	2.44E-04 0.010 (-13.261,-1.783)**	1.34E-04 0.068 (-14.359,0.503)	7.62E-05 0.109 (-14.378,1.448)
Regulation of Aβ formation	2.98E-04 0.010 (-3.186,-0.429)**	6.16E-05 0.203 (-4.726,1.002)	1.76E-04 0.033 (-12.236,-0.532)*	2.44E-04 0.010 (-13.265,-1.787)**	1.34E-04 0.067 (-14.368,0.494)	7.63E-05 0.109 (-14.379,1.448)
Protein-lipid complex	2.98E-04 0.010 (-3.186,-0.429)**	6.16E-05 0.203 (-4.726,1.002)	1.77E-04 0.032 (-12.243,-0.538)*	2.44E-04 0.010 (-13.270,-1.791)**	1.34E-04 0.067 (-14.371,0.491)	7.64E-05 0.109 (-14.384,1.443)
Regulation of amyloid precursor protein catabolism	2.98E-04 0.010 (-3.187,-0.430)**	6.17E-05 0.202 (-4.728,1.000)	1.77E-04 0.032 (-12.246,-0.542)*	2.44E-04 0.010 (-13.271,-1.793)**	1.34E-04 0.067 (-14.375,0.487)	7.64E-05 0.109 (-14.384,1.442)
Tau protein binding	2.98E-04 0.010 (-3.187,-0.430)**	6.18E-05 0.202 (-4.729,0.999)	1.77E-04 0.032 (-12.252,-0.548)*	2.45E-04 0.010 (-13.274,-1.796)**	1.35E-04 0.067 (-14.380,0.482)	7.65E-05 0.109 (-14.388,1.439)
Reverse cholesterol transport	2.98E-04 0.010 (-3.187,-0.430)**	6.18E-05 0.202 (-4.729,0.999)	1.77E-04 0.032 (-12.258,-0.554)*	2.45E-04 0.010 (-13.275,-1.797)**	1.35E-04 0.067 (-14.384,0.478)	7.66E-05 0.109 (-14.392,1.435)
Protein-lipid complex subunit organization	2.98E-04 0.010 (-3.187,-0.430)**	6.18E-05 0.202 (-4.730,0.999)	1.78E-04 0.032 (-12.263,-0.559)*	2.45E-04 0.010 (-13.276,-1.797)**	1.35E-04 0.067 (-14.389,0.474)	7.66E-05 0.108 (-14.395,1.432)
Plasma lipoprotein particle assembly	2.98E-04 0.010 (-3.187,-0.430)**	6.18E-05 0.202 (-4.730,0.998)	1.78E-04 0.032 (-12.266,-0.562)*	2.45E-04 0.010 (-13.277,-1.798)**	1.35E-04 0.066 (-14.391,0.471)	7.67E-05 0.108 (-14.398,1.428)
Activation of immune response	3.64E-04 0.005 (-3.376,-0.620)**	5.80E-05 0.216 (-4.670,1.057)	1.27E-04 0.070 (-11.267,0.434)	1.01E-04 0.098 (-10.576,0.901)	3.97E-04 0.002 (-19.352,-4.497)**	1.39E-04 0.031 (-16.630,-0.808)*
Genome-wide PRS	5.26E-04 0.001 (-3.780,-1.024)**	7.15E-06 0.664 (-3.498,2.230)	8.93E-05 0.128 (-10.399,1.306)	9.49E-05 0.109 (-10.432,1.048)	5.10E-05 0.260 (-4.204,1.135)	4.41E-05 0.046 (-15.957,-0.131)*

R2 and p values for subcortical volumes in the right hemisphere and each polygenic score at a P<sup>T</sup> of 0.001. The column names shows the region of interest, while the row names show the polygenic scores.

\* Nominally significant associations (p value < .05).

\*\* FDR corrected associations <0.05.

Acronyms: PRS = Polygenic Risk Score; PT = polygenic threshold; APOE = Apolipoprotein E; L = left; R = right; FDR = false discovery rate.

**Table 5.8 Results for UK Biobank subcortical volumes and PRS excluding APOE at P<sup>T</sup> 0.001**

Polygenic risk score	R Accumbens		R Amygdala		R Caudate		R Hippocampus		R Pallidum		R Putamen		R Thalamus	
	R <sup>2</sup>	p (CI)	R <sup>2</sup>	p (CI)	R <sup>2</sup>	p (CI)	R <sup>2</sup>	p (CI)	R <sup>2</sup>	p (CI)	R <sup>2</sup>	p (CI)	R <sup>2</sup>	p (CI)
<b>Protein-lipid complex assembly (-APOE)</b>	0.010 (-3.185,-0.428)**	2.97E-04	0.203 (-4.725,1.004)	6.15E-05	1.76E-04	0.033 (-12.230,-0.526)*	0.010 (-13.265,-1.786)**	2.44E-04	3.64E-05	0.341 (-3.966,1.374)	0.068 (-14.362,0.500)	1.34E-04	0.109 (-14.381,1.445)	7.63E-05
<b>Regulation of Aβ formation (-APOE)</b>	0.010 (-3.186,-0.429)**	2.98E-04	0.203 (-4.726,1.003)	6.16E-05	1.76E-04	0.032 (-12.239,-0.535)*	0.010 (-13.267,-1.788)**	2.44E-04	3.66E-05	0.340 (-3.969,1.370)	0.067 (-14.369,0.493)	1.34E-04	0.109 (-14.381,1.445)	7.63E-05
<b>Protein-lipid complex (-APOE)</b>	0.010 (-3.186,-0.429)**	2.98E-04	0.202 (-4.727,1.001)	6.16E-05	1.76E-04	0.032 (-12.242,-0.537)*	0.010 (-13.270,-1.791)**	2.44E-04	3.67E-05	0.339 (-3.972,1.368)	0.067 (-14.371,0.491)	1.34E-04	0.109 (-14.384,1.443)	7.64E-05
<b>Regulation of amyloid precursor protein catabolism (-APOE)</b>	0.010 (-3.187,-0.430)**	2.98E-04	0.202 (-4.728,1.000)	6.17E-05	1.77E-04	0.032 (-12.247,-0.543)*	0.010 (-13.272,-1.794)**	2.45E-04	3.69E-05	0.338 (-3.974,1.365)	0.067 (-14.376,0.486)	1.34E-04	0.109 (-14.385,1.441)	7.64E-05
<b>Tau protein binding (-APOE)</b>	0.010 (-3.187,-0.430)**	2.98E-04	0.202 (-4.729,0.999)	6.18E-05	1.77E-04	0.032 (-12.253,-0.549)*	0.010 (-13.275,-1.796)**	2.45E-04	3.70E-05	0.337 (-3.976,1.363)	0.067 (-14.380,0.482)	1.35E-04	0.109 (-14.388,1.439)	7.65E-05
<b>Reverse cholesterol transport (-APOE)</b>	0.010 (-3.187,-0.430)**	2.98E-04	0.202 (-4.730,0.999)	6.18E-05	1.77E-04	0.032 (-12.258,-0.554)*	0.010 (-13.276,-1.797)**	2.45E-04	3.71E-05	0.337 (-3.978,1.361)	0.067 (-14.384,0.478)	1.35E-04	0.109 (-14.392,1.435)	7.66E-05
<b>Protein-lipid complex subunit organization (-APOE)</b>	0.010 (-3.187,-0.430)**	2.98E-04	0.202 (-4.730,0.998)	6.18E-05	1.78E-04	0.032 (-12.263,-0.559)*	0.010 (-13.277,-1.798)**	2.45E-04	3.72E-05	0.336 (-3.980,1.360)	0.066 (-14.389,0.473)	1.35E-04	0.108 (-14.395,1.432)	7.66E-05
<b>Plasma lipoprotein particle assembly (-APOE)</b>	0.010 (-3.187,-0.430)**	2.98E-04	0.202 (-4.730,0.999)	6.18E-05	1.78E-04	0.032 (-12.267,-0.563)*	0.010 (-13.277,-1.798)**	2.45E-04	3.72E-05	0.336 (-3.981,1.359)	0.066 (-14.392,0.470)	1.35E-04	0.108 (-14.397,1.429)	7.67E-05
<b>Activation of immune response (-APOE)</b>	0.011 (-3.159,-0.403)*	2.89E-04	0.381 (-4.142,1.584)	2.91E-05	1.01E-04	0.106 (-10.672,1.030)	0.251 (-9.101,2.376)	4.87E-05	1.38E-04	0.064 (-5.190,0.148)	0.004 (-18.269,-3.413)*	3.28E-04	0.057 (-15.597,0.225)	1.08E-04
<b>Genome-wide PRS (-APOE)</b>	0.098 (-2.543,0.215)	1.24E-04	0.698 (-3.432,2.297)	5.71E-06	2.21E-08	0.981 (-5.925,5.782)	0.926 (-6.013,5.469)	3.18E-07	2.02E-05	0.478 (-3.637,1.703)	0.872 (-8.046,6.819)	1.05E-06	0.654 (-9.727,6.102)	5.99E-06
<b>APOE SNPs PRS</b>	4.60E-04 (-3.840,-1.085)**	5.53E-04	0.835 (-3.168,2.557)	1.66E-06	2.43E-04	0.012 (-13.342,-1.645)**	0.011 (-13.206,-1.735)**	2.41E-04	3.53E-05	0.348 (-3.945,1.391)	0.124 (-13.250,1.603)	9.47E-05	0.006 (-18.925,-3.110)**	2.22E-04

R<sup>2</sup> and p values for subcortical volumes in the right hemisphere and each polygenic score at a P<sup>T</sup> of 0.001. The column names show the region of interest, while the row names show the polygenic scores.

\* Nominally significant associations (p value < .05).

\*\* FDR corrected associations <0.05.

Acronyms: PRS = Polygenic Risk Score; PT = polygenic threshold; APOE = Apolipoprotein E; L = left; R = right; FDR = false discovery rate.

**Figure 5.4** Associations between genome-wide PRS and subcortical volumes in UK Biobank. Imaging phenotypes are shown on the X axis, the beta co-efficients (positive and negative) are shown on the Y axis. The height of the bars indicate the amount of variance explained ( $R^2$ ), and any nominally significant results are labelled with their p value. Each bar represents a version of the polygenic risk score. The bars are colour coded by the p value threshold used in the training data, shown on the legend.

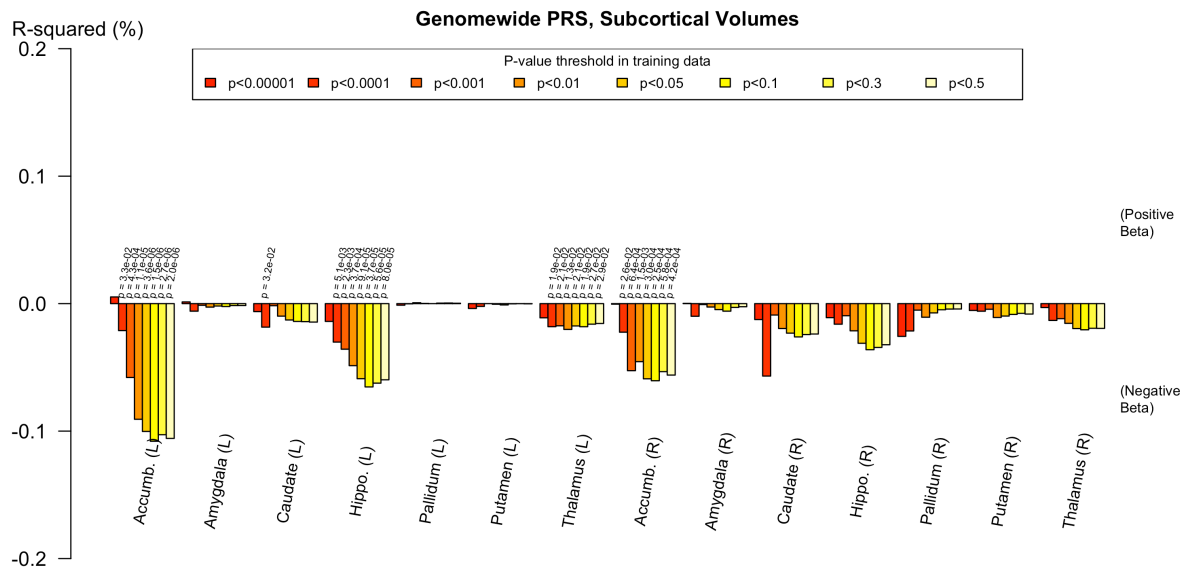


**Figure 5.5** Associations between protein-lipid complex assembly PRS and subcortical volumes in UK Biobank. Imaging phenotypes are shown on the X axis, the beta coefficients (positive and negative) are shown on the Y axis. The heights of the bars indicate the amount of variance explained ( $R^2$ ), and any nominally significant results are labelled with their p value. Each bar represents a version of the PRS. The bars are colour coded by the p value threshold used in the training data, shown on the legend.

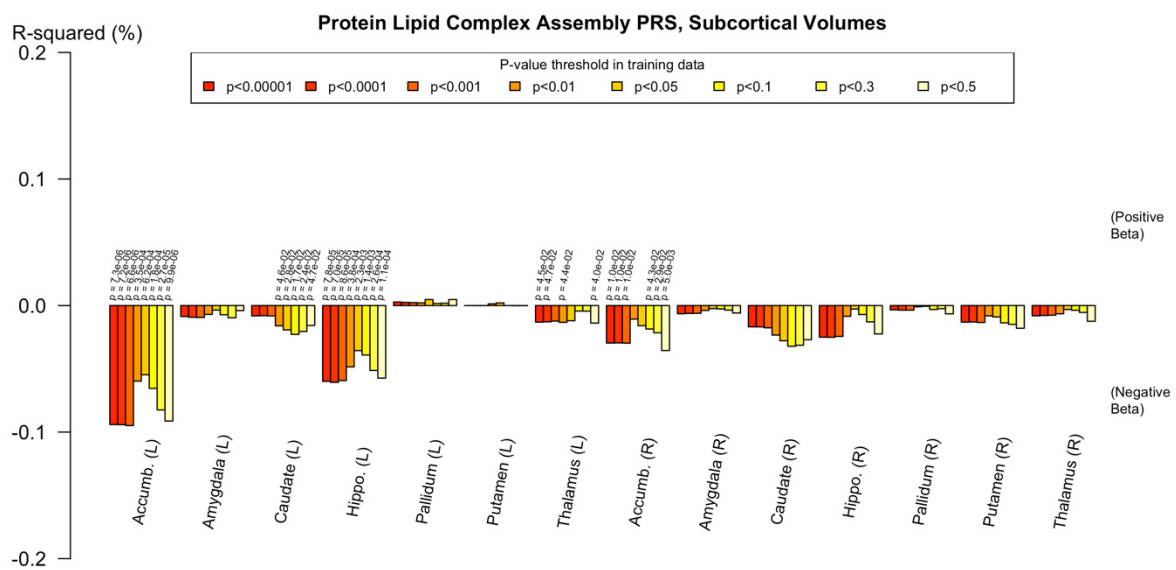
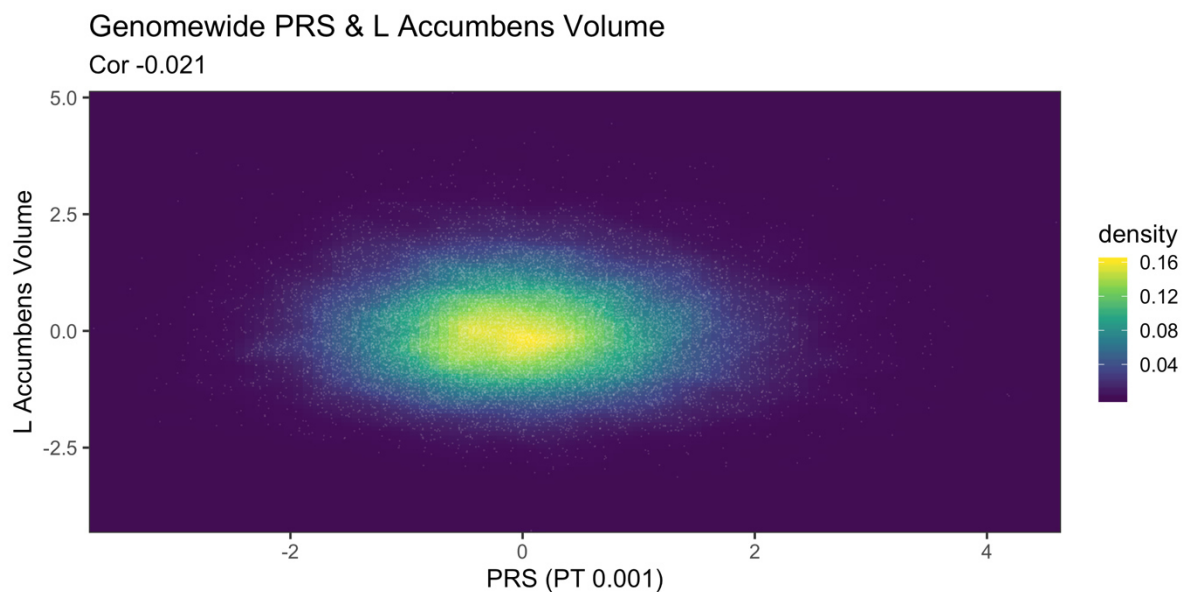


**Figure 5.6** Scatterplot showing normalised genome-wide PRS and normalised left accumbens volume. White circles indicate individual data points. Density represents the number of data points in each area.



### 5.4.3 Cortical Thickness in ALSPAC

In ALSPAC, the genome wide PRS showed evidence of association with reduced cortical thickness in the following regions: left inferior parietal ( $p = 0.008$ ,  $R^2 = 1.36 \times 10^{-2}$ ), left superior parietal ( $p = 0.005$ ,  $R^2 = 1.55 \times 10^{-2}$ ), left supramarginal ( $p = 0.022$ ,  $R^2 = 1.02 \times 10^{-2}$ ), left inferior temporal ( $p = 0.026$ ,  $R^2 = 9.64 \times 10^{-3}$ ), right precuneus ( $p = 0.001$ ,  $R^2 = 2.02 \times 10^{-2}$ ), and right superior parietal ( $p = 0.024$ ,  $R^2 = 9.90 \times 10^{-3}$ ). Only the association with the right precuneus remained significant when corrected for multiple comparisons and there were no significant associations when the *APOE* region was excluded from the PRS.

The pathway specific PRS were associated with reduced cortical thickness in similar regions. For example, the reverse cholesterol transport pathway PRS was negatively associated with cortical thickness in the following areas: left inferior parietal ( $p = 0.007$ ,  $R^2 = 1.43 \times 10^{-2}$ ), left precuneus ( $p = 0.022$ ,  $R^2 = 1.01 \times 10^{-2}$ ), left superior parietal ( $p = 1.83 \times 10^{-4}$ ,  $R^2 = 2.69 \times 10^{-2}$ ), left supramarginal ( $p = 0.022$ ,  $R^2 = 1.01 \times 10^{-2}$ ), left inferior temporal ( $p = 0.007$ ,  $R^2 = 1.43 \times 10^{-2}$ ), left middle temporal ( $p = 0.034$ ,  $R^2 = 8.65 \times 10^{-3}$ ), right inferior parietal ( $p = 0.008$ ,  $R^2 = 1.39 \times 10^{-2}$ ), right precuneus ( $p = 0.001$ ,  $R^2 = 2.30 \times 10^{-2}$ ) and right superior parietal ( $p = 0.003$ ,  $R^2 = 1.68 \times 10^{-2}$ ). The majority of these associations withstood correction for multiple testing. However, many attenuated when the *APOE* region was removed from the score. The immune response pathway PRS was associated with reduced cortical thickness in the right posterior cingulate only ( $p = 0.034$ ,  $R^2 = 8.73 \times 10^{-3}$ ) but this did not persist either with FDR correction or with the *APOE* region removed.

SNPs in the *APOE* region were associated with cortical thinning in the left inferior parietal ( $p = 0.018$ ,  $R^2 = 1.08 \times 10^{-2}$ ), left precuneus ( $p = 0.012$ ,  $R^2 = 1.21 \times 10^{-2}$ ), left superior parietal ( $p = 0.001$ ,  $R^2 = 2.0 \times 10^{-2}$ ), left supramarginal ( $p = 0.009$ ,  $R^2 = 1.34 \times 10^{-2}$ ), left inferior temporal ( $p = 0.001$ ,  $R^2 = 2.22 \times 10^{-2}$ ), left middle temporal ( $p = 0.004$ ,  $R^2 = 1.62 \times 10^{-2}$ ), right inferior parietal ( $p = 0.013$ ,  $R^2 = 1.22 \times 10^{-2}$ ), right precuneus ( $p = 2.78 \times 10^{-4}$ ,  $R^2 = 2.55 \times 10^{-2}$ ), right superior parietal ( $p = 0.003$ ,  $R^2 = 1.68 \times 10^{-2}$ ). Only the left inferior parietal association was no longer significant after FDR correction. The regions showing nominally significant associations with PRS, including and excluding the *APOE* region, are shown in Figures 5.7 and 5.8. The

results are summarised in Tables 5.9 to 5.16, and those surviving FDR correction for multiple comparisons of PRS and phenotype are indicated.

**Table 5.9 Results for ALSPAC cortical thickness in left parietal regions and PRS including APOE at  $P^T$  0.001**

	Left inferior parietal	Left isthmus cingulate	Left posterior cingulate	Left precuneus	Left superior parietal	Left supramarginal
Polygenic risk score	$R^2$ p (95% CI)	$R^2$ p (95% CI)	$R^2$ p (95% CI)	$R^2$ p (95% CI)	$R^2$ p (95% CI)	$R^2$ p (95% CI)
<b>Protein-lipid complex assembly</b>	1.36E-02 0.008 (-0.024,-0.004)*	1.66E-03 0.353 (-0.010,0.027)	3.92E-03 0.156 (-0.025,0.004)	8.97E-03 0.031 (-0.021,-0.001)*	2.32E-02 0.001 (-0.025,-0.007)**	8.64E-03 0.035 (-0.021,-0.001)*
<b>Regulation of A<math>\beta</math> formation</b>	2.05E-02 0.001 (-0.027,-0.007)**	3.91E-04 0.653 (-0.015,0.023)	5.56E-03 0.091 (-0.027,0.002)	1.25E-02 0.011 (-0.024,-0.003)*	2.12E-02 0.001 (-0.025,-0.006)**	9.93E-03 0.024 (-0.022,-0.002)*
<b>Protein-lipid complex</b>	1.19E-02 0.013 (-0.023,-0.003)*	2.16E-03 0.290 (-0.009,0.029)	3.06E-03 0.209 (-0.024,0.005)	9.63E-03 0.025 (-0.022,-0.001)*	2.42E-02 3.84E-04 (-0.025,-0.007)**	7.38E-03 0.051 (-0.020,3.32E-05)
<b>Regulation of amyloid precursor protein catabolic process</b>	2.05E-02 0.001 (-0.027,-0.007)**	3.91E-04 0.653 (-0.015,0.023)	5.56E-03 0.091 (-0.027,0.002)	1.25E-02 0.011 (-0.024,-0.003)*	2.12E-02 0.001 (-0.025,-0.006)**	9.93E-03 0.024 (-0.022,-0.002)*
<b>Tau protein binding</b>	1.45E-02 0.006 (-0.024,-0.004)**	2.08E-03 0.299 (-0.009,0.029)	3.28E-03 0.194 (-0.024,0.005)	1.01E-02 0.022 (-0.022,-0.002)*	2.60E-02 2.32E-04 (-0.026,-0.008)**	8.62E-03 0.035 (-0.021,-0.001)*
<b>Reverse cholesterol transport</b>	1.43E-02 0.007 (-0.024,-0.004)**	1.11E-03 0.449 (-0.011,0.026)	3.94E-03 0.154 (-0.025,0.004)	1.01E-02 0.022 (-0.022,-0.002)*	2.69E-02 1.83E-04 (-0.026,-0.008)**	1.01E-02 0.022 (-0.022,-0.002)*
<b>Protein-lipid complex subunit organization</b>	1.53E-02 0.005 (-0.024,-0.004)**	1.61E-03 0.361 (-0.010,0.027)	3.87E-03 0.158 (-0.025,0.004)	9.56E-03 0.026 (-0.022,-0.001)*	2.36E-02 4.60E-04 (-0.025,-0.007)**	9.07E-03 0.031 (-0.021,-0.001)*
<b>Plasma lipoprotein particle assembly</b>	1.03E-02 0.021 (-0.022,-0.002)*	2.92E-03 0.218 (-0.007,0.030)	2.73E-03 0.236 (-0.023,0.006)	6.86E-03 0.059 (-0.020,3.70E-04)	2.16E-02 0.001 (-0.024,-0.006)**	5.05E-03 0.107 (-0.018,0.002)
<b>Activation of immune response</b>	2.16E-04 0.740 (-0.012,0.008)	4.81E-04 0.618 (-0.024,0.014)	2.46E-05 0.911 (-0.015,0.014)	1.45E-03 0.387 (-0.015,0.006)	1.69E-07 0.993 (-0.009,0.009)	1.95E-03 0.317 (-0.015,0.005)
<b>Genome-wide PRS</b>	1.36E-02 0.008 (-0.024,-0.004)*	3.12E-04 0.688 (-0.015,0.023)	2.91E-04 0.699 (-0.017,0.012)	7.39E-03 0.050 (-0.021,-1.06E-05)	1.55E-02 0.005 (-0.022,-0.004)*	1.02E-02 0.022 (-0.022,-0.002)*

$R^2$  and p values for subcortical volumes in the left hemisphere and each polygenic score at a  $P^T$  of 0.001. The column names show the region of interest, while the row names show the polygenic scores.

\* Nominally significant associations (p value < .05).

\*\* FDR corrected associations <0.05.

Acronyms: PRS = Polygenic Risk Score;  $P^T$  = polygenic threshold; APOE = Apolipoprotein E; L = left; R = right; FDR = false discovery rate.

**Table 5.10 Results for ALSPAC cortical thickness in left temporal regions and PRS including APOE at P<sup>T</sup> 0.001**

	Left entorhinal	Left inferior temporal	Left middle temporal	Left parahippocampal	Superior temporal	Left temporal pole	Left transverse temporal
	R <sup>2</sup> p (95% CI)	R <sup>2</sup> p (95% CI)	R <sup>2</sup> p (95% CI)	R <sup>2</sup> p (95% CI)	R <sup>2</sup> p (95% CI)	R <sup>2</sup> p (95% CI)	R <sup>2</sup> p (95% CI)
<b>Polygenic risk score</b>							
<b>Protein-lipid complex assembly</b>	0.492 (-0.021,0.044) 9.75E-04	0.024 (-0.028,-0.002)* 9.90E-03	0.058 (-0.023,3.42E-04) 6.94E-03	0.550 (-0.016,0.030) 7.16E-04	0.557 (-0.015,0.008) 6.54E-04	0.769 (-0.038,0.028) 1.67E-04	0.280 (-0.028,0.008) 2.27E-03
<b>Regulation of Aβ formation</b>	0.550 (-0.023,0.043) 7.37E-04	0.076 (-0.025,0.001) 6.12E-03	0.114 (-0.022,0.002) 4.81E-03	0.904 (-0.022,0.025) 2.91E-05	0.695 (-0.014,0.010) 2.91E-04	0.958 (-0.033,0.034) 5.50E-06	0.147 (-0.032,0.005) 4.08E-03
<b>Protein-lipid complex</b>	0.497 (-0.021,0.044) 9.53E-04	0.005 (-0.032,-0.006)** 1.53E-02	0.043 (-0.024,-3.94E-04)* 7.85E-03	0.657 (-0.018,0.029) 3.96E-04	0.365 (-0.017,0.006) 1.55E-03	0.586 (-0.043,0.024) 5.75E-04	0.166 (-0.031,0.005) 3.72E-03
<b>Regulation of amyloid precursor protein catabolic process</b>	0.550 (-0.023,0.043) 7.37E-04	0.076 (-0.025,0.001) 6.12E-03	0.114 (-0.022,0.002) 4.81E-03	0.904 (-0.022,0.025) 2.91E-05	0.695 (-0.014,0.010) 2.91E-04	0.958 (-0.033,0.034) 5.50E-06	0.147 (-0.032,0.005) 4.08E-03
<b>Tau protein binding</b>	0.485 (-0.021,0.044) 1.01E-03	0.005 (-0.032,-0.006)** 1.54E-02	0.056 (-0.024,2.87E-04) 7.01E-03	0.519 (-0.018,0.031) 8.33E-04	0.470 (-0.016,0.008) 9.89E-04	0.544 (-0.044,0.023) 7.14E-04	0.200 (-0.030,0.006) 3.19E-03
<b>Reverse cholesterol transport</b>	0.679 (-0.026,0.039) 3.53E-04	0.007 (-0.031,-0.005)** 1.43E-02	0.034 (-0.025,-0.001)* 8.65E-03	0.566 (-0.016,0.030) 6.59E-04	0.353 (-0.017,0.006) 1.64E-03	0.466 (-0.045,0.021) 1.03E-03	0.152 (-0.032,0.005) 3.98E-03
<b>Protein-lipid complex subunit organization</b>	0.455 (-0.020,0.045) 1.15E-03	0.023 (-0.028,-0.002)* 9.99E-03	0.086 (-0.022,0.001) 5.68E-03	0.533 (-0.016,0.030) 7.77E-04	0.709 (-0.014,0.010) 2.63E-04	0.781 (-0.038,0.028) 1.50E-04	0.331 (-0.027,0.009) 1.84E-03
<b>Plasma lipoprotein particle assembly</b>	0.240 (-0.013,0.052) 2.84E-03	0.029 (-0.028,-0.002)* 9.29E-03	0.081 (-0.022,0.001) 5.89E-03	0.410 (-0.013,0.033) 1.36E-03	0.620 (-0.015,0.009) 4.68E-04	0.826 (-0.037,0.029) 9.36E-05	0.333 (-0.027,0.009) 1.82E-03
<b>Activation of immune response</b>	0.729 (-0.038,0.027) 2.48E-04	0.312 (-0.020,0.006) 2.00E-03	0.831 (-0.013,0.011) 8.83E-05	0.658 (-0.029,0.018) 3.93E-04	0.934 (-0.011,0.012) 1.29E-05	0.476 (-0.045,0.021) 9.88E-04	0.813 (-0.016,0.021) 1.09E-04
<b>Genome-wide PRS</b>	0.485 (-0.021,0.045) 1.01E-03	0.026 (-0.028,-0.002)* 9.64E-03	0.188 (-0.020,0.004) 3.35E-03	0.126 (-0.005,0.042) 4.67E-03	0.694 (-0.014,0.010) 2.94E-04	0.426 (-0.020,0.047) 1.23E-03	0.493 (-0.012,0.025) 9.15E-04

R2 and p values for subcortical volumes in the left hemisphere and each polygenic score at a P<sup>T</sup> of 0.001. The column names show the region of interest, while the row names show the polygenic scores.

\* Nominally significant associations (p value < .05).

\*\* FDR corrected associations <0.05.

Acronyms: PRS = Polygenic Risk Score; P<sup>T</sup> = polygenic threshold; APOE = Apolipoprotein E; L = left; R = right; FDR = false discovery rate.

**Table 5.11 Results for ALSPAC cortical thickness in left parietal regions and PRS excluding APOE at  $P \leq 0.001$**

	Left inferior parietal	Left isthmus cingulate	Left posterior cingulate	Left precuneus	Left superior parietal	Left supramarginal
Polygenic risk score	$R^2$ p (95% CI)	$R^2$ p (95% CI)	$R^2$ p (95% CI)	$R^2$ p (95% CI)	$R^2$ p (95% CI)	$R^2$ p (95% CI)
Protein-lipid complex assembly (-APOE)	7.76E-04 0.529 (-0.014,0.007)	2.58E-03 0.247 (-0.030,0.008)	3.41E-03 0.185 (-0.025,0.005)	6.99E-04 0.548 (-0.014,0.007)	7.36E-04 0.538 (-0.012,0.006)	6.05E-03 0.078 (-0.019,0.001)
Regulation of A $\beta$ formation (-APOE)	9.57E-03 0.027 (-0.021,-0.001)*	4.16E-03 0.142 (-0.032,0.005)	3.86E-03 0.159 (-0.025,0.004)	5.66E-03 0.087 (-0.019,0.001)	6.18E-04 0.573 (-0.012,0.006)	5.47E-03 0.094 (-0.018,0.001)
Protein-lipid complex (-APOE)	7.19E-04 0.544 (-0.007,0.014)	6.43E-04 0.564 (-0.013,0.025)	6.29E-04 0.570 (-0.019,0.010)	1.88E-04 0.755 (-0.012,0.009)	1.92E-04 0.753 (-0.008,0.011)	6.38E-05 0.856 (-0.009,0.011)
Regulation of amyloid precursor protein catabolic process (-APOE)	9.57E-03 0.027 (-0.021,-0.001)*	4.16E-03 0.142 (-0.032,0.005)	3.86E-03 0.159 (-0.025,0.004)	5.66E-03 0.087 (-0.019,0.001)	6.18E-04 0.573 (-0.012,0.006)	5.47E-03 0.094 (-0.018,0.001)
Tau protein binding (-APOE)	1.80E-03 0.337 (-0.015,0.005)	7.41E-04 0.536 (-0.013,0.025)	2.41E-03 0.265 (-0.023,0.006)	1.05E-03 0.462 (-0.014,0.007)	1.37E-04 0.791 (-0.010,0.008)	1.43E-03 0.392 (-0.015,0.006)
Reverse cholesterol transport (-APOE)	1.38E-03 0.401 (-0.015,0.006)	2.42E-03 0.263 (-0.030,0.008)	5.08E-03 0.106 (-0.027,0.003)	9.78E-04 0.477 (-0.014,0.007)	1.46E-03 0.387 (-0.013,0.005)	6.53E-03 0.067 (-0.020,0.001)
Protein-lipid complex subunit organization (-APOE)	1.10E-02 0.017 (-0.023,-0.002)*	9.16E-03 0.029 (-0.040,-0.002)*	7.77E-03 0.045 (-0.030,-3.54E-04)*	4.29E-03 0.136 (-0.019,0.003)	1.91E-03 0.321 (-0.014,0.005)	2.08E-02 0.001 (-0.027,-0.007)**
Plasma lipoprotein particle assembly (-APOE)	1.76E-03 0.342 (-0.005,0.015)	6.27E-05 0.857 (-0.017,0.021)	5.78E-05 0.863 (-0.016,0.013)	2.42E-04 0.724 (-0.009,0.012)	2.75E-06 0.970 (-0.009,0.009)	9.09E-05 0.829 (-0.009,0.011)
Activation of immune response (-APOE)	2.73E-05 0.906 (-0.011,0.009)	3.35E-05 0.895 (-0.017,0.020)	7.71E-04 0.529 (-0.010,0.019)	3.93E-05 0.887 (-0.011,0.009)	3.72E-04 0.662 (-0.007,0.011)	3.56E-04 0.669 (-0.012,0.008)
Genome-wide PRS (-APOE)	5.39E-03 0.096 (-0.019,0.002)	2.63E-04 0.712 (-0.015,0.022)	6.14E-04 0.574 (-0.010,0.019)	1.13E-03 0.444 (-0.014,0.006)	3.60E-03 0.173 (-0.015,0.003)	2.28E-03 0.280 (-0.016,0.005)
APOE SNPs PRS	1.08E-02 0.018 (-0.022,-0.002)*	5.62E-05 0.865 (-0.017,0.020)	5.34E-03 0.097 (-0.027,0.002)	1.21E-02 0.012 (-0.023,-0.003)**	2.00E-02 0.001 (-0.024,-0.006)**	1.34E-02 0.009 (-0.023,-0.003)**

R2 and p values for subcortical volumes in the left hemisphere and each polygenic score at a PT of 0.001. The column names shows the region of interest, while the row names show the polygenic scores.

\* Nominally significant associations (p value < .05).

\*\* FDR corrected associations <0.05.

Acronyms: PRS = Polygenic Risk Score; PT = polygenic threshold; APOE = Apolipoprotein E; L = left; R = right; FDR = false discovery rate.

**Table 5.12 Results for ALSPAC cortical thickness in left temporal regions and PRS excluding APOE at P<sup>T</sup> 0.001**

Polygenic risk score	Left entorhinal R <sup>2</sup> p (95% CI)	Left inferior temporal R <sup>2</sup> p (95% CI)	Left middle temporal R <sup>2</sup> p (95% CI)	Left parahippocampal R <sup>2</sup> p (95% CI)	Superior temporal R <sup>2</sup> p (95% CI)	Left temporal pole R <sup>2</sup> p (95% CI)	Left transverse temporal R <sup>2</sup> p (95% CI)
<b>Protein-lipid complex assembly (-APOE)</b>	1.06E-02 0.023 (-0.073,-0.005)*	6.98E-05 0.850 (-0.015,0.012)	6.91E-03 0.058 (-0.024,3.82E-04)	2.00E-03 0.317 (-0.036,0.012)	4.93E-03 0.107 (-0.022,0.002)	2.34E-04 0.729 (-0.040,0.028)	6.21E-03 0.074 (-0.036,0.002)
<b>Regulation of Aβ formation (-APOE)</b>	3.04E-03 0.225 (-0.052,0.012)	4.68E-04 0.624 (-0.010,0.016)	3.40E-04 0.675 (-0.014,0.009)	4.42E-03 0.137 (-0.041,0.006)	2.88E-04 0.696 (-0.014,0.009)	5.38E-04 0.599 (-0.024,0.042)	4.62E-03 0.123 (-0.032,0.004)
<b>Protein-lipid complex (-APOE)</b>	7.14E-04 0.557 (-0.044,0.024)	1.13E-03 0.446 (-0.019,0.008)	3.27E-03 0.193 (-0.020,0.004)	2.12E-03 0.304 (-0.037,0.011)	3.52E-03 0.173 (-0.020,0.004)	3.85E-04 0.656 (-0.026,0.041)	3.70E-03 0.168 (-0.032,0.005)
<b>Regulation of amyloid precursor protein catabolic process (-APOE)</b>	3.04E-03 0.225 (-0.052,0.012)	4.68E-04 0.624 (-0.010,0.016)	3.40E-04 0.675 (-0.014,0.009)	4.42E-03 0.137 (-0.041,0.006)	2.88E-04 0.696 (-0.014,0.009)	5.38E-04 0.599 (-0.024,0.042)	4.62E-03 0.123 (-0.032,0.004)
<b>Tau protein binding (-APOE)</b>	1.23E-03 0.441 (-0.046,0.020)	1.78E-03 0.339 (-0.020,0.007)	1.47E-03 0.383 (-0.017,0.007)	1.98E-05 0.921 (-0.022,0.025)	3.89E-04 0.651 (-0.015,0.009)	8.91E-05 0.830 (-0.030,0.037)	2.39E-03 0.267 (-0.029,0.008)
<b>Reverse cholesterol transport (-APOE)</b>	9.68E-03 0.030 (-0.071,-0.004)*	1.90E-04 0.755 (-0.016,0.011)	7.81E-03 0.044 (-0.025,-3.64E-04)*	1.68E-04 0.772 (-0.027,0.020)	4.82E-03 0.110 (-0.022,0.002)	7.64E-04 0.531 (-0.044,0.023)	6.01E-03 0.079 (-0.035,0.002)
<b>Protein-lipid complex subunit organization (-APOE)</b>	2.24E-02 0.001 (-0.090,-0.023)**	7.12E-05 0.849 (-0.015,0.012)	2.77E-03 0.231 (-0.020,0.005)	4.57E-03 0.130 (-0.043,0.005)	5.16E-04 0.601 (-0.016,0.009)	3.22E-04 0.684 (-0.041,0.027)	6.64E-03 0.064 (-0.037,0.001)
<b>Plasma lipoprotein particle assembly (-APOE)</b>	3.49E-04 0.681 (-0.041,0.026)	1.69E-05 0.926 (-0.014,0.013)	3.95E-03 0.152 (-0.021,0.003)	4.61E-05 0.879 (-0.026,0.022)	4.84E-03 0.110 (-0.022,0.002)	3.33E-05 0.896 (-0.036,0.031)	1.47E-03 0.384 (-0.027,0.010)
<b>Activation of immune response (-APOE)</b>	1.11E-04 0.817 (-0.036,0.028)	1.24E-04 0.801 (-0.015,0.011)	4.28E-04 0.638 (-0.009,0.015)	2.93E-05 0.904 (-0.024,0.022)	7.19E-04 0.538 (-0.008,0.015)	6.14E-04 0.574 (-0.042,0.023)	1.39E-03 0.398 (-0.010,0.026)
<b>Genome-wide PRS (-APOE)</b>	1.70E-04 0.774 (-0.028,0.038)	5.87E-04 0.584 (-0.017,0.010)	9.90E-05 0.821 (-0.011,0.013)	4.29E-03 0.143 (-0.006,0.041)	1.68E-05 0.925 (-0.011,0.013)	3.98E-03 0.152 (-0.009,0.058)	2.45E-03 0.262 (-0.008,0.029)
<b>APOE SNPs PRS</b>	1.60E-03 0.379 (-0.018,0.048)	2.22E-02 0.001 (-0.036,-0.010)**	1.62E-02 0.004 (-0.029,-0.006)**	6.31E-04 0.575 (-0.017,0.030)	1.57E-03 0.363 (-0.017,0.006)	1.26E-03 0.421 (-0.047,0.019)	5.11E-04 0.608 (-0.023,0.013)

R2 and p values for subcortical volumes in the left hemisphere and each polygenic score at a P<sup>T</sup> of 0.001. The column names shows the region of interest, while the row names show the polygenic scores.

\* Nominally significant associations (p value < .05).

\*\* FDR corrected associations <0.05.

Acronyms: PRS = Polygenic Risk Score; P<sup>T</sup> = polygenic threshold; APOE = Apolipoprotein E; L = left; R = right; FDR = false discovery rate.

**Table 5.13 Results for ALSPAC cortical thickness in right parietal regions and PRS including APOE at P<sup>T</sup> 0.001**

	Right inferior parietal		Right isthmus cingulate		Right posterior cingulate		Right precuneus		Right superior parietal		Right supramarginal	
Polygenic risk score	R <sup>2</sup>	p (95% CI)	R <sup>2</sup>	p (95% CI)	R <sup>2</sup>	p (95% CI)	R <sup>2</sup>	p (95% CI)	R <sup>2</sup>	p (95% CI)	R <sup>2</sup>	p (95% CI)
<b>Protein-lipid complex assembly</b>	1.07E-02	0.020 (-0.023,-0.002)*	5.50E-04	0.592 (-0.013,0.022)	4.81E-05	0.875 (-0.016,0.014)	1.88E-02	0.002 (-0.028,-0.006)**	1.27E-02	0.011 (-0.021,-0.003)*	2.44E-03	0.266 (-0.017,0.005)
<b>Regulation of Aβ formation</b>	1.10E-02	0.018 (-0.024,-0.002)*	2.27E-04	0.730 (-0.021,0.015)	2.30E-04	0.731 (-0.012,0.018)	1.56E-02	0.005 (-0.027,-0.005)**	1.07E-02	0.019 (-0.021,-0.002)*	2.88E-03	0.226 (-0.018,0.004)
<b>Protein-lipid complex</b>	1.16E-02	0.015 (-0.024,-0.003)*	6.42E-04	0.562 (-0.012,0.023)	1.55E-04	0.778 (-0.017,0.013)	1.77E-02	0.002 (-0.027,-0.006)**	1.35E-02	0.008 (-0.022,-0.003)*	3.25E-03	0.199 (-0.018,0.004)
<b>Regulation of amyloid precursor protein catabolic</b>	1.10E-02	0.018 (-0.024,-0.002)*	2.27E-04	0.730 (-0.021,0.015)	2.30E-04	0.731 (-0.012,0.018)	1.56E-02	0.005 (-0.027,-0.005)**	1.07E-02	0.019 (-0.021,-0.002)*	2.88E-03	0.226 (-0.018,0.004)
<b>Tau protein binding</b>	1.39E-02	0.008 (-0.025,-0.004)**	1.04E-04	0.815 (-0.015,0.020)	3.84E-04	0.657 (-0.018,0.012)	1.97E-02	0.001 (-0.028,-0.007)**	1.51E-02	0.005 (-0.023,-0.004)**	3.54E-03	0.180 (-0.018,0.003)
<b>Reverse cholesterol transport</b>	1.39E-02	0.008 (-0.025,-0.004)**	1.26E-04	0.797 (-0.015,0.020)	3.33E-04	0.679 (-0.018,0.012)	2.30E-02	0.001 (-0.029,-0.008)**	1.68E-02	0.003 (-0.023,-0.005)**	3.41E-03	0.188 (-0.018,0.003)
<b>Protein-lipid complex subunit organization</b>	1.09E-02	0.019 (-0.023,-0.002)*	1.27E-04	0.797 (-0.015,0.020)	1.90E-04	0.755 (-0.017,0.012)	1.94E-02	0.002 (-0.028,-0.007)**	1.33E-02	0.009 (-0.022,-0.003)*	2.47E-03	0.263 (-0.017,0.005)
<b>Plasma lipoprotein particle assembly</b>	8.37E-03	0.039 (-0.022,-0.001)*	1.96E-03	0.311 (-0.008,0.027)	2.07E-05	0.918 (-0.014,0.016)	1.49E-02	0.006 (-0.026,-0.004)*	1.00E-02	0.023 (-0.020,-0.002)*	1.98E-03	0.317 (-0.016,0.005)
<b>Activation of immune response</b>	1.48E-03	0.387 (-0.006,0.016)	4.54E-04	0.626 (-0.022,0.013)	8.73E-03	0.034 (-0.031,-0.001)*	2.33E-03	0.274 (-0.017,0.005)	8.56E-04	0.507 (-0.013,0.006)	4.01E-04	0.652 (-0.013,0.008)
<b>Genome-wide PRS</b>	5.40E-04	0.602 (-0.014,0.008)	7.45E-04	0.532 (-0.023,0.012)	5.18E-04	0.606 (-0.019,0.011)	2.02E-02	0.001 (-0.028,-0.007)**	9.90E-03	0.024 (-0.020,-0.001)*	5.40E-03	0.097 (-0.020,0.002)

R<sup>2</sup> and p values for subcortical volumes in the right hemisphere and each polygenic score at a PT of 0.001. The column names shows the region of interest, while the row names show the polygenic scores.  
 \* Nominally significant associations (p value < .05).  
 \*\* FDR corrected associations <0.05.

Acronyms: PRS = Polygenic Risk Score; PT = polygenic threshold; APOE = Apolipoprotein E; L = left; R = right; FDR = false discovery rate.

**Table 5.14 Results for ALSPAC cortical thickness in right temporal regions and PRS including APOE at P<sup>T</sup> 0.001**

	Right entorhinal	Right inferior temporal	Right middle temporal	Right parahippocampal	Right superior temporal	Right temporal pole	Right transverse temporal
	R <sup>2</sup> p (95% CI)	R <sup>2</sup> p (95% CI)	R <sup>2</sup> p (95% CI)	R <sup>2</sup> p (95% CI)	R <sup>2</sup> p (95% CI)	R <sup>2</sup> p (95% CI)	R <sup>2</sup> p (95% CI)
<b>Polygenic risk score</b>							
<b>Protein-lipid complex assembly</b>	2.01E-08 0.997 (-0.035,0.035)	3.42E-03 0.183 (-0.022,0.004)	1.22E-03 0.425 (-0.017,0.007)	6.16E-03 0.076 (-0.036,0.002)	2.36E-03 0.265 (-0.019,0.005)	4.57E-04 0.627 (-0.041,0.025)	4.66E-03 0.113 (-0.030,0.003)
<b>Regulation of Aβ formation</b>	1.07E-03 0.466 (-0.048,0.022)	2.43E-03 0.262 (-0.021,0.006)	2.22E-03 0.282 (-0.019,0.006)	1.65E-02 0.004 (-0.047,-0.009)**	3.96E-03 0.149 (-0.022,0.003)	1.02E-03 0.468 (-0.046,0.021)	4.75E-03 0.110 (-0.031,0.003)
<b>Protein-lipid complex</b>	8.11E-06 0.949 (-0.034,0.036)	6.95E-03 0.057 (-0.026,3.72E-04)	1.83E-03 0.329 (-0.018,0.006)	8.91E-03 0.032 (-0.039,-0.002)*	2.78E-03 0.226 (-0.020,0.005)	5.53E-05 0.866 (-0.036,0.030)	4.44E-03 0.123 (-0.030,0.004)
<b>Regulation of amyloid precursor protein catabolic</b>	1.07E-03 0.466 (-0.048,0.022)	2.43E-03 0.262 (-0.021,0.006)	2.22E-03 0.282 (-0.019,0.006)	1.65E-02 0.004 (-0.047,-0.009)**	3.96E-03 0.149 (-0.022,0.003)	1.02E-03 0.468 (-0.046,0.021)	4.75E-03 0.110 (-0.031,0.003)
<b>Tau protein binding</b>	5.28E-05 0.871 (-0.032,0.038)	7.51E-03 0.048 (-0.027,-1.38E-04)*	1.84E-03 0.328 (-0.018,0.006)	8.00E-03 0.043 (-0.038,-0.001)*	2.51E-03 0.250 (-0.020,0.005)	7.24E-05 0.847 (-0.037,0.030)	4.83E-03 0.107 (-0.031,0.003)
<b>Reverse cholesterol transport</b>	2.52E-06 0.972 (-0.034,0.035)	5.89E-03 0.080 (-0.025,0.001)	2.60E-03 0.245 (-0.019,0.005)	7.48E-03 0.050 (-0.038,-3.28E-05)	3.02E-03 0.207 (-0.020,0.004)	1.45E-04 0.784 (-0.038,0.028)	5.51E-03 0.085 (-0.032,0.002)
<b>Protein-lipid complex subunit organization</b>	7.90E-08 0.995 (-0.035,0.035)	3.54E-03 0.175 (-0.022,0.004)	9.65E-04 0.479 (-0.016,0.008)	5.45E-03 0.095 (-0.035,0.003)	1.91E-03 0.316 (-0.018,0.006)	5.41E-04 0.597 (-0.042,0.024)	4.78E-03 0.109 (-0.031,0.003)
<b>Plasma lipoprotein particle assembly</b>	2.15E-04 0.744 (-0.029,0.041)	3.18E-03 0.199 (-0.022,0.005)	6.40E-04 0.564 (-0.016,0.009)	5.02E-03 0.109 (-0.034,0.003)	1.21E-03 0.425 (-0.017,0.007)	2.41E-04 0.724 (-0.039,0.027)	3.09E-03 0.198 (-0.028,0.006)
<b>Activation of immune response</b>	3.71E-03 0.174 (-0.059,0.011)	3.78E-04 0.658 (-0.016,0.010)	7.55E-04 0.531 (-0.008,0.016)	4.90E-04 0.617 (-0.014,0.023)	4.93E-04 0.611 (-0.016,0.009)	9.47E-05 0.825 (-0.030,0.037)	1.44E-03 0.380 (-0.025,0.009)
<b>Genome-wide PRS</b>	1.38E-03 0.407 (-0.049,0.020)	2.88E-03 0.222 (-0.021,0.005)	1.50E-03 0.378 (-0.018,0.007)	6.74E-06 0.953 (-0.019,0.018)	2.63E-03 0.240 (-0.020,0.005)	1.55E-03 0.370 (-0.018,0.048)	1.90E-03 0.313 (-0.026,0.008)

R<sup>2</sup> and p values for subcortical volumes in the right hemisphere and each polygenic score at a PT of 0.001. The column names shows the region of interest, while the row names show the polygenic scores.

\* Nominally significant associations (p value < .05).

\*\* FDR corrected associations <0.05.

Acronyms: PRS = Polygenic Risk Score; PT = polygenic threshold; APOE = Apolipoprotein E; L = left; R = right; FDR = false discovery rate.

**Table 5.15 Results for ALSPAC cortical thickness in right parietal regions and PRS excluding APOE at P<sup>T</sup> 0.001**

	Right inferior parietal	Right isthmus cingulate	Right posterior cingulate	Right precuneus	Right superior parietal	Right supramarginal
Polygenic risk score	R <sup>2</sup> p (95% CI)	R <sup>2</sup> p (95% CI)	R <sup>2</sup> p (95% CI)	R <sup>2</sup> p (95% CI)	R <sup>2</sup> p (95% CI)	R <sup>2</sup> p (95% CI)
Protein-lipid complex assembly (-APOE)	4.48E-04 0.634 (-0.014,0.008)	4.83E-06 0.960 (-0.018,0.017)	2.05E-04 0.746 (-0.013,0.018)	7.00E-03 0.058 (-0.022,3.27E-04)	1.57E-03 0.369 (-0.014,0.005)	2.41E-04 0.727 (-0.013,0.009)
Regulation of Aβ formation (-APOE)	2.20E-03 0.291 (-0.016,0.005)	9.06E-03 0.029 (-0.036,-0.002)*	1.69E-03 0.351 (-0.008,0.022)	7.44E-04 0.537 (-0.014,0.007)	5.12E-04 0.608 (-0.012,0.007)	8.65E-04 0.508 (-0.014,0.007)
Protein-lipid complex (-APOE)	3.94E-04 0.656 (-0.008,0.013)	5.16E-03 0.100 (-0.003,0.033)	2.40E-03 0.266 (-0.007,0.024)	9.74E-05 0.823 (-0.010,0.012)	5.88E-04 0.583 (-0.007,0.012)	7.36E-05 0.847 (-0.012,0.010)
Regulation of amyloid precursor protein catabolic process (-APOE)	2.20E-03 0.291 (-0.016,0.005)	9.06E-03 0.029 (-0.036,-0.002)*	1.69E-03 0.351 (-0.008,0.022)	7.44E-04 0.537 (-0.014,0.007)	5.12E-04 0.608 (-0.012,0.007)	8.65E-04 0.508 (-0.014,0.007)
Tau protein binding (-APOE)	1.90E-03 0.327 (-0.016,0.005)	3.87E-04 0.653 (-0.022,0.014)	2.53E-04 0.718 (-0.012,0.018)	1.18E-03 0.437 (-0.015,0.007)	6.01E-05 0.861 (-0.010,0.009)	8.32E-04 0.516 (-0.015,0.007)
Reverse cholesterol transport (-APOE)	1.77E-03 0.344 (-0.016,0.006)	4.31E-05 0.881 (-0.019,0.016)	2.85E-04 0.702 (-0.012,0.018)	1.05E-02 0.020 (-0.024,-0.002)*	3.01E-03 0.214 (-0.016,0.003)	3.54E-04 0.672 (-0.013,0.009)
Protein-lipid complex subunit organization (-APOE)	1.13E-03 0.449 (-0.015,0.007)	1.62E-02 0.003 (-0.044,-0.009)**	1.84E-03 0.330 (-0.023,0.008)	2.19E-02 0.001 (-0.030,-0.008)**	6.65E-03 0.064 (-0.019,0.001)	6.04E-04 0.580 (-0.014,0.008)
Plasma lipoprotein particle assembly (-APOE)	1.30E-06 0.980 (-0.011,0.011)	8.02E-03 0.040 (0.001,0.036)*	2.44E-03 0.263 (-0.006,0.024)	2.33E-05 0.913 (-0.010,0.012)	1.05E-04 0.816 (-0.008,0.011)	2.72E-06 0.970 (-0.011,0.011)
Activation of immune response (-APOE)	4.66E-03 0.124 (-0.002,0.019)	8.69E-05 0.831 (-0.015,0.019)	3.01E-05 0.901 (-0.016,0.014)	9.84E-04 0.478 (-0.015,0.007)	4.87E-07 0.987 (-0.009,0.009)	4.48E-04 0.634 (-0.008,0.013)
Genome-wide PRS (-APOE)	1.63E-03 0.363 (-0.006,0.016)	4.27E-04 0.636 (-0.022,0.013)	2.85E-05 0.904 (-0.016,0.014)	4.84E-03 0.115 (-0.020,0.002)	1.41E-03 0.394 (-0.013,0.005)	2.54E-03 0.256 (-0.017,0.005)
APOE SNPs PRS	1.22E-02 0.013 (-0.024,-0.003)**	3.51E-04 0.668 (-0.021,0.014)	1.22E-03 0.427 (-0.021,0.009)	2.55E-02 2.78E-04 (-0.030,-0.009)**	1.68E-02 0.003 (-0.023,-0.005)**	3.48E-03 0.183 (-0.018,0.003)

R<sup>2</sup> and p values for subcortical volumes in the right hemisphere and each polygenic score at a PT of 0.001. The column names shows the region of interest, while the row names show the polygenic scores.

\* Nominally significant associations (p value < .05).

\*\* FDR corrected associations <0.05.

Acronyms: PRS = Polygenic Risk Score; PT = polygenic threshold; APOE = Apolipoprotein E; L = left; R = right; R = right; FDR = false discovery rate.

**Table 5.16 Results for ALSPAC cortical thickness in right temporal regions and PRS including APOE at P<sup>T</sup> 0.001**

	Right entorhinal	Right inferior temporal	Right middle temporal	Right parahippocampal	Right superior temporal	Right temporal pole	Right transverse temporal
Polygenic risk score	R <sup>2</sup> p (95% CI)	R <sup>2</sup> p (95% CI)	R <sup>2</sup> p (95% CI)	R <sup>2</sup> p (95% CI)	R <sup>2</sup> p (95% CI)	R <sup>2</sup> p (95% CI)	R <sup>2</sup> p (95% CI)
<b>Protein-lipid complex assembly (-APOE)</b>	3.98E-03 0.159 (-0.061,0.010)	3.17E-04 0.686 (-0.011,0.016)	5.24E-03 0.099 (-0.023,0.002)	4.40E-03 0.133 (-0.034,0.004)	8.08E-03 0.039 (-0.026,-0.001)*	2.37E-04 0.726 (-0.040,0.028)	7.72E-04 0.520 (-0.023,0.012)
<b>Regulation of Aβ formation (-APOE)</b>	1.07E-02 0.021 (-0.075,-0.006)*	5.28E-05 0.869 (-0.012,0.014)	4.12E-03 0.143 (-0.021,0.003)	2.35E-02 4.95E-04 (-0.051,-0.015)**	6.79E-03 0.058 (-0.024,3.83E-04)	1.30E-03 0.412 (-0.047,0.019)	1.61E-03 0.353 (-0.025,0.009)
<b>Protein-lipid complex (-APOE)</b>	4.31E-04 0.643 (-0.044,0.027)	7.66E-04 0.529 (-0.018,0.009)	1.41E-03 0.391 (-0.018,0.007)	9.63E-03 0.026 (-0.041,-0.003)*	5.55E-03 0.087 (-0.023,0.002)	1.62E-04 0.772 (-0.029,0.039)	4.68E-05 0.874 (-0.016,0.019)
<b>Regulation of amyloid precursor protein catabolic process (-APOE)</b>	1.07E-02 0.021 (-0.075,-0.006)*	5.28E-05 0.869 (-0.012,0.014)	4.12E-03 0.143 (-0.021,0.003)	2.35E-02 4.95E-04 (-0.051,-0.015)**	6.79E-03 0.058 (-0.024,3.83E-04)	1.30E-03 0.412 (-0.047,0.019)	1.61E-03 0.353 (-0.025,0.009)
<b>Tau protein binding (-APOE)</b>	3.03E-05 0.902 (-0.033,0.037)	3.88E-03 0.156 (-0.023,0.004)	2.94E-03 0.216 (-0.020,0.005)	9.76E-03 0.025 (-0.041,-0.003)*	7.48E-03 0.047 (-0.025,-2.06E-04)*	1.23E-04 0.801 (-0.029,0.038)	5.43E-05 0.864 (-0.019,0.016)
<b>Reverse cholesterol transport (-APOE)</b>	8.17E-04 0.524 (-0.047,0.024)	5.59E-05 0.865 (-0.012,0.015)	7.90E-03 0.042 (-0.025,-4.75E-04)*	3.38E-03 0.188 (-0.032,0.006)	8.50E-03 0.034 (-0.026,-0.001)*	1.92E-04 0.752 (-0.039,0.028)	1.54E-03 0.363 (-0.025,0.009)
<b>Protein-lipid complex subunit organization (-APOE)</b>	1.17E-02 0.016 (-0.079,-0.008)*	6.45E-04 0.563 (-0.010,0.018)	6.32E-03 0.070 (-0.024,0.001)	3.42E-03 0.186 (-0.032,0.006)	9.61E-03 0.024 (-0.027,-0.002)*	1.80E-03 0.335 (-0.051,0.017)	2.31E-03 0.265 (-0.027,0.007)
<b>Plasma lipoprotein particle assembly (-APOE)</b>	2.42E-07 0.991 (-0.035,0.035)	1.53E-05 0.929 (-0.013,0.014)	9.74E-04 0.477 (-0.017,0.008)	1.46E-03 0.388 (-0.027,0.011)	1.55E-03 0.367 (-0.018,0.007)	1.24E-04 0.800 (-0.029,0.038)	2.11E-10 1.000 (-0.017,0.017)
<b>Activation of immune response (-APOE)</b>	2.92E-03 0.228 (-0.055,0.013)	7.22E-08 0.995 (-0.013,0.013)	2.24E-03 0.280 (-0.005,0.019)	6.22E-04 0.573 (-0.013,0.024)	4.11E-05 0.883 (-0.011,0.013)	1.19E-03 0.434 (-0.046,0.020)	7.73E-05 0.839 (-0.018,0.015)
<b>Genome-wide PRS (-APOE)</b>	1.89E-03 0.333 (-0.052,0.018)	2.67E-04 0.710 (-0.016,0.011)	3.22E-04 0.683 (-0.015,0.010)	9.67E-04 0.482 (-0.012,0.026)	1.36E-03 0.398 (-0.018,0.007)	1.29E-03 0.414 (-0.019,0.047)	1.40E-03 0.386 (-0.025,0.009)
<b>APOE SNPs PRS</b>	3.37E-07 0.990 (-0.035,0.034)	5.84E-03 0.082 (-0.025,0.001)	2.03E-03 0.305 (-0.018,0.006)	3.16E-03 0.204 (-0.031,0.007)	1.49E-03 0.376 (-0.018,0.007)	2.99E-04 0.694 (-0.025,0.040)	5.20E-04 0.597 (-0.021,0.012)

R2 and p values for subcortical volumes in the right hemisphere and each polygenic score at a PT of 0.001. The column names show the region of interest, while the row names show the polygenic scores.

\* Nominally significant associations (p value < .05).

\*\* FDR corrected associations <0.05.

Acronyms: PRS = Polygenic Risk Score; PT = polygenic threshold; APOE = Apolipoprotein E; L = left; R = right; FDR = false discovery rate.

**Figure 5.7. Associations between PRS ( $P^T = 0.001$ ) and thickness in cortical and temporal regions of cortex in ALSPAC,  $p < 0.05$**

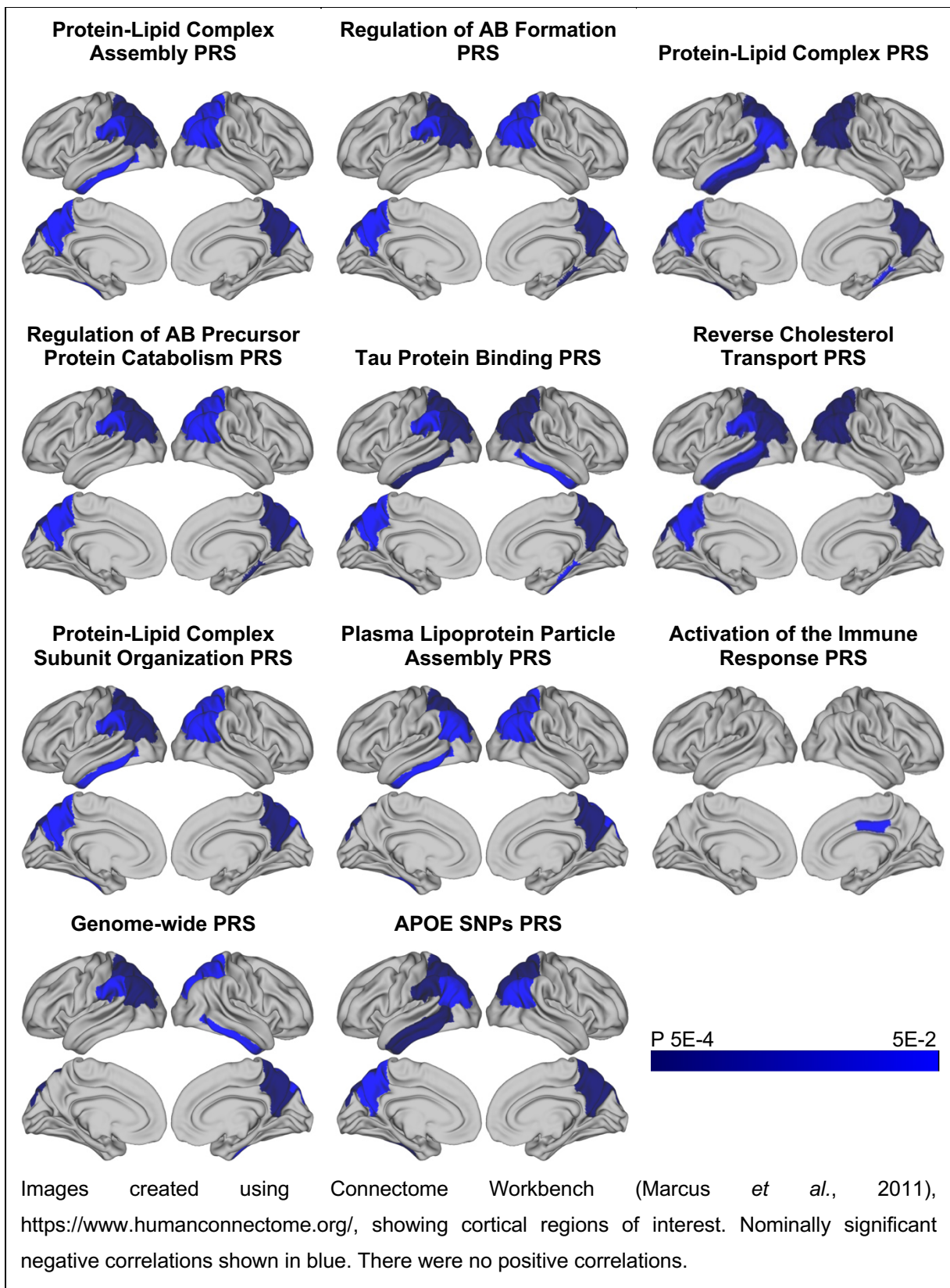
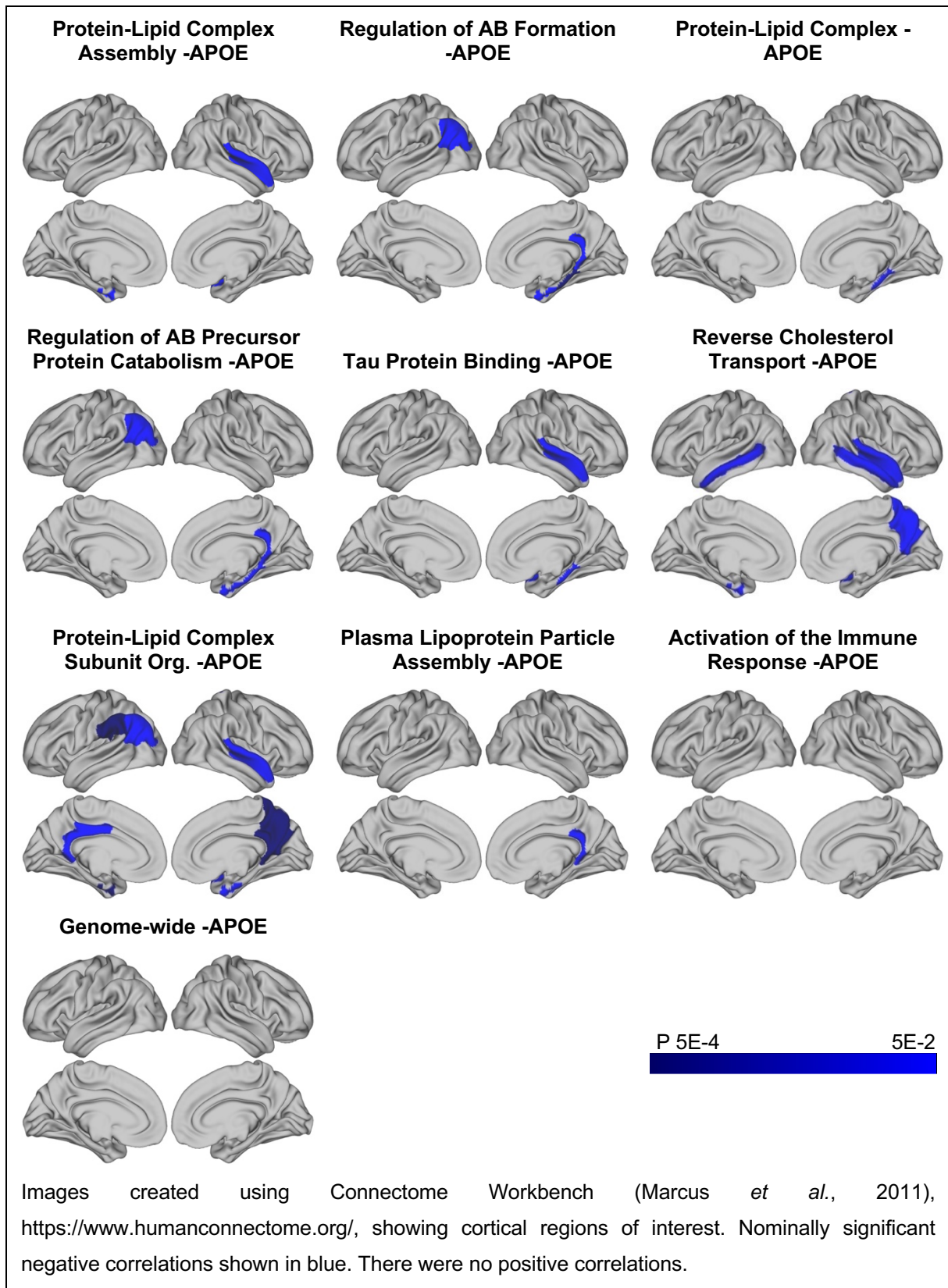


**Figure 5.8. Associations between PRS ( $P^T = 0.001$ ) excluding APOE and thickness in cortical and temporal regions of cortex in ALSPAC,  $p < 0.05$**



#### 5.4.4 Cortical thickness in UK Biobank

In UK Biobank, the genome-wide PRS was negatively associated with cortical thickness in the left and right entorhinal cortex ( $p = 0.019$ ,  $R^2 = 2.95 \times 10^{-4}$  and  $p = 0.006$ ,  $R^2 = 3.94 \times 10^{-4}$  respectively), and the left parahippocampal cortex ( $p = 0.024$ ,  $R^2 = 2.67 \times 10^{-4}$ ). When FDR correction was applied, none of these results remained significant. When the *APOE* region was excluded from the score, only the right entorhinal cortex remained significantly associated with the PRS ( $p = 0.005$ ,  $R^2 = 4.32 \times 10^{-4}$ ).

The pathway specific PRS were negatively associated with cortical thickness in similar regions. For example, the protein-lipid complex pathway was associated with reduced cortical thickness in the following regions: right inferior temporal ( $p = 0.003$ ,  $R^2 = 4.61 \times 10^{-4}$ ), right middle temporal ( $p = 0.008$ ,  $R^2 = 3.48 \times 10^{-4}$ ), right and left supra-marginal ( $p = 0.013$ ,  $R^2 = 2.86 \times 10^{-4}$  and  $p = 0.016$ ,  $R^2 = 2.69 \times 10^{-4}$  respectively), right inferior parietal ( $p = 0.025$ ,  $R^2 = 2.14 \times 10^{-4}$ ), right and left parahippocampal ( $p = 0.03$ ,  $R^2 = 2.42 \times 10^{-4}$  and  $p = 0.04$ ,  $R^2 = 2.22 \times 10^{-4}$  respectively) and right temporal pole regions ( $p = 0.041$ ,  $R^2 = 2.15 \times 10^{-5}$ ). These results were unchanged when the *APOE* region was excluded from the score, although they did not withstand correction for multiple comparisons. The immune response PRS showed a different pattern of association. It was negatively associated with the right posterior cingulate only ( $p = 0.011$ ,  $R^2 = 3.29 \times 10^{-4}$ ), and with the right posterior cingulate and left inferior temporal regions with the *APOE* region removed ( $p = 0.010$ ,  $R^2 = 3.37 \times 10^{-4}$  and  $0.043$ ,  $R^2 = 2.12 \times 10^{-4}$  respectively).

*APOE* region SNPs were associated with reduced thickness in the left entorhinal ( $p = 0.018$ ,  $R^2 = 3.04 \times 10^{-4}$ ) and right parahippocampal regions ( $p = 0.023$ ,  $R^2 = 2.67 \times 10^{-4}$ ). The regions showing nominally significant associations with PRS, including and excluding the *APOE* region, are shown in Figures 5.2 and 5.3. The results are summarised in Table 5.2, and those surviving FDR correction for multiple comparisons of PRS and phenotype are indicated.

**Table 5.17 Results for UK Biobank cortical thickness in left parietal regions and PRS including APOE at  $P^T$  0.001**

	Left inferior parietal		Left isthmus cingulate		Left posterior cingulate		Left precuneus		Left superior parietal		Left supramarginal	
	$R^2$	p (95% CI)	$R^2$	p (95% CI)	$R^2$	p (95% CI)	$R^2$	p (95% CI)	$R^2$	p (95% CI)	$R^2$	p (95% CI)
<b>Polygenic risk score</b>												
<b>Protein-lipid complex assembly</b>	5.62E-05	0.272 (-0.003,0.001)	1.51E-05	0.583 (-0.004,0.002)	1.76E-05	0.563 (-0.003,0.002)	2.90E-05	0.437 (-0.003,0.001)	2.74E-05	0.459 (-0.001,0.003)	2.69E-04	0.016 (-0.004,-4.59E-04)*
<b>Regulation of A<math>\beta</math> formation</b>	5.63E-05	0.272 (-0.003,0.001)	1.50E-05	0.584 (-0.004,0.002)	1.76E-05	0.564 (-0.003,0.002)	2.91E-05	0.436 (-0.003,0.001)	2.74E-05	0.459 (-0.001,0.003)	2.69E-04	0.016 (-0.004,-4.61E-04)*
<b>Protein-lipid complex</b>	5.64E-05	0.271 (-0.003,0.001)	1.52E-05	0.582 (-0.004,0.002)	1.76E-05	0.563 (-0.003,0.002)	2.93E-05	0.435 (-0.003,0.001)	2.73E-05	0.460 (-0.001,0.003)	2.69E-04	0.016 (-0.004,-4.61E-04)*
<b>Regulation of amyloid precursor protein catabolic process</b>	5.64E-05	0.271 (-0.003,0.001)	1.52E-05	0.582 (-0.004,0.002)	1.76E-05	0.563 (-0.003,0.002)	2.95E-05	0.434 (-0.003,0.001)	2.73E-05	0.460 (-0.001,0.003)	2.70E-04	0.016 (-0.004,-4.62E-04)*
<b>Tau protein binding</b>	5.66E-05	0.271 (-0.003,0.001)	1.53E-05	0.581 (-0.004,0.002)	1.76E-05	0.563 (-0.003,0.002)	2.96E-05	0.432 (-0.003,0.001)	2.73E-05	0.460 (-0.001,0.003)	2.70E-04	0.016 (-0.004,-4.62E-04)*
<b>Reverse cholesterol transport</b>	5.67E-05	0.270 (-0.003,0.001)	1.54E-05	0.580 (-0.004,0.002)	1.76E-05	0.564 (-0.003,0.002)	2.97E-05	0.432 (-0.003,0.001)	2.72E-05	0.461 (-0.001,0.003)	2.70E-04	0.016 (-0.004,-4.63E-04)*
<b>Protein-lipid complex subunit organization</b>	5.67E-05	0.270 (-0.003,0.001)	1.54E-05	0.580 (-0.004,0.002)	1.75E-05	0.564 (-0.003,0.002)	2.98E-05	0.431 (-0.003,0.001)	2.72E-05	0.461 (-0.001,0.003)	2.70E-04	0.016 (-0.004,-4.64E-04)*
<b>Plasma lipoprotein particle assembly</b>	5.67E-05	0.270 (-0.003,0.001)	1.54E-05	0.579 (-0.004,0.002)	1.75E-05	0.565 (-0.003,0.002)	2.99E-05	0.431 (-0.003,0.001)	2.72E-05	0.461 (-0.001,0.003)	2.70E-04	0.016 (-0.004,-4.64E-04)*
<b>Activation of immune response</b>	2.54E-05	0.460 (-0.003,0.001)	3.57E-06	0.790 (-0.003,0.003)	1.42E-05	0.604 (-0.003,0.002)	1.29E-04	0.101 (-0.004,3.21E-04)	1.37E-04	0.098 (-0.004,3.01E-04)	6.00E-05	0.255 (-0.003,0.001)
<b>Genome-wide PRS</b>	8.04E-07	0.896 (-0.002,0.002)	3.52E-05	0.402 (-0.002,0.004)	1.47E-04	0.095 (0.000,0.004)	5.38E-05	0.290 (-0.001,0.003)	1.95E-04	0.048 (0.000,0.004)*	1.05E-04	0.132 (-0.004,4.62E-04)

R2 and p values for subcortical volumes in the left hemisphere and each polygenic score at a  $P^T$  of 0.001. The column names shows the region of interest, while the row names show the polygenic scores.

\* Nominally significant associations (p value < .05).

\*\* FDR corrected associations <0.05.

Acronyms: PRS = Polygenic Risk Score;  $P^T$  = polygenic threshold; APOE = Apolipoprotein E; L = left; R = right; R = right; FDR = false discovery rate.

**Table 5.18 Results for UK Biobank cortical thickness in left temporal regions and PRS including APOE at  $P^T$  0.001**

	Left entorhinal	Left inferior temporal	Left middle temporal	Left parahippocampal	Superior temporal	Left temporal pole	Left transverse temporal
Polygenic risk score	$R^2$	$R^2$	$R^2$	$R^2$	$R^2$	$R^2$	$R^2$
	p (95% CI)	p (95% CI)	p (95% CI)	p (95% CI)	p (95% CI)	p (95% CI)	p (95% CI)
<b>Protein-lipid complex assembly</b>	1.80E-04 (-0.010,3.48E-04)	2.13E-05 (-0.0003,0.002)	2.69E-04 (-0.005,-4.58E-04)*	2.22E-04 (-0.010,-2.42E-04)*	7.30E-05 (-0.004,0.001)	9.59E-05 (-0.0008,0.002)	5.14E-05 (-0.002,0.005)
<b>Regulation of A<math>\beta</math> formation</b>	1.80E-04 (-0.010,3.40E-04)	2.13E-05 (-0.0003,0.002)	2.69E-04 (-0.005,-4.61E-04)*	2.22E-04 (-0.010,-2.48E-04)*	7.30E-05 (-0.004,0.001)	9.62E-05 (-0.0008,0.002)	5.14E-05 (-0.002,0.005)
<b>Protein-lipid complex</b>	1.80E-04 (-0.010,3.39E-04)	2.14E-05 (-0.0003,0.002)	2.69E-04 (-0.005,-4.59E-04)*	2.22E-04 (-0.010,-2.49E-04)*	7.31E-05 (-0.004,0.001)	9.62E-05 (-0.0008,0.002)	5.14E-05 (-0.002,0.005)
<b>Regulation of amyloid precursor protein catabolic process</b>	1.81E-04 (-0.010,3.36E-04)	2.15E-05 (-0.0003,0.002)	2.69E-04 (-0.005,-4.59E-04)*	2.22E-04 (-0.010,-2.50E-04)*	7.31E-05 (-0.004,0.001)	9.64E-05 (-0.0008,0.002)	5.15E-05 (-0.002,0.005)
<b>Tau protein binding</b>	1.81E-04 (-0.010,3.35E-04)	2.16E-05 (-0.0003,0.002)	2.69E-04 (-0.005,-4.58E-04)*	2.22E-04 (-0.010,-2.52E-04)*	7.32E-05 (-0.004,0.001)	9.64E-05 (-0.0008,0.002)	5.15E-05 (-0.002,0.005)
<b>Reverse cholesterol transport</b>	1.81E-04 (-0.010,3.37E-04)	2.16E-05 (-0.0003,0.002)	2.68E-04 (-0.005,-4.56E-04)*	2.22E-04 (-0.010,-2.51E-04)*	7.32E-05 (-0.004,0.001)	9.63E-05 (-0.0008,0.002)	5.15E-05 (-0.002,0.005)
<b>Protein-lipid complex subunit organization</b>	1.81E-04 (-0.010,3.38E-04)	2.17E-05 (-0.0003,0.002)	2.68E-04 (-0.005,-4.55E-04)*	2.22E-04 (-0.010,-2.50E-04)*	7.32E-05 (-0.004,0.001)	9.63E-05 (-0.0008,0.002)	5.15E-05 (-0.002,0.005)
<b>Plasma lipoprotein particle assembly</b>	1.81E-04 (-0.010,3.37E-04)	2.17E-05 (-0.0003,0.002)	2.68E-04 (-0.005,-4.54E-04)*	2.22E-04 (-0.010,-2.51E-04)*	7.32E-05 (-0.004,0.001)	9.64E-05 (-0.0008,0.002)	5.15E-05 (-0.002,0.005)
<b>Activation of immune response</b>	1.58E-04 (-0.010,0.001)	2.04E-04 (-0.005,-2.58E-05)*	1.19E-04 (-0.004,4.56E-04)	9.95E-05 (-0.008,0.001)	1.45E-04 (-0.004,1.93E-04)	2.06E-04 (-0.010,8.19E-06)	4.82E-05 (-0.005,0.002)
<b>Genome-wide PRS</b>	2.95E-04 (-0.011,-0.001)*	9.49E-07 (-0.002,0.003)	4.75E-05 (-0.003,0.001)	2.67E-04 (-0.011,-0.001)*	1.32E-06 (-0.002,0.002)	1.03E-04 (-0.008,0.001)	3.24E-06 (-0.003,0.004)

R<sup>2</sup> and p values for subcortical volumes in the left hemisphere and each polygenic score at a  $P^T$  of 0.001. The column names show the region of interest, while the row names show the polygenic scores.

\* Nominally significant associations (p value < .05).

\*\* FDR corrected associations <0.05.

Acronyms: PRS = Polygenic Risk Score;  $P^T$  = polygenic threshold; APOE = Apolipoprotein E; L = left; R = right; FDR = false discovery rate.

**Table 5.19 Results for UK Biobank cortical thickness in left parietal regions and PRS including APOE at P<sup>T</sup> 0.001**

	Left inferior Parietal	Left isthmus cingulate	Left posterior cingulate	Left precuneus	Left superior parietal	Left supramarginal
Polygenic risk score	R <sup>2</sup> p (95% CI)	R <sup>2</sup> p (95% CI)	R <sup>2</sup> p (95% CI)			
<b>Protein-lipid complex assembly (-APOE)</b>	5.63E-05 0.272 (-0.003,0.001)	1.51E-05 0.583 (-0.004,0.002)	1.76E-05 0.564 (-0.003,0.002)	2.90E-05 0.437 (-0.003,0.001)	2.74E-05 0.459 (-0.001,0.003)	2.69E-04 0.016 (-0.004,-4.60E-04)*
<b>Regulation of Aβ formation (-APOE)</b>	5.64E-05 0.271 (-0.003,0.001)	1.50E-05 0.584 (-0.004,0.002)	1.76E-05 0.563 (-0.003,0.002)	2.92E-05 0.436 (-0.003,0.001)	2.74E-05 0.460 (-0.001,0.003)	2.69E-04 0.016 (-0.004,-4.61E-04)*
<b>Protein-lipid complex (-APOE)</b>	5.64E-05 0.271 (-0.003,0.001)	1.52E-05 0.582 (-0.004,0.002)	1.76E-05 0.564 (-0.003,0.002)	2.93E-05 0.435 (-0.003,0.001)	2.73E-05 0.460 (-0.001,0.003)	2.69E-04 0.016 (-0.004,-4.61E-04)*
<b>Regulation of amyloid precursor protein catabolic process (-APOE)</b>	5.65E-05 0.271 (-0.003,0.001)	1.52E-05 0.582 (-0.004,0.002)	1.76E-05 0.563 (-0.003,0.002)	2.95E-05 0.434 (-0.003,0.001)	2.73E-05 0.460 (-0.001,0.003)	2.70E-04 0.016 (-0.004,-4.62E-04)*
<b>Tau protein binding (-APOE)</b>	5.66E-05 0.271 (-0.003,0.001)	1.53E-05 0.581 (-0.004,0.002)	1.76E-05 0.563 (-0.003,0.002)	2.96E-05 0.432 (-0.003,0.001)	2.73E-05 0.460 (-0.001,0.003)	2.70E-04 0.016 (-0.004,-4.62E-04)*
<b>Reverse cholesterol transport (-APOE)</b>	5.67E-05 0.270 (-0.003,0.001)	1.54E-05 0.580 (-0.004,0.002)	1.76E-05 0.564 (-0.003,0.002)	2.97E-05 0.432 (-0.003,0.001)	2.72E-05 0.461 (-0.001,0.003)	2.70E-04 0.016 (-0.004,-4.63E-04)*
<b>Protein-lipid complex subunit organization (-APOE)</b>	5.67E-05 0.270 (-0.003,0.001)	1.54E-05 0.580 (-0.004,0.002)	1.75E-05 0.564 (-0.003,0.002)	2.98E-05 0.431 (-0.003,0.001)	2.72E-05 0.461 (-0.001,0.003)	2.70E-04 0.016 (-0.004,-4.64E-04)*
<b>Plasma lipoprotein particle assembly (-APOE)</b>	5.68E-05 0.270 (-0.003,0.001)	1.54E-05 0.579 (-0.004,0.002)	1.75E-05 0.564 (-0.003,0.002)	2.99E-05 0.430 (-0.003,0.001)	2.72E-05 0.461 (-0.001,0.003)	2.70E-04 0.016 (-0.004,-4.64E-04)*
<b>Activation of immune response (-APOE)</b>	7.77E-06 0.683 (-0.002,0.001)	2.68E-06 0.817 (-0.003,0.003)	2.33E-05 0.507 (-0.003,0.001)	1.10E-04 0.130 (-0.004,4.51E-04)	1.21E-04 0.120 (-0.003,3.99E-04)	3.99E-05 0.353 (-0.003,0.001)
<b>Genome-wide PRS (-APOE)</b>	2.88E-05 0.432 (-0.001,0.003)	7.93E-05 0.209 (-0.001,0.005)	4.82E-05 0.339 (-0.001,0.003)	7.01E-05 0.227 (-0.001,0.003)	9.64E-05 0.165 (-0.001,0.003)	1.85E-05 0.527 (-0.003,0.001)
<b>APOE SNPs PRS</b>	3.17E-05 0.409 (-0.003,0.001)	3.72E-06 0.785 (-0.003,0.003)	1.21E-04 0.130 (-0.001,0.004)	1.26E-06 0.871 (-0.002,0.002)	1.06E-04 0.146 (0.000,0.003)	1.30E-04 0.094 (-0.004,2.90E-04)

R<sup>2</sup> and p values for subcortical volumes in the left hemisphere and each polygenic score at a PT of 0.001. The column names shows the region of interest, while the row names show the polygenic scores.

\* Nominally significant associations (p value < .05).

\*\* FDR corrected associations <0.05.

Acronyms: PRS = Polygenic Risk Score; PT = polygenic threshold; APOE = Apolipoprotein E; L = left; R = right; FDR = false discovery rate.

**Table 5.20 Results for UK Biobank cortical thickness in left temporal regions and PRS excluding APOE at P<sup>T</sup> 0.001**

	Left entorhinal	Left inferior temporal	Left middle temporal	Left parahippocampal	Superior temporal	Left temporal pole	Left transverse temporal
	R <sup>2</sup>	R <sup>2</sup>	R <sup>2</sup>	R <sup>2</sup>	R <sup>2</sup>	R <sup>2</sup>	R <sup>2</sup>
	p (95% CI)	p (95% CI)	p (95% CI)	p (95% CI)	p (95% CI)	p (95% CI)	p (95% CI)
<b>Polygenic risk score</b>							
<b>Protein-lipid complex assembly (-APOE)</b>	1.80E-04 0.067 (-0.010,3.43E-04)	2.12E-05 0.523 (-0.003,0.002)	2.69E-04 0.018 (-0.005,-4.60E-04)*	2.22E-04 0.040 (-0.010,-2.48E-04)*	7.30E-05 0.203 (-0.004,0.001)	9.61E-05 0.181 (-0.008,0.002)	5.13E-05 0.325 (-0.002,0.005)
<b>Regulation of Aβ formation (-APOE)</b>	1.80E-04 0.067 (-0.010,3.41E-04)	2.14E-05 0.521 (-0.003,0.002)	2.69E-04 0.018 (-0.005,-4.61E-04)*	2.22E-04 0.040 (-0.010,-2.48E-04)*	7.31E-05 0.202 (-0.004,0.001)	9.62E-05 0.181 (-0.008,0.002)	5.13E-05 0.325 (-0.002,0.005)
<b>Protein-lipid complex (-APOE)</b>	1.80E-04 0.067 (-0.010,3.39E-04)	2.14E-05 0.521 (-0.003,0.002)	2.69E-04 0.018 (-0.005,-4.59E-04)*	2.22E-04 0.039 (-0.010,-2.49E-04)*	7.31E-05 0.202 (-0.004,0.001)	9.63E-05 0.181 (-0.008,0.002)	5.14E-05 0.324 (-0.002,0.005)
<b>Regulation of amyloid precursor protein catabolic process (-APOE)</b>	1.81E-04 0.067 (-0.010,3.37E-04)	2.15E-05 0.520 (-0.003,0.002)	2.69E-04 0.018 (-0.005,-4.59E-04)*	2.22E-04 0.039 (-0.010,-2.50E-04)*	7.31E-05 0.202 (-0.004,0.001)	9.63E-05 0.180 (-0.008,0.002)	5.15E-05 0.324 (-0.002,0.005)
<b>Tau protein binding (-APOE)</b>	1.81E-04 0.067 (-0.010,3.36E-04)	2.16E-05 0.519 (-0.003,0.002)	2.69E-04 0.019 (-0.005,-4.58E-04)*	2.22E-04 0.039 (-0.010,-2.51E-04)*	7.32E-05 0.202 (-0.004,0.001)	9.64E-05 0.180 (-0.008,0.002)	5.15E-05 0.324 (-0.002,0.005)
<b>Reverse cholesterol transport (-APOE)</b>	1.81E-04 0.067 (-0.010,3.36E-04)	2.16E-05 0.519 (-0.003,0.002)	2.68E-04 0.019 (-0.005,-4.56E-04)*	2.22E-04 0.039 (-0.010,-2.51E-04)*	7.32E-05 0.202 (-0.004,0.001)	9.64E-05 0.180 (-0.008,0.002)	5.15E-05 0.324 (-0.002,0.005)
<b>Protein-lipid complex subunit organization (-APOE)</b>	1.81E-04 0.067 (-0.010,3.37E-04)	2.17E-05 0.518 (-0.003,0.002)	2.68E-04 0.019 (-0.005,-4.55E-04)*	2.22E-04 0.039 (-0.010,-2.51E-04)*	7.32E-05 0.202 (-0.004,0.001)	9.63E-05 0.180 (-0.008,0.002)	5.15E-05 0.324 (-0.002,0.005)
<b>Plasma lipoprotein particle assembly (-APOE)</b>	1.81E-04 0.067 (-0.010,3.38E-04)	2.17E-05 0.518 (-0.003,0.002)	2.68E-04 0.019 (-0.005,-4.54E-04)*	2.22E-04 0.039 (-0.010,-2.51E-04)*	7.32E-05 0.202 (-0.004,0.001)	9.63E-05 0.180 (-0.008,0.002)	5.15E-05 0.324 (-0.002,0.005)
<b>Activation of immune response (-APOE)</b>	1.52E-04 0.093 (-0.010,0.001)	2.12E-04 0.044 (-0.005,-7.08E-05)*	6.96E-05 0.231 (-0.004,0.001)	4.34E-05 0.363 (-0.007,0.003)	1.11E-04 0.116 (-0.004,4.54E-04)	1.60E-04 0.085 (-0.009,0.001)	3.97E-05 0.387 (-0.005,0.002)
<b>Genome-wide PRS (-APOE)</b>	7.17E-05 0.248 (-0.008,0.002)	7.93E-08 0.969 (-0.002,0.002)	5.98E-06 0.725 (-0.003,0.002)	1.42E-04 0.099 (-0.009,0.001)	9.82E-07 0.882 (-0.002,0.002)	3.97E-05 0.390 (-0.007,0.003)	1.43E-05 0.604 (-0.004,0.002)
<b>APOE SNPs PRS</b>	3.04E-04 0.018 (-0.011,-0.001)*	4.00E-06 0.781 (-0.002,0.003)	6.82E-05 0.235 (-0.004,0.001)	1.30E-04 0.115 (-0.009,0.001)	3.64E-07 0.928 (-0.002,0.002)	7.37E-05 0.241 (-0.008,0.002)	6.45E-05 0.270 (-0.001,0.005)

R<sup>2</sup> and p values for subcortical volumes in the left hemisphere and each polygenic score at a P<sup>T</sup> of 0.001. The column names show the region of interest, while the row names show the polygenic scores.

\* Nominally significant associations (p value < .05).

\*\* FDR corrected associations <0.05.

Acronyms: PRS = Polygenic Risk Score; P<sup>T</sup> = polygenic threshold; APOE = Apolipoprotein E; L = left; R = right; FDR = false discovery rate.

**Table 5.21 Results for UK Biobank cortical thickness in right parietal regions and PRS including APOE at P<sup>T</sup> 0.001**

	Right inferior parietal	Right isthmus cingulate	Right posterior cingulate	Right precuneus	Right superior parietal	Right supramarginal
	R <sup>2</sup> p (95% CI)	R <sup>2</sup> p (95% CI)	R <sup>2</sup> p (95% CI)	R <sup>2</sup> p (95% CI)	R <sup>2</sup> p (95% CI)	R <sup>2</sup> p (95% CI)
<b>Polygenic risk score</b>						
<b>Protein-lipid complex assembly</b>	2.14E-04 0.025 (-0.004,-2.82E-04)*	8.72E-05 0.182 (-0.005,0.001)	4.59E-05 0.345 (-0.003,0.001)	7.66E-05 0.201 (-0.003,0.001)	1.14E-05 0.627 (-0.001,0.002)	2.86E-04 0.013 (-0.005,-0.001)*
<b>Regulation of Aβ formation</b>	2.14E-04 0.025 (-0.004,-2.84E-04)*	8.73E-05 0.182 (-0.005,0.001)	4.62E-05 0.343 (-0.003,0.001)	7.66E-05 0.201 (-0.003,0.001)	1.14E-05 0.628 (-0.001,0.002)	2.87E-04 0.013 (-0.005,-0.001)*
<b>Protein-lipid complex</b>	2.14E-04 0.025 (-0.004,-2.84E-04)*	8.78E-05 0.181 (-0.005,0.001)	4.64E-05 0.342 (-0.003,0.001)	7.68E-05 0.200 (-0.003,0.001)	1.13E-05 0.629 (-0.001,0.002)	2.87E-04 0.013 (-0.005,-0.001)*
<b>Regulation of amyloid precursor protein catabolic</b>	2.14E-04 0.025 (-0.004,-2.84E-04)*	8.80E-05 0.180 (-0.005,0.001)	4.66E-05 0.341 (-0.003,0.001)	7.68E-05 0.200 (-0.003,0.001)	1.12E-05 0.630 (-0.001,0.002)	2.87E-04 0.013 (-0.005,-0.001)*
<b>Tau protein binding</b>	2.14E-04 0.025 (-0.004,-2.84E-04)*	8.82E-05 0.180 (-0.005,0.001)	4.68E-05 0.340 (-0.003,0.001)	7.69E-05 0.200 (-0.003,0.001)	1.12E-05 0.631 (-0.001,0.002)	2.87E-04 0.013 (-0.005,-0.001)*
<b>Reverse cholesterol transport</b>	2.14E-04 0.025 (-0.004,-2.84E-04)*	8.83E-05 0.179 (-0.005,0.001)	4.69E-05 0.340 (-0.003,0.001)	7.70E-05 0.200 (-0.003,0.001)	1.11E-05 0.632 (-0.001,0.002)	2.87E-04 0.013 (-0.005,-0.001)*
<b>Protein-lipid complex subunit organization</b>	2.14E-04 0.025 (-0.004,-2.84E-04)*	8.83E-05 0.179 (-0.005,0.001)	4.69E-05 0.340 (-0.003,0.001)	7.71E-05 0.200 (-0.003,0.001)	1.11E-05 0.632 (-0.001,0.002)	2.87E-04 0.013 (-0.005,-0.001)*
<b>Plasma lipoprotein particle assembly</b>	2.14E-04 0.025 (-0.004,-2.84E-04)*	8.82E-05 0.180 (-0.005,0.001)	4.70E-05 0.339 (-0.003,0.001)	7.70E-05 0.200 (-0.003,0.001)	1.11E-05 0.633 (-0.001,0.002)	2.87E-04 0.013 (-0.005,-0.001)*
<b>Activation of immune response</b>	3.40E-05 0.372 (-0.003,0.001)	9.90E-05 0.155 (-0.005,0.001)	3.29E-04 0.011 (-0.005,-0.001)*	1.19E-04 0.112 (-0.004,3.75E-04)	1.49E-04 0.079 (-0.004,2.04E-04)	6.95E-05 0.221 (-0.003,0.001)
<b>Genome-wide PRS</b>	6.25E-05 0.226 (-0.003,0.001)	3.76E-07 0.930 (-0.003,0.003)	1.74E-05 0.561 (-0.002,0.003)	6.86E-06 0.702 (-0.002,0.002)	1.16E-05 0.625 (-0.001,0.002)	7.21E-07 0.901 (-0.002,0.002)

R2 and p values for subcortical volumes in the left hemisphere and each polygenic score at a PT of 0.001. The column names shows the region of interest, while the row names show the polygenic scores.

\* Nominally significant associations (p value < .05).

\*\* FDR corrected associations <0.05.

Acronyms: PRS = Polygenic Risk Score; PT = polygenic threshold; APOE = Apolipoprotein E; L = left; R = right; FDR = false discovery rate.

**Table 5.22 Results for UK Biobank cortical thickness in right temporal regions and PRS including APOE at P<sup>T</sup> 0.001**

Polygenic risk score	Right entorhinal		Right inferior temporal		Right middle temporal		Right parahippocampal		Right superior temporal		Right temporal pole		Right transverse temporal	
	R <sup>2</sup>	p (95% CI)	R <sup>2</sup>	p (95% CI)	R <sup>2</sup>	p (95% CI)	R <sup>2</sup>	p (95% CI)	R <sup>2</sup>	p (95% CI)	R <sup>2</sup>	p (95% CI)	R <sup>2</sup>	p (95% CI)
<b>Protein-lipid complex assembly</b>	1.38E-04	0.109 (-0.010,0.001)	4.61E-04	0.003 (-0.006,-0.001)*	3.48E-04	0.008 (-0.005,-0.001)*	2.42E-04	0.030 (-0.009,-4.55E-04)*	2.15E-05	0.496 (-0.003,0.001)	2.27E-04	0.041 (-0.010,-2.26E-04)*	1.11E-04	0.151 (-0.006,0.001)
<b>Regulation of Aβ formation</b>	1.38E-04	0.108 (-0.010,0.001)	4.61E-04	0.003 (-0.006,-0.001)*	3.49E-04	0.008 (-0.005,-0.001)*	2.43E-04	0.030 (-0.009,-4.62E-04)*	2.15E-05	0.496 (-0.003,0.001)	2.27E-04	0.041 (-0.010,-2.29E-04)*	1.11E-04	0.150 (-0.006,0.001)
<b>Protein-lipid complex</b>	1.38E-04	0.108 (-0.010,0.001)	4.61E-04	0.003 (-0.006,-0.001)*	3.49E-04	0.008 (-0.005,-0.001)*	2.43E-04	0.030 (-0.009,-4.62E-04)*	2.16E-05	0.495 (-0.003,0.001)	2.27E-04	0.041 (-0.010,-2.28E-04)*	1.11E-04	0.150 (-0.006,0.001)
<b>Regulation of amyloid precursor protein catabolic</b>	1.38E-04	0.108 (-0.010,0.001)	4.61E-04	0.003 (-0.006,-0.001)*	3.49E-04	0.008 (-0.005,-0.001)*	2.43E-04	0.030 (-0.009,-4.65E-04)*	2.16E-05	0.495 (-0.003,0.001)	2.27E-04	0.041 (-0.010,-2.30E-04)*	1.11E-04	0.150 (-0.006,0.001)
<b>Tau protein binding</b>	1.38E-04	0.108 (-0.010,0.001)	4.60E-04	0.003 (-0.006,-0.001)*	3.49E-04	0.008 (-0.005,-0.001)*	2.43E-04	0.030 (-0.009,-4.66E-04)*	2.17E-05	0.494 (-0.003,0.001)	2.27E-04	0.041 (-0.010,-2.30E-04)*	1.12E-04	0.149 (-0.006,0.001)
<b>Reverse cholesterol transport</b>	1.38E-04	0.108 (-0.010,0.001)	4.60E-04	0.003 (-0.006,-0.001)*	3.48E-04	0.008 (-0.005,-0.001)*	2.43E-04	0.030 (-0.009,-4.65E-04)*	2.16E-05	0.495 (-0.003,0.001)	2.27E-04	0.041 (-0.010,-2.28E-04)*	1.12E-04	0.149 (-0.006,0.001)
<b>Protein-lipid complex subunit organization</b>	1.38E-04	0.108 (-0.010,0.001)	4.59E-04	0.003 (-0.006,-0.001)*	3.48E-04	0.008 (-0.005,-0.001)*	2.43E-04	0.030 (-0.009,-4.65E-04)*	2.16E-05	0.495 (-0.003,0.001)	2.27E-04	0.041 (-0.010,-2.26E-04)*	1.12E-04	0.148 (-0.006,0.001)
<b>Plasma lipoprotein particle assembly</b>	1.38E-04	0.108 (-0.010,0.001)	4.59E-04	0.003 (-0.006,-0.001)*	3.48E-04	0.008 (-0.005,-0.001)*	2.43E-04	0.030 (-0.009,-4.66E-04)*	2.16E-05	0.495 (-0.003,0.001)	2.27E-04	0.041 (-0.010,-2.25E-04)*	1.12E-04	0.148 (-0.006,0.001)
<b>Activation of immune response</b>	1.72E-04	0.073 (-0.011,4.78E-04)	4.75E-05	0.332 (-0.003,0.001)	4.15E-05	0.357 (-0.003,0.001)	2.34E-05	0.500 (-0.006,0.003)	3.69E-05	0.372 (-0.003,0.001)	8.68E-05	0.206 (-0.008,0.002)	1.78E-04	0.069 (-0.007,2.51E-04)
<b>Genome-wide PRS</b>	3.94E-04	0.007 (-0.013,-0.002)*	4.41E-05	0.351 (-0.003,0.001)	1.08E-04	0.137 (-0.004,0.001)	1.90E-04	0.055 (-0.008,8.70E-05)	4.68E-05	0.315 (-0.001,0.003)	9.00E-05	0.198 (-0.008,0.002)	7.11E-06	0.716 (-0.004,0.003)

R<sup>2</sup> and p values for subcortical volumes in the left hemisphere and each polygenic score at a PT of 0.001. The column names show the region of interest, while the row names show the polygenic scores.

\* Nominally significant associations (p value < .05).

\*\* FDR corrected associations <0.05.

Acronyms: PRS = Polygenic Risk Score; PT = polygenic threshold; APOE = Apolipoprotein E; L = left; R = right; FDR = false discovery rate.

**Table 5.23 Results for UK Biobank cortical thickness in right parietal regions and PRS excluding APOE at P<sup>T</sup> 0.001**

Polygenic risk score	Right inferior parietal R <sup>2</sup> p (95% CI)	Right isthmus cingulate R <sup>2</sup> p (95% CI)	Right posterior cingulate R <sup>2</sup> p (95% CI)	Right precuneus R <sup>2</sup> p (95% CI)	Right superior parietal R <sup>2</sup> p (95% CI)	Right supramarginal R <sup>2</sup> p (95% CI)
Protein-lipid complex assembly (-APOE)	2.14E-04 0.025 (-0.004,-2.83E-04)*	8.71E-05 0.182 (-0.005,0.001)	4.60E-05 0.345 (-0.003,0.001)	7.65E-05 0.201 (-0.003,0.001)	1.14E-05 0.627 (-0.001,0.002)	2.86E-04 0.013 (-0.005,-0.001)*
Regulation of Aβ formation (-APOE)	2.14E-04 0.025 (-0.004,-2.84E-04)*	8.74E-05 0.182 (-0.005,0.001)	4.62E-05 0.343 (-0.003,0.001)	7.67E-05 0.201 (-0.003,0.001)	1.13E-05 0.628 (-0.001,0.002)	2.87E-04 0.013 (-0.005,-0.001)*
Protein-lipid complex (-APOE)	2.14E-04 0.025 (-0.004,-2.84E-04)*	8.77E-05 0.181 (-0.005,0.001)	4.64E-05 0.342 (-0.003,0.001)	7.68E-05 0.200 (-0.003,0.001)	1.13E-05 0.629 (-0.001,0.002)	2.87E-04 0.013 (-0.005,-0.001)*
Regulation of amyloid precursor protein catabolic process (-APOE)	2.14E-04 0.025 (-0.004,-2.84E-04)*	8.80E-05 0.180 (-0.005,0.001)	4.66E-05 0.341 (-0.003,0.001)	7.69E-05 0.200 (-0.003,0.001)	1.12E-05 0.630 (-0.001,0.002)	2.87E-04 0.013 (-0.005,-0.001)*
Tau protein binding (-APOE)	2.14E-04 0.025 (-0.004,-2.84E-04)*	8.82E-05 0.180 (-0.005,0.001)	4.68E-05 0.340 (-0.003,0.001)	7.69E-05 0.200 (-0.003,0.001)	1.12E-05 0.631 (-0.001,0.002)	2.87E-04 0.013 (-0.005,-0.001)*
Reverse cholesterol transport (-APOE)	2.14E-04 0.025 (-0.004,-2.84E-04)*	8.82E-05 0.179 (-0.005,0.001)	4.69E-05 0.340 (-0.003,0.001)	7.70E-05 0.200 (-0.003,0.001)	1.11E-05 0.632 (-0.001,0.002)	2.87E-04 0.013 (-0.005,-0.001)*
Protein-lipid complex subunit organization (-APOE)	2.14E-04 0.025 (-0.004,-2.84E-04)*	8.83E-05 0.179 (-0.005,0.001)	4.70E-05 0.340 (-0.003,0.001)	7.71E-05 0.200 (-0.003,0.001)	1.11E-05 0.632 (-0.001,0.002)	2.87E-04 0.013 (-0.005,-0.001)*
Plasma lipoprotein particle assembly (-APOE)	2.14E-04 0.025 (-0.004,-2.84E-04)*	8.83E-05 0.179 (-0.005,0.001)	4.70E-05 0.339 (-0.003,0.001)	7.71E-05 0.199 (-0.003,0.001)	1.10E-05 0.633 (-0.001,0.002)	2.87E-04 0.013 (-0.005,-0.001)*
Activation of immune response (-APOE)	1.07E-05 0.617 (-0.002,0.001)	8.07E-05 0.199 (-0.005,0.001)	3.37E-04 0.010 (-0.005,-0.001)*	1.05E-04 0.135 (-0.004,4.71E-04)	1.30E-04 0.101 (-0.004,3.19E-04)	4.90E-05 0.304 (-0.003,0.001)
Genome-wide PRS (-APOE)	1.45E-06 0.854 (-0.002,0.002)	1.30E-06 0.871 (-0.003,0.003)	4.96E-05 0.326 (-0.001,0.003)	2.59E-05 0.457 (-0.001,0.003)	8.57E-06 0.674 (-0.002,0.002)	5.21E-05 0.289 (-0.001,0.003)
APOE SNPs PRS	1.34E-04 0.076 (-0.004,1.87E-04)	2.42E-07 0.944 (-0.003,0.003)	5.72E-06 0.739 (-0.003,0.002)	5.70E-06 0.727 (-0.002,0.002)	3.22E-06 0.797 (-0.002,0.002)	1.21E-04 0.106 (-0.004,3.64E-04)

R<sup>2</sup> and p values for subcortical volumes in the left hemisphere and each polygenic score at a PT of 0.001. The column names shows the region of interest, while the row names show the polygenic scores.

\* Nominally significant associations (p value < .05).

\*\* FDR corrected associations <0.05.

Acronyms: PRS = Polygenic Risk Score; PT = polygenic threshold; APOE = Apolipoprotein E; L = left; R = right; FDR = false discovery rate.

**Table 5.24 Results for UK Biobank cortical thickness in right temporal regions and PRS excluding APOE at P<sup>T</sup> 0.001**

Polygenic risk score	Right entorhinal R <sup>2</sup> p (95% CI)	Right inferior temporal R <sup>2</sup> p (95% CI)	Right middle temporal R <sup>2</sup> p (95% CI)	Right parahippocampal R <sup>2</sup> p (95% CI)	Right superior temporal R <sup>2</sup> p (95% CI)	Right temporal pole R <sup>2</sup> p (95% CI)	Right transverse temporal R <sup>2</sup> p (95% CI)
<b>Protein-lipid complex assembly (-APOE)</b>	1.38E-04 0.109 (-0.010,0.001)	4.62E-04 0.003 (-0.006,-0.001)*	3.49E-04 0.008 (-0.005,-0.001)*	2.43E-04 0.030 (-0.009,-4.59E-04)*	2.14E-05 0.497 (-0.003,0.001)	2.27E-04 0.041 (-0.010,-2.24E-04)*	1.11E-04 0.151 (-0.006,0.001)
<b>Regulation of Aβ formation (-APOE)</b>	1.38E-04 0.108 (-0.010,0.001)	4.61E-04 0.003 (-0.006,-0.001)*	3.49E-04 0.008 (-0.005,-0.001)*	2.43E-04 0.030 (-0.009,-4.61E-04)*	2.15E-05 0.496 (-0.003,0.001)	2.27E-04 0.041 (-0.010,-2.27E-04)*	1.11E-04 0.150 (-0.006,0.001)
<b>Protein-lipid complex (-APOE)</b>	1.38E-04 0.108 (-0.010,0.001)	4.61E-04 0.003 (-0.006,-0.001)*	3.49E-04 0.008 (-0.005,-0.001)*	2.43E-04 0.030 (-0.009,-4.62E-04)*	2.16E-05 0.495 (-0.003,0.001)	2.27E-04 0.041 (-0.010,-2.27E-04)*	1.11E-04 0.150 (-0.006,0.001)
<b>Regulation of amyloid precursor protein catabolic process (-APOE)</b>	1.38E-04 0.108 (-0.010,0.001)	4.61E-04 0.003 (-0.006,-0.001)*	3.49E-04 0.008 (-0.005,-0.001)*	2.43E-04 0.030 (-0.009,-4.64E-04)*	2.16E-05 0.495 (-0.003,0.001)	2.27E-04 0.041 (-0.010,-2.29E-04)*	1.12E-04 0.149 (-0.006,0.001)
<b>Tau protein binding (-APOE)</b>	1.38E-04 0.108 (-0.010,0.001)	4.60E-04 0.003 (-0.006,-0.001)*	3.49E-04 0.008 (-0.005,-0.001)*	2.43E-04 0.030 (-0.009,-4.65E-04)*	2.17E-05 0.494 (-0.003,0.001)	2.27E-04 0.041 (-0.010,-2.29E-04)*	1.12E-04 0.149 (-0.006,0.001)
<b>Reverse cholesterol transport (-APOE)</b>	1.38E-04 0.108 (-0.010,0.001)	4.60E-04 0.003 (-0.006,-0.001)*	3.48E-04 0.008 (-0.005,-0.001)*	2.43E-04 0.030 (-0.009,-4.66E-04)*	2.16E-05 0.495 (-0.003,0.001)	2.27E-04 0.041 (-0.010,-2.27E-04)*	1.12E-04 0.149 (-0.006,0.001)
<b>Protein-lipid complex subunit organization (-APOE)</b>	1.38E-04 0.108 (-0.010,0.001)	4.59E-04 0.003 (-0.006,-0.001)*	3.48E-04 0.008 (-0.005,-0.001)*	2.43E-04 0.030 (-0.009,-4.66E-04)*	2.16E-05 0.495 (-0.003,0.001)	2.27E-04 0.041 (-0.010,-2.26E-04)*	1.12E-04 0.148 (-0.006,0.001)
<b>Plasma lipoprotein particle assembly (-APOE)</b>	1.38E-04 0.108 (-0.010,0.001)	4.59E-04 0.003 (-0.006,-0.001)*	3.48E-04 0.008 (-0.005,-0.001)*	2.43E-04 0.030 (-0.009,-4.65E-04)*	2.16E-05 0.495 (-0.003,0.001)	2.27E-04 0.041 (-0.010,-2.25E-04)*	1.12E-04 0.148 (-0.006,0.001)
<b>Activation of immune response (-APOE)</b>	1.66E-04 0.078 (-0.011,0.001)	2.16E-05 0.514 (-0.003,0.001)	1.26E-05 0.612 (-0.003,0.002)	8.67E-06 0.681 (-0.005,0.003)	2.91E-05 0.429 (-0.003,0.001)	1.17E-04 0.142 (-0.009,0.001)	1.13E-04 0.146 (-0.006,0.001)
<b>Genome-wide PRS (-APOE)</b>	4.32E-04 0.005 (-0.014,-0.002)*	1.24E-09 0.996 (-0.002,0.002)	4.33E-05 0.347 (-0.003,0.001)	2.50E-05 0.485 (-0.006,0.003)	6.20E-05 0.248 (-0.001,0.004)	1.14E-04 0.146 (-0.009,0.001)	2.71E-06 0.822 (-0.004,0.003)
<b>APOE SNPs PRS</b>	3.02E-05 0.453 (-0.008,0.003)	1.24E-04 0.118 (-0.004,4.43E-04)	7.41E-05 0.218 (-0.004,0.001)	2.67E-04 0.023 (-0.009,-0.001)*	9.11E-07 0.889 (-0.002,0.002)	2.65E-06 0.825 (-0.006,0.005)	5.12E-06 0.757 (-0.004,0.003)

R2 and p values for subcortical volumes in the left hemisphere and each polygenic score at a PT of 0.001. The column names shows the region of interest, while the row names show the polygenic scores.

\* Nominally significant associations (p value < .05).

\*\* FDR corrected associations < 0.05.

Acronyms: PRS = Polygenic Risk Score; PT = polygenic threshold; APOE = Apolipoprotein E; L = left; R = right; FDR = false discovery rate.

**Figure 5.9. Associations between PRS ( $P^T = 0.001$ ) and thickness in cortical and temporal regions of cortex in UK Biobank,  $p < 0.05$**

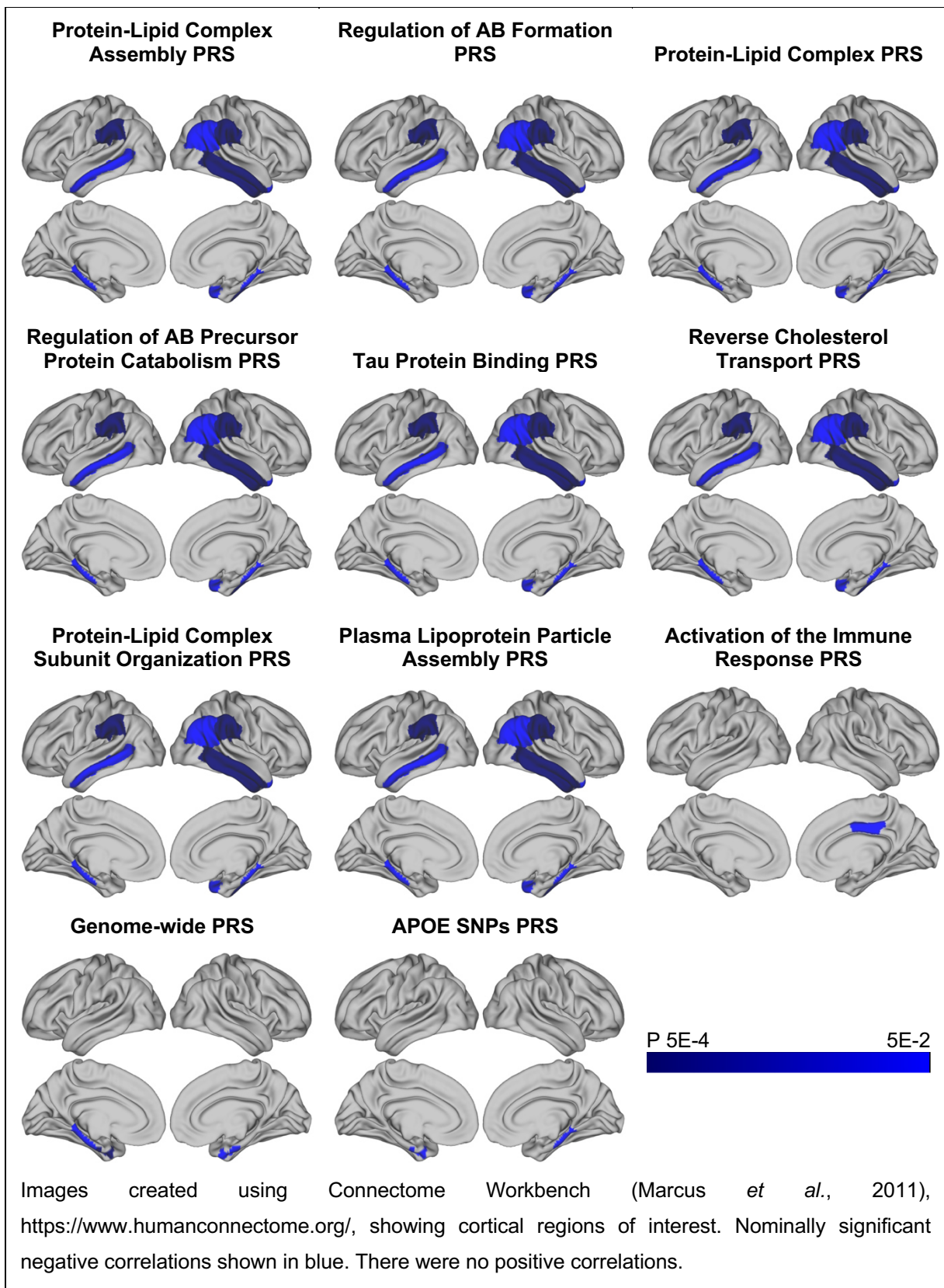
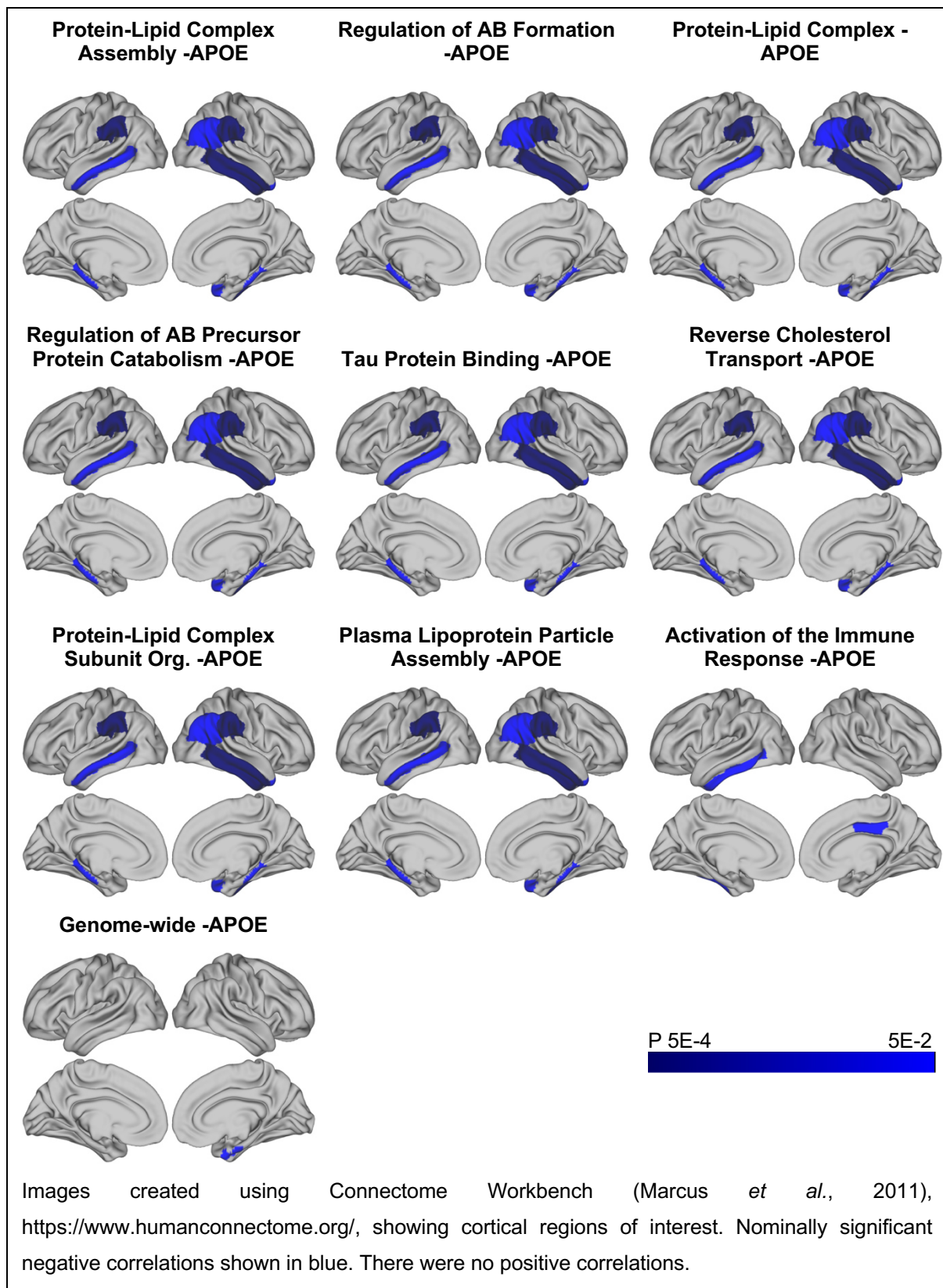


**Figure 5.10. Associations between PRS ( $P^T = 0.001$ ) excluding *APOE* and thickness in cortical and temporal regions of cortex in UK Biobank,  $p < 0.05$**



#### 5.4.5 Cortical Surface Area in ALSPAC

There were no significant associations between cortical surface area and the genome-wide PRS, pathway specific PRS or the *APOE* region. When the *APOE* region was excluded from the PRS, there were some nominally significant results. However, they did not withstand correction for multiple testing, and there was no consistent pattern between the scores. For example, the protein-lipid complex PRS without the *APOE* region was nominally associated with increased surface area in the left and right supramarginal regions ( $p = 0.015$ ,  $R^2 = 6.27 \times 10^{-3}$  and  $p = 0.021$ ,  $R^2 = 5.44 \times 10^{-3}$  respectively). The regulation of  $A\beta$  formation PRS without the *APOE* region was nominally associated with decreased surface area in the right inferior parietal ( $p = 0.011$ ,  $R^2 = 7.17 \times 10^{-3}$ ) and right posterior cingulate regions ( $p = 0.034$ ,  $R^2 = 5.91 \times 10^{-3}$ ). The results are summarised in Tables 5.25 to 5.32, and those surviving FDR correction for multiple comparisons of PRS and phenotype are indicated. The regions showing nominally significant associations with the PRS excluding the *APOE* region are shown in Figure 5.11.

**Table 5.25 Results for ALSPAC cortical surface area in left parietal regions and PRS including APOE at  $P^T$  0.001**

	Left inferior parietal	Left isthmus cingulate	Left posterior cingulate	Left precuneus	Left superior parietal	Left supramarginal
Polygenic risk score	$R^2$ p (95% CI)					
<b>Protein-lipid complex assembly</b>	1.94E-03 0.193 (-13.838,68.896)	1.07E-03 0.358 (-18.071,6.527)	3.49E-03 0.120 (-2.579,22.486)	1.04E-04 0.729 (-22.942,32.793)	1.08E-03 0.303 (-61.467,19.082)	3.34E-04 0.576 (-47.225,26.249)
<b>Regulation of A<math>\beta</math> formation</b>	2.19E-03 0.167 (-12.346,71.857)	1.65E-03 0.254 (-19.801,5.213)	9.45E-04 0.419 (-7.520,18.083)	1.27E-04 0.702 (-33.884,22.797)	1.67E-03 0.199 (-67.884,14.065)	2.65E-03 0.115 (-67.357,7.276)
<b>Protein-lipid complex</b>	2.41E-03 0.147 (-10.793,72.649)	1.11E-03 0.350 (-18.353,6.487)	3.75E-03 0.107 (-2.236,23.036)	3.90E-04 0.502 (-18.482,37.732)	9.31E-04 0.338 (-60.530,20.752)	7.05E-04 0.417 (-52.424,21.682)
<b>Regulation of amyloid precursor protein catabolic process</b>	2.19E-03 0.167 (-12.346,71.857)	1.65E-03 0.254 (-19.801,5.213)	9.45E-04 0.419 (-7.520,18.083)	1.27E-04 0.702 (-33.884,22.797)	1.67E-03 0.199 (-67.884,14.065)	2.65E-03 0.115 (-67.357,7.276)
<b>Tau protein binding</b>	2.23E-03 0.163 (-12.007,71.620)	1.12E-03 0.346 (-18.433,6.453)	4.38E-03 0.082 (-1.394,23.916)	1.94E-04 0.636 (-21.363,34.969)	8.22E-04 0.368 (-59.458,22.001)	1.00E-03 0.333 (-55.481,18.759)
<b>Reverse cholesterol transport</b>	1.76E-03 0.216 (-15.245,67.760)	5.66E-04 0.504 (-16.569,8.133)	4.25E-03 0.086 (-1.546,23.570)	3.30E-04 0.537 (-19.138,36.754)	8.85E-04 0.350 (-59.680,21.134)	3.19E-04 0.585 (-47.126,26.578)
<b>Protein-lipid complex subunit organization</b>	1.74E-03 0.218 (-15.364,67.502)	1.15E-03 0.342 (-18.293,6.332)	3.70E-03 0.110 (-2.292,22.803)	6.14E-05 0.790 (-24.111,31.691)	9.57E-04 0.331 (-60.346,20.326)	5.35E-04 0.479 (-50.066,23.499)
<b>Plasma lipoprotein particle assembly</b>	1.79E-03 0.211 (-15.053,68.232)	1.69E-03 0.247 (-19.697,5.062)	3.01E-03 0.149 (-3.323,21.909)	5.05E-05 0.809 (-24.593,31.507)	1.70E-03 0.195 (-67.352,13.672)	8.59E-04 0.370 (-53.883,20.035)
<b>Activation of immune response</b>	4.32E-03 0.052 (-0.224,83.173)	6.79E-05 0.817 (-10.969,13.908)	3.87E-04 0.605 (-16.025,9.336)	1.36E-04 0.692 (-33.805,22.430)	1.16E-04 0.735 (-33.687,47.753)	4.75E-04 0.505 (-24.470,49.737)
<b>Genome-wide PRS</b>	3.67E-03 0.073 (-3.505,79.597)	1.04E-04 0.775 (-14.185,10.569)	9.80E-07 0.979 (-12.464,12.800)	1.56E-05 0.893 (-26.101,29.935)	2.47E-03 0.118 (-8.174,72.744)	2.00E-03 0.171 (-11.086,62.711)

$R^2$  and p values for subcortical volumes in the left hemisphere and each polygenic score at a  $P^T$  of 0.001. The column names shows the region of interest, while the row names show the polygenic scores.

\* Nominally significant associations (p value < .05).

\*\* FDR corrected associations <0.05.

**Table 5.26 Results for ALSPAC cortical surface area in left temporal regions and PRS including APOE at  $P^T$  0.001**

Polygenic risk score	Left entorhinal		Left inferior temporal		Left middle temporal		Left parahippocampal		Left superior temporal		Left temporal pole		Left transverse temporal	
	$R^2$ p (95% CI)	$R^2$ p (95% CI)	$R^2$ p (95% CI)	$R^2$ p (95% CI)	$R^2$ p (95% CI)	$R^2$ p (95% CI)	$R^2$ p (95% CI)	$R^2$ p (95% CI)	$R^2$ p (95% CI)	$R^2$ p (95% CI)	$R^2$ p (95% CI)	$R^2$ p (95% CI)	$R^2$ p (95% CI)	$R^2$ p (95% CI)
<b>Protein-lipid complex assembly</b>	7.84E-04 0.504 (-3.896,7.924)	6.32E-05 0.802 (-34.248,26.484)	5.12E-04 0.494 (-16.424,34.068)	4.77E-04 0.595 (-8.108,14.143)	1.26E-04 0.731 (-34.287,24.060)	1.19E-03 0.401 (-3.246,8.122)	1.09E-03 0.401 (-7.809,3.119)							
<b>Regulation of A<math>\beta</math> formation</b>	9.98E-05 0.812 (-5.262,6.718)	3.22E-04 0.572 (-39.799,21.983)	9.68E-05 0.766 (-21.808,29.614)	2.58E-04 0.696 (-9.043,13.549)	1.51E-03 0.234 (-47.726,11.631)	6.02E-05 0.850 (-5.234,6.350)	2.41E-03 0.211 (-9.115,2.008)							
<b>Protein-lipid complex</b>	1.53E-03 0.352 (-3.128,8.801)	1.54E-05 0.902 (-32.585,28.720)	6.41E-04 0.444 (-15.532,35.454)	5.15E-04 0.581 (-8.078,14.412)	2.06E-04 0.661 (-36.094,22.882)	1.43E-03 0.357 (-3.048,8.455)	1.06E-03 0.407 (-7.848,3.178)							
<b>Regulation of amyloid precursor protein catabolic process</b>	9.98E-05 0.812 (-5.262,6.718)	3.22E-04 0.572 (-39.799,21.983)	9.68E-05 0.766 (-21.808,29.614)	2.58E-04 0.696 (-9.043,13.549)	1.51E-03 0.234 (-47.726,11.631)	6.02E-05 0.850 (-5.234,6.350)	2.41E-03 0.211 (-9.115,2.008)							
<b>Tau protein binding</b>	1.47E-03 0.360 (-3.179,8.757)	2.74E-05 0.869 (-33.302,28.129)	4.24E-04 0.534 (-17.424,33.653)	8.21E-04 0.486 (-7.249,15.256)	4.13E-04 0.535 (-38.923,20.181)	1.65E-03 0.322 (-2.852,8.679)	1.77E-03 0.284 (-8.543,2.500)							
<b>Reverse cholesterol transport</b>	1.28E-03 0.394 (-3.352,8.525)	1.24E-05 0.912 (-32.183,28.733)	3.91E-04 0.550 (-17.604,33.083)	2.67E-04 0.691 (-8.911,13.444)	1.51E-04 0.708 (-34.887,23.674)	1.26E-03 0.388 (-3.194,8.236)	1.07E-03 0.405 (-7.809,3.151)							
<b>Protein-lipid complex subunit organization</b>	7.32E-04 0.519 (-3.967,7.861)	1.15E-04 0.735 (-35.662,25.158)	2.99E-04 0.601 (-18.536,32.031)	7.83E-04 0.496 (-7.266,15.003)	3.01E-04 0.596 (-37.136,21.299)	1.44E-03 0.356 (-3.012,8.375)	1.75E-03 0.287 (-8.441,2.495)							
<b>Plasma lipoprotein particle assembly</b>	6.57E-04 0.541 (-4.091,7.801)	1.34E-04 0.715 (-36.270,24.880)	7.20E-04 0.417 (-14.887,35.953)	3.41E-04 0.653 (-8.638,13.775)	2.09E-04 0.658 (-36.040,22.770)	1.09E-03 0.422 (-3.381,8.073)	1.44E-03 0.333 (-8.218,2.782)							
<b>Activation of immune response</b>	1.30E-03 0.391 (-8.563,3.345)	2.96E-03 0.086 (-3.776,57.359)	2.50E-03 0.130 (-5.787,45.173)	1.65E-04 0.755 (-9.427,13.001)	3.83E-05 0.850 (-32.378,26.672)	1.49E-03 0.348 (-2.982,8.474)	2.82E-05 0.893 (-5.140,5.902)							
<b>Genome-wide PRS</b>	3.14E-05 0.894 (-5.600,6.419)	2.50E-03 0.115 (-5.933,55.024)	1.51E-03 0.240 (-10.148,40.593)	1.00E-03 0.441 (-15.692,6.829)	4.92E-05 0.830 (-32.736,26.276)	4.66E-05 0.868 (-6.225,5.252)	5.22E-04 0.561 (-3.881,7.156)							

$R^2$  and p values for subcortical volumes in the left hemisphere and each polygenic score at a  $P^T$  of 0.001. The column names show the region of interest, while the row names show the polygenic scores.

\* Nominally significant associations (p value < .05).

\*\* FDR corrected associations <0.05.

Acronyms: PRS = Polygenic Risk Score;  $P^T$  = polygenic threshold; APOE = Apolipoprotein E; L = left; R = right; FDR = false discovery rate.

**Table 5.27 Results for ALSPAC cortical surface area in left parietal regions and PRS excluding APOE at P<sup>T</sup> 0.001**

	Left inferior parietal R <sup>2</sup> p (95% CI)	Left isthmus cingulate R <sup>2</sup> p (95% CI)	Left posterior cingulate R <sup>2</sup> p (95% CI)	Left precuneus R <sup>2</sup> p (95% CI)	Left superior parietal R <sup>2</sup> p (95% CI)	Left supramarginal R <sup>2</sup> p (95% CI)
<b>Polygenic risk score</b>						
<b>Protein-lipid complex assembly (-APOE)</b>	8.04E-04 0.402 (-24.431,60.952)	6.41E-04 0.477 (-8.094,17.304)	9.30E-04 0.423 (-18.245,7.650)	8.05E-04 0.335 (-14.564,42.836)	8.48E-05 0.773 (-35.431,47.695)	6.27E-03 0.015 (9.166,84.497)*
<b>Regulation of Aβ formation (-APOE)</b>	6.13E-04 0.465 (-25.883,56.717)	1.89E-05 0.903 (-13.050,11.517)	2.24E-03 0.214 (-20.527,4.580)	1.17E-03 0.245 (-44.266,11.292)	1.47E-04 0.703 (-48.015,32.383)	1.93E-03 0.179 (-61.720,11.441)
<b>Protein-lipid complex (-APOE)</b>	3.88E-03 0.065 (-2.449,82.113)	5.72E-04 0.502 (-16.936,8.283)	1.80E-03 0.265 (-20.153,5.524)	4.01E-04 0.496 (-18.620,38.442)	2.86E-05 0.867 (-37.743,44.811)	1.44E-04 0.713 (-30.561,44.678)
<b>Regulation of amyloid precursor protein catabolic process (-APOE)</b>	6.13E-04 0.465 (-25.883,56.717)	1.89E-05 0.903 (-13.050,11.517)	2.24E-03 0.214 (-20.527,4.580)	1.17E-03 0.245 (-44.266,11.292)	1.47E-04 0.703 (-48.015,32.383)	1.93E-03 0.179 (-61.720,11.441)
<b>Tau protein binding (-APOE)</b>	5.53E-03 0.028 (5.332,89.765)*	1.25E-03 0.320 (-18.977,6.192)	8.30E-04 0.449 (-17.812,7.879)	4.03E-04 0.495 (-38.422,18.577)	6.96E-04 0.408 (-23.804,58.688)	4.82E-04 0.502 (-50.500,24.708)
<b>Reverse cholesterol transport (-APOE)</b>	6.03E-04 0.468 (-26.744,58.181)	8.69E-04 0.407 (-7.287,17.973)	3.72E-04 0.612 (-16.202,9.542)	1.51E-04 0.676 (-22.486,34.664)	8.49E-05 0.772 (-35.229,47.436)	3.92E-03 0.055 (-0.690,74.389)
<b>Protein-lipid complex subunit organization (-APOE)</b>	3.83E-04 0.563 (-30.210,55.514)	1.20E-03 0.331 (-6.398,19.022)	1.64E-03 0.287 (-20.049,5.931)	5.51E-04 0.425 (-17.064,40.515)	1.41E-03 0.239 (-16.578,66.742)	7.66E-03 0.007 (14.208,89.713)*
<b>Plasma lipoprotein particle assembly (-APOE)</b>	4.33E-04 0.539 (-28.985,55.475)	3.65E-05 0.865 (-11.482,13.660)	7.77E-05 0.817 (-14.313,11.288)	3.07E-04 0.552 (-19.789,37.050)	2.64E-04 0.610 (-51.789,30.398)	1.10E-03 0.311 (-18.045,56.810)
<b>Activation of immune response (-APOE)</b>	3.84E-03 0.067 (-2.583,79.571)	9.23E-05 0.787 (-13.962,10.581)	3.27E-05 0.881 (-11.539,13.455)	3.31E-04 0.537 (-36.420,18.955)	6.60E-05 0.799 (-34.877,45.319)	7.68E-04 0.397 (-20.711,52.339)
<b>Genome-wide PRS (-APOE)</b>	3.62E-03 0.075 (-3.765,79.793)	4.72E-05 0.847 (-11.222,13.676)	2.14E-04 0.701 (-15.190,10.211)	8.06E-06 0.923 (-26.806,29.581)	4.39E-03 0.037 (2.688,83.892)*	3.43E-03 0.073 (-3.084,71.015)
<b>APOE SNPs PRS</b>	3.33E-04 0.590 (-30.130,52.991)	9.44E-04 0.388 (-17.773,6.896)	6.60E-04 0.500 (-8.251,16.925)	8.72E-06 0.920 (-26.503,29.363)	1.57E-04 0.694 (-48.557,32.328)	8.95E-05 0.772 (-42.310,31.420)

R<sup>2</sup> and p values for subcortical volumes in the left hemisphere and each polygenic score at a P<sup>T</sup> of 0.001. The column names shows the region of interest, while the row names show the polygenic scores.

\* Nominally significant associations (p value < .05).

\*\* FDR corrected associations <0.05.

**Table 5.28 Results for ALSPAC cortical surface area in left temporal regions and PRS excluding APOE at P<sup>T</sup> 0.001**

Polygenic risk score	Left entorhinal R <sup>2</sup> p (95% CI)	Left inferior temporal R <sup>2</sup> p (95% CI)	Left middle temporal R <sup>2</sup> p (95% CI)	Left parahippocampal R <sup>2</sup> p (95% CI)	Left superior temporal R <sup>2</sup> p (95% CI)	Left temporal pole R <sup>2</sup> p (95% CI)	Left transverse temporal R <sup>2</sup> p (95% CI)
<b>Protein-lipid complex assembly (-APOE)</b>	4.62E-07 0.987 (-6.124,6.226)	1.64E-03 0.202 (-10.883,51.755)	1.51E-04 0.710 (-21.168,31.076)	1.23E-03 0.394 (-16.504,6.501)	1.85E-03 0.188 (-9.866,50.373)	3.59E-06 0.963 (-5.983,5.708)	2.92E-03 0.169 (-1.667,9.573)
<b>Regulation of Aβ formation (-APOE)</b>	7.52E-04 0.514 (-7.877,3.936)	9.74E-05 0.756 (-35.108,25.495)	3.91E-04 0.550 (-32.789,17.460)	2.59E-04 0.696 (-13.389,8.932)	1.86E-03 0.187 (-48.725,9.464)	3.31E-03 0.161 (-9.687,1.605)	1.29E-04 0.772 (-6.254,4.643)
<b>Protein-lipid complex (-APOE)</b>	5.37E-04 0.581 (-4.425,7.901)	1.56E-03 0.213 (-11.268,50.778)	1.47E-03 0.246 (-10.514,4.1049)	3.02E-04 0.672 (-14.048,9.060)	1.12E-03 0.305 (-14.193,45.422)	1.32E-04 0.780 (-4.979,6.636)	1.68E-03 0.296 (-2.606,8.564)
<b>Regulation of amyloid precursor protein catabolic process (-APOE)</b>	7.52E-04 0.514 (-7.877,3.936)	9.74E-05 0.756 (-35.108,25.495)	3.91E-04 0.550 (-32.789,17.460)	2.59E-04 0.696 (-13.389,8.932)	1.86E-03 0.187 (-48.725,9.464)	3.31E-03 0.161 (-9.687,1.605)	1.29E-04 0.772 (-6.254,4.643)
<b>Tau protein binding (-APOE)</b>	6.60E-04 0.540 (-4.144,7.912)	2.45E-03 0.119 (-6.287,55.702)	2.73E-04 0.618 (-19.231,32.392)	4.84E-04 0.593 (-8.271,14.483)	6.78E-06 0.937 (-28.649,31.075)	1.39E-03 0.365 (-3.110,8.469)	1.98E-04 0.720 (-6.635,4.585)
<b>Reverse cholesterol transport (-APOE)</b>	3.02E-05 0.896 (-5.731,6.553)	1.91E-03 0.169 (-9.256,53.077)	7.42E-05 0.795 (-22.520,29.422)	2.95E-03 0.186 (-19.105,3.701)	2.19E-03 0.152 (-8.023,51.795)	9.83E-08 0.994 (-5.836,5.791)	1.70E-03 0.294 (-2.595,8.590)
<b>Protein-lipid complex subunit organization (-APOE)</b>	1.23E-04 0.791 (-7.021,5.350)	1.73E-03 0.190 (-10.395,52.625)	1.21E-03 0.292 (-40.295,12.111)	2.37E-08 0.997 (-11.692,11.647)	1.63E-04 0.696 (-24.239,36.314)	7.04E-04 0.519 (-3.926,7.784)	5.52E-05 0.850 (-5.117,6.211)
<b>Plasma lipoprotein particle assembly (-APOE)</b>	8.43E-05 0.827 (-5.438,6.805)	3.81E-04 0.538 (-21.217,40.646)	1.62E-03 0.224 (-9.725,41.704)	1.81E-03 0.301 (-17.435,5.378)	1.86E-03 0.187 (-9.652,49.677)	4.55E-04 0.604 (-7.301,4.242)	3.74E-03 0.119 (-1.134,9.990)
<b>Activation of immune response (-APOE)</b>	4.72E-03 0.101 (-10.767,0.947)	1.88E-03 0.172 (-9.096,51.227)	1.90E-03 0.188 (-8.197,41.974)	1.48E-04 0.767 (-12.742,9.397)	3.74E-05 0.852 (-26.288,31.836)	1.21E-03 0.397 (-3.215,8.107)	8.98E-04 0.446 (-3.315,7.543)
<b>Genome-wide PRS (-APOE)</b>	4.24E-04 0.624 (-7.525,4.509)	3.46E-03 0.064 (-1.569,59.617)	1.56E-03 0.232 (-9.936,41.097)	2.74E-03 0.203 (-18.772,3.967)	1.83E-04 0.679 (-35.831,23.347)	8.12E-04 0.488 (-7.803,3.724)	5.29E-04 0.558 (-3.881,7.191)
<b>APOE SNPs PRS</b>	2.00E-03 0.286 (-2.745,9.314)	7.12E-09 0.998 (-30.449,30.532)	1.04E-04 0.758 (-21.331,29.306)	5.72E-04 0.561 (-7.873,14.526)	7.39E-05 0.793 (-25.477,33.369)	1.11E-03 0.418 (-3.352,8.078)	3.95E-05 0.873 (-5.044,5.940)

R<sup>2</sup> and p values for subcortical volumes in the left hemisphere and each polygenic score at a P<sup>T</sup> of 0.001. The column names shows the region of interest, while the row names show the polygenic scores.

\* Nominally significant associations (p value < .05).

\*\* FDR corrected associations <0.05.

Acronyms: PRS = Polygenic Risk Score; P<sup>T</sup> = polygenic threshold; APOE = Apolipoprotein E; L = left; R = right; FDR = false discovery rate.

**Table 5.29 Results for ALSPAC cortical surface area in right parietal regions and PRS including APOE at P<sup>T</sup> 0.001**

Polygenic risk score	Right inferior parietal		Right isthmus cingulate		Right posterior cingulate		Right precuneus		Right superior parietal		Right supramarginal	
	R <sup>2</sup> p (95% CI)	R <sup>2</sup> p (95% CI)	R <sup>2</sup> p (95% CI)	R <sup>2</sup> p (95% CI)	R <sup>2</sup> p (95% CI)	R <sup>2</sup> p (95% CI)						
<b>Protein-lipid complex assembly</b>	9.02E-04 0.372 (-25.563,68.480)	1.11E-04 0.770 (-9.722,13.142)	2.54E-06 0.965 (-13.547,12.955)	2.18E-03 0.135 (-7.667,57.341)	6.20E-04 0.434 (-55.444,23.772)	7.04E-05 0.793 (-39.818,30.427)						
<b>Regulation of Aβ formation</b>	1.95E-04 0.678 (-58.047,37.746)	2.91E-04 0.636 (-14.452,8.828)	1.85E-03 0.237 (-21.606,5.343)	1.46E-03 0.222 (-12.446,53.775)	1.20E-03 0.275 (-62.747,17.847)	2.81E-05 0.869 (-32.738,38.773)						
<b>Protein-lipid complex</b>	1.47E-03 0.253 (-19.757,75.078)	6.93E-05 0.817 (-10.179,12.901)	1.05E-04 0.779 (-15.291,11.457)	3.52E-03 0.057 (-0.903,64.587)	3.13E-04 0.578 (-51.333,28.617)	4.54E-05 0.833 (-39.243,31.633)						
<b>Regulation of amyloid precursor protein catabolic process</b>	1.95E-04 0.678 (-58.047,37.746)	2.91E-04 0.636 (-14.452,8.828)	1.85E-03 0.237 (-21.606,5.343)	1.46E-03 0.222 (-12.446,53.775)	1.20E-03 0.275 (-62.747,17.847)	2.81E-05 0.869 (-32.738,38.773)						
<b>Tau protein binding</b>	1.44E-03 0.259 (-20.146,74.880)	1.65E-04 0.721 (-9.458,13.672)	1.19E-04 0.765 (-15.452,11.356)	3.42E-03 0.061 (-1.360,64.274)	2.44E-04 0.623 (-50.111,30.009)	2.34E-04 0.633 (-44.161,26.848)						
<b>Reverse cholesterol transport</b>	1.42E-03 0.262 (-20.155,74.168)	4.74E-05 0.849 (-10.354,12.590)	3.99E-05 0.862 (-14.473,12.117)	3.22E-03 0.069 (-2.281,62.852)	4.72E-04 0.494 (-53.608,25.866)	9.96E-05 0.755 (-40.831,29.630)						
<b>Protein-lipid complex subunit organization</b>	5.96E-04 0.468 (-29.636,64.551)	3.05E-04 0.628 (-8.616,14.280)	2.93E-05 0.882 (-14.277,12.265)	2.57E-03 0.105 (-5.546,59.531)	4.22E-04 0.518 (-52.759,26.585)	2.33E-04 0.634 (-43.711,26.622)						
<b>Plasma lipoprotein particle assembly</b>	1.07E-03 0.329 (-23.745,70.877)	1.19E-05 0.924 (-12.070,10.947)	2.57E-05 0.889 (-14.285,12.391)	1.92E-03 0.161 (-9.258,56.186)	9.80E-04 0.325 (-59.895,19.810)	2.12E-04 0.649 (-43.555,27.138)						
<b>Activation of immune response</b>	9.21E-05 0.775 (-40.603,54.455)	9.61E-04 0.389 (-16.633,6.477)	9.17E-05 0.793 (-11.601,15.200)	9.61E-05 0.754 (-27.624,38.160)	1.62E-03 0.205 (-14.101,65.837)	1.70E-03 0.197 (-12.095,58.748)						
<b>Genome-wide PRS</b>	5.65E-05 0.823 (-52.732,41.927)	4.03E-04 0.578 (-14.769,8.230)	1.32E-06 0.975 (-13.117,13.547)	5.36E-04 0.458 (-20.348,45.138)	3.39E-03 0.067 (-2.482,76.988)	8.20E-04 0.371 (-19.190,51.423)						

R<sup>2</sup> and p values for subcortical volumes in the right hemisphere and each polygenic score at a P<sup>T</sup> of 0.001. The column names shows the region of interest, while the row names show the polygenic scores.

\* Nominally significant associations (p value < .05).

\*\* FDR corrected associations <0.05.

Acronyms: PRS = Polygenic Risk Score; P<sup>T</sup> = polygenic threshold; APOE = Apolipoprotein E; L = left; R = right; FDR = false discovery rate.

**Table 5.30 Results for ALSPAC cortical surface area in right temporal regions and PRS including APOE at  $P^T$  0.001**

	Right entorhinal	Right inferior temporal	Right middle temporal	Right parahippocampal	Right superior temporal	Right temporal pole	Right transverse temporal
Polygenic risk score	$R^2$ p (95% CI)	$R^2$ p (95% CI)	$R^2$ p (95% CI)	$R^2$ p (95% CI)	$R^2$ p (95% CI)	$R^2$ p (95% CI)	$R^2$ p (95% CI)
<b>Protein-lipid complex assembly</b>	0.658 (-4.711,7.460)	0.248 (-46.014,11.874)	0.174 (-8.424,46.762)	0.438 (-4.933,11.406)	0.163 (-7.492,44.814)	0.089 (-9.907,0.685)	0.461 (-2.704,5.966)
<b>Regulation of A<math>\beta</math> formation</b>	0.989 (-6.175,6.263)	0.417 (-41.766,17.289)	0.248 (-11.524,44.719)	0.215 (-3.057,13.597)	0.347 (-13.880,39.521)	0.066 (-10.444,0.317)	0.940 (-4.584,4.247)
<b>Protein-lipid complex</b>	0.679 (-4.822,7.408)	0.264 (-45.837,12.549)	0.144 (-7.073,48.568)	0.433 (-4.940,11.535)	0.243 (-10.673,42.156)	0.179 (-9.011,1.674)	0.501 (-2.871,5.878)
<b>Regulation of amyloid precursor protein catabolic process</b>	0.989 (-6.175,6.263)	0.417 (-41.766,17.289)	0.248 (-11.524,44.719)	0.215 (-3.057,13.597)	0.347 (-13.880,39.521)	0.066 (-10.444,0.317)	0.940 (-4.584,4.247)
<b>Tau protein binding</b>	0.840 (-5.493,6.756)	0.335 (-43.649,14.844)	0.126 (-6.103,49.617)	0.417 (-4.826,11.661)	0.316 (-12.921,40.047)	0.132 (-9.470,1.231)	0.741 (-3.646,5.124)
<b>Reverse cholesterol transport</b>	0.574 (-4.339,7.827)	0.240 (-46.428,11.606)	0.199 (-9.495,45.844)	0.519 (-5.496,10.884)	0.261 (-11.170,41.320)	0.127 (-9.455,1.165)	0.468 (-2.736,5.961)
<b>Protein-lipid complex subunit organization</b>	0.699 (-4.890,7.296)	0.317 (-43.785,14.176)	0.173 (-8.391,46.867)	0.500 (-5.361,10.395)	0.211 (-9.469,42.927)	0.081 (-10.037,0.569)	0.655 (-3.353,5.333)
<b>Plasma lipoprotein particle assembly</b>	0.809 (-5.364,6.874)	0.115 (-52.542,5.666)	0.236 (-10.955,44.611)	0.404 (-4.716,11.713)	0.194 (-8.867,43.806)	0.063 (-10.401,0.256)	0.437 (-2.633,6.094)
<b>Activation of immune response</b>	0.391 (-3.446,8.810)	0.252 (-12.146,46.422)	0.899 (-29.728,26.106)	0.620 (-10.207,6.086)	0.284 (-12.085,41.324)	0.398 (-3.045,7.668)	0.825 (-4.876,3.886)
<b>Genome-wide PRS</b>	0.191 (-2.021,10.155)	0.413 (-16.980,41.347)	0.843 (-24.998,30.621)	0.460 (-5.081,11.243)	0.150 (-6.328,45.640)	0.276 (-2.363,8.284)	0.289 (-2.000,6.720)

R2 and p values for subcortical volumes in the right hemisphere and each polygenic score at a  $P^T$  of 0.001. The column names shows the region of interest, while the row names show the polygenic scores.

\* Nominally significant associations (p value < .05).

\*\* FDR corrected associations <0.05.

Acronyms: PRS = Polygenic Risk Score;  $P^T$  = polygenic threshold; APOE = Apolipoprotein E; L = left; R = right; FDR = false discovery rate.

**Table 5.31 Results for ALSPAC cortical surface area in right parietal regions and PRS excluding APOE at P<sup>T</sup> 0.001**

	Right inferior parietal	Right isthmus cingulate	Right posterior cingulate	Right precuneus	Right superior parietal	Right supramarginal
Polygenic risk score	R <sup>2</sup>	R <sup>2</sup>	R <sup>2</sup>	R <sup>2</sup>	R <sup>2</sup>	R <sup>2</sup>
	p (95% CI)	p (95% CI)	p (95% CI)	p (95% CI)	p (95% CI)	p (95% CI)
<b>Protein-lipid complex assembly (-APOE)</b>	2.31E-04 0.651 (-37.516,60.005)	1.67E-04 0.720 (-13.946,9.630)	7.75E-04 0.444 (-8.322,18.989)	1.47E-04 0.698 (-26.916,40.220)	1.41E-04 0.709 (-48.651,33.059)	5.44E-03 0.021 (6.522,78.565)*
<b>Regulation of Aβ formation (-APOE)</b>	7.17E-03 0.012 (-106.981,-13.681)*	2.25E-03 0.188 (-19.034,3.720)	5.91E-03 0.034 (-27.389,-1.090)*	1.71E-04 0.675 (-39.407,25.527)	5.96E-04 0.443 (-54.981,24.018)	3.39E-03 0.069 (-2.434,67.390)
<b>Protein-lipid complex (-APOE)</b>	1.09E-03 0.327 (-24.029,72.265)	7.51E-04 0.447 (-16.237,7.150)	1.19E-06 0.976 (-13.353,13.767)	2.74E-05 0.867 (-30.486,36.192)	7.66E-06 0.931 (-38.774,42.379)	6.16E-03 0.014 (9.230,80.722)*
<b>Regulation of amyloid precursor protein catabolic process (-APOE)</b>	7.17E-03 0.012 (-106.981,-13.681)*	2.25E-03 0.188 (-19.034,3.720)	5.91E-03 0.034 (-27.389,-1.090)*	1.71E-04 0.675 (-39.407,25.527)	5.96E-04 0.443 (-54.981,24.018)	3.39E-03 0.069 (-2.434,67.390)
<b>Tau protein binding (-APOE)</b>	1.80E-03 0.206 (-17.027,79.151)	2.05E-05 0.900 (-12.450,10.950)	9.09E-06 0.934 (-14.133,12.987)	2.14E-05 0.882 (-35.854,30.817)	5.38E-04 0.466 (-25.452,55.652)	2.33E-03 0.132 (-8.235,63.519)
<b>Reverse cholesterol transport (-APOE)</b>	9.93E-04 0.348 (-25.273,71.719)	1.36E-03 0.307 (-17.821,5.596)	5.59E-04 0.516 (-9.074,18.082)	6.19E-05 0.801 (-37.676,29.092)	4.51E-04 0.504 (-54.469,26.763)	3.95E-03 0.049 (0.174,71.923)*
<b>Protein-lipid complex subunit organization (-APOE)</b>	1.13E-03 0.318 (-73.726,23.922)	2.08E-03 0.205 (-4.170,19.450)	8.67E-05 0.798 (-11.918,15.498)	3.04E-03 0.077 (-3.236,63.956)	6.59E-04 0.419 (-24.086,57.879)	3.29E-03 0.073 (-3.043,69.414)
<b>Plasma lipoprotein particle assembly (-APOE)</b>	1.85E-03 0.200 (-16.599,79.366)	2.38E-03 0.175 (-19.695,3.572)	7.38E-04 0.456 (-8.357,18.643)	6.28E-04 0.423 (-46.751,19.606)	1.12E-03 0.293 (-62.029,18.693)	2.37E-03 0.128 (-7.945,63.511)
<b>Activation of immune response (-APOE)</b>	1.95E-04 0.678 (-36.905,56.743)	1.27E-03 0.323 (-17.154,5.639)	3.89E-04 0.588 (-9.561,16.873)	1.07E-05 0.916 (-30.658,34.126)	1.68E-03 0.197 (-13.391,65.317)	3.58E-04 0.555 (-24.389,45.459)
<b>Genome-wide PRS (-APOE)</b>	9.66E-04 0.355 (-70.004,25.100)	9.44E-04 0.394 (-16.587,6.521)	6.79E-04 0.474 (-8.498,18.289)	8.41E-06 0.926 (-31.390,34.512)	5.53E-03 0.019 (8.001,87.733)*	1.72E-03 0.196 (-12.027,58.907)
<b>APOE SNPs PRS</b>	1.31E-03 0.282 (-21.242,73.054)	1.33E-04 0.749 (-9.595,13.340)	1.62E-03 0.269 (-20.768,5.783)	1.58E-03 0.203 (-11.418,53.831)	8.83E-05 0.768 (-45.755,33.761)	1.56E-04 0.697 (-42.239,28.229)

R<sup>2</sup> and p values for subcortical volumes in the right hemisphere and each polygenic score at a P<sup>T</sup> of 0.001. The column names shows the region of interest, while the row names show the polygenic scores.

\* Nominally significant associations (p value < .05).

\*\* FDR corrected associations <0.05.

Acronyms: PRS = Polygenic Risk Score; P<sup>T</sup> = polygenic threshold; APOE = Apolipoprotein E; L = left; R = right; FDR = false discovery rate.

**Table 5.32 Results for ALSPAC cortical surface area in right temporal regions and PRS excluding APOE at P<sup>T</sup> 0.001**

Polygenic risk score	Right entorhinal		Right inferior temporal		Right middle temporal		Right parahippocampal		Right superior temporal		Right temporal pole		Right transverse temporal	
	R <sup>2</sup>	p (95% CI)	R <sup>2</sup>	p (95% CI)	R <sup>2</sup>	p (95% CI)	R <sup>2</sup>	p (95% CI)	R <sup>2</sup>	p (95% CI)	R <sup>2</sup>	p (95% CI)	R <sup>2</sup>	p (95% CI)
<b>Protein-lipid complex assembly (-APOE)</b>	5.14E-03	0.078 (-0.613,1.1.828)	3.65E-04	0.564 (-21.043,38.643)	3.93E-05	0.847 (-25.716,31.337)	2.57E-04	0.676 (-6.558,10.118)	1.49E-03	0.228 (-10.384,43.643)	3.94E-04	0.641 (-4.159,6.753)	5.61E-03	0.061 (-0.191,8.740)
<b>Regulation of Aβ formation (-APOE)</b>	1.65E-04	0.752 (-7.071,5.108)	1.18E-03	0.299 (-13.630,44.384)	3.22E-05	0.861 (-25.204,30.138)	2.54E-03	0.189 (-2.658,13.518)	3.49E-05	0.854 (-28.603,23.686)	1.03E-04	0.812 (-5.948,4.660)	1.74E-03	0.297 (-6.623,2.020)
<b>Protein-lipid complex (-APOE)</b>	3.07E-04	0.667 (-4.885,7.634)	5.13E-04	0.494 (-19.268,39.978)	2.13E-03	0.155 (-7.728,48.721)	2.72E-03	0.174 (-2.542,14.134)	1.67E-03	0.201 (-9.295,44.208)	2.74E-03	0.219 (-2.010,8.810)	2.10E-03	0.252 (-1.842,7.033)
<b>Regulation of amyloid precursor protein catabolic process (-APOE)</b>	1.65E-04	0.752 (-7.071,5.108)	1.18E-03	0.299 (-13.630,44.384)	3.22E-05	0.861 (-25.204,30.138)	2.54E-03	0.189 (-2.658,13.518)	3.49E-05	0.854 (-28.603,23.686)	1.03E-04	0.812 (-5.948,4.660)	1.74E-03	0.297 (-6.623,2.020)
<b>Tau protein binding (-APOE)</b>	2.24E-03	0.245 (-9.848,2.505)	6.39E-03	0.015 (7.106,66.183)*	7.15E-03	0.009 (9.472,65.680)*	7.23E-03	0.026 (1.129,17.616)*	2.21E-04	0.643 (-20.550,33.304)	7.36E-04	0.524 (-3.658,7.185)	2.30E-03	0.231 (-7.149,1.720)
<b>Reverse cholesterol transport (-APOE)</b>	2.83E-03	0.191 (-2.047,10.283)	1.27E-04	0.733 (-24.499,34.833)	2.79E-04	0.607 (-20.933,35.832)	5.65E-04	0.535 (-5.642,10.867)	1.30E-03	0.260 (-11.386,42.223)	5.93E-05	0.857 (-4.927,5.928)	3.74E-03	0.126 (-0.974,7.926)
<b>Protein-lipid complex subunit organization (-APOE)</b>	9.41E-03	0.017 (1.390,13.856)*	7.50E-03	0.009 (10.281,69.809)*	5.02E-05	0.827 (-25.392,31.752)	1.93E-04	0.717 (-9.922,6.824)	1.98E-04	0.661 (-21.023,33.154)	5.25E-04	0.591 (-3.976,6.985)	5.77E-05	0.850 (-4.055,4.924)
<b>Plasma lipoprotein particle assembly (-APOE)</b>	3.43E-04	0.649 (-4.717,7.571)	1.53E-03	0.237 (-47.377,11.697)	7.47E-06	0.933 (-27.049,29.475)	9.34E-04	0.426 (-4.877,11.568)	1.37E-03	0.248 (-10.949,42.420)	5.90E-05	0.857 (-4.898,5.892)	7.64E-03	0.029 (0.525,9.343)*
<b>Activation of immune response (-APOE)</b>	1.18E-03	0.399 (-3.431,8.615)	9.60E-04	0.349 (-15.056,42.675)	5.58E-05	0.818 (-24.314,30.779)	2.90E-04	0.657 (-9.861,6.217)	1.05E-03	0.311 (-12.706,39.956)	8.17E-04	0.502 (-3.471,7.089)	9.50E-05	0.808 (-3.784,4.856)
<b>Genome-wide PRS (-APOE)</b>	2.97E-03	0.181 (-1.931,10.289)	1.68E-03	0.215 (-10.768,48.052)	4.26E-04	0.525 (-37.108,18.924)	2.73E-04	0.667 (-6.379,9.975)	5.40E-04	0.468 (-16.705,36.340)	4.34E-03	0.122 (-1.116,9.580)	8.46E-04	0.468 (-2.762,6.016)
<b>APOE SNPs PRS</b>	1.77E-04	0.744 (-5.083,7.120)	2.12E-04	0.660 (-35.599,22.526)	2.10E-03	0.158 (-7.708,47.570)	7.62E-04	0.472 (-5.185,11.208)	2.59E-03	0.112 (-4.923,47.557)	3.36E-04	0.667 (-6.505,4.163)	1.17E-03	0.394 (-2.457,6.242)

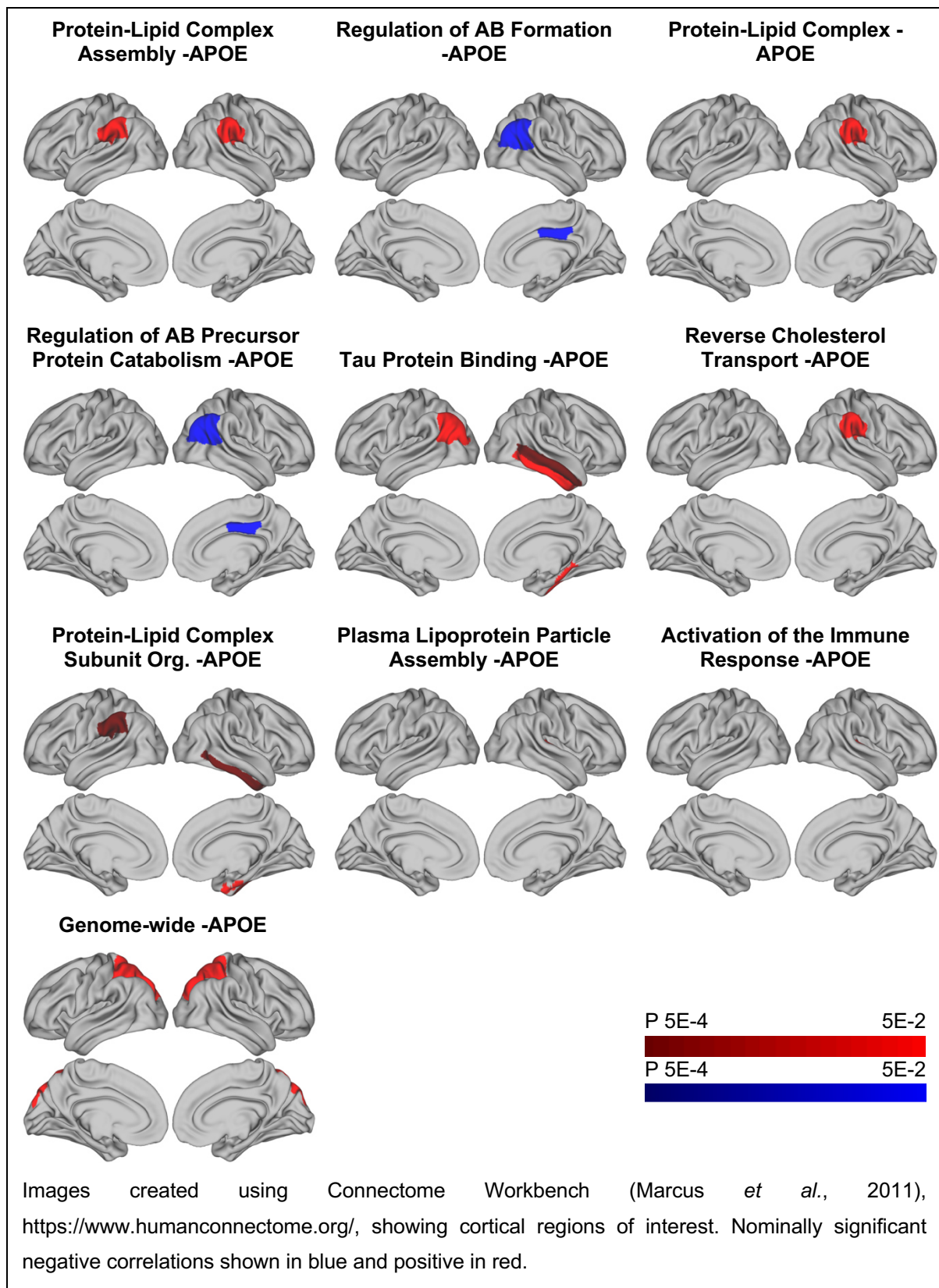
R<sup>2</sup> and p values for subcortical volumes in the right hemisphere and each polygenic score at a P<sup>T</sup> of 0.001. The column names shows the region of interest, while the row names show the polygenic scores.

\* Nominally significant associations (p value < .05).

\*\* FDR corrected associations <0.05.

Acronyms: PRS = Polygenic Risk Score; P<sup>T</sup> = polygenic threshold; APOE = Apolipoprotein E; L = left; R = right; FDR = false discovery rate.

**Figure 5.11. Associations between PRS ( $P^T = 0.001$ ) excluding APOE and surface area in cortical and temporal regions of cortex in ALSPAC,  $p < 0.05$ .**



#### 5.4.6 Cortical Surface Area in UK Biobank

In UK Biobank, there were a number of associations with cortical surface area that were beneath the FDR corrected significance threshold. The genome wide PRS was negatively associated with cortical surface area in the left and right inferior temporal regions ( $p = 0.002$ ,  $R^2 = 3.14 \times 10^{-4}$  and  $p = 0.046$ ,  $R^2 = 1.29 \times 10^{-4}$  respectively). When the *APOE* region was removed, the genome wide PRS correlated with those regions ( $p = 0.009$ ,  $R^2 = 2.25 \times 10^{-4}$  and  $p = 0.019$ ,  $R^2 = 1.78 \times 10^{-4}$  respectively) and the left posterior cingulate ( $p = 0.026$ ,  $R^2 = 1.96 \times 10^{-4}$ ).

The pathway specific PRS were positively associated with cortical surface area in the left supramarginal and left precuneus with very similar results (approximately  $p = 0.005$ ,  $R^2 = 2.43 \times 10^{-4}$  and  $p = 0.035$ ,  $R^2 = 1.32 \times 10^{-4}$  respectively). The left inferior temporal region showed a negative association with the pathway PRS ( $p = 0.035$ ,  $R^2 = 1.48 \times 10^{-4}$ ). These results were unchanged when the *APOE* region was removed from the score ( $p$  range 0.005 – 0.035). The results for the immune response PRS were distinct, with negative associations with cortical surface area in the left and right inferior temporal regions ( $p = 0.009$ ,  $R^2 = 2.22 \times 10^{-4}$  and  $p = 0.011$ ,  $R^2 = 2.07 \times 10^{-4}$  respectively), and was negatively associated with surface area in the left inferior parietal area ( $p = 0.038$ ,  $R^2 = 1.43 \times 10^{-4}$ ). This was maintained when the *APOE* region was excluded from the score ( $p$  range 0.014 – 0.044). SNPs in the *APOE* region showed no associations with cortical surface area.

The regions showing nominally significant associations with PRS, including and excluding the *APOE* region, are shown in Figures 5.12 and 5.13. The results are summarised in Tables 5.33 and 5.40. Those surviving FDR correction for multiple comparisons of PRS and phenotype are indicated.

**Table 5.33 Results for UK Biobank cortical surface area in left parietal regions and PRS including APOE at P<sup>T</sup> 0.001**

Polygenic risk score	Left inferior parietal		Left isthmus cingulate		Left posterior cingulate		Left precuneus		Left superior parietal		Left supramarginal	
	R <sup>2</sup> p (95% CI)	R <sup>2</sup> p (95% CI)	R <sup>2</sup> p (95% CI)	R <sup>2</sup> p (95% CI)	R <sup>2</sup> p (95% CI)	R <sup>2</sup> p (95% CI)	R <sup>2</sup> p (95% CI)	R <sup>2</sup> p (95% CI)	R <sup>2</sup> p (95% CI)	R <sup>2</sup> p (95% CI)	R <sup>2</sup> p (95% CI)	
<b>Protein-lipid complex assembly</b>	1.85E-05 0.455 (-4.255,9.499)	4.30E-07 0.908 (-2.237,1.987)	4.45E-05 0.288 (-1.038,3.495)	1.32E-04 0.035 (0.373,10.312)*	5.56E-05 0.208 (-2.592,11.932)	2.43E-04 0.005 (2.523,14.293)*						
<b>Regulation of Aβ formation</b>	1.84E-05 0.456 (-4.262,9.493)	4.27E-07 0.908 (-2.236,1.988)	4.42E-05 0.289 (-1.041,3.492)	1.32E-04 0.035 (0.379,10.318)*	5.57E-05 0.207 (-2.587,11.937)	2.44E-04 0.005 (2.529,14.299)*						
<b>Protein-lipid complex</b>	1.83E-05 0.457 (-4.269,9.486)	4.26E-07 0.908 (-2.236,1.988)	4.42E-05 0.290 (-1.042,3.490)	1.32E-04 0.035 (0.376,10.315)*	5.55E-05 0.208 (-2.595,11.929)	2.44E-04 0.005 (2.526,14.296)*						
<b>Regulation of amyloid precursor protein catabolic process</b>	1.82E-05 0.459 (-4.277,9.478)	4.18E-07 0.909 (-2.235,1.989)	4.40E-05 0.291 (-1.045,3.488)	1.32E-04 0.035 (0.379,10.318)*	5.56E-05 0.208 (-2.594,11.930)	2.44E-04 0.005 (2.528,14.298)*						
<b>Tau protein binding</b>	1.81E-05 0.460 (-4.284,9.471)	4.15E-07 0.909 (-2.234,1.989)	4.39E-05 0.291 (-1.046,3.487)	1.32E-04 0.035 (0.380,10.318)*	5.55E-05 0.208 (-2.596,11.928)	2.44E-04 0.005 (2.529,14.299)*						
<b>Reverse cholesterol transport</b>	1.80E-05 0.461 (-4.290,9.465)	4.14E-07 0.910 (-2.234,1.990)	4.39E-05 0.291 (-1.047,3.486)	1.32E-04 0.035 (0.381,10.320)*	5.55E-05 0.208 (-2.597,11.927)	2.44E-04 0.005 (2.533,14.303)*						
<b>Protein-lipid complex subunit organization</b>	1.80E-05 0.462 (-4.294,9.461)	4.14E-07 0.910 (-2.234,1.989)	4.38E-05 0.292 (-1.047,3.486)	1.33E-04 0.035 (0.384,10.323)*	5.55E-05 0.208 (-2.596,11.928)	2.44E-04 0.005 (2.537,14.307)*						
<b>Plasma lipoprotein particle assembly</b>	1.80E-05 0.462 (-4.296,9.458)	4.11E-07 0.910 (-2.234,1.990)	4.38E-05 0.292 (-1.048,3.485)	1.33E-04 0.035 (0.386,10.325)*	5.56E-05 0.208 (-2.594,11.930)	2.44E-04 0.005 (2.542,14.312)*						
<b>Activation of immune response</b>	1.43E-04 0.038 (-14.169,-0.420)*	1.14E-06 0.850 (-2.314,1.908)	1.27E-04 0.072 (-4.343,0.189)	4.71E-06 0.691 (-5.978,3.959)	1.08E-07 0.956 (-7.055,7.466)	3.04E-05 0.323 (-8.854,2.915)						
<b>Genome-wide PRS</b>	3.36E-05 0.314 (-10.408,3.346)	8.94E-05 0.095 (-3.910,0.314)	1.41E-04 0.059 (-4.452,0.080)	2.98E-06 0.752 (-4.168,5.772)	1.72E-06 0.825 (-6.441,8.083)	3.91E-06 0.723 (-4.821,6.951)						

R2 and p values for subcortical volumes in the left hemisphere and each polygenic score at a P<sup>T</sup> of 0.001. The column names shows the region of interest, while the row names show the polygenic scores.

\* Nominally significant associations (p value < .05).

\*\* FDR corrected associations <0.05.

Acronyms: PRS = Polygenic Risk Score; P<sup>T</sup> = polygenic threshold; APOE = Apolipoprotein E; L = left; R = right; FDR = false discovery rate.

**Table 5.34 Results for UK Biobank cortical surface area in left temporal regions and PRS including APOE at  $P^T$  0.001**

	Left entorhinal	Left inferior temporal	Left middle temporal	Left parahippocampal	Left superior temporal	Left temporal pole	Left transverse temporal
Polygenic risk score	$R^2$ p (95% CI)	$R^2$ p (95% CI)	$R^2$ p (95% CI)	$R^2$ p (95% CI)	$R^2$ p (95% CI)	$R^2$ p (95% CI)	$R^2$ p (95% CI)
<b>Protein-lipid complex assembly</b>	3.14E-05 0.401 (-1.391,0.557)	1.48E-04 0.035 (-10.693,-0.393)*	3.51E-05 0.284 (-6.504,1.908)	8.55E-05 0.145 (-0.320,2.167)	2.64E-05 0.331 (-2.230,6.609)	1.06E-05 0.628 (-0.603,1.000)	6.41E-05 0.225 (-0.385,1.637)
<b>Regulation of A<math>\beta</math> formation</b>	3.15E-05 0.400 (-1.392,0.556)	1.48E-04 0.035 (-10.691,-0.391)*	3.50E-05 0.285 (-6.502,1.910)	8.58E-05 0.145 (-0.318,2.168)	2.64E-05 0.331 (-2.229,6.610)	1.05E-05 0.628 (-0.603,0.999)	6.42E-05 0.224 (-0.384,1.638)
<b>Protein-lipid complex</b>	3.15E-05 0.400 (-1.392,0.556)	1.48E-04 0.035 (-10.693,-0.393)*	3.49E-05 0.285 (-6.499,1.912)	8.60E-05 0.144 (-0.317,2.169)	2.63E-05 0.332 (-2.231,6.608)	1.05E-05 0.629 (-0.604,0.999)	6.42E-05 0.224 (-0.384,1.638)
<b>Regulation of amyloid precursor protein catabolic process</b>	3.15E-05 0.400 (-1.392,0.556)	1.48E-04 0.035 (-10.693,-0.393)*	3.49E-05 0.285 (-6.498,1.914)	8.63E-05 0.144 (-0.315,2.171)	2.64E-05 0.332 (-2.230,6.609)	1.04E-05 0.630 (-0.604,0.998)	6.43E-05 0.224 (-0.383,1.638)
<b>Tau protein binding</b>	3.16E-05 0.400 (-1.392,0.556)	1.48E-04 0.035 (-10.695,-0.395)*	3.48E-05 0.286 (-6.496,1.916)	8.65E-05 0.143 (-0.314,2.172)	2.64E-05 0.332 (-2.230,6.609)	1.04E-05 0.631 (-0.605,0.998)	6.44E-05 0.224 (-0.383,1.639)
<b>Reverse cholesterol transport</b>	3.16E-05 0.400 (-1.392,0.555)	1.48E-04 0.035 (-10.696,-0.396)*	3.48E-05 0.286 (-6.494,1.918)	8.66E-05 0.143 (-0.314,2.172)	2.64E-05 0.331 (-2.229,6.610)	1.03E-05 0.632 (-0.605,0.997)	6.45E-05 0.223 (-0.383,1.639)
<b>Protein-lipid complex subunit organization</b>	3.17E-05 0.400 (-1.392,0.555)	1.48E-04 0.035 (-10.695,-0.395)*	3.47E-05 0.287 (-6.492,1.920)	8.67E-05 0.143 (-0.313,2.173)	2.65E-05 0.331 (-2.227,6.612)	1.03E-05 0.632 (-0.606,0.997)	6.46E-05 0.223 (-0.382,1.640)
<b>Plasma lipoprotein particle assembly</b>	3.17E-05 0.399 (-1.393,0.555)	1.48E-04 0.035 (-10.693,-0.393)*	3.46E-05 0.287 (-6.490,1.922)	8.68E-05 0.142 (-0.312,2.174)	2.65E-05 0.331 (-2.225,6.613)	1.03E-05 0.632 (-0.606,0.997)	6.46E-05 0.223 (-0.382,1.640)
<b>Activation of immune response</b>	9.68E-06 0.641 (-1.205,0.742)	2.22E-04 0.010 (-11.926,-1.629)*	1.15E-05 0.540 (-5.520,2.889)	4.27E-05 0.304 (-1.895,0.591)	7.72E-06 0.599 (-3.234,5.603)	4.50E-06 0.752 (-0.930,0.672)	3.22E-06 0.785 (-0.870,1.151)
<b>Genome-wide PRS</b>	4.17E-05 0.334 (-1.454,0.493)	3.14E-04 0.002 (-13.217,-2.918)*	3.33E-05 0.297 (-6.445,1.967)	3.82E-06 0.758 (-1.438,1.048)	4.03E-06 0.704 (-3.563,5.276)	1.65E-04 0.055 (-0.017,1.586)	2.06E-05 0.491 (-0.656,1.366)

R2 and p values for subcortical volumes in the left hemisphere and each polygenic score at a  $P^T$  of 0.001. The column names show the region of interest, while the row names show the polygenic scores.

\* Nominally significant associations (p value < .05).

\*\* FDR corrected associations <0.05.

Acronyms: PRS = Polygenic Risk Score;  $P^T$  = polygenic threshold; APOE = Apolipoprotein E; L = left; R = right; FDR = false discovery rate.

**Table 5.35 Results for UK Biobank cortical surface area in left parietal regions and PRS excluding APOE at P<sup>T</sup> 0.001**

Polygenic risk score	Left inferior parietal R <sup>2</sup> p (95% CI)	Left isthmus cingulate R <sup>2</sup> p (95% CI)	Left posterior cingulate R <sup>2</sup> p (95% CI)	Left precuneus R <sup>2</sup> p (95% CI)	Left superior parietal R <sup>2</sup> p (95% CI)	Left supramarginal R <sup>2</sup> p (95% CI)
Protein–lipid complex assembly (-APOE)	1.85E-05 0.455 (-4.256,9.498)	4.30E-07 0.908 (-2.237,1.987)	4.44E-05 0.289 (-1.039,3.494)	1.32E-04 0.035 (0.374,10.313)*	5.57E-05 0.207 (-2.590,11.935)	2.43E-04 0.005 (2.525,14.295)*
Regulation of Aβ formation (-APOE)	1.85E-05 0.456 (-4.260,9.494)	4.34E-07 0.907 (-2.237,1.987)	4.42E-05 0.289 (-1.042,3.491)	1.32E-04 0.035 (0.376,10.315)*	5.56E-05 0.207 (-2.591,11.933)	2.44E-04 0.005 (2.527,14.297)*
Protein–lipid complex (-APOE)	1.83E-05 0.457 (-4.269,9.485)	4.25E-07 0.908 (-2.236,1.988)	4.41E-05 0.290 (-1.043,3.490)	1.32E-04 0.035 (0.377,10.315)*	5.56E-05 0.208 (-2.594,11.930)	2.44E-04 0.005 (2.527,14.297)*
Regulation of amyloid precursor protein catabolic process (-APOE)	1.82E-05 0.458 (-4.276,9.479)	4.22E-07 0.909 (-2.235,1.988)	4.40E-05 0.291 (-1.045,3.488)	1.32E-04 0.035 (0.378,10.317)*	5.55E-05 0.208 (-2.596,11.928)	2.44E-04 0.005 (2.527,14.297)*
Tau protein binding (-APOE)	1.81E-05 0.460 (-4.284,9.471)	4.17E-07 0.909 (-2.235,1.989)	4.39E-05 0.291 (-1.046,3.487)	1.32E-04 0.035 (0.379,10.318)*	5.55E-05 0.208 (-2.597,11.927)	2.44E-04 0.005 (2.529,14.299)*
Reverse cholesterol transport (-APOE)	1.80E-05 0.461 (-4.290,9.465)	4.14E-07 0.910 (-2.234,1.990)	4.39E-05 0.292 (-1.047,3.486)	1.32E-04 0.035 (0.381,10.320)*	5.55E-05 0.208 (-2.597,11.927)	2.44E-04 0.005 (2.533,14.303)*
Protein–lipid complex subunit organization (-APOE)	1.80E-05 0.462 (-4.294,9.460)	4.14E-07 0.910 (-2.234,1.989)	4.38E-05 0.292 (-1.047,3.486)	1.33E-04 0.035 (0.384,10.323)*	5.55E-05 0.208 (-2.595,11.929)	2.44E-04 0.005 (2.538,14.308)*
Plasma lipoprotein particle assembly (-APOE)	1.79E-05 0.462 (-4.297,9.457)	4.14E-07 0.910 (-2.234,1.990)	4.38E-05 0.292 (-1.048,3.485)	1.33E-04 0.035 (0.386,10.325)*	5.55E-05 0.208 (-2.595,11.929)	2.44E-04 0.005 (2.541,14.311)*
Activation of immune response (-APOE)	1.34E-04 0.044 (-13.925,-0.176)*	7.38E-07 0.880 (-1.948,2.275)	9.20E-05 0.126 (-4.032,0.499)	4.92E-06 0.684 (-5.999,3.938)	6.74E-07 0.890 (-6.746,7.774)	4.13E-05 0.249 (-9.347,2.421)
Genome-wide PRS (-APOE)	8.02E-05 0.120 (-12.332,1.423)	3.73E-05 0.281 (-3.274,0.950)	1.96E-04 0.026 (-4.848,-0.315)*	1.86E-05 0.427 (-6.986,2.955)	2.70E-06 0.781 (-8.293,6.233)	2.55E-05 0.365 (-8.608,3.165)
APOE SNPs PRS	4.94E-06 0.700 (-5.521,8.226)	5.88E-05 0.176 (-3.568,0.653)	1.41E-06 0.850 (-2.484,2.046)	7.47E-05 0.113 (-0.950,8.983)	1.92E-05 0.460 (-4.519,9.997)	1.00E-04 0.072 (-0.489,11.276)

R<sup>2</sup> and p values for subcortical volumes in the left hemisphere and each polygenic score at a PT of 0.001. The column names shows the region of interest, while the row names show the polygenic scores.

\* Nominally significant associations (p value < .05).

\*\* FDR corrected associations <0.05.

Acronyms: PRS = Polygenic Risk Score; PT = polygenic threshold; APOE = Apolipoprotein E; L = left; R = right; FDR = false discovery rate.

**Table 5.36 Results for UK Biobank cortical surface area in left temporal regions and PRS excluding APOE at  $P \leq 0.001$**

	Left entorhinal	Left inferior temporal	Left middle temporal	Left parahippocampal	Left superior temporal	Left temporal pole	Left transverse temporal
Polygenic risk score	$R^2$ p (95% CI)	$R^2$ p (95% CI)	$R^2$ p (95% CI)	$R^2$ p (95% CI)	$R^2$ p (95% CI)	$R^2$ p (95% CI)	$R^2$ p (95% CI)
Protein-lipid complex assembly (-APOE)	3.15E-05 0.401 (-1.392,0.556)	1.48E-04 0.035 (-10.692,-0.392)*	3.51E-05 0.284 (-6.506,1.906)	8.55E-05 0.145 (-0.319,2.167)	2.63E-05 0.332 (-2.231,6.607)	1.05E-05 0.628 (-0.603,0.999)	6.40E-05 0.225 (-0.385,1.637)
Regulation of A $\beta$ formation (-APOE)	3.15E-05 0.400 (-1.392,0.556)	1.48E-04 0.035 (-10.691,-0.391)*	3.50E-05 0.285 (-6.501,1.911)	8.57E-05 0.145 (-0.318,2.168)	2.64E-05 0.332 (-2.230,6.608)	1.05E-05 0.628 (-0.603,0.999)	6.41E-05 0.224 (-0.384,1.638)
Protein-lipid complex (-APOE)	3.15E-05 0.400 (-1.392,0.556)	1.48E-04 0.035 (-10.693,-0.393)*	3.50E-05 0.285 (-6.500,1.912)	8.60E-05 0.144 (-0.317,2.169)	2.64E-05 0.332 (-2.231,6.608)	1.05E-05 0.629 (-0.604,0.999)	6.42E-05 0.224 (-0.384,1.638)
Regulation of amyloid precursor protein catabolic process (-APOE)	3.15E-05 0.400 (-1.392,0.556)	1.48E-04 0.035 (-10.693,-0.393)*	3.49E-05 0.286 (-6.497,1.914)	8.63E-05 0.144 (-0.315,2.171)	2.64E-05 0.332 (-2.231,6.608)	1.04E-05 0.630 (-0.604,0.998)	6.43E-05 0.224 (-0.384,1.638)
Tau protein binding (-APOE)	3.16E-05 0.400 (-1.392,0.556)	1.48E-04 0.035 (-10.695,-0.395)*	3.48E-05 0.286 (-6.496,1.916)	8.65E-05 0.143 (-0.314,2.172)	2.64E-05 0.332 (-2.230,6.609)	1.04E-05 0.631 (-0.605,0.998)	6.44E-05 0.224 (-0.383,1.639)
Reverse cholesterol transport (-APOE)	3.16E-05 0.400 (-1.392,0.555)	1.48E-04 0.035 (-10.696,-0.396)*	3.48E-05 0.286 (-6.494,1.918)	8.66E-05 0.143 (-0.314,2.172)	2.64E-05 0.331 (-2.229,6.610)	1.03E-05 0.632 (-0.605,0.997)	6.45E-05 0.223 (-0.383,1.639)
Protein-lipid complex subunit organization (-APOE)	3.17E-05 0.399 (-1.393,0.555)	1.48E-04 0.035 (-10.695,-0.395)*	3.47E-05 0.287 (-6.492,1.920)	8.67E-05 0.143 (-0.313,2.173)	2.65E-05 0.331 (-2.227,6.612)	1.03E-05 0.632 (-0.606,0.997)	6.46E-05 0.223 (-0.382,1.640)
Plasma lipoprotein particle assembly (-APOE)	3.17E-05 0.399 (-1.393,0.555)	1.48E-04 0.035 (-10.694,-0.394)*	3.46E-05 0.287 (-6.490,1.922)	8.68E-05 0.142 (-0.312,2.174)	2.65E-05 0.331 (-2.226,6.613)	1.03E-05 0.632 (-0.606,0.997)	6.47E-05 0.223 (-0.382,1.640)
Activation of immune response (-APOE)	2.28E-06 0.821 (-1.086,0.861)	2.01E-04 0.014 (-11.603,-1.306)*	3.49E-06 0.735 (-4.330,3.480)	4.98E-05 0.266 (-1.948,0.538)	1.71E-05 0.434 (-2.654,6.182)	1.57E-06 0.852 (-0.878,0.725)	8.61E-06 0.656 (-0.781,1.240)
Genome-wide PRS (-APOE)	6.05E-05 0.244 (-1.553,0.395)	2.25E-04 0.009 (-11.982,-1.681)*	1.47E-08 0.982 (-4.254,4.159)	3.63E-05 0.343 (-1.845,0.642)	3.52E-05 0.262 (-1.890,6.950)	1.65E-04 0.055 (-0.018,1.585)	4.15E-05 0.329 (-0.507,1.515)
APOE SNPs PRS	1.99E-07 0.947 (-1.006,0.940)	9.31E-05 0.095 (-9.537,0.757)	8.98E-05 0.087 (-7.878,0.529)	2.25E-05 0.455 (-0.769,1.715)	2.06E-05 0.391 (-6.348,2.485)	1.94E-05 0.512 (-0.533,1.069)	9.56E-07 0.882 (-1.087,0.934)

R2 and p values for subcortical volumes in the left hemisphere and each polygenic score at a PT of 0.001. The column names show the region of interest, while the row names show the polygenic scores.

\* Nominally significant associations (p value < .05).

\*\* FDR corrected associations <0.05.

Acronyms: PRS = Polygenic Risk Score; PT = polygenic threshold; APOE = Apolipoprotein E; L = left; R = right; FDR = false discovery rate.

**Table 5.37 Results for UK Biobank cortical surface area in right parietal regions and PRS including APOE at P<sup>T</sup> 0.001**

Polygenic risk score	Right inferior parietal R <sup>2</sup> p (95% CI)	Right isthmus cingulate R <sup>2</sup> p (95% CI)	Right posterior cingulate R <sup>2</sup> p (95% CI)	Right precuneus R <sup>2</sup> p (95% CI)	Right superior parietal R <sup>2</sup> p (95% CI)	Right supramarginal R <sup>2</sup> p (95% CI)
<b>Protein-lipid complex assembly</b>	6.03E-05 0.166 (-2.297, 13.354)	6.69E-05 0.156 (-0.515, 3.200)	3.19E-06 0.770 (-1.928, 2.606)	1.13E-04 0.049 (0.013, 10.906)*	6.33E-05 0.173 (-2.175, 12.076)	2.27E-05 0.415 (-3.464, 8.389)
<b>Regulation of Aβ formation</b>	6.03E-05 0.166 (-2.297, 13.355)	6.70E-05 0.156 (-0.513, 3.201)	3.24E-06 0.768 (-1.926, 2.609)	1.13E-04 0.050 (0.010, 10.904)*	6.34E-05 0.173 (-2.171, 12.079)	2.27E-05 0.416 (-3.466, 8.388)
<b>Protein-lipid complex</b>	6.02E-05 0.167 (-2.302, 13.349)	6.71E-05 0.156 (-0.513, 3.202)	3.22E-06 0.769 (-1.927, 2.608)	1.13E-04 0.050 (0.008, 10.901)*	6.33E-05 0.173 (-2.176, 12.075)	2.26E-05 0.417 (-3.471, 8.382)
<b>Regulation of amyloid precursor protein catabolic process</b>	6.01E-05 0.167 (-2.303, 13.348)	6.71E-05 0.156 (-0.512, 3.203)	3.24E-06 0.768 (-1.926, 2.609)	1.13E-04 0.050 (0.008, 10.901)*	6.34E-05 0.173 (-2.174, 12.076)	2.25E-05 0.417 (-3.474, 8.379)
<b>Tau protein binding</b>	6.01E-05 0.167 (-2.304, 13.348)	6.71E-05 0.156 (-0.512, 3.203)	3.26E-06 0.767 (-1.925, 2.610)	1.13E-04 0.050 (0.006, 10.900)*	6.33E-05 0.173 (-2.177, 12.074)	2.24E-05 0.418 (-3.480, 8.374)
<b>Reverse cholesterol transport</b>	6.01E-05 0.167 (-2.304, 13.348)	6.71E-05 0.156 (-0.513, 3.202)	3.27E-06 0.767 (-1.924, 2.610)	1.13E-04 0.050 (0.006, 10.900)*	6.33E-05 0.174 (-2.178, 12.073)	2.23E-05 0.419 (-3.484, 8.370)
<b>Protein-lipid complex subunit organization</b>	6.01E-05 0.167 (-2.303, 13.348)	6.70E-05 0.156 (-0.513, 3.201)	3.29E-06 0.766 (-1.923, 2.611)	1.13E-04 0.050 (0.007, 10.900)*	6.33E-05 0.173 (-2.177, 12.074)	2.23E-05 0.419 (-3.485, 8.368)
<b>Plasma lipoprotein particle assembly</b>	6.02E-05 0.167 (-2.302, 13.349)	6.70E-05 0.156 (-0.514, 3.201)	3.31E-06 0.766 (-1.922, 2.612)	1.13E-04 0.050 (0.006, 10.900)*	6.33E-05 0.173 (-2.176, 12.075)	2.23E-05 0.420 (-3.486, 8.367)
<b>Activation of immune response</b>	1.62E-06 0.820 (-8.730, 6.918)	2.10E-06 0.802 (-2.095, 1.619)	2.41E-05 0.421 (-3.197, 1.336)	5.13E-06 0.675 (-6.610, 4.282)	6.63E-05 0.164 (-12.185, 2.061)	6.23E-05 0.177 (-10.006, 1.844)
<b>Genome-wide PRS</b>	1.48E-06 0.828 (-8.693, 6.959)	1.17E-05 0.553 (-2.420, 1.295)	7.52E-05 0.155 (-3.912, 0.622)	3.14E-09 0.992 (-5.419, 5.476)	1.20E-06 0.851 (-6.444, 7.807)	1.04E-07 0.956 (-5.760, 6.094)

R<sup>2</sup> and p values for subcortical volumes in the right hemisphere and each polygenic score at a PT of 0.001. The column names shows the region of interest, while the row names show the polygenic scores.

\* Nominally significant associations (p value < .05).

\*\* FDR corrected associations <0.05.

Acronyms: PRS = Polygenic Risk Score; PT = polygenic threshold; APOE = Apolipoprotein E; L = left; R = right; FDR = false discovery rate.

**Table 5.38 Results for UK Biobank cortical surface area in right temporal regions and PRS including APOE at PT 0.001**

	Right entorhinal	Right inferior temporal	Right middle temporal	Right parahippocampal	Right superior temporal	Right temporal pole	Right transverse temporal
Polygenic risk score	R <sup>2</sup>	R <sup>2</sup>	R <sup>2</sup>	R <sup>2</sup>	R <sup>2</sup>	R <sup>2</sup>	R <sup>2</sup>
	p (95% CI)	p (95% CI)	p (95% CI)	p (95% CI)	p (95% CI)	p (95% CI)	p (95% CI)
<b>Protein-lipid complex assembly</b>	1.09E-04 0.125 (-0.224, 1.833)	1.77E-05 0.459 (-6.610, 2.986)	9.09E-06 0.573 (-5.537, 3.062)	2.70E-05 0.393 (-0.671, 1.705)	8.41E-05 0.081 (-0.426, 7.419)	4.60E-06 0.756 (-0.675, 0.929)	1.49E-05 0.551 (-0.522, 0.978)
<b>Regulation of Aβ formation</b>	1.09E-04 0.124 (-0.222, 1.835)	1.76E-05 0.461 (-6.603, 2.993)	9.09E-06 0.573 (-5.537, 3.062)	2.72E-05 0.392 (-0.669, 1.707)	8.42E-05 0.081 (-0.425, 7.420)	4.63E-06 0.755 (-0.674, 0.929)	1.50E-05 0.551 (-0.521, 0.978)
<b>Protein-lipid complex</b>	1.09E-04 0.124 (-0.222, 1.836)	1.77E-05 0.460 (-6.608, 2.988)	9.11E-06 0.572 (-5.538, 3.060)	2.71E-05 0.392 (-0.669, 1.707)	8.42E-05 0.081 (-0.425, 7.420)	4.57E-06 0.757 (-0.675, 0.929)	1.51E-05 0.549 (-0.521, 0.979)
<b>Regulation of amyloid precursor protein catabolic process</b>	1.10E-04 0.123 (-0.220, 1.837)	1.76E-05 0.460 (-6.605, 2.991)	9.13E-06 0.572 (-5.539, 3.060)	2.72E-05 0.392 (-0.669, 1.707)	8.43E-05 0.080 (-0.423, 7.422)	4.58E-06 0.757 (-0.675, 0.929)	1.51E-05 0.548 (-0.520, 0.979)
<b>Tau protein binding</b>	1.10E-04 0.123 (-0.220, 1.838)	1.77E-05 0.460 (-6.608, 2.988)	9.14E-06 0.572 (-5.540, 3.059)	2.72E-05 0.392 (-0.669, 1.707)	8.43E-05 0.080 (-0.422, 7.423)	4.56E-06 0.757 (-0.675, 0.928)	1.52E-05 0.547 (-0.519, 0.980)
<b>Reverse cholesterol transport</b>	1.10E-04 0.123 (-0.219, 1.838)	1.77E-05 0.459 (-6.611, 2.985)	9.14E-06 0.572 (-5.540, 3.058)	2.72E-05 0.392 (-0.669, 1.707)	8.44E-05 0.080 (-0.420, 7.425)	4.53E-06 0.758 (-0.676, 0.928)	1.53E-05 0.546 (-0.519, 0.981)
<b>Protein-lipid complex subunit organization</b>	1.10E-04 0.123 (-0.219, 1.839)	1.77E-05 0.459 (-6.611, 2.985)	9.15E-06 0.571 (-5.541, 3.058)	2.71E-05 0.392 (-0.669, 1.707)	8.45E-05 0.080 (-0.417, 7.428)	4.53E-06 0.758 (-0.676, 0.928)	1.54E-05 0.544 (-0.518, 0.982)
<b>Plasma lipoprotein particle assembly</b>	1.10E-04 0.123 (-0.218, 1.839)	1.77E-05 0.459 (-6.609, 2.987)	9.14E-06 0.572 (-5.540, 3.058)	2.72E-05 0.391 (-0.668, 1.708)	8.46E-05 0.080 (-0.415, 7.430)	4.52E-06 0.758 (-0.676, 0.928)	1.55E-05 0.544 (-0.518, 0.982)
<b>Activation of immune response</b>	2.92E-05 0.427 (-0.612, 1.445)	2.07E-04 0.011 (-10.985, -1.393)*	4.34E-05 0.218 (-7.001, 1.595)	3.63E-05 0.322 (-1.787, 0.588)	2.31E-05 0.360 (-5.753, 2.090)	4.53E-05 0.329 (-1.201, 0.403)	3.23E-06 0.781 (-0.856, 0.643)
<b>Genome-wide PRS</b>	3.62E-06 0.780 (-1.176, 0.882)	1.29E-04 0.046 (-9.692, -0.097)*	6.84E-05 0.122 (-7.694, 0.904)	1.94E-05 0.469 (-1.627, 0.749)	1.87E-05 0.410 (-2.272, 5.573)	4.68E-05 0.322 (-1.207, 0.397)	5.52E-05 0.251 (-1.189, 0.311)

R2 and p values for subcortical volumes in the right hemisphere and each polygenic score at a PT of 0.001. The column names show the region of interest, while the row names show the polygenic scores.

\* Nominally significant associations (p value < .05).

\*\* FDR corrected associations <0.05.

Acronyms: PRS = Polygenic Risk Score; PT = polygenic threshold; APOE = Apolipoprotein E; L = left; R = right; FDR = false discovery rate.

**Table 5.39 Results for UK Biobank cortical surface area in right parietal regions and PRS excluding APOE at P<sup>T</sup> 0.001**

Polygenic risk score	Right inferior parietal		Right isthmus cingulate		Right posterior cingulate		Right precuneus		Right superior parietal		Right supramarginal	
	R <sup>2</sup>	p (95% CI)	R <sup>2</sup>	p (95% CI)	R <sup>2</sup>	p (95% CI)	R <sup>2</sup>	p (95% CI)	R <sup>2</sup>	p (95% CI)	R <sup>2</sup>	p (95% CI)
Protein-lipid complex assembly (-APOE)	0.166 (-2.300,13.351)	6.02E-05	0.156 (-0.514,3.200)	6.69E-05	0.769 (-1.927,2.607)	3.21E-06	0.050 (0.008,10.902)*	1.13E-04	0.173 (-2.173,12.078)	6.34E-05	0.415 (-3.463,8.391)	2.27E-05
Regulation of Aβ formation (-APOE)	0.166 (-2.298,13.354)	6.03E-05	0.156 (-0.514,3.201)	6.70E-05	0.769 (-1.927,2.607)	3.22E-06	0.050 (0.009,10.902)*	1.13E-04	0.173 (-2.174,12.076)	6.33E-05	0.416 (-3.467,8.387)	2.26E-05
Protein-lipid complex (-APOE)	0.167 (-2.302,13.349)	6.02E-05	0.156 (-0.513,3.202)	6.70E-05	0.768 (-1.927,2.608)	3.23E-06	0.050 (0.007,10.901)*	1.13E-04	0.173 (-2.175,12.076)	6.33E-05	0.417 (-3.471,8.383)	2.26E-05
Regulation of amyloid precursor protein catabolic process (-APOE)	0.167 (-2.304,13.348)	6.01E-05	0.156 (-0.512,3.202)	6.71E-05	0.768 (-1.926,2.608)	3.23E-06	0.050 (0.007,10.901)*	1.13E-04	0.173 (-2.176,12.075)	6.33E-05	0.417 (-3.475,8.379)	2.25E-05
Tau protein binding (-APOE)	0.167 (-2.304,13.348)	6.01E-05	0.156 (-0.512,3.202)	6.71E-05	0.768 (-1.925,2.609)	3.25E-06	0.050 (0.006,10.900)*	1.13E-04	0.173 (-2.177,12.073)	6.33E-05	0.418 (-3.480,8.374)	2.24E-05
Reverse cholesterol transport (-APOE)	0.167 (-2.304,13.347)	6.01E-05	0.156 (-0.513,3.202)	6.71E-05	0.767 (-1.924,2.610)	3.27E-06	0.050 (0.006,10.899)*	1.13E-04	0.173 (-2.177,12.073)	6.33E-05	0.419 (-3.483,8.370)	2.23E-05
Protein-lipid complex subunit organization (-APOE)	0.167 (-2.304,13.348)	6.01E-05	0.156 (-0.513,3.201)	6.70E-05	0.766 (-1.923,2.611)	3.29E-06	0.050 (0.006,10.900)*	1.13E-04	0.173 (-2.177,12.074)	6.33E-05	0.419 (-3.485,8.368)	2.23E-05
Plasma lipoprotein particle assembly (-APOE)	0.167 (-2.304,13.348)	6.01E-05	0.156 (-0.514,3.201)	6.70E-05	0.766 (-1.922,2.612)	3.31E-06	0.050 (0.006,10.900)*	1.13E-04	0.173 (-2.176,12.075)	6.33E-05	0.420 (-3.486,8.367)	2.23E-05
Activation of immune response (-APOE)	0.993 (-7.789,7.859)	2.44E-09	0.876 (-2.005,1.709)	8.13E-07	0.520 (-3.010,1.523)	1.54E-05	0.799 (-6.154,4.737)	1.90E-06	0.166 (-12.154,2.092)	6.54E-05	0.140 (-10.381,1.469)	7.43E-05
Genome-wide PRS (-APOE)	0.593 (-9.961,5.692)	8.98E-06	0.875 (-1.708,2.007)	8.29E-07	0.275 (-3.531,1.004)	4.44E-05	0.474 (-7.438,3.458)	1.50E-05	0.649 (-8.781,5.472)	7.07E-06	0.437 (-8.280,3.575)	2.07E-05
APOE SNPs PRS	0.728 (-6.432,9.210)	3.81E-06	0.230 (-2.994,0.719)	4.81E-05	0.356 (-3.333,1.199)	3.17E-05	0.332 (-2.752,8.136)	2.75E-05	0.359 (-3.786,10.456)	2.88E-05	0.260 (-2.519,9.327)	4.34E-05

R<sup>2</sup> and p values for subcortical volumes in the right hemisphere and each polygenic score at a PT of 0.001. The column names shows the region of interest, while the row names show the polygenic scores.

\* Nominally significant associations (p value < .05).

\*\* FDR corrected associations <0.05.

Acronyms: PRS = Polygenic Risk Score; PT = polygenic threshold; APOE = Apolipoprotein E; L = left; R = right; FDR = false discovery rate.

**Table 5.40 Results for UK Biobank cortical surface area in right temporal regions and PRS excluding APOE at P<sup>T</sup> 0.001**

	Right entorhinal	Right inferior temporal	Right middle temporal	Right parahippocampal	Right superior temporal	Right temporal pole	Right transverse temporal
	R <sup>2</sup>	R <sup>2</sup>	R <sup>2</sup>	R <sup>2</sup>	R <sup>2</sup>	R <sup>2</sup>	R <sup>2</sup>
	p (95% CI)	p (95% CI)	p (95% CI)	p (95% CI)	p (95% CI)	p (95% CI)	p (95% CI)
<b>Polygenic risk score</b>							
<b>Protein-lipid complex assembly (-APOE)</b>	1.09E-04 0.125 (-0.224, 1.834)	1.77E-05 0.459 (-6.609, 2.987)	9.10E-06 0.573 (-5.537, 3.061)	2.71E-05 0.392 (-0.669, 1.706)	8.40E-05 0.081 (-0.429, 7.416)	4.60E-06 0.756 (-0.675, 0.929)	1.49E-05 0.552 (-0.522, 0.977)
<b>Regulation of Aβ formation (-APOE)</b>	1.09E-04 0.125 (-0.223, 1.835)	1.76E-05 0.460 (-6.605, 2.991)	9.09E-06 0.573 (-5.537, 3.062)	2.71E-05 0.392 (-0.669, 1.707)	8.41E-05 0.081 (-0.426, 7.419)	4.60E-06 0.756 (-0.675, 0.929)	1.50E-05 0.550 (-0.521, 0.978)
<b>Protein-lipid complex (-APOE)</b>	1.09E-04 0.124 (-0.222, 1.836)	1.77E-05 0.460 (-6.607, 2.989)	9.12E-06 0.572 (-5.538, 3.060)	2.71E-05 0.392 (-0.669, 1.707)	8.42E-05 0.081 (-0.425, 7.420)	4.58E-06 0.757 (-0.675, 0.929)	1.50E-05 0.549 (-0.521, 0.979)
<b>Regulation of amyloid precursor protein catabolic process (-APOE)</b>	1.10E-04 0.124 (-0.220, 1.837)	1.77E-05 0.460 (-6.606, 2.990)	9.12E-06 0.572 (-5.539, 3.060)	2.71E-05 0.392 (-0.669, 1.707)	8.42E-05 0.080 (-0.423, 7.422)	4.57E-06 0.757 (-0.675, 0.929)	1.51E-05 0.548 (-0.520, 0.979)
<b>Tau protein binding (-APOE)</b>	1.10E-04 0.123 (-0.220, 1.838)	1.77E-05 0.459 (-6.609, 2.987)	9.14E-06 0.572 (-5.540, 3.059)	2.72E-05 0.392 (-0.669, 1.707)	8.43E-05 0.080 (-0.422, 7.423)	4.55E-06 0.757 (-0.676, 0.928)	1.52E-05 0.547 (-0.519, 0.980)
<b>Reverse cholesterol transport (-APOE)</b>	1.10E-04 0.123 (-0.219, 1.838)	1.77E-05 0.459 (-6.611, 2.985)	9.15E-06 0.571 (-5.541, 3.058)	2.72E-05 0.392 (-0.669, 1.707)	8.44E-05 0.080 (-0.420, 7.425)	4.53E-06 0.758 (-0.676, 0.928)	1.53E-05 0.546 (-0.519, 0.981)
<b>Protein-lipid complex subunit organization (-APOE)</b>	1.10E-04 0.123 (-0.219, 1.839)	1.77E-05 0.459 (-6.611, 2.985)	9.15E-06 0.571 (-5.541, 3.058)	2.72E-05 0.392 (-0.669, 1.707)	8.45E-05 0.080 (-0.417, 7.428)	4.53E-06 0.758 (-0.676, 0.928)	1.54E-05 0.544 (-0.518, 0.982)
<b>Plasma lipoprotein particle assembly (-APOE)</b>	1.10E-04 0.123 (-0.219, 1.839)	1.77E-05 0.459 (-6.611, 2.985)	9.15E-06 0.571 (-5.541, 3.058)	2.72E-05 0.392 (-0.669, 1.707)	8.46E-05 0.080 (-0.416, 7.429)	4.52E-06 0.758 (-0.676, 0.928)	1.55E-05 0.543 (-0.517, 0.982)
<b>Activation of immune response (-APOE)</b>	3.02E-05 0.419 (-0.605, 1.452)	1.71E-04 0.021 (-10.430, -0.838)*	3.05E-05 0.302 (-6.563, 2.033)	4.74E-05 0.258 (-1.873, 0.502)	9.27E-06 0.562 (-5.082, 2.761)	3.18E-05 0.414 (-1.136, 0.468)	4.72E-06 0.737 (-0.878, 0.621)
<b>Genome-wide PRS (-APOE)</b>	1.77E-05 0.537 (-1.353, 0.705)	1.78E-04 0.019 (-10.547, -0.951)*	2.81E-05 0.322 (-6.475, 2.125)	7.20E-05 0.163 (-2.033, 0.343)	3.34E-05 0.271 (-1.719, 6.127)	3.19E-05 0.413 (-1.137, 0.467)	7.65E-05 0.177 (-1.266, 0.233)
<b>APOE SNPs PRS</b>	5.82E-06 0.723 (-0.842, 1.214)	1.53E-06 0.828 (-5.328, 4.263)	4.59E-05 0.205 (-7.074, 1.519)	1.54E-05 0.519 (-0.797, 1.577)	2.08E-07 0.931 (-4.094, 3.747)	1.53E-05 0.571 (-1.033, 0.570)	6.13E-07 0.904 (-0.796, 0.703)

R<sup>2</sup> and p values for subcortical volumes in the right hemisphere and each polygenic score at a PT of 0.001. The column names shows the region of interest, while the row names show the polygenic scores.

\* Nominally significant associations (p value < .05).

\*\* FDR corrected associations <0.05.

Acronyms: PRS = Polygenic Risk Score; PT = polygenic threshold; APOE = Apolipoprotein E; L = left; R = right; FDR = false discovery rate.

**Figure 5.12. Associations between PRS ( $P^T = 0.001$ ) and surface area in cortical and temporal regions of cortex in UK Biobank,  $p < 0.05$ .**

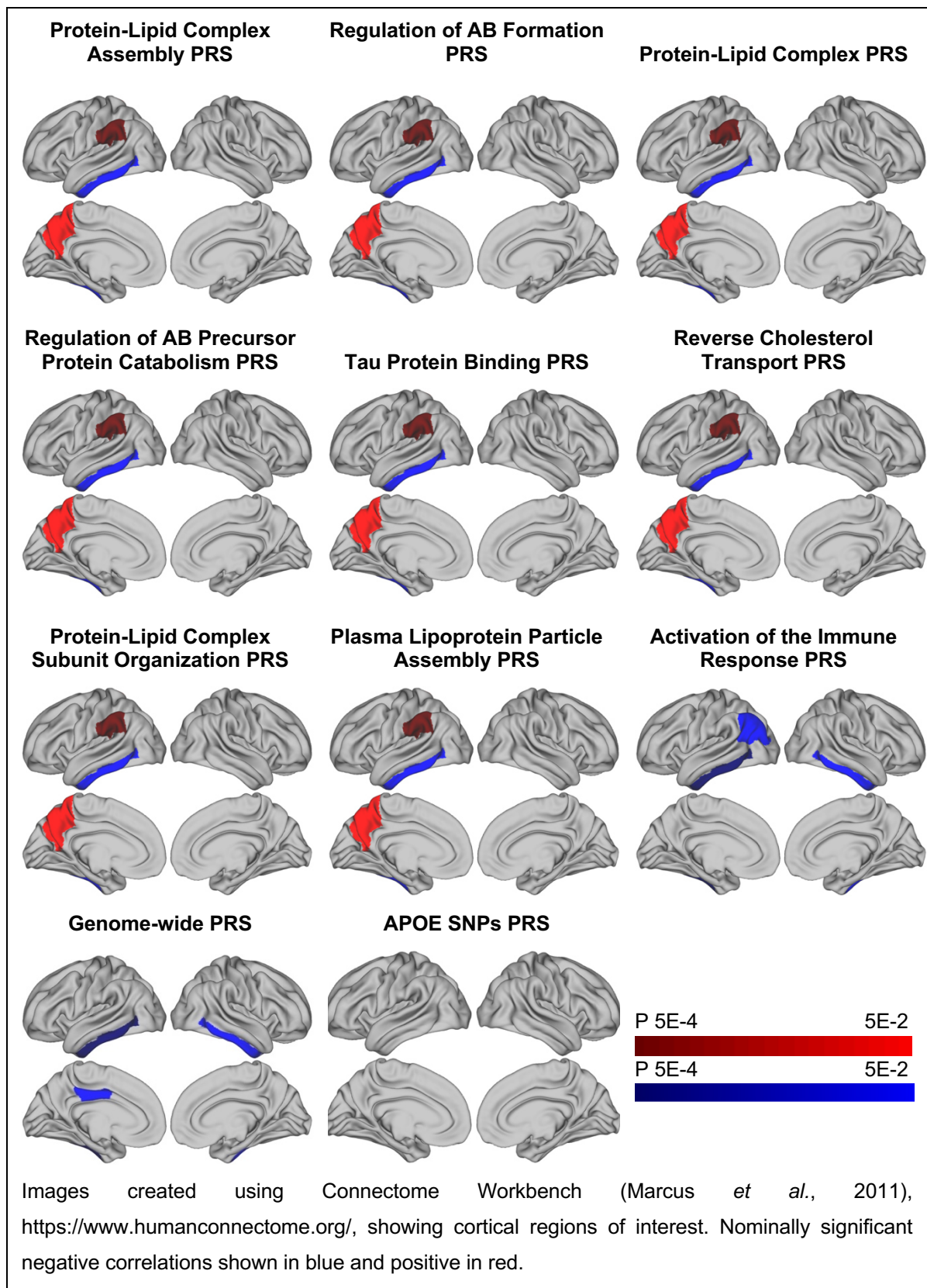
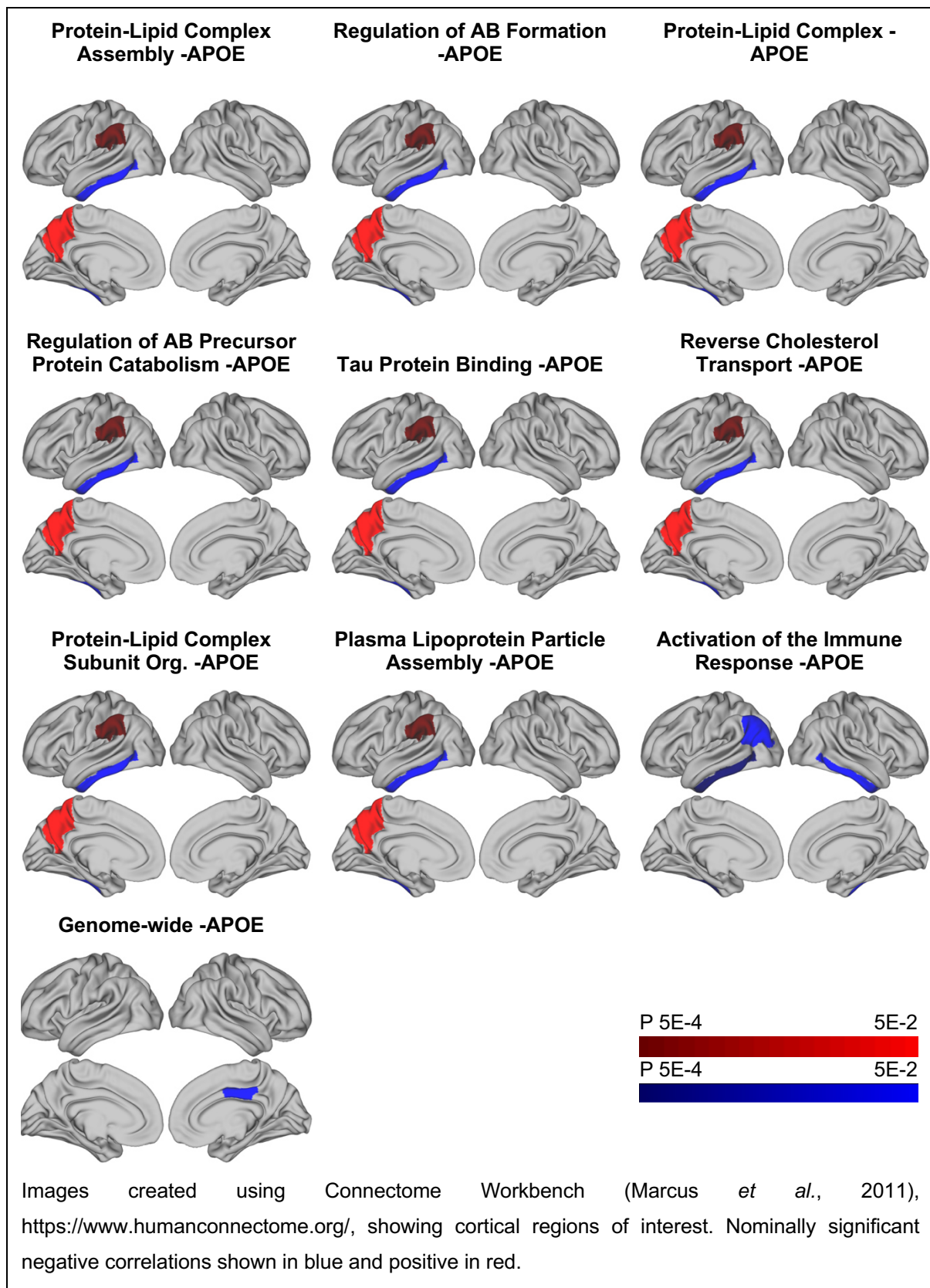


**Figure 5.13. Associations between PRS ( $P^T = 0.001$ ) excluding *APOE* and surface area in cortical and temporal regions of cortex in UK Biobank,  $p < 0.05$ .**



## 5.5 Discussion

As predicted, increased genetic burden for AD, measured by PRS, was associated with lower subcortical volumes and reduced cortical thickness in older adults who are cognitively healthy. In younger adults, increased polygenic risk was also associated with lower cortical thickness, but it was associated with greater volumes in subcortical structures. The strongest evidence of association with AD polygenic risk was found in the subcortical regions in the left hemisphere, with many of the pathway specific PRS associations remaining significant after the *APOE* region was removed in the older cohort.

As discussed above, reduced hippocampal volume in AD is a robust finding (Serra *et al.*, 2009; Clerx *et al.*, 2012) and hippocampal atrophy can predict progression from MCI to AD (Korf *et al.*, 2004; Jack *et al.*, 2005). Previous studies exploring the effect of AD genetic risk on hippocampal volume across the lifespan report mixed results. While studies of older adults commonly report reduced hippocampal volume among *APOE* carriers, findings in young participants are varied. Some studies report an association between *APOE* and decreased hippocampal volume in samples with mean ages ranging from 23.9 to 39.7 years (Alexopoulos *et al.*, 2011; O'Dwyer, Lamberton, Matura, Tanner, *et al.*, 2012; Foley *et al.*, 2016) whereas others observe no significant differences in samples aged 14.4 to 28.8 years (Filippini *et al.*, 2009b; Heise *et al.*, 2011; Khan *et al.*, 2013). Increased hippocampal volume, as observed in the present study in the young adult sample, has also been reported in samples of children who are *APOE4* carriers (Chang *et al.*, 2016) and in some studies of healthy adult *APOE4* carriers (Striepens *et al.*, 2011). Greater frontal grey matter volumes have been observed in infant *APOE4* carriers (Dean *et al.*, 2014), and increased temporal grey matter volumes have been reported in children with autosomal dominant AD genes (Quiroz *et al.*, 2015). Young *APOE4* carriers also show increased activation in the hippocampus on fMRI (Filippini *et al.*, 2009a).

In the older adult cohort, this experiment found significant associations between increased PRS and decreased volume in the nucleus accumbens, which has also been associated with AD. In a study of striatal morphology in AD cases compared to controls, AD patients showed significant reductions in nucleus accumbens volumes

bilaterally (Pievani *et al.*, 2013). Other studies have identified sub-regional structural changes in the nucleus accumbens and the hippocampus in MCI and AD which correlated with the cognitive impairment (Nie *et al.*, 2017). Further studies have reported evidence of functional changes in the accumbens. For example, using Alzheimer's Disease Neuroimaging Initiative (ADNI) data, Kazemifar *et al.* found that activity shown on resting state MRI was significantly lower in the accumbens of AD cases compared to healthy controls (Kazemifar *et al.*, 2017). A study using an *APP/PS1* mouse model identified significant intracellular A $\beta$  accumulation, increased excitability and synaptic alterations in the nucleus accumbens of transgenic mice compared to wild type (Fernández-Pérez *et al.*, 2020).

In the present study, there was a preponderance of associations in subcortical regions in the left hemisphere. This is broadly consistent with the findings of previous studies. Although one group reported reduced hippocampal volume in *APOE4* compared to *APOE3* carriers on the right only (Lind *et al.*, 2006), the literature predominantly observed greater evidence of changes in the left hemisphere, especially in preclinical or early stage AD (Shi *et al.*, 2009), which corresponds with the findings of the present study.

Cortical thinning, particularly in medial temporal regions, may be an early morphometric biomarker. Normal aging has little effect on cortical thickness in medial temporal regions (Salat *et al.*, 2004; Dickerson, Feczko, *et al.*, 2009). This is thought to correspond to laminar thinning observed in these areas early in the disease (Dickerson, Feczko, *et al.*, 2009). In the older cohort, we found the genome-wide PRS and SNPs in the *APOE* region were associated with cortical thinning in the entorhinal and parahippocampal regions. This is consistent with previous studies which have implicated the entorhinal (Köhler *et al.*, 1998; Killiany *et al.*, 2002; Burggren *et al.*, 2008) and parahippocampal cortex (Shaw *et al.*, 2007; Dowell *et al.*, 2016). Results for the genome-wide PRS attenuated partly when the *APOE* region was excluded, with only the right entorhinal cortex remaining significant.

There was little evidence of association between entorhinal cortex thickness and any PRS in the younger cohort. Neither were the pathway specific PRS in the older cohort associated with entorhinal thinning. However, there were negative associations with

several other areas in the temporal and parietal cortex. Many of these regions show the most marked cortical thinning in incipient AD compared to healthy older adults (Sabuncu *et al.*, 2011). Furthermore, a previous study reported that AD PRS is associated with cortical thinning in these regions (Sabuncu *et al.*, 2012). Cortical thinning has also been demonstrated even in *APOE* carriers in children and adolescents (Shaw *et al.*, 2007). Unlike the genome-wide PRS, the results were maintained even when *APOE* was excluded from the score. The immune response PRS was only associated with cortical thinning in the right posterior cingulate gyrus in older and younger adults. Both AD genetic risk and established AD have been associated with reduced thickness in the posterior cingulate (Knight *et al.*, 2009; Lehmann *et al.*, 2010).

Whilst these results concur with the findings of previous studies, many results were no longer significant when corrected for multiple comparisons. Interestingly, whilst the cortical results in the younger adult cohort attenuated when *APOE* was excluded, the associations in the older adult cohort were maintained. This suggests that beyond *APOE*, polygenic burden for AD may not manifest in brain structure changes until later in life.

Few studies have reported associations between cortical surface area and manifest AD or pre-clinical AD. One study, which primarily explored networks based on cortical morphometry, reported a mixture of positive and negative associations with cortical surface area in AD and Frontotemporal dementia patients (Vuksanović *et al.*, 2019). Another reported difference in entorhinal and posterior parahippocampal cingulate surface area between established AD and controls, although the overall loss of volume in AD was driven by significant cortical thinning rather than surface area change (Dickerson, Feczko, *et al.*, 2009). The present study observed similar results to Vuksanović and colleagues, although none of the cortical surface area results remained after correction for multiple comparisons. Compared to thinning, cortical surface area is less clearly linked with AD pathophysiology, and it does not correlate with cognitive function (Dickerson, Feczko, *et al.*, 2009). Measurements of cortical thinning in AD appear to relate more closely to neuronal loss, degeneration of synapses and dendritic branching than surface area, factors which probably underpin cognitive decline in AD (Dickerson, Feczko, *et al.*, 2009).

Whilst it was hypothesised that genetic burden in different disease pathways might be associated with distinct patterns of association in the grey matter, as suggested by Caspers and colleagues (Caspers *et al.*, 2020), the results did not support this. There was close correspondence between the genome-wide and pathway specific PRS in terms of the regions implicated, variance explained and associated p values. This is probably explained by the significant overlap in the SNPs included in each pathway, and by the *APOE* gene which is included in the full genome PRS and in the majority of the pathways (all apart from the immune response pathway). See Table 4.2 in Chapter 4 for a breakdown of genes and SNPs included in each pathway PRS. The full genome wide PRS, constructed from SNPs with p-values <0.001, contained a relatively small number of SNPs (n = 404) and it is likely that *APOE* effect dominated the genome wide PRS. The immune response PRS, which was associated with fewer morphological changes, contains a much greater number of genes than the other pathway PRS, which might have introduced more noise into the score.

The findings are broadly in line with three previous studies that have used PRS specific to disease pathways to explore neuroimaging phenotypes relevant to AD. All studied dementia-free population samples of older adults. Corlier et al (sample n = 355) found that an immune response PRS (n SNPs = 11) was significantly associated with a general measure of cortical thinning (Corlier *et al.*, 2018). Ahmad and colleagues (sample n = 4521) found no significant associations between seven different pathway polygenic scores (n SNPs = 20), hippocampal volume and whole brain volume (Ahmad *et al.*, 2018). Caspers et al (sample n = 544) reported that cortical thinning associated with PRS (n SNPs = 20) for specific biological processes. The pathway-specific effects showed a more bilateral pattern and two unique pathway-specific patterns were reported, involving the superior parietal and mid/anterior cingulate regions (Caspers *et al.*, 2020). All of these studies used PRS that only included Bonferroni significant loci, thereby excluding relevant genetic information that is below the stringent threshold for genome-wide significance. The present study, using threshold-based PRS, may have seen significant effects where previous studies have observed mixed results.

### 5.5.1 Strength and limitations

This study benefited from using results from the largest AD GWAS performed to date as our discovery data (Kunkle *et al.*, 2019). Consequently, estimates of SNP effects on disease risk used in this analysis are the most accurate available, with improved power compared to previous estimates. It has been demonstrated that PRS and  $R^2$  are highly sensitive to the size of discovery dataset (Schizophrenia Working Group of the Psychiatric Genomics, 2014). It also benefitted from large target sample sizes in population cohorts, which resulted in greater statistical power than previous studies.

There are disadvantages of studying the ALSPAC and UK Biobank cohorts. Due to the inclusion criteria of ALSPAC imaging sub-studies, males were over-represented, and a minority of participants reported psychotic experiences which might have represented incipient psychiatric disorders. However, sex was included as a co-variate in the analysis, and the number of participants reporting experiences which may have met criteria for a neuropsychiatric disorder was very small. In both ALSPAC and UK Biobank analyses have shown participants to be generally healthier and from higher socio-economic backgrounds (Abigail Fraser *et al.*, 2013; Fry *et al.*, 2017). This may affect the generalisability of the results.

Although we attempted to dissect the PRS signal into disease pathway groups (see Table 4.2 in Chapter 4), as PRS inherently pools risk variants, it remains difficult to draw firm conclusions regarding the exact molecular mechanisms underpinning the observed differences in brain structure. It is also difficult to interpret the biological or functional significance of changes seen in the younger cohort. Neurofibrillary tangles have been found in subcortical regions in young adults (Braak and Del Tredici, 2011), and according to the Braak staging model, areas of cortex such as the entorhinal region can be affected even earlier by this process (Braak and Braak, 1991). Amyloid deposition has been reported in young carriers of autosomal dominant AD genes (Fleisher *et al.*, 2012) and in trisomy 21 (Braak and Del Tredici, 2011), however the ALSPAC sample was probably not old enough to show detectable amyloid burden.

Further studies will be required to confirm these findings and assess their biological significance. Longitudinal studies will be necessary to determine the effects of genetic burden for AD across the life course. Combining advanced MRI techniques with CSF and neuroradiology biomarkers can advance our understanding of how early changes in brain structure relate to subsequent biomarker derangement. However, future pathway-based analyses will need large samples and ways to address the problem of multiple comparisons.

### **5.5.2 Conclusion**

This Chapter explores the associations between polygenic risk scores for disease pathways implicated in AD, subcortical volumes, cortical thickness and cortical surface area. Increased genetic burden across pathway groups was associated with increased subcortical volume in the younger group, and decreased subcortical volumes in the older cohort, particularly in the left hemisphere. Increased pathway specific polygenic risk was also associated with cortical thinning in younger and older cohorts. Although there was no evidence of distinct patterns of changes associated with each disease pathway, the pathway specific scores showed greater evidence of association with grey matter phenotypes than the genome-wide score, suggesting that this may be a helpful way to reduce noise inherent within polygenic scores. Chapter 6 will explore associations between polygenic risk for AD and white matter microstructure assessed using diffusion MRI.

## CHAPTER 6: ALZHEIMER'S POLYGENIC RISK SCORES & WHITE MATTER MICROSTRUCTURE

*The chapter includes some material that was previously published as an abstract Harrison J, Caseras X, Foley S, Baker E, Williams J, Linden D, Holmans P, Escott-Price V, Jones D. Pathway-specific polygenic scores for Alzheimer's disease are associated with multi-modal structural brain imaging markers in young adults. Proceedings of the 28th ISMRM Annual Scientific Meeting & Exhibition, 2020 August.*

*Dr Xavier Caseras, Ms Sonya Foley and Dr Matthew Bracher-Smith assisted with the initial curation of imaging data, pre-processing and quality control, as this dataset was also used for other projects. Dr Emily Baker provided the lists of SNPs in the Kunkle et al 2019 disease pathways and calculated the polygenic scores in the UK Biobank data, as they were used for separate analyses. Dr Katherine Tansey assisted with genotyping quality control in ALSPAC.*

*Some information from previous chapters is repeated here for convenience, particularly background from Chapter 3 and some methods descriptions from Chapter 5.*

### 6.1 Summary

Diffusion MRI (dMRI) allows the investigation of tissue microstructure. Extensive changes have been identified in AD, particularly in the frontal and temporal lobes, cingulum, corpus callosum, superior longitudinal fasciculi and uncinate fasciculi. Longitudinal studies report increasing diffusivity and decreasing anisotropy in parallel with increasing cognitive impairment and worsening grey matter atrophy. White matter microstructural changes are also evident in AD prodromes, such as Mild Cognitive Impairment (MCI). Changes in areas such as the parahippocampal cingulum and the fornix have been suggested as early AD biomarkers. Increasing diffusivity and decreasing anisotropy are evident in pre-symptomatic carriers of autosomal dominant AD genes and in healthy carriers of the AD risk gene *APOE4*. One previous study

found that increased polygenic risk for AD was associated with decreased anisotropy in the cingulum in a cohort of young adults.

Pathway analyses of data from genome-wide association studies (GWAS) have implicated various physiological processes in AD pathogenesis. Few studies have investigated neuroimaging phenotypes using pathway specific polygenic profiles. Those that have used only Bonferroni significant SNPs in their PRS, and only explored grey matter changes.

This study aimed to investigate white matter microstructure in healthy adults and AD polygenic risk, using genome-wide and AD pathway specific polygenic scores, a novel analysis. Data from two population cohorts were used: the Avon Longitudinal Study of Parents and Children (ALSPAC) and UK Biobank, with respective samples of over 500 young adults and over 18,000 mature adults. PRS were computed in PLINK using summary statistics from the largest GWAS of AD to date. Pathway-specific polygenic scores were generated using lists of SNPs from a recent pathway analysis. In ALSPAC, dMRI data were analysed using ExploreDTI and whole-brain tractography was implemented using the damped Richardson Lucy pipeline. In UK Biobank, a skeleton-based analysis was conducted, with distinct regions of interest (ROIs) defined from the Johns Hopkins University tract atlas. Relationships between imaging phenotypes, genome-wide and pathway specific PRS were assessed with linear regression.

Increasing PRS was associated with increased diffusivity and decreased anisotropy in the older adult cohort. The strongest associations were between the pathway specific PRS and increased mean diffusivity (MD) in the parahippocampal cingulum and cingulate gyrus. There were also significant negative correlations between the pathway specific PRS and fractional anisotropy (FA) in the parahippocampal cingulum. We saw no association with diffusion metrics in the fornix in the UK Biobank cohort using a p value threshold ( $P^T$ ) of 0.001, although there was some evidence of association on secondary analysis with more liberal  $P^T$ . The results were maintained when APOE was removed from the PRS, and APOE SNPs alone were slightly less strongly associated with the same phenotypes. The genome-wide PRS showed less evidence of association than the pathway specific PRS, with no significant results

withstanding correction for multiple comparisons. In the younger cohort there were no statistically significant findings. Whilst there was some evidence of association between increased PRS and increased MD in the younger cohort, particularly in the left cingulum, the results were no longer significant after correction for multiple comparisons. Further longitudinal studies, using multimodal imaging and biomarker techniques, as well as functional genomic studies of individual variants will be needed to understand the biological significance of these findings.

## **6.2 Introduction**

Diffusion MRI (dMRI) is an imaging technique that uses the movement of water molecules to infer the microstructural configuration of tissue (Jones, 2011; Winston, 2012). Chapter 3 discussed dMRI methodology in detail. To summarise, dMRI measures represent how easily water molecules can diffuse within and around tissues. Structures, such as cell bodies or axons, limit diffusion (Stejskal and Tanner, 1965; Bihan, 1995; Strijkers, Drost and Nicolay, 2011; Johansen-Berg and Behrens, 2013). In white matter tracts, several microstructural characteristics affect the rate of diffusion, including the density, diameter and myelination of axons (Jones, 2011). In large, coherently aligned and densely packed fibre bundles, diffusion is anisotropic. As mentioned in previous Chapters, this is commonly indexed by FA (Basser and Pierpaoli, 1996). An FA of 0 represents isotropic diffusion, in which rates of diffusion are the same in all directions. FA of 1 represents anisotropic diffusion, where diffusion is limited to one axis (Beaulieu and Allen, 1994; Pierpaoli and Basser, 1996; Beaulieu, 2009; Winston, 2012). Changes in anisotropy are often interpreted as a measure of tissue integrity (Thomason and Thompson, 2011), but as explained in Chapter 3, this should be treated with caution (Jones, Knösche and Turner, 2013). MD is another commonly reported metric. MD denotes the orientationally-averaged rate of diffusion. Detailed descriptions of dMRI techniques and associated pitfalls are in Chapter 3.

The advent of dMRI has allowed the investigation of white matter microstructure in AD. Extensive changes have been identified. For example, Sexton et al conducted a meta-analysis of 41 studies comparing AD cases to controls. They observed reduced FA and increased MD in AD patients, particularly in the frontal and temporal lobes,

posterior cingulum, corpus callosum, superior longitudinal fasciculi and uncinate fasciculi (Sexton *et al.*, 2011). Patients with MCI also had lower FA in all white matter areas except parietal and occipital regions, and higher MD except in occipital and frontal regions (Sexton *et al.*, 2011).

Diffusivity changes in some regions have been proposed as early biomarkers of AD. There is some evidence that AD pathology preferentially affects late-myelinating tracts (Benitez *et al.*, 2014), as discussed in Chapter 3. The parahippocampal cingulum (Mayo *et al.*, 2017), and the fornix (Ringman *et al.*, 2007; Perea *et al.*, 2018) are both suggested to be preferentially degraded in AD. As with conventional markers of atrophy, longitudinal studies report that increased diffusivity and decreased anisotropy are more evident with increasing cognitive impairment (Mayo *et al.*, 2017). dMRI metrics in the fornix are associated with cognitive decline (Fletcher *et al.*, 2013). They can distinguish MCI from AD (Egli *et al.*, 2015; Tang *et al.*, 2017), and can predict conversion from healthy cognition to MCI and from MCI to AD (Mielke *et al.*, 2012; Oishi *et al.*, 2012). Subtle fornix changes may even precede hippocampal atrophy (Zhuang *et al.*, 2012).

As described in Chapter 3, the effect of AD genetic risks on white matter microstructure has been widely investigated (Harrison *et al.*, 2020). Most previous studies compared *APOE* E4 carriers (homozygotes and heterozygotes) with those without an E4 allele, although some were able to assess the effect of *APOE* gene dosage (Lyll *et al.*, 2014), but the findings are discrepant. Although most studies reported some significant changes in diffusion metrics in *APOE*4 carriers, five studies reported no significant differences (Honea *et al.*, 2009; Bendlin *et al.*, 2012; Nyberg and Salami, 2014; Dell'Acqua *et al.*, 2015; R. Wang *et al.*, 2015). Of the positive results, reduced FA was commonly reported, often with increased MD, RD or LD. Please see the Table 3.1 in Chapter 3 for a breakdown of the white matter regions implicated in *APOE* studies.

How autosomal dominant AD risk manifests in the white matter microstructure of pre-symptomatic individuals is less widely studied. As discussed in Chapter 3, sample sizes are modest, reflecting the rarity of these genes. Three studies have addressed this in *PS1* carriers (Ryan *et al.*, 2013; Parra *et al.*, 2015; Sanchez-Valle *et al.*, 2016)

and three in mixed cohorts of *PS1/2* and *APP* carriers (Ringman *et al.*, 2007; X. Li *et al.*, 2015; Caballero *et al.*, 2018). Whilst there were widespread changes in symptomatic carriers, only one study identified significant changes in pre-symptomatic *PS1* carriers: reduced MD and LD in the right cingulum (Ryan *et al.*, 2013). Two studies with mixed cohorts of *PS1* or *APP* carriers reported a number of changes in pre-symptomatic carriers: reduced FA in the fornix and frontal white matter (Ringman *et al.* 2007); increased MD in the left inferior longitudinal fasciculus, left forceps major, left cingulum and bilateral superior longitudinal fasciculus (X Li *et al.*, 2015). A further study of *PS1/2* and *APP* carriers found increased MD in the forceps minor, forceps major and long projecting fibres 5-10 years before cognitive problems were anticipated (Caballero *et al.*, 2018). Please see Table 3.2 in Chapter 3 for a summary of dMRI studies in autosomal dominant AD.

Few studies have been able to assess the effect of AD risk loci with small effect sizes identified through GWAS. Braskie *et al.* observed that each C allele copy of the *CLU* allele was associated with lower FA in the splenium of the corpus callosum, the fornix, cingulum, and superior and inferior longitudinal fasciculi in healthy young adults (Braskie *et al.*, 2011). Shorter genotypes of the poly-T repeat in TOMM40 are associated with FA in the cingulum, irrespective of *APOE* genotype (Lyll *et al.*, 2014).

As described in Chapter 2, GWAS risk variants can be combined in polygenic risk score (PRS), the weighted sum of the risk loci from GWAS, computed for each individual in a dataset (Wray *et al.*, 2014). Only one previous study explored associations between PRS and white matter phenotypes. Foley *et al.* studied healthy young adults (aged approximately 24 years, dMRI data  $n = 197$ ). They used a threshold-based genome-wide PRS using the International Genomics of Alzheimer's Project GWAS (Lambert *et al.*, 2013) as training data. They identified an association between increased AD PRS and decreased FA in the right cingulum (Foley *et al.*, 2016).

### 6.2.1 Rationale and Aims

dMRI studies in humans have demonstrated that changes in white matter microstructure are evident in AD neurodegeneration and are associated with cognitive impairment. Chapter 3 systematically reviewed the literature and found evidence of significant associations between AD genetic risk and diffusivity in white matter tracts, specifically, lower anisotropy and increased diffusivity, and provides evidence of the effect of AD risk genes on white matter microstructure in healthy, pre-clinical individuals.

Chapter 2 found evidence that AD PRS can predict AD case/control status. It also described the evidence that AD PRS are associated with neurodegeneration phenotypes such as cognition and biomarkers. As discussed in Chapters 1 and 2, loci identified by GWAS are enriched for SNPs involved in certain biological pathways including lipid metabolism, immune response, and synaptic processes (Jones *et al.*, 2010; Holmans and Jones, 2012; Kunkle *et al.*, 2019). As discussed in previous Chapters, polygenic scores can be informed by these pathway analyses, to allow genetic burden associated with disease pathway groups to be delineated. Each of these disease pathway groups explains only a small amount of the variance (Darst *et al.*, 2017), consequently large discovery and target sample sizes are necessary (Dudbridge, 2013).

Few studies have applied this pathway specific PRS technique to neuroimaging data (Ahmad *et al.*, 2018; Corlier *et al.*, 2018; Caspers *et al.*, 2020). These previous studies only explored grey matter, and included only Bonferroni significant SNPs in their PRS, excluding loci of smaller effect sizes that may be involved in the disease.

In Chapter 5, it was demonstrated that AD pathway specific PRS are associated with decreased volume in subcortical structures and cortical thinning in cognitively healthy participants. The primary aim of this chapter is to explore associations between disease pathway specific PRS and white matter microstructure in areas preferentially affected by AD pathology. This will be achieved using the same large population cohorts of younger and older adults. A secondary objective is to apply a range of

different p value thresholds, used to select relevant SNPs for the polygenic analysis, to assess which explains the most variance in the phenotype.

## **6.2.2 Hypothesis**

It is hypothesised that increasing genetic burden for AD, indexed by PRS, will be associated with i) decreasing anisotropy (measured with FA) in the fornix, cingulum and hippocampal cingulum, in tandem with ii) increasing diffusivity (measured with MD) in the same regions. It is further hypothesised that PRS for different disease pathway groups will show distinct patterns of changes in white matter microstructure.

## **6.3 Methods**

### **6.3.1 Participants**

As described in Chapters 4 and 5, participants were recruited by the Avon Longitudinal Study of Parents and Children (ALSPAC) and UK Biobank. Chapter 4 contains a detailed description of recruitment methods and sample characteristics which are summarised here for convenience.

This experiment uses data from two population neuroimaging studies conducted by ALSPAC (Sharp *et al.*, 2020). As discussed in Chapter 4 and Chapter 5, the first investigated the effect of testosterone on the structure of the brain (ALSPAC project ID B648; n = 513) (Björnholm *et al.*, 2017). The second explored psychotic experiences and brain structure (ALSPAC project ID B709, n = 152) (Drakesmith *et al.*, 2016). Ethical approval for the neuroimaging sub-studies was given by the ALSPAC Ethics and Law Committee and Local Research Ethics Committees (North Somerset and South Bristol Research Ethics Committee: 08/H0106/96) and participants provided written informed consent. Chapter 4 includes details of the inclusion criteria for the sub-studies.

As described in Chapters 4 and 5, the first 20,000 datasets released by UK Biobank are analysed here (Sudlow *et al.*, 2015). UK Biobank granted approval for the analyses reported in this thesis (UK Biobank Application 15175). UK Biobank obtained approval

from a number of external bodies (UK Biobank, 2007) and participants gave informed consent. As discussed in Chapter 5, this study excluded UK Biobank participants if they self-reported a history of neurological or major psychiatric disorders, such as dementia, cerebrovascular disease, intellectual disability, at an assessment visit or during online follow-up, or had a hospital admission ICD-10 code for a relevant disorder. Further participants were removed from ALSPAC and UK Biobank if they had non-white British or Irish ancestry or if they had asked to have their data removed from the cohorts. Data was retained if it successfully reconstructed and passed quality control.

After genotyping and imaging data quality control procedures, 517 individuals with dMRI and structural T1-weighted data remained (19.3% female, 80.7% male) in ALSPAC and 18172 in UK Biobank (52.7% female, 47.3% male). At the time of inclusion, the average ages of ALSPAC and UK Biobank participants were 19.81 years (SD 0.02) and 64.2 (SD 7.75) respectively.

### **6.3.2 MRI Acquisition**

As described in Chapter 5, neuroimaging data were acquired for ALSPAC at Cardiff University Brain Research Imaging Centre (CUBRIC). A 3 Tesla General Electric HDx (GE Medical Systems) scanner was used with an 8 channel head coil. Acquisition parameters were harmonised between ALSPAC sub-studies as far as practicable.

dMRI data were acquired with a dual spin-echo (SE), single shot echo-planar imaging (EPI) sequence. 30 gradient orientations and 3 non-diffusion weighted images were obtained using the following parameters: isotropic resolution = 2.4mm x 2.4mm x 2.4mm; FOV = 230mm x 230mm; acquisition matrix = 96 x 96; slice thickness = 2.4mm; 60 oblique-axial AC-PC slices; TR/TE = cardiac gated/87ms; b = 0, 1200 s/mm<sup>2</sup>, T1 = 0; flip angle = 90°; number of excitations (NEX) = 1; acquisition time approximately 15-20 minutes.

For UK Biobank, as discussed in Chapter 5, data was gathered at three recruitment centres in Stockport, Newcastle and Reading using identical Siemens Skyra 3T scanners with a standard Siemens 32 channel head coil. Multi-shell dMRI data was

acquired using a monopolar Stejskal-Tanner pulse sequence with SE-EPI. 50 diffusion-encoding directions were acquired with the following parameters: resolution: 2 mm x 2mm x 2mm; FOV: 104mm x 104mm x 72mm matrix; 5 x b = 0 s/mm<sup>2</sup> (plus 3 x b = 0 s/mm<sup>2</sup> blip-reversed), 50 x b=1000 s/mm<sup>2</sup>, 50 x b=2000 s/mm<sup>2</sup>; gradient timings  $\delta = 21.4\text{ms}$ ,  $\Delta = 45.5\text{ms}$ ; echo time (TE) = 92ms. Acquisition time approximately 7-8 minutes (Alfaro-Almagro *et al.*, 2018).

### 6.3.3 Analysis Pipeline

For ALSPAC, neuroimaging data was analysed in-house using ROI-based probabilistic tractography in ExploreDTI (Leemans *et al.*, 2009) version 4.8.6. Eddy current distortions and subject motion were corrected with affine registration to T1-weighted images, with reorienting of the encoding vectors (Leemans and Jones, 2009). An echo planar imaging (EPI) correction was used to warp the dMRI data to the fast, spoiled gradient recalled images (Wu *et al.*, 2008). This produced an output with a resolution of 1 × 1 × 1 mm<sup>3</sup>. Corrections were run, including: RESTORE (Chang, Jones and Pierpaoli, 2005) and RESDORE (Parker *et al.*, 2013), aiming to reduce the influence of outliers on the eventual model estimates; and free water corrections (Pasternak *et al.*, 2009), aiming to separate the diffusion properties of brain tissue from surrounding free water.

Whole-brain tractography was implemented using the damped Richardson Lucy pipeline (Dell'Acqua *et al.*, 2010). Streamline termination criteria were: a decline in the magnitude of minimally subtending fibre orientation density function peak amplitude (below 0.05); fractional anisotropy < 0.2; or an angle threshold greater than 45°. In-house automated tractography software was used to obtain tracts (Parker *et al.*, 2013b). Automated tractography models for the cingulum, parahippocampal cingulum and fornix were based on manual tractography. Anatomical regions of interest (ROIs) were placed to determine which streamlines are included in the analysis. These are based on Boolean logical operations, e.g. selecting fibres that traverse ROI-1 AND ROI-2 but NOT ROI-3. Therefore, inclusive ROIs, that a tract must pass through to be included, are known as 'AND' gates, and exclusive ROIs, that a tract must not pass through, are 'NOT' gates (Conturo *et al.*, 1999; Jones *et al.*, 2013). Tracts are segmented in the native space of the individual, providing a representation of tract

anatomy for each person (Bastin *et al.*, 2013). Automated tracts were quality controlled by visual inspection. Where tracts had not successfully reconstructed, they were excluded.

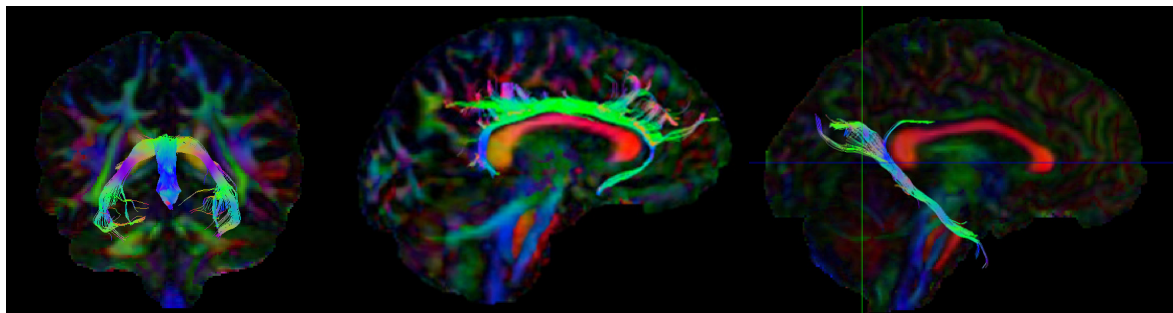
The fornix was segmented as described by Metzler-Baddeley and colleagues (Metzler-Baddeley *et al.*, 2011). AND ROIs were placed on a coronal slice on the fornix at point where the fornix anterior pillars enter the body, and on an axial slice at the level of the lower border of the splenium. NOT gates aimed to exclude streamlines in the corpus callosum and corticospinal tract. The fornix can be difficult to reconstruct because it runs in close to other white matter tracts, such as the anterior commissure, and may be especially susceptible to signal contamination from the cerebrospinal fluid (CSF) in the ventricles nearby (Concha, Gross and Beaulieu, 2005; Jones and Cercignani, 2010). The fornix was not always successfully reconstructed by the automated models used in the present study, with a relatively high number failing quality control ( $n = 18$ ). The cingulum was segmented using the standard method outlined by Jones and colleagues (Jones *et al.*, 2013), with two AND gates placed above the body of the corpus callosum, around 18 millimetres apart in the rostral–caudal plane. The parahippocampal cingulum was segmented using the ‘restricted’ method. Two AND gates placed just behind and below the splenium, and a NOT gate was placed above the body of the corpus callosum to exclude tracts projecting forward into the frontal cortex (Jones *et al.*, 2013). Examples of the segmented tracts are shown in Figure 6.1. Diffusion metrics were extracted with custom MATLAB scripts (The MathWorks, Inc., Natick, MA).

UK Biobank undertook pre-processing and dMRI analysis using automated pipelines (Smith, Alfaro-Almagro and Miller, 2015; Alfaro-Almagro *et al.*, 2018). First, the data were corrected for head motion and eddy currents and had outlier-slices corrected with the FSL Eddy tool <http://fsl.fmrib.ox.ac.uk/fsl/fslwiki/EDDY> (Andersson and Sotiropoulos, 2015, 2016). Gradient distortion correction was implemented to produce a 4D output file. Subsequently, the dMRI FA image was processed using TBSS (Tract-Based Spatial Statistics (Smith *et al.*, 2006). TBSS uses a non-linear registration to a template using the FMRIB's non-linear image registration tool (FNIRT), followed by projection on to a tract representation of mean FA, known as the white matter skeleton. High-dimensional warping based on the Oxford Centre for Functional MRI of the Brain

(FMRIB) linear image registration tool (FNIRT) (De Groot *et al.*, 2013) was used to improve alignment. The Johns Hopkins University standard-space tract masks were overlaid on skeleton-projected data (Mori *et al.*, 2005; Wakana *et al.*, 2007). UK Biobank provided these imaging derived phenotypes (IDPs) for distinct ROIs defined from Johns Hopkins University tract atlas. IDPs for FA and MD in the cingulum, the parahippocampal cingulum and the fornix were downloaded from UK Biobank. IDPs received from UK Biobank were checked and cleaned.

For each region of interest, the final numbers included in the ALSPAC analysis were: the fornix (n = 499), parahippocampal cingulum right and left (n = 517), the cingulum right and left (n = 516). For UK Biobank, the final numbers were: the fornix and left and right cingulum (n = 16529), the parahippocampal cingulum right and left (n = 16527). Metrics were curated and stored in files compatible with R.

**Figure 6.1 Showing the dMRI regions of interest defined for ALSPAC. Left image: the fornix; Centre image: the cingulum; Right image: the parahippocampal cingulum.**



#### 6.3.4 Genotyping

The genotyping procedures in ALSPAC and UK Biobank are described in detail in Chapter 4 and were summarised in Chapter 5. Briefly, ALSPAC genotyped participants with the Illumina HumanHap550 quad genome-wide SNP genotyping platform (Illumina Inc., San Diego, California, USA). UK Biobank used the Affymetrix UK BiLEVE Axiom array for the first 500 participants followed by the Affymetrix UK Biobank Axiom array. Quality control was undertaken in PLINK (Purcell *et al.*, 2007).

As described in Chapter 4, participants were excluded for the following reasons: i) ambiguous sex; ii) cryptic relatedness; iii) < 97% genotyping completeness; and iv) non-British or Irish ancestry in ALSPAC and i) < 97% genotyping completeness and ii) non-British or Irish ancestry in UK Biobank. For both datasets, SNPs were filtered by: i) minor allele frequency (MAF) < 1%; ii) SNP call rate < 98%; iii)  $\chi^2$  test for Hardy-Weinberg equilibrium  $p < 1 \times 10^{-4}$ .

### 6.3.5 Polygenic Score (PRS) Calculations

PRS computation was performed using the International Schizophrenia Consortium procedure (Purcell *et al.*, 2009). Please see Chapter 4 for a detailed description. To summarise, the discovery sample was the Genome-wide Association Study (GWAS) conducted by Kunkle *et al.* (Kunkle *et al.*, 2019). SNPs with a low MAF (< .01) were excluded. The data were pruned for linkage disequilibrium using clumping (--clump) in PLINK (Purcell *et al.*, 2007) (parameters:  $r^2 > 0.2$  (--clump-r2) and 500 kilobase (--clump-kb)). PRS were calculated using PLINK --score (Purcell *et al.*, 2007). The primary analysis used a p value threshold ( $P^T$ ) of 0.001 to select relevant SNPs as a previous study (Foley *et al.*, 2016) found that this explained the most variance in structural neuroimaging phenotypes. Seven progressive thresholds were applied for the secondary analysis ( $p = 0.5, 0.3, 0.1, 0.01, 0.0001, 0.00001, 0.000001$ ). Lists of SNPs in disease pathways implicated by Kunkle and colleagues were used to compute pathway specific PRS (Kunkle *et al.*, 2019). Please see Chapter 4 for further information on the polygenic score calculations and disease pathways.

### 6.3.6 Statistical Analysis

As with the analyses presented in Chapter 5, statistical analyses were conducted using R Studio version 1.1.383 for Mac, [www.rstudio.com](http://www.rstudio.com) (R Development Core Team 3.0.1., 2013). The relationships between dMRI phenotypes and PRS were tested using linear multiple regression. Analyses were performed on the overall genome-wide AD PRS and the pathway-specific PRS separately. The analysis was repeated using a polygenic risk score which excluded the *APOE* region SNPs (chromosome 19 between 44.4Mb and 46.5Mb), thereby assessing the extent that the *APOE* region

explained the signal. As described in Chapter 4 and Chapter 5, the resulting p values were corrected for multiple comparisons of phenotype and PRS using the False Discovery Rate (FDR) in the R (R Development Core Team 3.0.1., 2013). SNPs in the *APOE* region (chromosome 19 between 44.4Mb and 46.5Mb) were also analysed separately so the variance explained by the PRS could be compared to the *APOE* region. Regression analyses adjusted for population structure using 10 principal components for ALSPAC and 15 for UK Biobank as covariates. Additional covariates were gender and intracranial volume in ALSPAC and gender, intracranial volume, age, scanning site and genotyping array in UK Biobank. Although dMRI studies often do not correct for the volume of the cranium, some studies have shown an effect of intracranial volume on FA and MD (Takao *et al.*, 2011) and therefore it was included as a covariate.

## 6.4 Results

P values reported correspond only to the PRS variable in the regression model. The primary analysis, reported below, used a  $P^T$  of 0.001.

### 6.4.1 Fornix dMRI metrics

In the ALSPAC cohort, there were no statistically significant associations between any PRS and either FA or MD in the fornix. There were some apparent trends towards association. For example, the protein lipid complex PRS (excluding the *APOE* region) was nominally associated with lower FA in the fornix ( $p = 0.049$ ,  $R^2 = 6.36 \times 10^{-3}$ ). However, the genome-wide PRS (excluding the *APOE* region) was also nominally associated with increased FA in the fornix ( $p = 0.021$ ,  $R^2 = 8.73 \times 10^{-3}$ ). There were no associations between any PRS and fornix MD.

In UK Biobank, there were also no significant associations between FA or MD in the fornix. However, the genome-wide PRS, immune response PRS and the *APOE* region SNPs showed trends towards decreased FA and increased MD in the fornix at  $P^T = 0.001$ , however these were not significant ( $R^2 < 1.2-1.5 \times 10^{-4}$ ,  $p > 0.05$ ). There were no significant associations with the pathway specific PRS for protein–lipid complex assembly, regulation of A $\beta$  formation, protein–lipid complex, regulation of amyloid

precursor protein catabolic process, tau protein binding, reverse cholesterol transport, protein–lipid complex subunit organization or plasma lipoprotein particle assembly ( $R^2 < 1.5 \times 10^{-5}$ ,  $p > 0.05$ ).

Secondary analysis of UK Biobank results at more liberal  $P^T$  showed nominally significant associations between the genome-wide PRS and decreased FA ( $p = 0.03$ - $0.04$  at  $P^T 0.05$ - $0.5$ ) and increased MD in the fornix ( $p = 0.007$ - $0.02$  at  $P^T 0.01$ - $0.5$ ), although these attenuated slightly when the *APOE* region was removed from the PRS. There were also nominal associations between the immune response PRS and decreased FA ( $p = 0.03$  at  $P^T 0.05$ ;  $p = 0.02$  & at  $P^T 0.5$ ) and increased MD ( $p = 0.03$  at  $P^T 0.05$ ;  $p = 0.01$  at  $P^T 0.5$ ), however these were no longer significant when *APOE* was excluded. SNPs in the *APOE* region also showed a nominally significant association with increased MD in the fornix at two more liberal thresholds ( $p = 0.045$  at  $P^T 0.05$ ;  $p = 0.04$  at  $P^T 0.01$ ).

#### **6.4.2 Cingulum dMRI metrics**

In ALSPAC, there were trends toward association with increased MD in the left cingulum for the regulation of  $A\beta$  formation PRS, the regulation of amyloid precursor protein catabolic process and the protein–lipid complex subunit organization PRS ( $p = 0.042$ - $0.043$ ,  $R^2 = 7.84$ - $7.94 \times 10^{-3}$ ) although these did not withstand correction for multiple comparisons and were not maintained when the *APOE* region was excluded.

Secondary analysis in ALSPAC of other  $P^T$  showed further trends of association between increased MD and lower FA in the right and left cingulum with more liberal  $P^T$ . This pattern was particularly evident with the tau protein binding PRS without *APOE* (see Figure 6.3), although these associations would not have survived correction for multiple testing ( $p$  values  $1.4$ - $3.9 \times 10^{-2}$ ).

In UK Biobank, neither the genome-wide PRS, pathway specific PRS or the *APOE* region SNPs showed evidence of association with reduced FA in the cingulum (right or left,  $R^2 < 2.1 \times 10^{-5}$ ,  $p > 0.05$ ). Secondary analysis at more liberal  $P^T$  did not reveal any associations with FA.

The genome-wide PRS was positively associated with MD in the left cingulum ( $R^2 = 2.48 \times 10^{-4}$ ,  $p = 0.03$ ) but not the right ( $R^2 = 1.36 \times 10^{-4}$ ,  $p = 0.12$ ). However, the result for the left cingulum did not survive correction for multiple testing. The pathway specific PRS for protein–lipid complex assembly, regulation of A $\beta$  formation, protein–lipid complex, regulation of amyloid precursor protein catabolic process, tau protein binding, reverse cholesterol transport, protein–lipid complex subunit organization and plasma lipoprotein particle assembly were all significantly positively associated with MD in the right and the left cingulum ( $R^2$  range  $7.3 - 8.2 \times 10^{-4}$ ,  $p$  range  $1.6 - 3.9 \times 10^{-4}$ ). These results survived multiple testing correction and were maintained when the *APOE* region was removed from the score. Activation of immune response did not show evidence of association with MD in either the right or left cingulum ( $R^2 < 1.3 \times 10^{-4}$ ,  $p > 0.05$ ). SNPs in the *APOE* region were also significantly positively associated with MD in the right ( $R^2 = 4.9 \times 10^{-4}$ ,  $p = 0.004$ ) and left ( $R^2 = 7.1 \times 10^{-4}$ ,  $p = 0.001$ ) cingulum.

#### 6.4.3 Parahippocampal dMRI metrics

There were no statistically significant associations between any PRS and parahippocampal FA or MD in ALSPAC. The only nominally significant association was with the protein-lipid subunit organisation PRS (excluding the *APOE* region) and higher FA in the parahippocampal cingulum ( $R^2 = 8.53 \times 10^{-3}$ ,  $p = 0.03$ ), however there was no corresponding change in MD ( $R^2 = 5.69 \times 10^{-4}$ ,  $p = 0.24$ ).

In UK Biobank, the genome-wide PRS was negatively associated with FA in the right parahippocampal cingulum ( $R^2 = 3.4 \times 10^{-4}$ ,  $p = 0.01$ ) but not the left ( $R^2 = 1.2 \times 10^{-4}$ ,  $p = 0.14$ ). However, the result for the right parahippocampal cingulum did not survive correction for multiple testing. The pathway specific PRS for protein–lipid complex assembly, regulation of A $\beta$  formation, protein–lipid complex, regulation of amyloid precursor protein catabolic process, tau protein binding, reverse cholesterol transport, protein–lipid complex subunit organization and plasma lipoprotein particle assembly were all significantly negatively associated with FA in the right and the left parahippocampal cingulum ( $R^2$  range  $5.8 - 9.4 \times 10^{-4}$ ,  $p$  range  $1.0 \times 10^{-3} - 3.9 \times 10^{-5}$ ). These results withstood correction for multiple testing and remained significant when

the *APOE* region was excluded from the PRS. Activation of immune response PRS did not show evidence of association with FA in either the right or left parahippocampal cingulum ( $R^2 < 1.3 \times 10^{-5}$ ,  $p > 0.05$ ). SNPs in the *APOE* region were significantly negatively associated with FA in the right ( $R^2 = 6.7 \times 10^{-4}$ ,  $p = 0.001$ ) and left ( $R^2 = 5.0 \times 10^{-4}$ ,  $p = 0.003$ ) parahippocampal cingulum.

There was no association between the genome-wide PRS and MD in the right or left hippocampal cingulum ( $R^2 < 7.2 \times 10^{-6}$ ,  $p > 0.05$ ). The pathway specific PRS were significantly positively correlated with hippocampal cingulum MD ( $R^2$  range  $5.8 - 9.4 \times 10^{-4}$ ,  $p$  range  $1.0 \times 10^{-3} - 3.9 \times 10^{-5}$ ). SNPs in the *APOE* region only showed trends towards association with increased MD in the left parahippocampal cingulum ( $R^2 = 2.1 \times 10^{-4}$ ,  $p = 0.06$ ). In the right parahippocampal cingulum, the *APOE* region were only nominally associated with increased MD ( $R^2 = 2.9 \times 10^{-4}$ ,  $p = 0.049$ ).

For ALSPAC, results for all regions of interest are summarised in Tables 6.1 - 6.4 and Figures 6.2 – 6.4. For UK Biobank, results are summarised in Tables 6.5 – 6.8 and Figures 6.5 – 6.7. Those surviving FDR correction for multiple comparisons of PRS and phenotype are indicated on the tables.

**Figure 6.2** ALSPAC Genome-wide PRS and dMRI metrics, showing no significant results. Imaging phenotypes are shown on the X axis, the beta coefficients (positive and negative) are shown on the Y axis. The heights of the bars indicate the amount of variance explained ( $R^2$ ), and any nominally significant results are labelled with their p value. Each bar represents a version of the polygenic risk score. The bars are colour coded by the p value threshold used in the training data, shown on the legend.

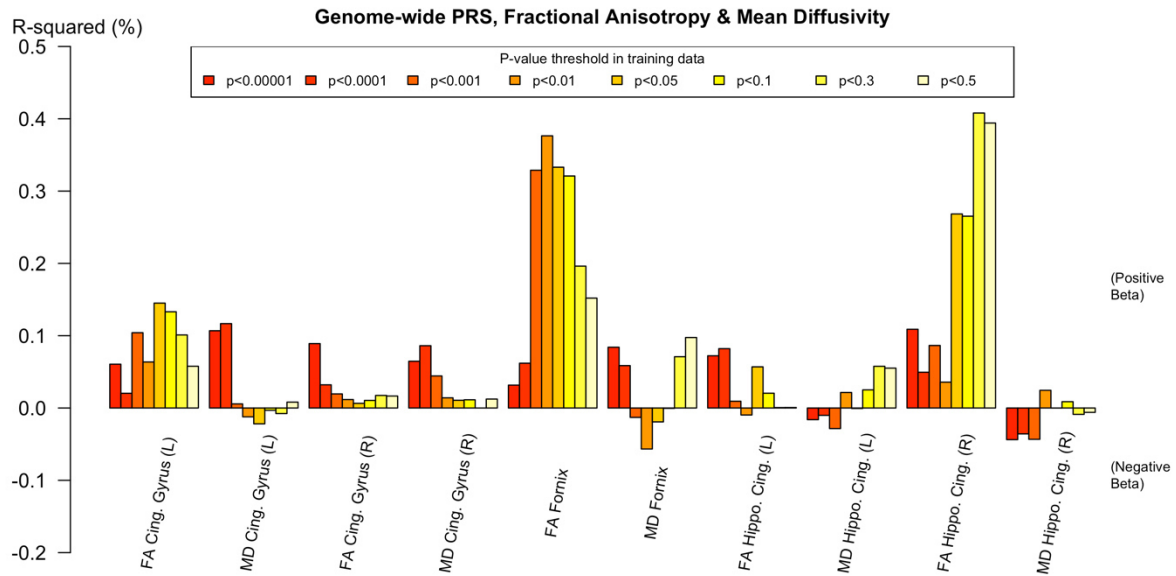


**Figure 6.3** ALSPAC tau protein binding PRS (excluding the APOE region) and diffusion metrics, showing trends towards significance in more liberal PT in the cingulum. Imaging phenotypes are shown on the X axis, the beta coefficients (positive and negative) are shown on the Y axis. The heights of the bars indicate the amount of variance explained ( $R^2$ ), and any nominally significant results are labelled with their p value. Each bar represents a version of the polygenic risk score. The bars are colour coded by the p value threshold used in the training data, shown on the legend.

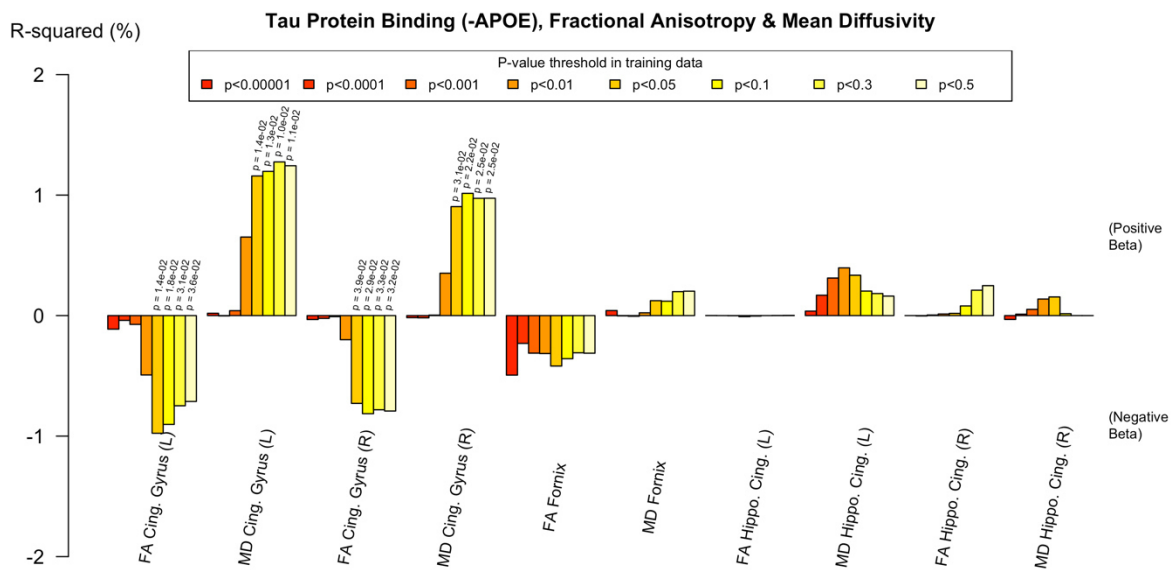


**Figure 6.4** Scatter plot showing ALSPAC non-significant association between normalised genome-wide PRS and normalised MD in the left cingulum. White circles indicate individual data points. Density represents the number of data points in each area.

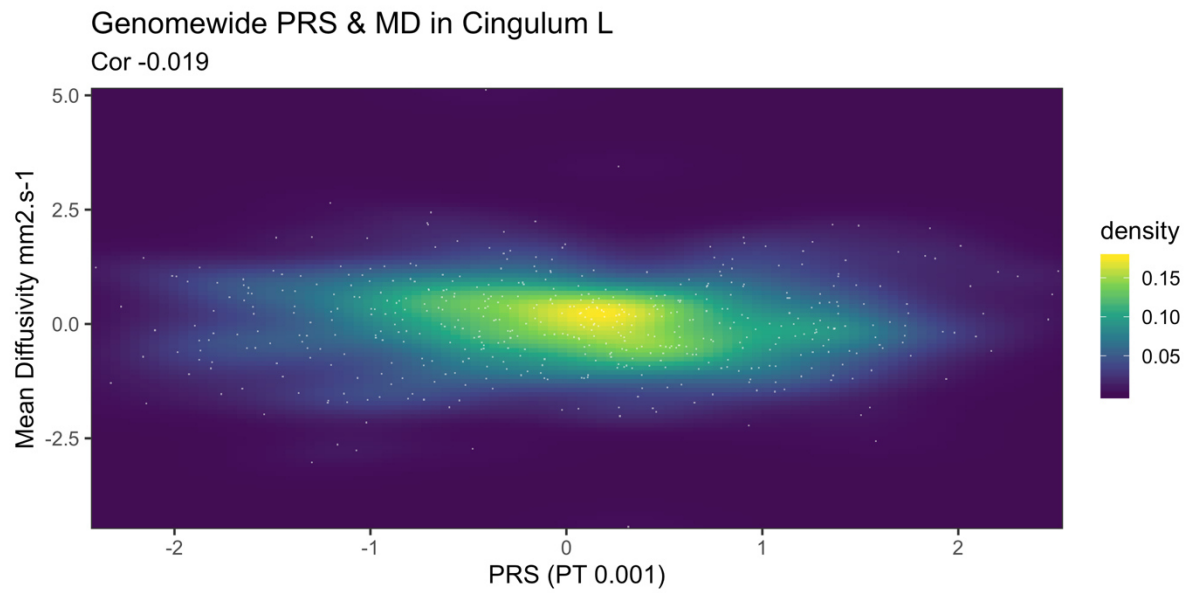


**Table 6.1 Results for ALSPAC fractional anisotropy area and PRS including APOE at  $P^T$  0.001**

	FA Cingulum Left	FA Cingulum Right	FA Parahipp. Cingulum Left	FA Parahipp. Cingulum Right	FA Fornix
	$R^2$	$R^2$	$R^2$	$R^2$	$R^2$
	p (95% CI)				
<b>Polygenic risk score</b>					
<b>Protein-lipid complex assembly</b>	4.58E-04 0.595 (-0.003,0.002)	1.12E-05 0.936 (-0.003,0.003)	3.33E-07 0.989 (-0.002,0.003)	1.66E-04 0.759 (-0.003,0.003)	2.50E-04 0.696 (-0.002,0.001)
<b>Regulation of A<math>\beta</math> formation</b>	1.17E-03 0.395 (-0.004,0.002)	1.36E-09 0.999 (-0.003,0.003)	3.36E-05 0.893 (-0.002,0.003)	3.35E-04 0.663 (-0.004,0.002)	2.76E-04 0.682 (-0.001,0.002)
<b>Protein-lipid complex</b>	3.96E-04 0.621 (-0.003,0.002)	2.48E-08 0.997 (-0.003,0.003)	1.33E-05 0.933 (-0.002,0.003)	6.59E-04 0.541 (-0.004,0.002)	1.94E-03 0.277 (-0.002,0.001)
<b>Regulation of amyloid precursor protein catabolic process</b>	1.17E-03 0.395 (-0.004,0.002)	1.36E-09 0.999 (-0.003,0.003)	3.36E-05 0.893 (-0.002,0.003)	3.35E-04 0.663 (-0.004,0.002)	2.76E-04 0.682 (-0.001,0.002)
<b>Tau protein binding</b>	4.65E-04 0.592 (-0.003,0.002)	1.73E-05 0.920 (-0.003,0.003)	8.36E-06 0.946 (-0.002,0.003)	7.36E-04 0.518 (-0.004,0.002)	1.35E-03 0.365 (-0.002,0.001)
<b>Reverse cholesterol transport</b>	8.94E-05 0.814 (-0.003,0.002)	2.59E-05 0.902 (-0.003,0.003)	1.08E-06 0.981 (-0.003,0.002)	4.57E-04 0.611 (-0.004,0.002)	9.91E-04 0.437 (-0.002,0.001)
<b>Protein-lipid complex subunit organization</b>	6.80E-04 0.523 (-0.004,0.002)	3.09E-06 0.966 (-0.003,0.003)	2.11E-05 0.915 (-0.002,0.003)	1.26E-04 0.790 (-0.003,0.003)	1.27E-04 0.781 (-0.002,0.001)
<b>Plasma lipoprotein particle assembly</b>	9.42E-04 0.445 (-0.004,0.002)	2.26E-05 0.909 (-0.003,0.003)	6.25E-05 0.854 (-0.003,0.002)	8.58E-04 0.486 (-0.004,0.002)	3.75E-04 0.633 (-0.002,0.001)
<b>Activation of immune response</b>	3.98E-04 0.620 (-0.002,0.003)	1.14E-04 0.797 (-0.002,0.003)	1.78E-03 0.326 (-0.004,0.001)	7.71E-06 0.947 (-0.003,0.003)	9.11E-04 0.457 (-0.002,0.001)
<b>Genome-wide PRS</b>	1.04E-03 0.423 (-0.002,0.004)	1.95E-04 0.736 (-0.002,0.003)	9.36E-05 0.822 (-0.002,0.003)	8.65E-04 0.484 (-0.002,0.004)	3.29E-03 0.157 (-4.25E-04,0.003)

R2 and p values for subcortical volumes in the right hemisphere and each polygenic score at a  $P^T$  of 0.001. The column names shows the region of interest, while the row names show the polygenic scores.

\* Nominally significant associations (p value < .05).

\*\* FDR corrected associations <0.05.

Acronyms: PRS = Polygenic Risk Score;  $P^T$  = polygenic threshold; APOE = Apolipoprotein E; L = left; R = right; FDR = false discovery rate; FA = fractional anisotropy; Parahipp. = parahippocampal

**Table 6.2 Results for ALSPAC fractional anisotropy area and PRS excluding APOE at P<sup>T</sup> 0.001**

Polygenic risk score	FA Cingulum Left R <sup>2</sup> p (95% CI)	FA Cingulum Right R <sup>2</sup> p (95% CI)	FA Parahipp. Cingulum Left R <sup>2</sup> p (95% CI)	FA Parahipp. Cingulum Right R <sup>2</sup> p (95% CI)	FA Fornix R <sup>2</sup> p (95% CI)
Protein-lipid complex assembly (-APOE)	2.46E-03 0.217 (-0.001,0.004)	3.49E-03 0.154 (-0.001,0.005)	1.18E-04 0.801 (-0.003,0.002)	1.93E-03 0.295 (-0.001,0.005)	8.84E-04 0.463 (-0.002,0.001)
Regulation of Aβ formation (-APOE)	1.44E-05 0.925 (-0.003,0.003)	4.98E-04 0.590 (-0.002,0.003)	3.95E-04 0.644 (-0.002,0.003)	2.35E-04 0.715 (-0.002,0.004)	4.38E-03 0.102 (-2.51E-04,0.003)
Protein-lipid complex (-APOE)	9.56E-05 0.808 (-0.003,0.002)	2.54E-04 0.701 (-0.002,0.003)	5.33E-06 0.957 (-0.002,0.003)	1.21E-04 0.794 (-0.003,0.003)	6.36E-03 0.049 (-0.003,-1.29E-05)*
Regulation of amyloid precursor protein catabolic process (-APOE)	1.44E-05 0.925 (-0.003,0.003)	4.98E-04 0.590 (-0.002,0.003)	3.95E-04 0.644 (-0.002,0.003)	2.35E-04 0.715 (-0.002,0.004)	4.38E-03 0.102 (-2.51E-04,0.003)
Tau protein binding (-APOE)	7.32E-04 0.501 (-0.004,0.002)	8.78E-05 0.821 (-0.003,0.002)	9.70E-06 0.942 (-0.003,0.002)	4.90E-05 0.868 (-0.003,0.003)	3.12E-03 0.168 (-0.003,4.62E-04)
Reverse cholesterol transport (-APOE)	2.47E-03 0.217 (-0.001,0.004)	2.24E-03 0.254 (-0.001,0.004)	6.18E-04 0.563 (-0.003,0.002)	1.29E-03 0.393 (-0.002,0.004)	1.27E-04 0.781 (-0.002,0.001)
Protein-lipid complex subunit organization (-APOE)	1.90E-03 0.279 (-0.001,0.004)	2.40E-03 0.237 (-0.001,0.004)	4.61E-04 0.617 (-0.002,0.003)	8.53E-03 0.028 (3.92E-04,0.007)*	1.32E-05 0.929 (-0.002,0.002)
Plasma lipoprotein particle assembly (-APOE)	8.48E-04 0.469 (-0.002,0.004)	1.39E-03 0.369 (-0.001,0.004)	7.96E-04 0.512 (-0.003,0.002)	1.46E-04 0.774 (-0.003,0.003)	1.10E-03 0.413 (-0.002,0.001)
Activation of immune response (-APOE)	1.44E-04 0.765 (-0.003,0.002)	1.94E-04 0.737 (-0.003,0.002)	3.11E-03 0.195 (-0.004,0.001)	9.16E-04 0.471 (-0.002,0.004)	4.82E-04 0.588 (-0.001,0.002)
Genome-wide PRS (-APOE)	7.42E-04 0.498 (-0.002,0.004)	1.83E-04 0.744 (-0.002,0.003)	8.58E-04 0.496 (-0.002,0.003)	4.56E-03 0.108 (-0.001,0.005)	8.73E-03 0.021 (2.81E-04,0.003)*
<b>APOE SNPs PRS</b>	3.18E-04 0.658 (-0.002,0.003)	2.28E-05 0.908 (-0.003,0.003)	8.47E-04 0.498 (-0.003,0.002)	2.86E-03 0.203 (-0.005,0.001)	1.77E-03 0.299 (-0.002,0.001)

R<sup>2</sup> and p values for subcortical volumes in the right hemisphere and each polygenic score at a P<sup>T</sup> of 0.001. The column names shows the region of interest, while the row names show the polygenic scores.

\* Nominally significant associations (p value < .05).

\*\* FDR corrected associations <0.05.

Acronyms: PRS = Polygenic Risk Score; P<sup>T</sup> = polygenic threshold; APOE = Apolipoprotein E; L = left; R = right; FDR = false discovery rate; FA = fractional anisotropy; Parahipp. = parahippocampal

**Table 6.3 Results for ALSPAC mean diffusivity and PRS including APOE at P<sup>T</sup> 0.001**

Polygenic risk score	MD Cingulum Left		MD Cingulum Right		MD Parahipp. Cingulum Left		MD Parahipp. Cingulum Right		MD Fornix	
	R <sup>2</sup> p (95% CI)	R <sup>2</sup> p (95% CI)	R <sup>2</sup> p (95% CI)	R <sup>2</sup> p (95% CI)	R <sup>2</sup> p (95% CI)					
<b>Protein-lipid complex assembly</b>	0.057 (6.96E-03, -5.82E-08, 4.13E-06)	0.231 (2.78E-03, -7.99E-07, 3.31E-06)	0.615 (5.01E-04, -1.64E-06, 2.77E-06)	0.986 (5.58E-07, -2.67E-06, 2.71E-06)	0.209 (3.02E-03, -1.53E-06, 7.01E-06)					
<b>Regulation of Aβ formation</b>	0.042 (7.94E-03, 8.25E-08, 4.34E-06)*	0.320 (1.92E-03, -1.03E-06, 3.16E-06)	0.419 (1.29E-03, -1.32E-06, 3.17E-06)	0.998 (1.26E-08, -2.74E-06, 2.73E-06)	0.172 (3.57E-03, -1.31E-06, 7.38E-06)					
<b>Protein-lipid complex</b>	0.083 (5.79E-03, -2.41E-07, 3.99E-06)	0.201 (3.18E-03, -7.18E-07, 3.43E-06)	0.467 (1.04E-03, -1.40E-06, 3.05E-06)	0.760 (1.77E-04, -2.29E-06, 3.14E-06)	0.235 (2.70E-03, -1.69E-06, 6.92E-06)					
<b>Regulation of amyloid precursor protein catabolic process</b>	0.042 (7.94E-03, 8.25E-08, 4.34E-06)*	0.320 (1.92E-03, -1.03E-06, 3.16E-06)	0.419 (1.29E-03, -1.32E-06, 3.17E-06)	0.998 (1.26E-08, -2.74E-06, 2.73E-06)	0.172 (3.57E-03, -1.31E-06, 7.38E-06)					
<b>Tau protein binding</b>	0.088 (5.61E-03, -2.70E-07, 3.97E-06)	0.202 (3.15E-03, -7.25E-07, 3.43E-06)	0.480 (9.86E-04, -1.43E-06, 3.04E-06)	0.806 (1.15E-04, -2.38E-06, 3.06E-06)	0.288 (2.16E-03, -1.97E-06, 6.66E-06)					
<b>Reverse cholesterol transport</b>	0.120 (4.67E-03, -4.30E-07, 3.78E-06)	0.234 (2.75E-03, -8.08E-07, 3.32E-06)	0.527 (7.91E-04, -1.50E-06, 2.93E-06)	0.832 (8.55E-05, -2.40E-06, 2.99E-06)	0.275 (2.29E-03, -1.89E-06, 6.67E-06)					
<b>Protein-lipid complex subunit organization</b>	0.043 (7.85E-03, 6.94E-08, 4.26E-06)*	0.196 (3.24E-03, -6.99E-07, 3.42E-06)	0.653 (4.00E-04, -1.70E-06, 2.72E-06)	0.951 (7.14E-06, -2.78E-06, 2.61E-06)	0.184 (3.37E-03, -1.38E-06, 7.17E-06)					
<b>Plasma lipoprotein particle assembly</b>	0.054 (7.16E-03, -2.99E-08, 4.18E-06)	0.203 (3.14E-03, -7.25E-07, 3.41E-06)	0.518 (8.27E-04, -1.49E-06, 2.95E-06)	0.760 (1.77E-04, -2.28E-06, 3.13E-06)	0.307 (2.00E-03, -2.05E-06, 6.54E-06)					
<b>Activation of immune response</b>	0.932 (1.39E-05, -2.01E-06, 2.20E-06)	0.723 (2.44E-04, -1.71E-06, 2.46E-06)	0.762 (1.81E-04, -1.88E-06, 2.57E-06)	0.677 (3.29E-04, -2.14E-06, 3.29E-06)	0.662 (3.67E-04, -3.35E-06, 5.28E-06)					
<b>Genome-wide PRS</b>	0.864 (5.67E-05, -1.91E-06, 2.28E-06)	0.633 (4.44E-04, -1.57E-06, 2.58E-06)	0.705 (2.84E-04, -2.65E-06, 1.79E-06)	0.633 (4.33E-04, -3.36E-06, 2.04E-06)	0.795 (1.30E-04, -4.87E-06, 3.73E-06)					

R<sup>2</sup> and p values for subcortical volumes in the right hemisphere and each polygenic score at a P<sup>T</sup> of 0.001. The column names shows the region of interest, while the row names show the polygenic scores.

\* Nominally significant associations (p value < .05).

\*\* FDR corrected associations <0.05.

Acronyms: PRS = Polygenic Risk Score; P<sup>T</sup> = polygenic threshold; APOE = Apolipoprotein E; L = left; R = right; FDR = false discovery rate; MD = mean diffusivity; Parahipp. = parahippocampal

**Table 6.4 Results for ALSPAC mean diffusivity and PRS excluding APOE at P<sup>T</sup> 0.001**

Polygenic risk score	MD Cingulum Left		MD Cingulum Right		MD Parahipp. Cingulum Left		MD Parahipp. Cingulum Right		MD Fornix	
	R <sup>2</sup>	p (95% CI)	R <sup>2</sup>	p (95% CI)	R <sup>2</sup>	p (95% CI)	R <sup>2</sup>	p (95% CI)	R <sup>2</sup>	p (95% CI)
Protein-lipid complex assembly (-APOE)	2.88E-04	0.699 (-2.57E-06, 1.72E-06)	6.50E-04	0.563 (-2.75E-06, 1.50E-06)	2.81E-05	0.905 (-2.41E-06, 2.14E-06)	1.06E-04	0.813 (-3.11E-06, 2.44E-06)	1.16E-03	0.437 (-2.66E-06, 6.16E-06)
Regulation of Aβ formation (-APOE)	2.32E-04	0.729 (-1.71E-06, 2.44E-06)	6.85E-04	0.553 (-2.68E-06, 1.43E-06)	7.50E-04	0.538 (-1.51E-06, 2.89E-06)	3.90E-04	0.650 (-3.30E-06, 2.06E-06)	1.29E-03	0.413 (-2.48E-06, 6.04E-06)
Protein-lipid complex (-APOE)	5.83E-04	0.583 (-1.53E-06, 2.73E-06)	7.97E-05	0.839 (-1.90E-06, 2.33E-06)	1.91E-03	0.325 (-1.12E-06, 3.39E-06)	9.07E-04	0.489 (-1.78E-06, 3.72E-06)	8.13E-04	0.515 (-2.92E-06, 5.83E-06)
Regulation of amyloid precursor protein catabolic process (-APOE)	2.32E-04	0.729 (-1.71E-06, 2.44E-06)	6.85E-04	0.553 (-2.68E-06, 1.43E-06)	7.50E-04	0.538 (-1.51E-06, 2.89E-06)	3.90E-04	0.650 (-3.30E-06, 2.06E-06)	1.29E-03	0.413 (-2.48E-06, 6.04E-06)
Tau protein binding (-APOE)	4.08E-04	0.646 (-1.63E-06, 2.63E-06)	4.00E-05	0.886 (-1.96E-06, 2.26E-06)	3.12E-03	0.209 (-8.08E-07, 3.71E-06)	5.19E-04	0.601 (-2.02E-06, 3.49E-06)	5.56E-05	0.865 (-4.76E-06, 4.00E-06)
Reverse cholesterol transport (-APOE)	3.06E-04	0.691 (-2.57E-06, 1.70E-06)	1.42E-04	0.787 (-2.40E-06, 1.82E-06)	4.88E-04	0.619 (-1.69E-06, 2.84E-06)	6.58E-05	0.852 (-2.49E-06, 3.02E-06)	4.61E-05	0.877 (-4.04E-06, 4.73E-06)
Protein-lipid complex subunit organization (-APOE)	2.08E-04	0.743 (-1.79E-06, 2.52E-06)	4.57E-05	0.878 (-2.31E-06, 1.97E-06)	1.22E-03	0.431 (-3.20E-06, 1.37E-06)	2.64E-03	0.238 (-4.45E-06, 1.10E-06)	6.84E-03	0.058 (-1.43E-07, 8.67E-06)
Plasma lipoprotein particle assembly (-APOE)	9.77E-04	0.477 (-2.90E-06, 1.35E-06)	7.09E-04	0.546 (-2.76E-06, 1.46E-06)	3.21E-04	0.687 (-1.79E-06, 2.71E-06)	5.69E-04	0.584 (-1.97E-06, 3.51E-06)	3.23E-04	0.681 (-5.27E-06, 3.44E-06)
Activation of immune response (-APOE)	3.52E-03	0.177 (-6.41E-07, 3.50E-06)	3.93E-03	0.155 (-5.59E-07, 3.54E-06)	3.45E-05	0.895 (-2.05E-06, 2.34E-06)	1.49E-04	0.779 (-3.06E-06, 2.29E-06)	6.14E-06	0.955 (-4.38E-06, 4.13E-06)
Genome-wide PRS (-APOE)	1.58E-05	0.928 (-2.01E-06, 2.21E-06)	2.44E-04	0.723 (-1.71E-06, 2.46E-06)	3.65E-03	0.174 (-3.78E-06, 6.81E-07)	3.37E-03	0.182 (-4.56E-06, 8.65E-07)	1.91E-03	0.318 (-6.52E-06, 2.12E-06)
APOE SNPs PRS	6.51E-05	0.854 (-1.91E-06, 2.31E-06)	2.24E-04	0.734 (-1.71E-06, 2.43E-06)	4.35E-03	0.138 (-5.33E-07, 3.89E-06)	2.98E-03	0.210 (-9.89E-07, 4.42E-06)	2.43E-03	0.260 (-1.82E-06, 6.75E-06)

R<sup>2</sup> and p values for subcortical volumes in the right hemisphere and each polygenic score at a P<sup>T</sup> of 0.001. The column names shows the region of interest, while the row names show the polygenic scores.

\* Nominally significant associations (p value < .05).

\*\* FDR corrected associations <0.05.

Acronyms: PRS = Polygenic Risk Score; P<sup>T</sup> = polygenic threshold; APOE = Apolipoprotein E; L = left; R = right; FDR = false discovery rate; MD = mean diffusivity; Parahipp. = parahippocampal

**Figure 6.5** UK Biobank genome-wide PRS and dMRI metrics, showing associations with reduced FA and increased MD. Imaging phenotypes are shown on the X axis, the beta coefficients (positive and negative) are shown on the Y axis. The heights of the bars indicate the amount of variance explained ( $R^2$ ), and any nominally significant results are labelled with their p value. Each bar represents a version of the polygenic risk score. The bars are colour coded by the p value threshold used in the training data, shown on the legend.

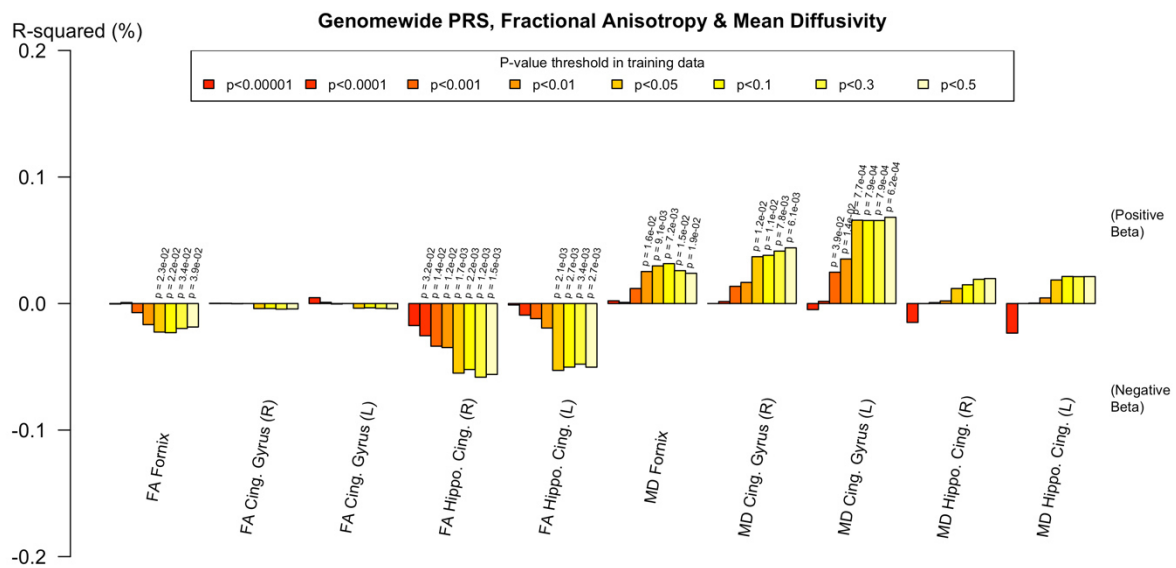


**Figure 6.6** UK Biobank protein lipid complex subunit PRS and dMRI metrics, showing associations with decreased FA and increased MD. Imaging phenotypes are shown on the X axis, the beta coefficients (positive and negative) are shown on the Y axis. The heights of the bars indicate the amount of variance explained ( $R^2$ ), and any nominally significant results are labelled with their p value. Each bar represents a version of the polygenic risk score. The bars are colour coded by the p value threshold used in the training data, shown on the legend.

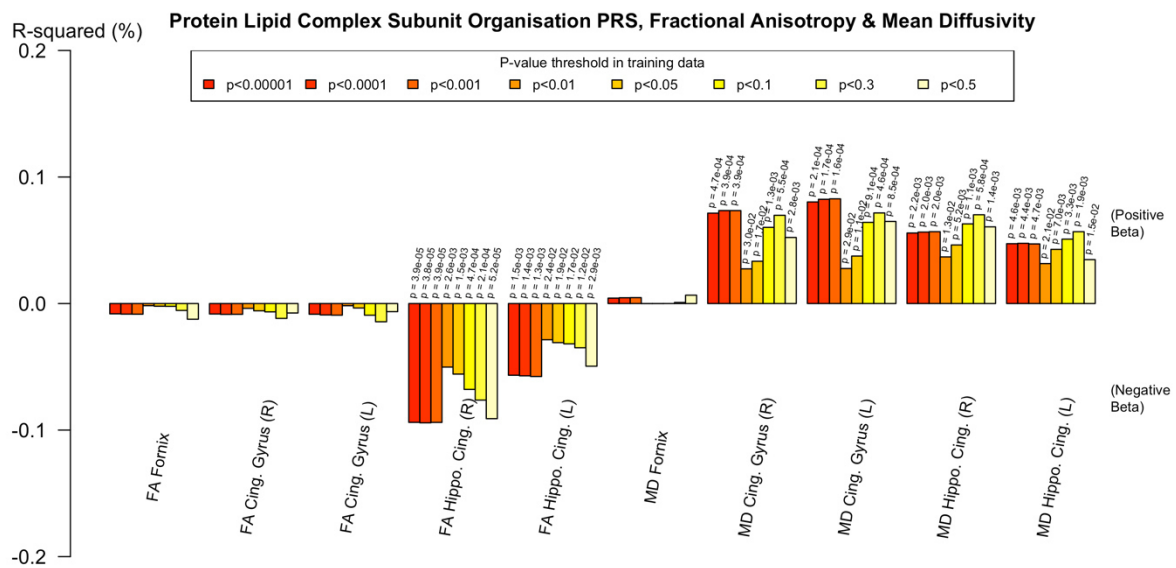


**Figure 6.7** Scatter plot showing UK Biobank association between normalised genome-wide PRS and normalised MD in the right parahippocampal cingulum. White circles indicate individual data points. Density represents the number of data points in each area.

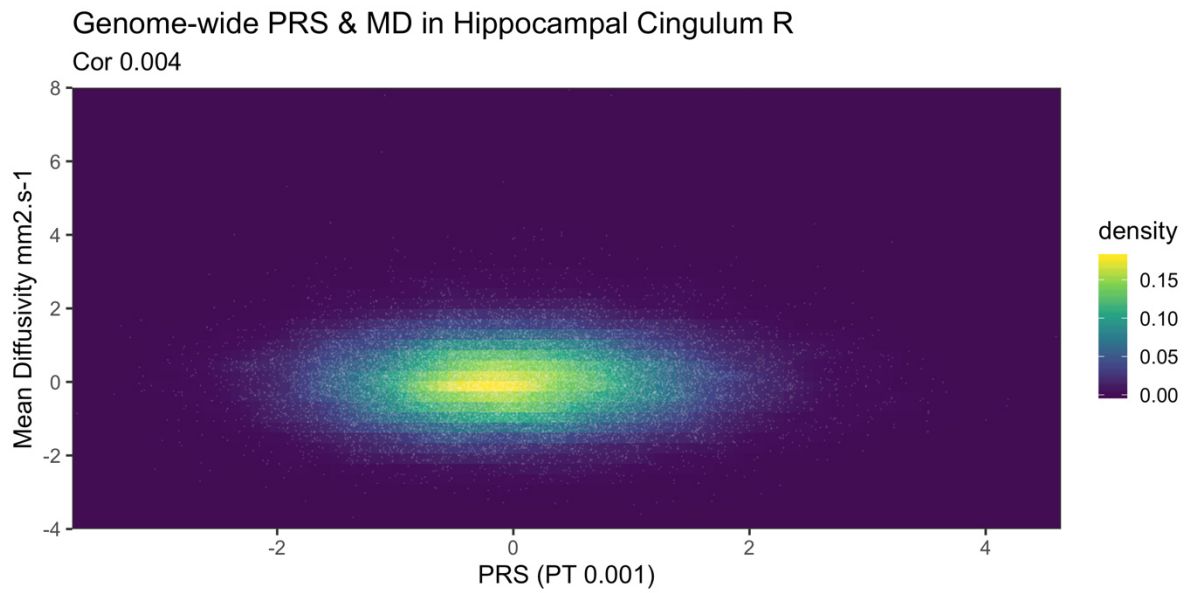


**Table 6.5 Results for UK Biobank fractional anisotropy and PRS including APOE at  $P^T$  0.001**

Polygenic risk score	FA Cingulum Left		FA Cingulum Right		FA Parahipp. Cingulum Left		FA Parahipp. Cingulum Right		FA Fornix	
	R <sup>2</sup>	p (95% CI)	R <sup>2</sup>	p (95% CI)	R <sup>2</sup>	p (95% CI)	R <sup>2</sup>	p (95% CI)	R <sup>2</sup>	p (95% CI)
Protein-lipid complex assembly	0.195 (-0.001,1.62E-04)	9.29E-05	0.220 (-0.001,1.85E-04)	8.47E-05	0.001 (-0.001,-3.28E-04)**	5.76E-04	3.94E-05 (-0.002,-0.001)**	9.38E-04	8.52E-05	0.162 (-0.002,3.21E-04)
Regulation of A $\beta$ formation	0.196 (-0.001,1.62E-04)	9.28E-05	0.220 (-0.001,1.84E-04)	8.49E-05	0.001 (-0.001,-3.28E-04)**	5.76E-04	3.92E-05 (-0.002,-0.001)**	9.39E-04	8.50E-05	0.163 (-0.002,3.22E-04)
Protein-lipid complex	0.196 (-0.001,1.62E-04)	9.27E-05	0.220 (-0.001,1.84E-04)	8.49E-05	0.001 (-0.001,0.000)**	5.76E-04	3.92E-05 (-0.002,-0.001)**	9.39E-04	8.50E-05	0.163 (-0.002,3.22E-04)
Regulation of amyloid precursor protein catabolic process	0.196 (-0.001,1.62E-04)	9.26E-05	0.219 (-0.001,1.84E-04)	8.51E-05	0.001 (-0.001,-3.28E-04)**	5.76E-04	3.91E-05 (-0.002,-0.001)**	9.39E-04	8.47E-05	0.164 (-0.002,3.23E-04)
Tau protein binding	0.197 (-0.001,1.63E-04)	9.24E-05	0.219 (-0.001,1.84E-04)	8.51E-05	0.001 (-0.001,-3.28E-04)**	5.76E-04	3.91E-05 (-0.002,-0.001)**	9.39E-04	8.45E-05	0.164 (-0.002,3.24E-04)
Reverse cholesterol transport	0.197 (-0.001,1.63E-04)	9.21E-05	0.219 (-0.001,1.84E-04)	8.50E-05	0.001 (-0.001,-3.28E-04)**	5.76E-04	3.91E-05 (-0.002,-0.001)**	9.39E-04	8.43E-05	0.165 (-0.002,3.26E-04)
Protein-lipid complex subunit organization	0.198 (-0.001,1.63E-04)	9.19E-05	0.219 (-0.001,1.84E-04)	8.50E-05	0.001 (-0.001,-3.28E-04)**	5.77E-04	3.89E-05 (-0.002,-0.001)**	9.40E-04	8.40E-05	0.166 (-0.002,3.27E-04)
Plasma lipoprotein particle assembly	0.198 (-0.001,1.64E-04)	9.18E-05	0.219 (-0.001,1.84E-04)	8.50E-05	0.001 (-0.001,-3.29E-04)**	5.77E-04	3.88E-05 (-0.002,-0.001)**	9.40E-04	8.38E-05	0.166 (-0.002,3.28E-04)
Activation of immune response	0.993 (-4.73E-04,4.78E-04)	4.73E-09	0.894 (-0.001,4.59E-04)	9.99E-07	0.918 (-0.001,4.87E-04)	5.87E-07	0.635 (-3.94E-04,6.46E-04)	1.25E-05	3.66E-05	0.360 (-0.002,0.001)
Genome-wide PRS	0.799 (-0.001,4.15E-04)	3.58E-06	0.868 (-0.001,4.52E-04)	1.56E-06	0.144 (-0.001,-1.34E-04)	1.19E-04	0.014 (-0.001,-1.34E-04)*	3.37E-04	7.18E-05	0.200 (-0.002,3.87E-04)

R2 and p values for diffusion metrics and each polygenic score at a  $P^T$  of 0.001. The column names shows the region of interest, while the row names show the polygenic scores.

\* Nominally significant associations (p value < .05).

\*\* FDR corrected associations <0.05.

Acronyms: PRS = Polygenic Risk Score;  $P^T$  = polygenic threshold; APOE = Apolipoprotein E; L = left; R = right; FDR = false discovery rate; FA = fractional anisotropy; Parahipp. = parahippocampal

**Table 6.6 Results for UK Biobank fractional anisotropy and PRS excluding APOE at  $P^T$  0.001**

Polygenic risk score	FA Cingulum Left		FA Cingulum Right		FA Parahipp. Cingulum Left		FA Parahipp. Cingulum Right		FA Fornix		
	$R^2$ p (95% CI)	$R^2$ p (95% CI)	$R^2$ p (95% CI)	$R^2$ p (95% CI)							
<b>Protein-lipid complex assembly (-APOE)</b>	0.195 (-0.001, 1.62E-04)	9.30E-05	0.220 (-0.001, 1.85E-04)	8.47E-05	0.001 (-0.001, -3.28E-04)**	5.76E-04	9.39E-04	3.93E-05 (-0.002, -0.001)**	9.39E-04	0.162 (-0.002, 3.21E-04)	8.53E-05
<b>Regulation of A<math>\beta</math> formation (-APOE)</b>	0.196 (-0.001, 1.62E-04)	9.27E-05	0.220 (-0.001, 1.85E-04)	8.48E-05	0.001 (-0.001, -3.28E-04)**	5.76E-04	9.39E-04	3.93E-05 (-0.002, -0.001)**	9.39E-04	0.163 (-0.002, 3.22E-04)	8.51E-05
<b>Protein-lipid complex (-APOE)</b>	0.196 (-0.001, 1.62E-04)	9.27E-05	0.220 (-0.001, 1.84E-04)	8.49E-05	0.001 (-0.001, -3.28E-04)**	5.76E-04	9.39E-04	3.92E-05 (-0.002, -0.001)**	9.39E-04	0.163 (-0.002, 3.22E-04)	8.50E-05
<b>Regulation of amyloid precursor protein catabolic process (-APOE)</b>	0.196 (-0.001, 1.62E-04)	9.26E-05	0.219 (-0.001, 1.84E-04)	8.50E-05	0.001 (-0.001, -3.28E-04)**	5.76E-04	9.39E-04	3.91E-05 (-0.002, -0.001)**	9.39E-04	0.164 (-0.002, 3.23E-04)	8.48E-05
<b>Tau protein binding (-APOE)</b>	0.197 (-0.001, 1.63E-04)	9.23E-05	0.219 (-0.001, 1.84E-04)	8.50E-05	0.001 (-0.001, -3.28E-04)**	5.76E-04	9.39E-04	3.92E-05 (-0.002, -0.001)**	9.39E-04	0.164 (-0.002, 3.24E-04)	8.45E-05
<b>Reverse cholesterol transport (-APOE)</b>	0.197 (-0.001, 1.63E-04)	9.21E-05	0.219 (-0.001, 1.84E-04)	8.50E-05	0.001 (-0.001, -3.28E-04)**	5.76E-04	9.39E-04	3.91E-05 (-0.002, -0.001)**	9.39E-04	0.165 (-0.002, 3.26E-04)	8.43E-05
<b>Protein-lipid complex subunit organization (-APOE)</b>	0.198 (-0.001, 1.63E-04)	9.19E-05	0.219 (-0.001, 1.84E-04)	8.50E-05	0.001 (-0.001, -3.29E-04)**	5.77E-04	9.40E-04	3.89E-05 (-0.002, -0.001)**	9.40E-04	0.166 (-0.002, 3.27E-04)	8.40E-05
<b>Plasma lipoprotein particle assembly (-APOE)</b>	0.198 (-0.001, 1.64E-04)	9.18E-05	0.219 (-0.001, 1.84E-04)	8.50E-05	0.001 (-0.001, -3.29E-04)**	5.77E-04	9.40E-04	3.88E-05 (-0.002, -0.001)**	9.40E-04	0.166 (-0.002, 3.28E-04)	8.38E-05
<b>Activation of immune response (-APOE)</b>	0.874 (-4.37E-04, 5.14E-04)	1.39E-06	0.949 (-0.001, 4.76E-04)	2.32E-07	0.624 (-3.85E-04, 6.42E-04)	1.34E-05	4.08E-05	0.392 (-2.93E-04, 7.48E-04)	4.08E-05	0.532 (-0.001, 0.001)	1.71E-05
<b>Genome-wide PRS (-APOE)</b>	0.885 (-4.42E-04, 5.12E-04)	1.16E-06	0.801 (-4.30E-04, 5.57E-04)	3.59E-06	0.686 (-4.09E-04, 6.21E-04)	9.12E-06	1.30E-05	0.629 (-0.001, 3.93E-04)	1.30E-05	0.739 (-0.001, 0.001)	4.85E-06
<b>APOE SNPs PRS</b>	0.537 (-0.001, 3.27E-04)	2.11E-05	0.539 (-0.001, 3.39E-04)	2.12E-05	0.003 (-0.001, -2.67E-04)**	4.96E-04	6.70E-04	0.001 (-0.001, -4.03E-04)**	6.70E-04	0.090 (-0.002, 1.49E-04)	1.26E-04

$R^2$  and p values for diffusion metrics and each polygenic score at a  $P^T$  of 0.001. The column names show the region of interest, while the row names show the polygenic scores.

\* Nominally significant associations (p value < .05).

\*\* FDR corrected associations <0.05.

Acronyms: PRS = Polygenic Risk Score;  $P^T$  = polygenic threshold; APOE = Apolipoprotein E; L = left; R = right; FDR = false discovery rate; FA = fractional anisotropy; Parahipp. = parahippocampal.

**Table 6.7 Results for UK Biobank mean diffusivity and PRS including APOE at  $P^T$  0.001**

Polygenic risk score	MD Cingulum Left		MD Cingulum Right		MD Parahipp. Cingulum Left		MD Parahipp. Cingulum Right		MD Fornix	
	R <sup>2</sup>	p (95% CI)	R <sup>2</sup>	p (95% CI)	R <sup>2</sup>	p (95% CI)	R <sup>2</sup>	p (95% CI)	R <sup>2</sup>	p (95% CI)
<b>Protein-lipid complex assembly</b>	1.63E-04 (4.03E-07, 1.28E-06)**	8.28E-04	3.90E-04 (3.60E-07, 1.25E-06)**	7.36E-04	0.005 (2.35E-07, 1.28E-06)**	4.73E-04	0.002 (3.00E-07, 1.34E-06)**	5.67E-04	0.296 (-1.85E-06, 6.07E-06)	4.78E-05
<b>Regulation of A<math>\beta</math> formation</b>	1.63E-04 (4.03E-07, 1.28E-06)**	8.28E-04	3.91E-04 (3.60E-07, 1.25E-06)**	7.35E-04	0.005 (2.34E-07, 1.28E-06)**	4.73E-04	0.002 (3.00E-07, 1.34E-06)**	5.67E-04	0.297 (-1.85E-06, 6.07E-06)	4.76E-05
<b>Protein-lipid complex</b>	1.63E-04 (4.03E-07, 1.28E-06)**	8.28E-04	3.92E-04 (3.60E-07, 1.25E-06)**	7.35E-04	0.005 (2.34E-07, 1.28E-06)**	4.72E-04	0.002 (3.00E-07, 1.34E-06)**	5.67E-04	0.297 (-1.85E-06, 6.07E-06)	4.76E-05
<b>Regulation of amyloid precursor protein catabolic process</b>	1.63E-04 (4.03E-07, 1.28E-06)**	8.28E-04	3.92E-04 (3.60E-07, 1.25E-06)**	7.35E-04	0.005 (2.34E-07, 1.28E-06)**	4.72E-04	0.002 (3.00E-07, 1.34E-06)**	5.67E-04	0.298 (-1.86E-06, 6.07E-06)	4.74E-05
<b>Tau protein binding</b>	1.64E-04 (4.03E-07, 1.28E-06)**	8.28E-04	3.93E-04 (3.60E-07, 1.25E-06)**	7.35E-04	0.005 (2.33E-07, 1.28E-06)**	4.72E-04	0.002 (3.00E-07, 1.34E-06)**	5.68E-04	0.299 (-1.86E-06, 6.06E-06)	4.72E-05
<b>Reverse cholesterol transport</b>	1.64E-04 (4.03E-07, 1.28E-06)**	8.28E-04	3.94E-04 (3.59E-07, 1.25E-06)**	7.35E-04	0.005 (2.33E-07, 1.28E-06)**	4.71E-04	0.002 (3.00E-07, 1.34E-06)**	5.68E-04	0.300 (-1.87E-06, 6.06E-06)	4.70E-05
<b>Protein-lipid complex subunit organization</b>	1.64E-04 (4.03E-07, 1.28E-06)**	8.28E-04	3.94E-04 (3.59E-07, 1.25E-06)**	7.35E-04	0.005 (2.33E-07, 1.28E-06)**	4.71E-04	0.002 (0.000, 1.34E-06)**	5.68E-04	0.301 (-1.87E-06, 6.05E-06)	4.68E-05
<b>Plasma lipoprotein particle assembly</b>	1.64E-04 (4.03E-07, 1.28E-06)**	8.28E-04	3.93E-04 (3.60E-07, 1.25E-06)**	7.35E-04	0.005 (2.33E-07, 1.28E-06)**	4.71E-04	0.002 (3.01E-07, 1.34E-06)**	5.68E-04	0.302 (-1.87E-06, 6.05E-06)	4.67E-05
<b>Activation of immune response</b>	0.400 (-6.23E-07, 2.48E-07)	4.14E-05	0.131 (-7.85E-07, 1.02E-07)	1.34E-04	0.137 (-9.21E-07, 1.26E-07)	1.30E-04	0.154 (-8.94E-07, 1.41E-07)	1.21E-04	0.693 (-3.15E-06, 4.75E-06)	6.83E-06
<b>Genome-wide PRS</b>	0.039 (2.27E-08, 8.96E-07)*	2.48E-04	0.127 (-9.86E-08, 7.91E-07)	1.36E-04	0.810 (-4.61E-07, 5.90E-07)	3.40E-06	0.727 (-4.26E-07, 6.11E-07)	7.20E-06	0.099 (-6.29E-07, 7.29E-06)	1.19E-04

R2 and p values for diffusion metrics and each polygenic score at a  $P^T$  of 0.001. The column names shows the region of interest, while the row names show the polygenic scores.

\* Nominally significant associations (p value < .05).

\*\* FDR corrected associations <0.05.

Acronyms: PRS = Polygenic Risk Score;  $P^T$  = polygenic threshold; APOE = Apolipoprotein E; L = left; R = right; FDR = false discovery rate; MD = mean diffusivity; Parahipp. = parahippocampal

**Table 6.8 Results for UK Biobank mean diffusivity and PRS excluding APOE at  $P^T$  0.001**

	MD Cingulum Left		MD Cingulum Right		MD Parahipp. Cingulum Left		MD Parahipp. Cingulum Right		MD Fornix	
Polygenic risk score	$R^2$	p (95% CI)	$R^2$	p (95% CI)	$R^2$	p (95% CI)	$R^2$	p (95% CI)	$R^2$	p (95% CI)
<b>Protein-lipid complex assembly (-APOE)</b>	1.63E-04 (4.04E-07, 1.28E-06)**	8.29E-04 (4.03E-07, 1.28E-06)**	7.36E-04 (3.60E-07, 1.25E-06)**	3.89E-04 (3.60E-07, 1.28E-06)**	4.73E-04 (2.35E-07, 1.28E-06)**	0.005 (2.35E-07, 1.28E-06)**	5.66E-04 (2.99E-07, 1.34E-06)**	0.002 (2.99E-07, 1.34E-06)**	4.79E-05	0.295 (-1.85E-06, 6.08E-06)
<b>Regulation of A<math>\beta</math> formation (-APOE)</b>	1.64E-04 (4.03E-07, 1.28E-06)**	8.28E-04 (4.03E-07, 1.28E-06)**	7.35E-04 (3.60E-07, 1.25E-06)**	3.92E-04 (3.60E-07, 1.28E-06)**	4.72E-04 (2.34E-07, 1.28E-06)**	0.005 (2.34E-07, 1.28E-06)**	5.67E-04 (3.00E-07, 1.34E-06)**	0.002 (3.00E-07, 1.34E-06)**	4.77E-05	0.296 (-1.85E-06, 6.07E-06)
<b>Protein-lipid complex (-APOE)</b>	1.63E-04 (4.03E-07, 1.28E-06)**	8.28E-04 (4.03E-07, 1.28E-06)**	7.35E-04 (3.60E-07, 1.25E-06)**	3.91E-04 (3.60E-07, 1.25E-06)**	4.72E-04 (2.34E-07, 1.28E-06)**	0.005 (2.34E-07, 1.28E-06)**	5.67E-04 (3.00E-07, 1.34E-06)**	0.002 (3.00E-07, 1.34E-06)**	4.76E-05	0.297 (-1.85E-06, 6.07E-06)
<b>Regulation of amyloid precursor protein catabolism (-APOE)</b>	1.64E-04 (4.03E-07, 1.28E-06)**	8.28E-04 (4.03E-07, 1.28E-06)**	7.35E-04 (3.60E-07, 1.25E-06)**	3.92E-04 (3.60E-07, 1.28E-06)**	4.72E-04 (2.34E-07, 1.28E-06)**	0.005 (2.34E-07, 1.28E-06)**	5.67E-04 (3.00E-07, 1.34E-06)**	0.002 (3.00E-07, 1.34E-06)**	4.74E-05	0.298 (-1.86E-06, 6.07E-06)
<b>Tau protein binding (-APOE)</b>	1.64E-04 (4.03E-07, 1.28E-06)**	8.28E-04 (4.03E-07, 1.28E-06)**	7.35E-04 (3.59E-07, 1.25E-06)**	3.94E-04 (3.59E-07, 1.25E-06)**	4.72E-04 (2.33E-07, 1.28E-06)**	0.005 (2.33E-07, 1.28E-06)**	5.68E-04 (3.00E-07, 1.34E-06)**	0.002 (3.00E-07, 1.34E-06)**	4.72E-05	0.299 (-1.86E-06, 6.06E-06)
<b>Reverse cholesterol transport (-APOE)</b>	1.64E-04 (4.03E-07, 1.28E-06)**	8.28E-04 (4.03E-07, 1.28E-06)**	7.35E-04 (3.59E-07, 1.25E-06)**	3.94E-04 (3.59E-07, 1.25E-06)**	4.71E-04 (2.33E-07, 1.28E-06)**	0.005 (2.33E-07, 1.28E-06)**	5.68E-04 (3.00E-07, 1.34E-06)**	0.002 (3.00E-07, 1.34E-06)**	4.70E-05	0.300 (-1.87E-06, 6.06E-06)
<b>Protein-lipid complex subunit organization (-APOE)</b>	1.64E-04 (4.03E-07, 1.28E-06)**	8.28E-04 (4.03E-07, 1.28E-06)**	7.35E-04 (3.59E-07, 1.25E-06)**	3.94E-04 (3.59E-07, 1.25E-06)**	4.71E-04 (2.33E-07, 1.28E-06)**	0.005 (2.33E-07, 1.28E-06)**	5.68E-04 (3.00E-07, 1.34E-06)**	0.002 (3.00E-07, 1.34E-06)**	4.68E-05	0.301 (-1.87E-06, 6.05E-06)
<b>Plasma lipoprotein particle assembly (-APOE)</b>	1.64E-04 (4.03E-07, 1.28E-06)**	8.28E-04 (4.03E-07, 1.28E-06)**	7.35E-04 (3.59E-07, 1.25E-06)**	3.94E-04 (3.59E-07, 1.25E-06)**	4.71E-04 (2.33E-07, 1.28E-06)**	0.005 (2.33E-07, 1.28E-06)**	5.68E-04 (3.00E-07, 1.34E-06)**	0.002 (3.00E-07, 1.34E-06)**	4.67E-05	0.302 (-1.87E-06, 6.05E-06)
<b>Activation of immune response (-APOE)</b>	0.264 (-6.84E-07, 1.87E-07)	7.27E-05 (-6.84E-07, 1.87E-07)	1.87E-04 (-8.48E-07, 3.94E-08)	0.074 (-8.48E-07, 3.94E-08)	1.40E-04 (-9.36E-07, 1.12E-07)	0.123 (-9.36E-07, 1.12E-07)	1.37E-04 (-9.19E-07, 1.16E-07)	0.129 (-9.19E-07, 1.16E-07)	3.35E-07	0.930 (-3.78E-06, 4.13E-06)
<b>Genome-wide PRS (-APOE)</b>	0.979 (-4.43E-07, 4.31E-07)	4.03E-08 (-4.43E-07, 4.31E-07)	3.73E-06 (-5.02E-07, 3.87E-07)	0.801 (-5.02E-07, 3.87E-07)	7.41E-05 (-8.26E-07, 2.25E-07)	0.262 (-8.26E-07, 2.25E-07)	6.41E-05 (-7.94E-07, 2.43E-07)	0.299 (-7.94E-07, 2.43E-07)	1.58E-05	0.548 (-2.75E-06, 5.18E-06)
<b>APOE SNPs PRS</b>	0.001 (3.38E-07, 1.21E-06)**	7.05E-04 (3.38E-07, 1.21E-06)**	4.86E-04 (2.10E-07, 1.10E-06)**	0.004 (2.10E-07, 1.10E-06)**	2.11E-04 (-1.78E-08, 1.03E-06)	0.058 (-1.78E-08, 1.03E-06)	2.29E-04 (1.36E-09, 1.04E-06)*	0.049 (1.36E-09, 1.04E-06)*	1.67E-04	0.051 (-1.19E-08, 7.91E-06)

R2 and p values for diffusion metrics and each polygenic score at a  $P^T$  of 0.001. The column names shows the region of interest, while the row names show the polygenic scores.

\* Nominally significant associations (p value < .05).

\*\* FDR corrected associations <0.05.

Acronyms: PRS = Polygenic Risk Score;  $P^T$  = polygenic threshold; APOE = Apolipoprotein E; L = left; R = right; FDR = false discovery rate; MD = mean diffusivity; Parahipp. = parahippocampal.

## 6.5 Discussion

In line with the hypothesis, increasing PRS was associated with increased diffusivity, measured with MD, and decreased anisotropy, measured with FA, in the older adult cohort. The strongest associations were between the pathway specific PRS and increased MD in the parahippocampal cingulum and cingulate gyrus, although there were also significant negative correlations between the pathway specific PRS and FA in the parahippocampal cingulum. We saw no association with either FA or MD in the fornix in the UK Biobank cohort at  $P^T = 0.001$ , although there was some evidence of association on secondary analysis with more generous  $P^T$ . These results were not driven by the *APOE* locus, and SNPs in the *APOE* region alone were slightly less strongly associated with the same phenotypes. The genome-wide polygenic scores showed less evidence of association than the pathway specific PRS, with no significant results withstanding multiple comparisons correction with FDR. In the younger cohort there were no statistically significant findings. Whilst there was some evidence of association between increased PRS and increased MD in the younger cohort, particularly in the left cingulum, these results did not withstand correction for multiple comparisons.

As discussed in previous chapters, other studies have applied PRS based on AD pathways to investigate associations with subcortical brain volumes (Ahmad *et al.*, 2018) and cortical thinning (Corlier *et al.*, 2018; Caspers *et al.*, 2020). The present study was the first to apply this approach to investigate white matter microstructure. Furthermore, this experiment has used a threshold-based PRS, allowing us to include a much greater amount of genetic information than previous studies which used only Bonferroni significant loci (Ahmad *et al.*, 2018; Corlier *et al.*, 2018; Caspers *et al.*, 2020).

Findings from UK Biobank are consistent with the previous literature. As discussed in Chapter 3, changes in the left parahippocampal cingulum (Honea *et al.*, 2009), and cingulum (Douaud *et al.*, 2011) have previously been identified in AD patients and in MCI (Sexton *et al.*, 2011). Decreased FA in medial temporal areas is evident in healthy *APOE* carriers (Persson *et al.*, 2006; Bagepally *et al.*, 2012) and in pre-symptomatic autosomal dominant AD (Ringman *et al.*, 2007).

Contrary to the hypothesis, there was little evidence of association between white matter metrics and PRS in the younger adult cohort. This was unexpected, as a number of previous studies with samples of comparable age have observed associations between AD genetic risk and changes in white matter microstructure. One study of healthy young participants ( $n = 73$ , mean age 28.6 years, SD 4.20) observed extensive decreases in FA among *APOE* carriers (Heise *et al.*, 2011). A study of young and healthy carriers of a clusterin risk locus ( $n = 398$ , mean age 23.6, SD 2.2) also reported decreased FA in a number of areas, including in the cingulum and the fornix (Braskie *et al.*, 2011). Similarly, Foley *et al.* used an AD PRS in a cohort of young adults ( $n = 197$ , mean age 23.9, SD 5.1) and found reduced FA in the right cingulum (Foley *et al.*, 2016). Associations have even been reported in infant carriers of *APOE4*. Dean and colleagues reported changes in white matter myelin water fraction in the precuneus, cingulum, lateral temporal, and medial occipitotemporal areas among a cohort of infants ( $n = 162$ , 2-25 months old) (Dean *et al.*, 2014). The same group demonstrated longitudinal differences between infant *APOE4* carriers compared to non-carriers ( $n = 233$ , aged 2-68 months), with differences in myelin water fraction in the uncinate fasciculus, temporal lobe, internal capsule and occipital lobe in the *APOE4* group (Remer *et al.*, 2020). Little is known about the effect of polygenic risk for AD on brain structure across the life course, particularly during neurodevelopment. However, it is clear that white matter structural maturation progresses during adolescence and continues in early adulthood. This is evident in age-related changes in white matter volume and microstructure (Paus, 2010). It is possible that the effect of polygenic risk for AD in brain structure at age 20 are masked by concurrent neurodevelopmental white matter changes. It is also possible that measures of specific white matter microstructure components, such as myelin water fraction, may be more sensitive to AD-related changes in childhood and early adulthood, as the development myelin from precursory lipids may be affected by lipid dysregulation associated with AD risk loci (Deoni *et al.*, 2012; Dean *et al.*, 2014).

Contrary to expectations, there were no significant associations observed between the PRS and changes in the fornix in the older age cohort at  $P^T = 0.001$ . This is surprising considering previous studies reported changes in the fornix in healthy carriers of *APOE* (Zhang *et al.*, 2015). This might be explained by the neuroanatomy of the fornix, which is narrow, highly curved and close to the ventricles. The tract specificity of the

TBSS projection step is unclear, and TBSS may have particular difficulty in differentiating the fornix (Smith *et al.*, 2006; Bach *et al.*, 2014).

It was hypothesised that distinct patterns of signal would be observed with genetic burden in different disease pathways, as reported in some previous studies (Corlier *et al.*, 2018; Caspers *et al.*, 2020). As with grey matter volumes, described in Chapter 5, the results did not support this. For tracts which showed changes, the variance explained and associated p values were similar between the pathway specific PRS. This mirrored patterns of cortical thinning and subcortical volumes described in Chapter 5 and may reflect the significant overlap in the SNPs included in each pathway.

The associations observed in UK Biobank between PRS and white matter metrics were not driven by the *APOE* locus. The associations remained when *APOE* was removed from each PRS. The *APOE* region alone explained a smaller amount of variance in the phenotype than the pathway PRS. This also corroborates the findings of the only previous study to use an AD PRS to explore white matter microstructure which also reported that the signal was independent of *APOE* genotype (Foley *et al.*, 2016). The genome-wide PRS and the immune response PRS showed less evidence of association with alterations in white matter microstructure. Each of these PRS included a much greater number of genes (Kunkle *et al.*, 2019), which may have resulted in more noise in the PRS.

It is unclear whether FA or MD is the more sensitive marker of AD related changes. Increasing diffusivity and decreasing anisotropy occur in tandem. In the present study we found more evidence of association between MD and polygenic burden than FA. A number of studies have only reported significant decreases in FA, although some have reported only significant increases in MD (Adluru *et al.*, 2014; Kljajevic *et al.*, 2014; Cai *et al.*, 2017). Foley and colleagues identified an association between AD PRS and FA in the right cingulum (Foley *et al.*, 2016), whereas the present study found AD PRS to be associated with MD in the right and left cingulum in older adults. Furthermore, interpreting decreased FA or increased MD is not straight forward. Unlike grey matter morphology, water diffusion does not measure neuroanatomy directly. As discussed in Chapter 3, there is degeneracy in dMRI signal changes, and

decreased anisotropy and increased diffusivity can represent a number of structural and pathological ground-truths. Lower anisotropy can reflect fibres running at different orientations. Pathological states such as demyelination, oedema, axonal loss or axonal growth can also affect dMRI signals, as explained in Chapter 3. Therefore, it is a mistake to indiscriminately interpret changes in diffusion signal as evidence of neurodegeneration. However, other biomarkers of neurodegeneration correlate with reduced FA and increased MD in AD, such as amyloid on PET (Kantarci *et al.*, 2014), and CSF amyloid and tau (Amlie *et al.*, 2013; Gold *et al.*, 2014; X Li *et al.*, 2015). Furthermore, cognitive function has been shown to be associated with FA and MD changes (Fletcher *et al.*, 2013). For further dMRI methodological considerations, please see Chapter 3.

### **6.5.1 Strength and limitations**

A number of strengths and limitations of Chapter 5 also apply to this analysis. The present study had superior statistical power compared to previous studies for two reasons. First, it also used the largest and most recent GWAS of clinically assessed AD, Kunkle *et al.* (Kunkle *et al.*, 2019), as the discovery dataset. Effect size estimates for each SNP are therefore the most accurate available, with greater power than previous estimates. PRS and  $R^2$  have been shown to be highly sensitive to the size of discovery dataset (Schizophrenia Working Group of the Psychiatric Genomics, 2014). Second, it used population cohorts which provided large target sample sizes.

As explained in Chapter 5, the use of large population imaging cohorts has some disadvantages. For example, the ALSPAC imaging sub-studies has specific inclusion criteria (see Chapter 4) meaning the sample over-represents males, and a small number of participants reported psychotic experiences. However, the regression analysis co-varied for sex, and only a minority of the number of individuals reporting experiences could have met criteria for a neuropsychiatric disorder. As described in Chapters 4 and 5, a criticism of both ALSPAC and UK Biobank is that participants tend to be healthier and from higher socio-economic backgrounds (Abigail Fraser *et al.*, 2013; Fry *et al.*, 2017) which could affect the generalisability of the results.

Whilst the polygenic scoring methods applied to ALSPAC and UK Biobank were the same, the dMRI methodology was significantly different, and thus likely to lead to different results. Therefore, it is difficult to be sure whether differences in results were due to differences in the sample or were due to measurement bias. As described in Chapter 5, even though the present study delineated pathway specific polygenic profiles, it is not possible to determine the exact molecular mechanisms responsible for changes in phenotype because PRS combine the effect of risk variants. Elucidating that will require further functional genomic studies of individual variants. Further longitudinal genetic imaging studies, including even younger samples than the present study, will be needed to improve our understanding of how AD polygenic risk is manifest throughout development. Similarly, longitudinal studies combining neuroradiology and CSF biomarkers with advanced MRI and genetics can put these findings into context of biomarker abnormalities seen in incipient AD. As discussed in Chapter 5, future pathway-based studies will also require large samples and would benefit from new approaches to correcting for multiple comparisons.

### **6.5.2 Conclusion**

Increasing PRS was associated with increased diffusivity and decreased anisotropy, in the older adult cohort. The strongest associations were between the pathway specific PRS and increased MD in the parahippocampal cingulum and cingulate gyrus. There were also significant negative correlations between the pathway specific PRS and FA in the parahippocampal cingulum. There were no significant associations in the younger cohort. Further longitudinal studies, using multimodal imaging and biomarker techniques, as well as functional genomic studies of individual variants will be needed to understand the biological significance of these findings.

## CHAPTER 7: ALZHEIMER'S POLYGENIC RISK SCORES, BLOOD LIPID & INFLAMMATORY MARKERS

*Dr Emily Baker provided the lists of SNPs in the Kunkle et al 2019 disease pathways, as they were used for separate analyses. Dr Katherine Tansey assisted with genotyping quality control in ALSPAC.*

*Some information from previous Chapters is repeated here for convenience, particularly information on polygenic scoring methods from Chapters 4, 5 and 6.*

### 7.1 Summary

There is significant evidence of a link between dyslipidaemia, inflammatory dysregulation and AD. Epidemiological studies have found associations between blood lipid levels, inflammatory markers and dementia. Raised lipids and inflammatory markers are also risk factors for cardiovascular disease, and tools designed to measure cardiovascular risk are associated with neurodegenerative phenotypes. There is pleiotropy between late onset AD and cardiovascular risk loci. The *APOE4* allele confers significant increased risk for both AD and cardiovascular disease. AD genome-wide association studies (GWAS) have established associations with SNPs involved in lipid metabolism, such as *ABCA7* and *CLU*, and those implicated in inflammatory processes, such as *HLA-DRB5* and *CR1*. A recently identified rare variant in *TREM-2* with anti-inflammatory functions also confers increased risk for AD. Pathway analysis using data from GWAS have further implicated lipid metabolism and the innate immune system in AD pathophysiology.

Previous studies have investigated pleiotropic genetic enrichment in AD as a function of blood lipid profiles, and a small preliminary study identified associations between genome-wide and immune specific AD polygenic risk scores (PRS) and inflammatory markers. To date, no studies have yet applied AD pathway specific PRS to investigate blood lipid phenotypes.

This study aimed to investigate associations between disease pathway specific PRS and blood lipid and inflammatory markers in adults using a large population cohort. As a secondary aim, it compared the associations using more and less liberal p value thresholds.

Increased polygenic risk for AD was associated with increased blood lipids, particularly LDL and total cholesterol. These results were reflected across the genome-wide PRS and most of the pathway-specific PRS, and withstood corrections for multiple comparisons. CRP was negatively associated with increased genome-wide PRS and with most of the pathway PRS. The results attenuated when SNPs in the *APOE* region were excluded from the PRS. This is in keeping with the findings of previous investigations. Although none of the PRS were significant when *APOE* was omitted, some of the PRS including the *APOE* region explained greater variance in phenotypes than *APOE* alone. The contribution of the polygenic component of AD to these phenotypes (besides the *APOE* region) will need to be confirmed by further studies. Further investigation is needed into the exact biological mechanisms by which loci within PRS contribute to AD pathophysiology.

## 7.2 Introduction

Growing evidence points to an association between AD and metabolic processes, such as lipid metabolism and inflammation. Dyslipidaemia and systematic inflammatory dysregulation are overlapping risk factors for cardiovascular disease and AD (Stampfer, 2006).

Some epidemiological studies have found that increased serum cholesterol is associated with an increased risk of AD, although the findings of other studies contradict this (Li *et al.*, 2005; Reitz *et al.*, 2010; Tynkkynen *et al.*, 2018; Wagner *et al.*, 2018; Ferguson *et al.*, 2020). This discrepancy in findings could be partly attributed to the smaller sample sizes in the earlier studies. Recent evidence from a lipidomic analysis found a combination of 24 lipid molecules could distinguish AD cases from controls with >70% accuracy. Specific lipid profiles could also predict disease progression and brain atrophy (Proitsi *et al.*, 2017).

Further evidence of overlapping AD and cardiovascular risk comes from studies using tools designed to predict cardiovascular morbidity, such as the Framingham Cardiovascular Risk Profile (FCRP). The FCRP has been shown to be associated with cortical thinning (Cardenas *et al.*, 2012) and cognitive decline in both cognitively healthy individuals and those with Mild Cognitive Impairment (MCI) (Jefferson *et al.*, 2015). High FCRP scores can also predict progression from MCI to AD (Viticchi *et al.*, 2015). Observational studies of older adults suggest that elevated levels of serum inflammatory markers are linked to worsening cognitive abilities (Dik *et al.*, 2005) and may be associated with incident dementia (Tan *et al.*, 2007).

Molecular and biomarker studies suggest a role for phospholipids in AD pathogenesis (Di Paolo and Kim, 2011; Mapstone *et al.*, 2014). Cholesterol is essential for synapse maturation and maintaining synaptic plasticity (Koudinov and Koudinova, 2001; Mauch *et al.*, 2001). Levels of cholesterol also modulate A $\beta$  clearance and neurofibrillary tangles formation via lipid rafts present in neurone membranes (Rushworth and Hooper, 2011). Complement factors and activated microglia are established histopathological features in AD (Eikelenboom *et al.*, 2012).

There is genetic overlap between late-onset AD and cardiovascular risk loci. The *APOE* alleles, Epsilon 2, 3 and 4, encode protein isoforms with different lipid interactions in serum (Liu *et al.*, 2013). *APOE4* homozygotes have an eight-fold increase in risk of AD compared to non-carriers (Corder *et al.*, 1993). *APOE4* is associated with higher low density lipoprotein (LDL) cholesterol and significantly increased cardiovascular risk (Lahoz *et al.*, 2001). *APOE4* carriers with cardiovascular disease often have comorbid AD (Hofman *et al.*, 1997; Eichner *et al.*, 2002). *APOE* is involved in cholesterol transport and catabolism of lipoprotein components rich in triglycerides (Kalaria, Akinyemi and Ihara, 2012).

Late-onset AD GWAS have established associations with SNPs involved in lipid metabolism, such as *ABCA7* and *CLU*, and those implicated in inflammatory processes, such as *HLA-DRB5* and *CR1* (Jones *et al.*, 2010; Karch, Cruchaga and Goate, 2014). Recently, a rare variant in *TREM-2* has been shown to confer increased risk for AD. It is also implicated in anti-inflammatory functions (Guerreiro, Wojtas, Bras, Carrasquillo, Rogaeva, Majounie, Cruchaga, Sassi, John S.K. Kauwe, *et al.*, 2013;

Jonsson *et al.*, 2013). As discussed in previous Chapters, pathway analysis using data from genome-wide association studies have further implicated lipid metabolism and the innate immune system in AD pathophysiology (Jones *et al.*, 2010; Kunkle *et al.*, 2019).

There are polygenic contributions to inflammatory markers and lipid levels. For example, a meta-analysis of GWAS including more than 80,000 participants identified multiple SNPs for C-Reactive Protein (CRP) levels. Loci were linked to pathways involved in metabolic syndrome or the immune system, and regions not previously implicated in chronic inflammation (Dehghan *et al.*, 2011). A GWAS of plasma lipids in over 100,000 subjects reported significant associations with 95 loci. These included SNPs near genes known to function as lipid regulators and a number of loci that had not been previously implicated in lipid metabolism (Teslovic, 2013). There is evidence of genetic pleiotropy between risk loci for AD, CRP and lipoprotein metabolism. Desikan and colleagues used the summary statistics from three large GWAS to investigate overlap between SNPs associated with AD, CRP, triglycerides, high-density lipoprotein (HDL) and low-density lipoprotein (LDL) levels. They found that AD SNPs were enriched for SNPs associated with HDL, LDL, triglyceride and CRP SNPs up to 50-fold. By conditioning on SNPs associated with these phenotypes, they observed enhanced statistical power in gene discovery analyses, identifying 55 novel AD risk loci (Desikan *et al.*, 2015). A small preliminary study (n = 93 AD cases) tested a range of inflammatory markers for association with a threshold-based PRS and found that CRP was associated with an increased PRS specific for the immune response (Morgan *et al.*, 2017).

As blood lipids and inflammatory markers are established biomarkers used in clinical practice, standardised methods exist to measure these at scale. For lipids, enzymatic assays are commonly used in automated analysers. These techniques involve hydrolyzing esterified cholesterol to free cholesterol, then oxidizing to cholest-4-en-3-one. The hydrogen peroxide produced during the oxidation is then measured using fluorometric probes (Li *et al.*, 2019). CRP is commonly measured by immunoturbidimetric assays in clinical laboratories. These involve microparticle latex reagents, non-immunopurified antibodies to assay against CRP (Price *et al.*, 1987). This method is reproducible and fully automated.

### 7.2.1 Rationale and Aims

Taken together, findings from epidemiological studies, molecular and genetic research suggest that processes involved with lipid metabolism and inflammation also affect AD pathogenesis. Recent literature provides evidence of the effect of AD risk genes on blood lipids and inflammatory markers.

In Chapter 2, existing studies exploring the use of AD polygenic scores (PRS) were systematically reviewed and summarised. There was evidence of association between AD PRS and a variety of phenotypes, including cognitive health, neuroimaging and CSF biomarkers. Although studies have explored the effect of *APOE* on metabolic markers (Ferguson *et al.*, 2020), how the polygenic component of AD risk is manifest in blood lipids and inflammatory markers is not well understood.

As discussed in previous chapters, GWAS have identified further susceptibility loci in addition to *APOE4* (Lambert *et al.*, 2013; Kunkle *et al.*, 2019). These novel loci are associated with a number of biological pathways, such as lipid metabolism, the innate immune response, and synaptic processes (Jones *et al.*, 2010; Holmans and Jones, 2012). By detecting pathways enriched for risk alleles, PRS can allow molecular sub-classification. Only one study has used AD pathway polygenic scores to assess inflammatory blood markers. It was limited by a small sample size, therefore the findings can only be considered preliminary (Morgan *et al.*, 2017). As mentioned in previous Chapters, the variance explained by each pathway is small (Darst *et al.*, 2017), consequently large ‘discovery’ GWAS and large target sample sizes are necessary (Dudbridge, 2013).

The primary aim of this chapter is to investigate associations between disease pathway specific PRS and blood lipid and inflammatory markers in adults using a large population cohort. As a secondary aim, it will compare the associations using more and less liberal p value thresholds to assess which cut off explains the most variance in the phenotype.

## **7.2.2 Hypothesis**

It is hypothesised that increasing genetic burden for AD, measured in increasing PRS, will be associated with i) increased very Low Density Lipoprotein (vLDL) and Low Density Lipoprotein (LDL) cholesterol, ii) decreased High Density Lipoprotein (HDL) cholesterol and iii) increased C-Reactive Protein (CRP). Additionally, it is hypothesised that lipid-related disease pathways PRS will show greater association with lipid biomarkers, and that CRP will be associated with the immune response pathway PRS.

## **7.3 Methods**

### **7.3.1 Participants**

Participants were enrolled through the Avon Longitudinal Study of Parents and Children (ALSPAC). Chapter 4 contains a detailed description of ALSPAC's recruitment methods and sample characteristics. Briefly, it recruited pregnant women living in a specific area of South West England who were expected to deliver their babies in the period between 1st April 1991 - 31st December 1992. A total of 13,761 women were recruited. Follow-up assessment clinics took place at 17–18 years later. 4834 women attended and provided fasting blood samples.

This experiment excluded participants if: they reported non-British/Irish ancestry; if they were recruited into ALSPAC twice during the study period; if they had missing data for the variables of interest; or if they had asked to have their data removed from the cohort. After blood assay and genotyping quality control procedures, 2776 participants with serum lipid and CRP data remained (100% female). At the time of inclusion, their average age was 47.97 years (SD 4.28).

### **7.3.2 Blood marker processing**

Participants were asked to fast overnight or for a minimum of six hours before their clinic visit. Blood samples were taken using standard procedures, and the blood was centrifuged immediately and frozen at a temperature of  $-80^{\circ}\text{C}$ . The measurements

were assayed between three and nine months later, with no previous freeze-thaw cycles during this period. Plasma lipids (total cholesterol, triglycerides, and LDL and HDL cholesterol) were assayed using the Lipid Research Clinics Protocol with enzymatic reagents (Technicon RA500). LDL cholesterol concentration was calculated using the Friedewald equation:  $LDL = TC - HDL - (TG/2.2)$  (Friedewald, Levy and Fredrickson, 1972). CRP was measured using an automated particle-enhanced immunoturbidimetric assay (Roche UK, Welwyn Garden City, UK). Assay coefficients of variation were less than 5%.

CRP is an acute phase reactant, increasing in response to systemic insults, such as infection (Osei-Bimpong, Meek and Lewis, 2007). Participants with CRP values  $>10\text{mg/l}$  ( $n = 104$ ), which may have been a response to intercurrent illness, were removed from the analysis. There are a number of single gene disorders that cause dyslipidaemias, known as Familial Hypercholesterolaemia. These are common autosomal dominant conditions, with a frequency of around 1 in 200–500 in European populations (Nordestgaard *et al.*, 2013). A number of gene carriers have been identified among the ALSPAC offspring (Futema *et al.*, 2017). According to the Simon Broome criteria for Familial Hypercholesterolaemia, possible single gene disorders are indicated by LDL cholesterol of greater than  $4.9\text{mmol/L}$  or total cholesterol greater than  $7.5\text{mmol/L}$  in an adult, either untreated or the highest on treatment (Marks *et al.*, 2003). Participants who met these criteria ( $n = 12$ ) were excluded from the analysis. Metrics were curated and stored in files compatible with R.

### **7.3.3 Genotyping**

The genotyping procedures for ALSPAC have been described in detail in Chapter 4 and summarised in previous experimental chapters. Briefly, participants were genotyped using the Illumina HumanHap550 quad genome-wide SNP genotyping platform (Illumina Inc., San Diego, California, USA). Quality control was executed in PLINK (Purcell *et al.*, 2007). As described in Chapter 4, participants were excluded for: i) ambiguous sex; ii) cryptic relatedness; iii) suboptimal genotyping completeness; and iv) non-British or Irish ancestry. SNPs were excluded based on the following

criteria: i) minor allele frequency (MAF) < 1%; ii) SNP call rate < 98%; iii)  $\chi^2$  test for Hardy-Weinberg equilibrium  $p < 1 \times 10^{-4}$ .

### 7.3.4 Polygenic Score Calculations

As described in Chapters 4, 5 and 6, PRS were calculated using the procedure developed by the International Schizophrenia Consortium (Purcell *et al.*, 2009). SNPs were selected from the discovery sample, the largest Genome-wide Association Study (GWAS) of late onset AD to date (Kunkle *et al.*, 2019). First, SNPs with a low MAF (< .01) were excluded. Second, the data were pruned for linkage disequilibrium in PLINK (Purcell *et al.*, 2007) using the clumping function (--clump; parameters  $r^2 > 0.2$  (--clump-r2) and 500 kilobases (--clump-kb)). Finally, PRS were computed in PLINK (--score) (Purcell *et al.*, 2007). As in previous experiments, a  $P^T$  of 0.001 was applied for the primary analysis, and seven graduated thresholds were used ( $p = 0.5, 0.3, 0.1, 0.01, 0.0001, 0.00001, 0.000001$ ) for a secondary analysis. Pathway gene sets reported by Kunkle and colleagues (Kunkle *et al.*, 2019) were used to produce lists of SNPs which were then matched to the discovery sample. Polygenic scores were computed using the methods described above. These are summarised in Table 4.2 in Chapter 4.

### 7.3.5 Statistical Analysis

As for the experiments described in Chapters 5 and 6, statistical analyses were conducted in R Studio version 1.1.383 for Mac, [www.rstudio.com](http://www.rstudio.com) (R Development Core Team 3.0.1., 2013). Linear multiple regression was used to investigate associations between PRS and blood marker phenotypes, co-varying for age and ten principal components to adjust for population structure. As for previous experiments, the False Discovery Rate (FDR) was used to correct for multiple comparisons of phenotype and PRS in the R statistical computing package (R Development Core Team 3.0.1., 2013). To determine how much of the signal was explained by *APOE* alone, results were re-analysed using genome-wide and pathway PRS that excluded the *APOE* region (chromosome 19 between 44.4Mb and 46.5Mb) and using a PRS comprising only SNPs in the *APOE* region.

## 7.4 Results

P values reported correspond only to the PRS variable in the regression model. The primary analysis, reported below, used a  $P^T$  of 0.001.

### 7.4.1 C-Reactive Protein

There were significant associations between increased genome wide PRS and decreased CRP in the PRS for protein–lipid complex assembly ( $p = 3.11 \times 10^{-5}$ ,  $R^2 = 6.24 \times 10^{-3}$ ), regulation of A $\beta$  formation ( $p = 1.10 \times 10^{-4}$ ,  $R^2 = 5.39 \times 10^{-3}$ ), protein–lipid complex ( $p = 1.48 \times 10^{-4}$ ,  $R^2 = 5.18 \times 10^{-3}$ ), regulation of amyloid precursor protein catabolic process ( $p = 1.10 \times 10^{-4}$ ,  $R^2 = 5.39 \times 10^{-3}$ ), tau protein binding ( $p = 1.73 \times 10^{-4}$ ,  $R^2 = 5.08 \times 10^{-3}$ ), reverse cholesterol transport ( $p = 1.14 \times 10^{-4}$ ,  $R^2 = 5.36 \times 10^{-3}$ ), protein–lipid complex subunit organization ( $p = 3.96 \times 10^{-5}$ ,  $R^2 = 6.08 \times 10^{-3}$ ), plasma lipoprotein particle assembly ( $p = 6.00 \times 10^{-5}$ ,  $R^2 = 5.80 \times 10^{-3}$ ), genome-wide PRS ( $p = 1.24 \times 10^{-4}$ ,  $R^2 = 5.30 \times 10^{-3}$ ). There was no association between CRP and the activation of immune response PRS ( $p = 0.542$ ,  $R^2 = 1.34 \times 10^{-4}$ ). None of the PRS were associated with CRP when the *APOE* region was excluded from the score, although the direction of the effect was the same. See Table 7.1 and 7.2 for a summary of results with those surviving FDR correction indicated. Figures 7.1-7.5 show the p values, variance explained ( $R^2$ ) and direction of effect across p value thresholds. Figure 7.6 shows a density plot of the correlation between genome-wide PRS and CRP.

### 7.4.2 Blood Lipids

There were significant positive associations between the genome-wide PRS, LDL and total cholesterol ( $p = 0.014$ ,  $R^2 = 2.07 \times 10^{-3}$  and  $p = 0.044$ ,  $R^2 = 1.37 \times 10^{-3}$  respectively), although the result for total cholesterol was no longer significant after correction for multiple comparisons. There were also significant positive correlations between PRS for protein–lipid complex assembly, regulation of A $\beta$  formation, protein–lipid complex, regulation of amyloid precursor protein catabolic process, tau protein binding, reverse cholesterol transport, protein–lipid complex subunit organization, plasma lipoprotein particle assembly and LDL, vLDL and total

cholesterol ( $p$  range = 0.014 -  $6.0 \times 10^{-7}$ ,  $R^2$  range 2.15 -  $8.56 \times 10^{-3}$ ). None of these positive correlations remained when the *APOE* region was removed from the PRS. When the *APOE* region was excluded, the protein-lipid complex and tau protein binding PRS showed a significant negative correlation with LDL ( $p = 0.012$ ,  $R^2 = 2.15 \times 10^{-3}$  and  $p = 0.015$ ,  $R^2 = 2.03 \times 10^{-3}$  respectively) and total cholesterol ( $p = 0.004$ ,  $R^2 = 2.73 \times 10^{-3}$  and  $p = 0.008$ ,  $R^2 = 2.34 \times 10^{-3}$  respectively). See Table 7.1 and 7.2 for a summary of results with those surviving FDR correction indicated. Figures 7.1-7.5 show the  $p$  values, variance explained ( $R^2$ ) and direction of effect across  $p$  value thresholds.

**Figure 7.1** Associations between genome-wide PRS, CRP and blood lipids across  $p$  value thresholds. Serum phenotypes are shown on the X axis, the beta coefficients (positive and negative) are shown on the Y axis. The heights of the bars indicate the amount of variance explained ( $R^2$ ), and any nominally significant results are labelled with their  $p$  value. Each bar represents a version of the polygenic risk score. The bars are colour coded by the  $p$  value threshold used in the training data, shown on the legend.

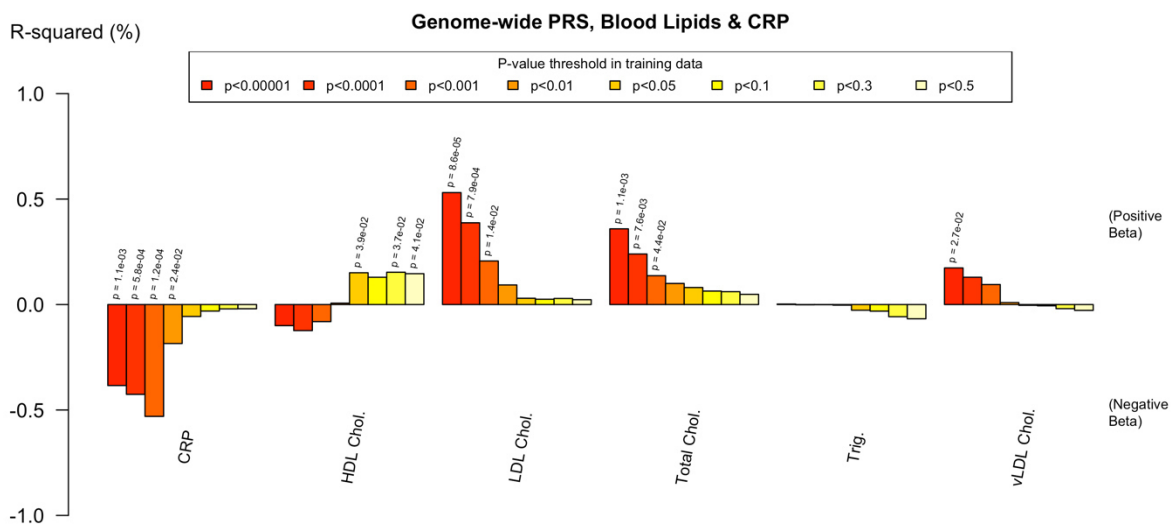


**Figure 7.2** Associations between genome wide PRS excluding APOE, CRP and blood lipids across p value thresholds. Serum phenotypes are shown on the X axis, the beta coefficients (positive and negative) are shown on the Y axis. The heights of the bars indicate the amount of variance explained ( $R^2$ ), and any nominally significant results are labelled with their p value. Each bar represents a version of the polygenic risk score. The bars are colour coded by the p value threshold used in the training data, shown on the legend.

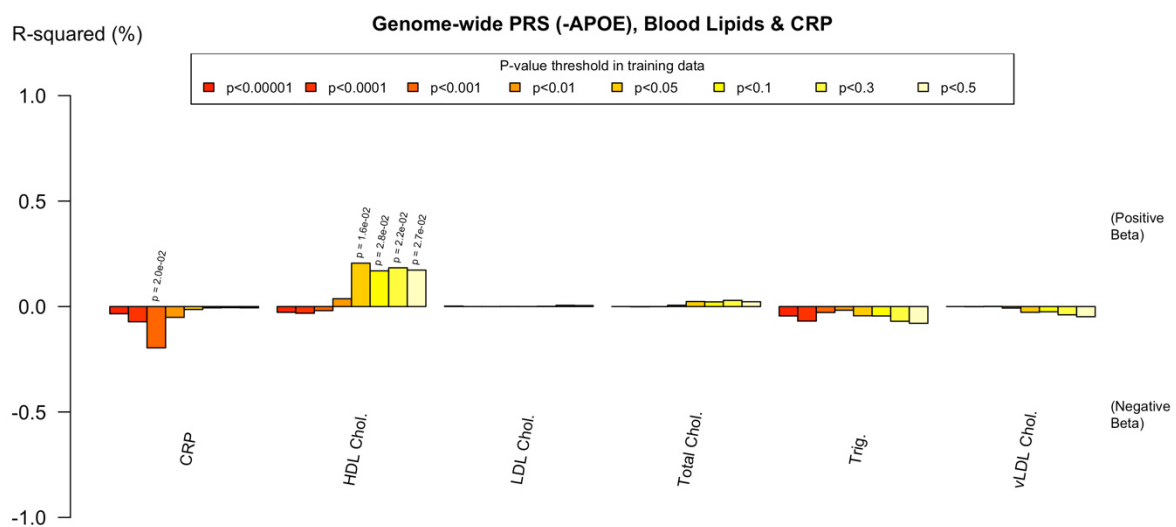


**Figure 7.3** Associations between APOE region SNPs only, CRP and blood lipids across p value thresholds. Serum phenotypes are shown on the X axis, the beta coefficients (positive and negative) are shown on the Y axis. The heights of the bars indicate the amount of variance explained ( $R^2$ ), and any nominally significant results are labelled with their p value. Each bar represents a version of the polygenic risk score. The bars are colour coded by the p value threshold used in the training data, shown on the legend.

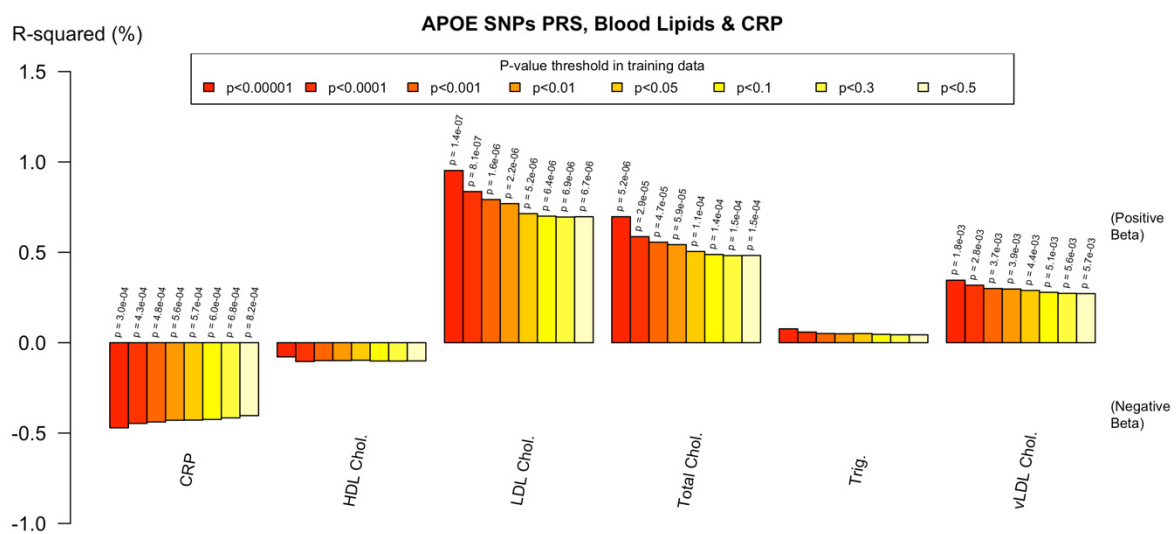


**Figure 7.4.** Associations between tau protein-binding PRS, CRP and blood lipids across p value thresholds. Serum phenotypes are shown on the X axis, the beta coefficients (positive and negative) are shown on the Y axis. The heights of the bars indicate the amount of variance explained ( $R^2$ ), and any nominally significant results are labelled with their p value. Each bar represents a version of the polygenic risk score. The bars are colour coded by the p value threshold used in the training data, shown on the legend.

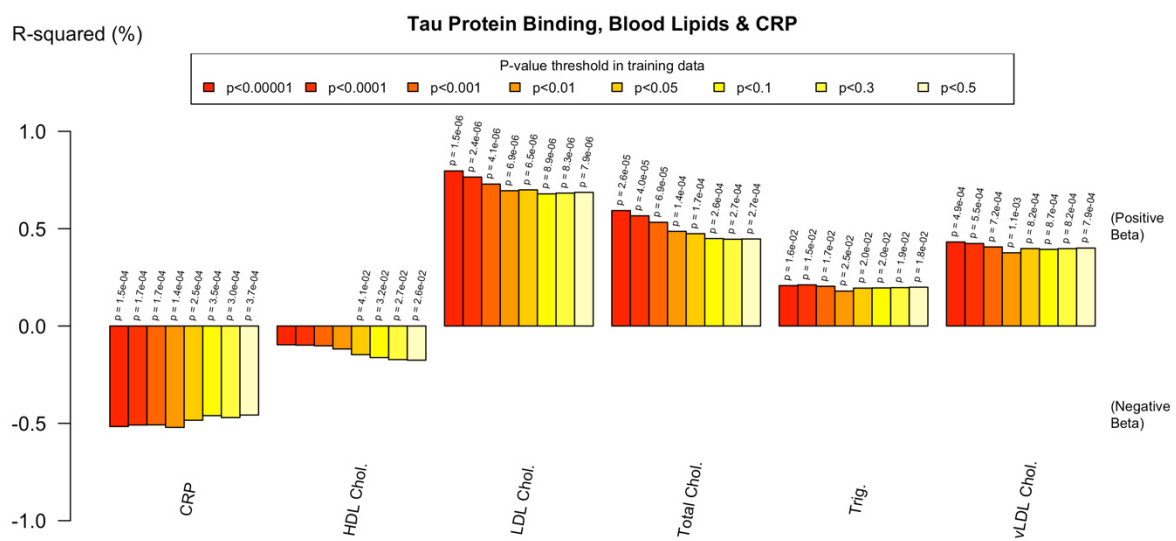


**Figure 7.5.** Associations between tau protein-binding PRS excluding the APOE region, CRP and blood lipids across p value thresholds. Serum phenotypes are shown on the X axis, the beta coefficients (positive and negative) are shown on the Y axis. The heights of the bars indicate the amount of variance explained ( $R^2$ ), and any nominally significant results are labelled with their p value. Each bar represents a version of the PRS. The bars are colour coded by the p value threshold used in the training data, shown on the legend.

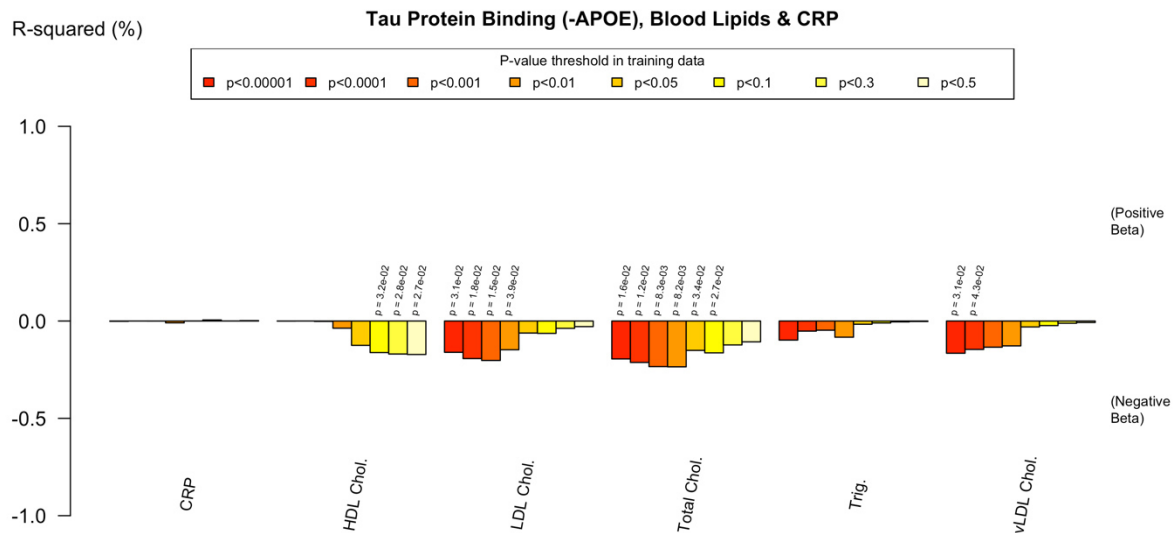


**Figure 7.6** A scatter plot showing the correlation between normalised genome-wide PRS and normalised CRP. White circles indicate individual data points. Density represents the number of data points in each area.

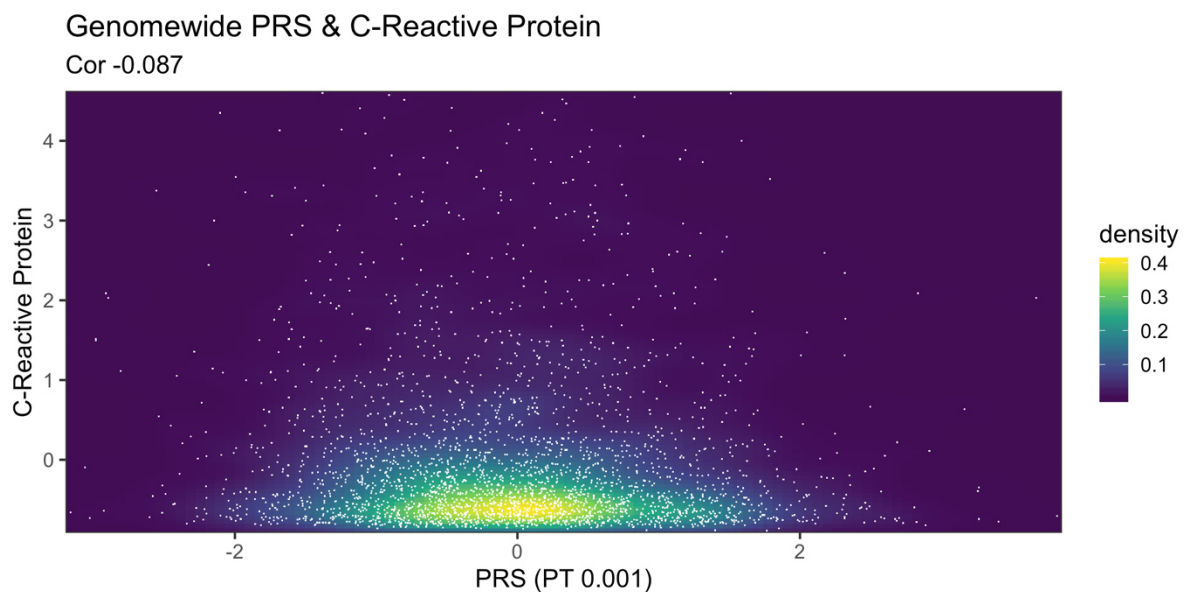


**Table 7.1 Results for maternal blood marker phenotypes and PRS including APOE at P<sup>T</sup> 0.001**

Polygenic risk score	C-Reactive Protein		HDL Cholesterol		LDL Cholesterol		Total Cholesterol		Triglycerides		vLDL Cholesterol	
	R <sup>2</sup> p (95% CI)	R <sup>2</sup> p (95% CI)	R <sup>2</sup> p (95% CI)	R <sup>2</sup> p (95% CI)	R <sup>2</sup> p (95% CI)	R <sup>2</sup> p (95% CI)	R <sup>2</sup> p (95% CI)	R <sup>2</sup> p (95% CI)	R <sup>2</sup> p (95% CI)	R <sup>2</sup> p (95% CI)	R <sup>2</sup> p (95% CI)	
<b>Protein-lipid complex assembly</b>	6.24E-03 3.11E-05 (-0.208,-0.075)**	1.19E-03 0.066 (-0.023,0.001)	8.06E-03 1.28E-06 (0.026,0.061)**	5.65E-03 4.10E-05 (0.033,0.092)**	1.29E-03 0.058 (-0.001,0.039)							
<b>Regulation of Aβ formation</b>	5.39E-03 1.10E-04 (-0.201,-0.066)**	5.97E-04 0.193 (-0.020,0.004)	4.23E-03 4.54E-04 (0.014,0.050)**	3.14E-03 0.002 (0.017,0.078)**	6.33E-04 0.184 (-0.007,0.034)							
<b>Protein-lipid complex</b>	5.18E-03 1.48E-04 (-0.196,-0.063)**	1.14E-03 0.072 (-0.023,0.001)	6.62E-03 1.14E-05 (0.022,0.057)**	4.68E-03 1.90E-04 (0.027,0.087)**	1.58E-03 0.036 (0.001,0.041)**							
<b>Regulation of amyloid precursor protein catabolic process</b>	5.39E-03 1.10E-04 (-0.201,-0.066)**	5.97E-04 0.193 (-0.020,0.004)	4.23E-03 4.54E-04 (0.014,0.050)**	3.14E-03 0.002 (0.017,0.078)**	6.33E-04 0.184 (-0.007,0.034)							
<b>Tau protein binding</b>	5.08E-03 1.73E-04 (-0.195,-0.061)**	1.02E-03 0.089 (-0.022,0.002)	7.29E-03 4.11E-06 (0.024,0.059)**	5.33E-03 6.86E-05 (0.031,0.091)**	2.04E-03 0.017 (0.004,0.044)**							
<b>Reverse cholesterol transport</b>	5.36E-03 1.14E-04 (-0.197,-0.065)**	1.24E-03 0.061 (-0.023,0.001)	7.19E-03 4.81E-06 (0.024,0.059)**	5.14E-03 9.14E-05 (0.030,0.089)**	2.00E-03 0.018 (0.004,0.044)**							
<b>Protein-lipid complex subunit organization</b>	6.08E-03 3.96E-05 (-0.206,-0.073)**	1.06E-03 0.083 (-0.022,0.001)	8.56E-03 6.00E-07 (0.027,0.062)**	6.17E-03 1.83E-05 (0.036,0.095)**	1.55E-03 0.038 (0.001,0.041)**							
<b>Plasma lipoprotein particle assembly</b>	5.80E-03 6.00E-05 (-0.202,-0.070)**	9.00E-04 0.110 (-0.021,0.002)	7.48E-03 3.16E-06 (0.024,0.059)**	5.40E-03 6.10E-05 (0.031,0.091)**	1.07E-03 0.084 (-0.002,0.037)							
<b>Activation of immune response</b>	1.34E-04 0.542 (-0.088,0.046)	3.16E-04 0.344 (-0.006,0.018)	3.35E-03 0.002 (0.011,0.046)**	2.95E-03 0.003 (0.015,0.076)**	4.03E-04 0.290 (-0.031,0.009)							
<b>Genome-wide PRS</b>	5.30E-03 1.24E-04 (-0.196,-0.064)**	8.08E-04 0.130 (-0.021,0.003)	2.07E-03 0.014 (0.004,0.039)**	1.37E-03 0.044 (0.001,0.060)**	7.79E-06 0.883 (-0.021,0.018)							

R<sup>2</sup> and p values for diffusion metrics and each polygenic score at a P<sup>T</sup> of 0.001. The column names shows the phenotypes, while the row names show the polygenic scores.

\* Nominally significant associations (p value < .05).

\*\* FDR corrected associations <0.05.

Acronyms: PRS = Polygenic Risk Score; p<sup>T</sup> = polygenic threshold; APOE = Apolipoprotein E; FDR = false discovery rate; HDL = High Density Lipoprotein; LDL = Low Density Lipoprotein; vLDL = very Low Density Lipoprotein.

**Table 7.2 Results for maternal blood marker phenotypes and PRS excluding APOE at  $P^T$  0.001**

Polygenic risk score	C-Reactive Protein		HDL Cholesterol		LDL Cholesterol		Total Cholesterol		Triglycerides		VLDL Cholesterol	
	$R^2$	p (95% CI)	$R^2$	p (95% CI)	$R^2$	p (95% CI)	$R^2$	p (95% CI)	$R^2$	p (95% CI)	$R^2$	p (95% CI)
Protein-lipid complex assembly (-APOE)	2.73E-04	0.384 (-0.096,0.037)	7.74E-04	0.138 (-0.021,0.003)	3.85E-04	0.291 (-0.027,0.008)	7.65E-04	0.132 (-0.053,0.007)	2.01E-04	0.454 (-0.027,0.012)	7.16E-05	0.654 (-0.011,0.007)
Regulation of A $\beta$ formation (-APOE)	1.44E-04	0.528 (-0.089,0.046)	2.39E-06	0.934 (-0.011,0.012)	1.41E-03	0.043 (-0.036,-0.001)*	1.08E-03	0.074 (-0.058,0.003)	3.54E-04	0.321 (-0.030,0.010)	3.80E-04	0.302 (-0.014,0.004)
Protein-lipid complex (-APOE)	7.80E-05	0.642 (-0.082,0.050)	2.08E-04	0.443 (-0.016,0.007)	2.15E-03	0.012 (-0.040,-0.005)**	2.73E-03	0.004 (-0.073,-0.013)**	1.71E-03	0.029 (-0.042,-0.002)*	1.60E-03	0.034 (-0.018,-0.001)*
Regulation of amyloid precursor protein catabolic process (-APOE)	1.44E-04	0.528 (-0.089,0.046)	2.39E-06	0.934 (-0.011,0.012)	1.41E-03	0.043 (-0.036,-0.001)*	1.08E-03	0.074 (-0.058,0.003)	3.54E-04	0.321 (-0.030,0.010)	3.80E-04	0.302 (-0.014,0.004)
Tau protein binding (-APOE)	2.49E-06	0.934 (-0.069,0.064)	1.85E-05	0.819 (-0.013,0.010)	2.03E-03	0.015 (-0.039,-0.004)**	2.34E-03	0.008 (-0.070,-0.010)**	4.72E-04	0.252 (-0.031,0.008)	0.052 (-0.018,6.90E-05)	1.34E-03
Reverse cholesterol transport (-APOE)	3.33E-04	0.337 (-0.099,0.034)	6.05E-04	0.190 (-0.020,0.004)	7.27E-04	0.146 (-0.031,0.005)	1.16E-03	0.063 (-0.058,0.002)	1.90E-04	0.468 (-0.027,0.012)	0.489 (-0.012,0.006)	1.71E-04
Protein-lipid complex subunit organization (-APOE)	7.66E-05	0.645 (-0.082,0.051)	5.79E-04	0.200 (-0.019,0.004)	2.93E-04	0.356 (-0.026,0.009)	5.39E-04	0.206 (-0.049,0.011)	2.56E-05	0.790 (-0.017,0.023)	0.982 (-0.009,0.009)	1.87E-07
Plasma lipoprotein particle assembly (-APOE)	1.93E-04	0.465 (-0.091,0.042)	2.86E-04	0.368 (-0.017,0.006)	1.38E-04	0.528 (-0.023,0.012)	2.98E-04	0.347 (-0.044,0.016)	4.48E-04	0.264 (-0.031,0.009)	0.592 (-0.011,0.006)	1.02E-04
Activation of immune response (-APOE)	2.30E-04	0.424 (-0.039,0.094)	2.06E-04	0.445 (-0.007,0.016)	1.17E-03	0.065 (-0.001,0.034)	1.03E-03	0.081 (-0.003,0.056)	3.62E-04	0.315 (-0.030,0.010)	0.864 (-0.010,0.008)	1.05E-05
Genome-wide PRS (-APOE)	1.96E-03	0.020 (-0.143,-0.012)*	1.94E-04	0.458 (-0.016,0.007)	1.10E-06	0.955 (-0.018,0.017)	4.59E-06	0.907 (-0.031,0.028)	2.82E-04	0.375 (-0.028,0.011)	0.889 (-0.008,0.009)	6.95E-06
APOE SNPs PRS	4.38E-03	4.84E-04 (-0.184,-0.052)**	9.89E-04	0.094 (-0.022,0.002)	7.92E-03	1.59E-06 (0.025,0.060)**	5.56E-03	4.75E-05 (0.032,0.091)**	5.09E-04	0.234 (-0.008,0.032)	0.004 (0.004,0.022)**	3.00E-03

R<sup>2</sup> and p values for diffusion metrics and each polygenic score at a  $P^T$  of 0.001. The column names shows the phenotypes, while the row names show the polygenic scores.

\* Nominally significant associations (p value < .05).

\*\* FDR corrected associations <0.05.

Acronyms: PRS = Polygenic Risk Score;  $P^T$  = polygenic threshold; APOE = Apolipoprotein E; FDR = false discovery rate; HDL = High Density Lipoprotein; LDL = Low Density Lipoprotein; vLDL = very Low Density Lipoprotein.

## 7.5 Discussion

In line with the hypothesis, increased polygenic risk for AD was associated with increased blood lipids, particularly LDL and total cholesterol. These results were reflected across the genome-wide PRS and the pathway-specific PRS, and withstood corrections for multiple comparisons. CRP was negatively associated with increased genome-wide PRS and with most of the pathway PRS. The results attenuated when SNPs in the *APOE* region were excluded from the PRS.

Previous studies have investigated pleiotropic genetic enrichment in AD as a function of blood lipid profiles (Broce *et al.*, 2018), and associations between genome-wide and immune specific AD PRS and inflammatory markers (Morgan *et al.*, 2017). This was the first study to use AD pathway specific PRS to investigate blood lipid phenotypes. Although Morgan *et al.* took a similar approach to investigate inflammatory markers including CRP, the findings can only be considered preliminary as the study had limited statistical power (smaller discovery sample (Lambert *et al.*, 2013); target sample  $n = 93$  AD cases (Morgan *et al.*, 2017)).

The associations identified between AD polygenic profiles and blood lipids were consistent with the previous literature. A previous study identified an association between AD PRS and blood lipids, particularly LDL cholesterol, both in infancy and longitudinally throughout childhood. However, there were no consistent associations excluding variants in the *APOE* region (Korologou-Linden, O’Keeffe, *et al.*, 2019). A phenome-wide association study (PheWAS) by the same group found that higher PRS for AD was associated with prescriptions of cholesterol-lowering medicines (Korologou-Linden, Anderson, *et al.*, 2019).

Significant genetic pleiotropy has been identified between plasma lipids and AD. Broce and colleagues identified 90 SNPs on 19 different chromosomes excluding *APOE* that jointly increased risk for AD and cardiovascular disease. There was significant enrichment of the polygenic component of AD and blood lipids (Broce *et al.*, 2019). Desikan *et al.* also demonstrated significant genetic overlap between AD, blood lipids and CRP. By conditioning SNPs on the association with cardiovascular phenotypes,

they also identified a number of novel loci conferring increased risk for AD (Desikan *et al.*, 2015).

Mendelian randomization (MR) is a novel method for determining causal relationships between exposures and outcomes. MR estimates the causal association between an exposure (e.g. hypercholesterolaemia) and an outcome (e.g. dementia) using genetic variants as proxies for exposures (Davey Smith and Ebrahim, 2003). Andrews and colleagues used MR to demonstrate a causal relationship between serum cholesterol levels and AD (Andrews, Marcora and Goate, 2019). A further study by Andrews *et al.* used both PRS and MR methods to identify a causal association between total and LDL cholesterol and increased neuritic plaques, however the effects were driven by SNPs in the *APOE* locus. In addition, total serum cholesterol was associated with lower hippocampal volume (Andrews *et al.*, 2021).

Although the link between aberrant lipid metabolism and AD is undisputed, the exact molecular mechanisms by which altered blood lipids contribute to neurodegeneration are not clear. Peripheral cholesterol concentrations do not reflect cholesterol levels within the blood brain barrier. The brain synthesises cholesterol internally, in astrocytes and microglia. The *APOE* gene codes for the ApoE protein, and ApoE lipoprotein particles convey the cholesterol to neurons and oligodendrocytes, where it is used for synaptogenesis, synapse repair and dendritic spine integrity. *APOE4* is less effective in this than *APOE3* (Bu, 2009). Furthermore, ApoE protein and ApoE receptors clear amyloid- $\beta$  ( $A\beta$ ) from the brain. *APOE3* binds  $A\beta$  more effectively than *APOE4*. Therefore, *APOE3* mediates  $A\beta$  clearance more efficiently via ApoE receptors (Bu, 2009). In serum,  $A\beta$  is transported to the liver for elimination in HDL cholesterol particles (Koudinov *et al.*, 1998). It has been suggested that *APOE* may also modulate AD susceptibility by affecting the systemic clearance of  $A\beta$ -HDL in the liver (Jones *et al.*, 2010).

Contrary to the hypothesis, this study found no association between CRP and the immune response pathway PRS, as reported by an earlier study (Morgan *et al.*, 2017). In the present study, there was a significant negative association between CRP and the genome-wide PRS. A trend toward significance remained at  $P^T = 0.001$  when SNPs in the *APOE* locus were removed. Of note, the Morgan *et al.* study was based

on an earlier GWAS and a previous pathways analysis (Jones *et al.*, 2010; Lambert *et al.*, 2013). Therefore, the immune response PRS used in that study did not contain exactly the same SNPs as the equivalent PRS in the present study. Please see Chapter 2 for a detailed description of the factors that can influence the selection of SNPs in PRS studies.

CRP is an acute-phase reactant produced by the liver in response to inflammatory stimuli such as acute infection or injury. A number of studies have reported links between AD and CRP. Significant genetic pleiotropy has been reported between CRP and AD risk loci (Desikan *et al.*, 2015). Histological analyses have observed associations between CRP, neurofibrillary tangles (Duong, Nikolaeva and Acton, 1997) and senile plaques (Iwamoto *et al.*, 1994) in the brain tissue of AD patients. One study also found CRP was associated with cortical thinning (Corlier *et al.*, 2018).

One might expect that elevated CRP would be associated with AD. However, the literature is contradictory. CRP is not associated with cognitive decline in older people (Dik *et al.*, 2005). Whilst a longitudinal study reported an association between raised CRP in midlife and increased risk for AD (Schmidt *et al.*, 2002), and one case-control study reported higher CRP in AD patients (Song *et al.*, 2015), other studies find that there is either no difference between cases and controls (Licastro *et al.*, 2000; Swardfager *et al.*, 2010; Miwa *et al.*, 2016; Ng *et al.*, 2018) or that CRP is *lower* in AD cases (Hu *et al.*, 2012; O'Bryant *et al.*, 2013; Yarchoan *et al.*, 2013). Similarly, a study of post-surgical neurodegeneration showed that lower CRP was associated with greater atrophy in the post-operative period. This effect was only evident in *APOE4* carriers (Kline and Cuadrado, 2014). A number of other studies have demonstrated that *APOE4* carriers (both AD cases and healthy controls) have significantly lower CRP concentrations compared to non-carriers (Chasman *et al.*, 2006; Haan *et al.*, 2008; Soares *et al.*, 2012). The estimated variance in plasma CRP explained by *APOE* alleles is around 3.5-4.1% (Chasman *et al.*, 2006).

Studies exploring the effect of loci associated with the immune response are also discrepant. Pro-inflammatory polymorphisms for CRP have no effect on brain atrophy in healthy participants (Persson *et al.*, 2014) and are not associated with incident dementia (Miwa *et al.*, 2016). Whilst a previous study reported some evidence of

association between CRP levels and an inflammatory-specific AD PRS (Morgan *et al.*, 2017) this study was limited by low statistical power. A more recent study reported that a higher PRS comprising AD risk variants linked to immunity (besides *APOE*) was associated with cortical thinning, however levels of CRP did not mediate the effect (Corlier *et al.*, 2018). A recent MR study investigating the effect of inflammatory cytokines found no evidence of association with AD risk, however the authors noted that systemic inflammatory regulators could be downstream effects of AD or inflammation and AD could both result from common factors (Yeung and Schooling, 2020). Taken together, the literature supports the association between increased polygenic risk for AD and decreased CRP observed in this experiment, suggesting that other mechanisms, involving other inflammatory signals, may underlie the relationship between immune-associated variants and elevated AD risk.

The molecular mechanisms through which *APOE* affects CRP are not well understood. The effect of *APOE* genotype on LDL and total cholesterol appears to be mediated by the level of ApoE protein produced from the  $\epsilon 4$  allele compared to  $\epsilon 2$  or  $\epsilon 3$  alleles (Chasman *et al.*, 2006). Conversely, there is much less evidence of association between CRP and ApoE protein levels (Chasman *et al.*, 2006). Instead, the effect of *APOE* on CRP may be mediated by functional differences such as the amino acid substitution from cysteine to arginine at residue 112 present in *APOE4* (Chasman *et al.*, 2006).

This study found some evidence that polygenic risk for AD contributes to levels of blood lipids and CRP beyond *APOE* alone. For example, the protein–lipid complex subunit organization PRS was positively associated with total cholesterol, LDL, vLDL and triglycerides with *APOE* included. Whilst the associations were no longer significant when *APOE* was omitted, some of the PRS, the protein–lipid complex subunit organization PRS for example, showed slightly more evidence of association with these phenotypes than *APOE* alone (greater explained variance and smaller p values). This is in keeping with the findings of a previous study that reported enrichment of the polygenic AD serum lipids besides *APOE* (Broce *et al.*, 2019), although in contrast to findings in children (Korologou-Linden, O’Keeffe, *et al.*, 2019). Similarly, the genome-wide PRS was significantly negatively associated with decreased CRP with *APOE*, and when *APOE* was excluded the association remained

at  $P^T = 0.001$ . However, it was not significant at other  $P^T$ , and did not withstand correction for multiple comparisons. In line with the results of other experiments reported in this thesis, and in contrast to the findings of one previous study (Caspers *et al.*, 2020), there was a similar pattern of association between pathway PRS associated with different areas of pathophysiology.

### **7.5.1 Strengths and limitations**

This study has a number of advantages, many of which are similar to those described in Chapters 5 and 6. For example, this study used a large target sample size and summary statistics from the largest clinically confirmed AD GWAS available (Kunkle *et al.*, 2019). PRS and  $R^2$  are heavily influenced by the size of the discovery sample (Schizophrenia Working Group of the Psychiatric Genomics, 2014).

There are a number of limitations which must be taken into account. For example, the use of lipid lowering medications is not allowed for in this analysis. Possible autosomal dominant familial hypercholesterolaemia cases were removed by phenotype rather than genotype. It is possible that some may have remained if they had particularly well-controlled disease. Participants in ALSPAC tend to be slightly healthier and from higher socio-economic backgrounds than the general UK population (Abigail Fraser *et al.*, 2013). Those who had a genetic predisposition toward high blood lipids may have made lifestyle modifications to address their cardiovascular risk. Socioeconomic and lifestyle factors were also not accounted for in this analysis. All of these factors would reduce the likelihood of detecting a significant effect of polygenic burden on serum lipid levels. As discussed in previous Chapters, PRS combines risk variants, making it impossible to draw conclusions regarding the exact molecular mechanisms relating to alterations in phenotype.

The potential therapeutic implications of these findings are not clear. The association between raised cholesterol and AD has led a number of groups to investigate whether the cholesterol lowering drugs statins might have a role in prevention or slowing progression of AD (Jick *et al.*, 2000; Santos *et al.*, 2017). Similarly, epidemiological studies suggesting non-steroidal anti-inflammatory drugs (NSAIDs) were associated with decreased risk of AD also raised hopes that they may prove useful for AD

prevention (Szekely *et al.*, 2004). However, large-scale randomized controlled trials found little evidence of clinical benefit for either treatment (McGuinness *et al.*, 2009; Pasqualetti *et al.*, 2009; Imbimbo, Solfrizzi and Panza, 2010), showing that an improved understanding of the disease processes mediating these effects is required.

Future studies would benefit from longitudinal follow-up, assessment of other relevant biomarkers such as CSF and neuroimaging changes, detailed modelling of potential socioeconomic, lifestyle and treatment confounders, and use of techniques such as MR to assess causality. Such studies will also require large sample sizes to allow further pathway-based analyses.

### **7.5.2 Conclusion**

Increased polygenic risk for AD was associated with increased blood lipids, particularly LDL and total cholesterol, and decreased CRP. This is in keeping with the findings of previous investigations. Although none of the PRS were significant when *APOE* was omitted, some of the PRS explained greater variance in phenotypes than *APOE* alone. The pattern of associations was similar across all versions of PRS. The contribution of the polygenic component of AD to these phenotypes (besides *APOE*) will need to be confirmed by further studies. Additional investigations into the exact biological mechanisms through which they contribute to AD pathophysiology is also needed.

## **CHAPTER 8: DISCUSSION**

In this thesis, volumetric and diffusion MRI and serum lipid and inflammatory markers were used to investigate manifestations of AD polygenic risk. Specifically, these analyses sought to determine 1) whether AD polygenic risk scores (PRS) were associated with neuroimaging and blood marker phenotypes linked to neurodegeneration in younger and older adult cohorts; and 2) whether PRS informed by disease pathways were associated with different patterns of alteration in brain structure, serum lipids or inflammatory markers.

Two systematic reviews were conducted to assess the current literature on 1) the association between AD PRS and dementia-relevant phenotypes and 2) the effect of AD risk genes on white matter microstructure assessed with diffusion MRI. Three experiments were conducted to address the above questions. First, as described in Chapter 5, volumetric MRI, specifically surface-based analysis of T1 MRI data, was used to investigate grey matter structure. Second, as described in Chapter 6, both region-of-interest and tract-skeleton based diffusion MRI analyses were used to assess white matter microstructure. Finally, as described in Chapter 7, serum lipid and inflammatory markers, specifically low density lipoprotein (LDL), high density lipoprotein (HDL), total cholesterol, triglycerides and C-Reactive Protein (CRP), were used to determine how polygenic risk for AD manifested in the metabolome.

### **8.1 Summary of findings**

Findings from the analyses described in this thesis contribute to our understanding of how polygenic risk for AD manifests in brain structure and serum markers of lipids and inflammation. Furthermore, it demonstrated how sets of SNPs involved in disease pathway groups can be used to inform polygenic analyses.

Chapter 2 systematically reviewed the literature that used PRS to study phenotypes relevant to AD. This chapter presented a narrative synthesis of 57 published studies found to meet the criteria for inclusion in the ten years sampled (2008-2018). Many of the studies were published toward the end of this period, showing the increasing popularity of the method. The evidence suggests that PRS can predict AD relatively

accurately (AUC 70-75%) (Escott-Price, Sims, Bannister, *et al.*, 2015; Altmann *et al.*, 2020). A number of studies demonstrate evidence of association with cognitive problems, and other phenotypes associated with dementia. The PRS approach has also been used to study neuroimaging changes and biomarkers in cerebrospinal fluid (CSF). A few more recent studies have also attempted to create gene sets based on evidence of enrichment in functional categories. However, none of the studies included in the review had been sufficiently powered to combine this pathway-based approach with selecting SNPs using p-value cut offs, as undertaken in this thesis.

Chapter 3 presented a systematic review of studies that explored the effect of genetic risks for AD on white matter using diffusion MRI (dMRI). It comprised a narrative synthesis of the 37 studies that met criteria for inclusion (2000-2019) and gave a detailed review of dMRI methods and their pitfalls. There was evidence that individuals with increased genetic risk for AD show increased diffusivity and reduced anisotropy throughout the white matter of the brain, particularly in temporal and frontal areas, the cingulum and the corpus callosum. Those with established disease showed more changes than pre-clinical individuals. Although dMRI lacks specificity to disease pathology, as the field develops it may prove useful in early diagnosis or disease staging.

In the first experiment, described in Chapter 5, it was demonstrated that the effect of AD polygenic risk is evident in grey matter changes even in young adults. Higher polygenic risk was associated with cortical thinning and changes in subcortical volumes. In older adults, reduced volume was particularly marked in the left accumbens and the left hippocampus. In younger adults, increased subcortical volumes was observed, particularly in the left amygdala, left hippocampus and left caudate. This is in keeping with the previous literature suggesting that genetic risk for AD may be associated with increased subcortical volume in young adults and decreased hippocampal volume in older adults. For cortical surface area, some regions showing a positive association with polygenic risk and other regions showed negative associations without a consistent pattern. Results for the cortical thickness and surface area generally did not withstand correction for multiple testing, although there was a consistent pattern of association with cortical thickness. Whilst the cortical thickness association in older adults was independent of *APOE*, in younger adults it

attenuated with *APOE* excluded. Excepting the immune response PRS, the pathway specific PRS explained a greater amount of variance than the genome-wide polygenic score in most phenotypes. The amount of variance (and significance of the p values) between most of the pathway-specific polygenic scores was comparable with that of *APOE*. However, there was no evidence of distinct patterns of grey matter alterations with different functional groups, as had been suggested by a previous study (Caspers *et al.*, 2020). Thus, the results of this experiment suggest that changes in grey matter occur very early in the life course of those at high genetic risk of AD, and that delineating SNPs sets into pathway groups enhances their association with phenotypes when compared to a standard genome-wide approach.

In the second experiment, discussed in Chapter 6, it was demonstrated that AD polygenic risk also manifests in the white matter microstructure of older adults. In keeping with the previous literature, summarised in Chapter 3, it was shown that those with increased polygenic risk for AD have reduced anisotropy and increased diffusivity in white matter tracts that are known to be affected by AD pathology, in particular the hippocampal cingulum. There was less evidence of association between polygenic risk scores and changes in white matter in younger adults, apart from some nominal associations with increased diffusivity in the left cingulum. As mentioned in Chapter 6, there were differences in the diffusion analysis frameworks implemented in the two cohorts. The patterns of association between the different PRS and white matter phenotypes were similar to the grey matter. The pathway specific PRS showed greater evidence of association and explained more of the variance than the genome wide PRS except the immune response PRS, which showed little association. The pathway specific effects were also independent of *APOE* and explained greater variance than *APOE* alone. In the older cohort, many of the associations with changes in the white matter measures remained significant after correction for multiple testing. Thus, the results of this experiment suggest that polygenic risk for AD is evident in white matter changes in mature individuals, and less so in younger people. It provides further evidence that informing the PRS using SNPs associated with functional categories is helpful to reduce noise inherent in the PRS method.

In the final experiment, described in Chapter 7, it was demonstrated that there are associations between PRS for AD, blood lipids and CRP in adults in mid-life. There

was particular evidence of association between increased PRS and increased LDL and total cholesterol. There was also evidence of a negative association between the PRS and CRP. Unlike the neuroimaging phenotypes, the pathway-specific PRS did not show greater evidence of association than the genome-wide score. The results were driven by *APOE* to a great extent, with few remaining even nominally significant when *APOE* was excluded from the polygenic score. The effect of *APOE* on blood lipids and CRP is already established. Thus, the results of this thesis suggest that variation in serum lipids is primarily influenced by *APOE*, with little effect from other AD susceptibility loci, even those implicated in pathway groups related to lipids. Similarly, there was no evidence of association between SNPs in the immune response PRS (besides the *APOE* region) and CRP.

## **8.2 Implications of this research**

The results discussed in this thesis build on our understanding of how AD polygenic risk affects the brain and body metabolism. To my knowledge, no previous study has used a threshold based PRS delineated by sets of SNPs in functional categories to explore brain structure phenotypes. Although one previous study took this approach to assess blood inflammatory markers, it was significantly underpowered (Morgan *et al.*, 2017). This series of analyses therefore brings novel insights into imaging and serum markers of AD polygenic burden in healthy adults. Here, the wider implications of these findings for translational research and clinical practice are discussed.

### **8.2.1 How should we use AD polygenic scores?**

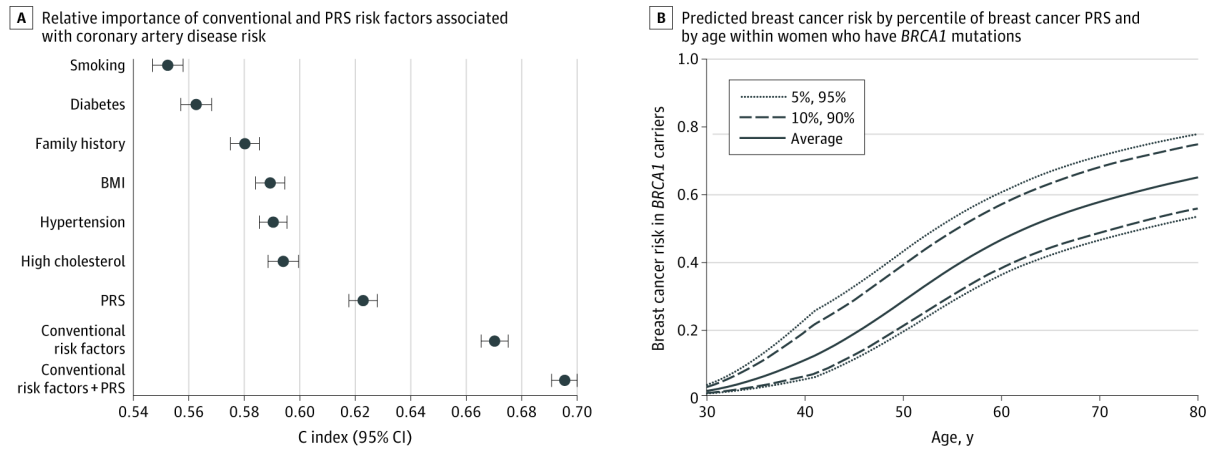
Genetic testing is an established part of clinical care. It is possible to test for thousands of monogenic diseases (*NCBI Genetic Testing Registry*, 2020). Specific services exist for the diagnosis and counselling of patients and family members affected by conditions such as Huntington's Disease and Cystic Fibrosis. As discussed in Chapter 2, PRS for AD have been shown to accurately predict disease (Escott-Price, Sims, Harold, *et al.*, 2015; Sleegers *et al.*, 2015; Xiao *et al.*, 2015; Yokoyama, Bonham, *et al.*, 2015; Escott-Price *et al.*, 2017; Chaudhury *et al.*, 2018). Therefore, some have

discussed how the information might be used in clinical practice (Khoury, Janssens and Ransohoff, 2013; Wray *et al.*, 2020).

Currently, risk stratification based on phenotypic and lifestyle risk factors is used to prevent conditions such as cardiovascular disease (D'Agostino *et al.*, 2008). These prediction tools combine multiple clinical risk factors including age, sex, blood pressure, smoking status, family history, cholesterol levels and diabetes into a total risk score. Individually, none of these risk factors are useful in predicting disease risk. However, on aggregate, they indicate the need for interventions such as the prescription of lipid lowering drugs and preventative lifestyle changes. A study using data from UK Biobank (Inouye *et al.*, 2018) found that a combined clinical risk score was more effective at predicating coronary artery disease than a PRS for coronary heart disease. However, when the PRS and clinical risk score were combined, they were more accurate than either alone (Inouye *et al.*, 2018) (Figure 8.1A). If these findings extrapolate to the wider UK population in the same age group, this might change the risk category of thousands of people (Wray *et al.*, 2020). Those with high PRS may move upward to a risk category where pharmacological treatment is advised, whereas those in a lower PRS group others may move downwards to a category in which intervention can be avoided (Wray *et al.*, 2020).

Incorporating polygenic profiles into existing screening protocols could be particularly useful where the screening tests are particularly invasive or have significant side-effects. It might be possible to focus screening on those at highest risk of disease. Screening frequency could be tailored to the individual's risk profile, with those at greatest risk receiving more frequent assessment (Wray *et al.*, 2020). At the population level, this could lower the risks relating to screening programmes and could be more cost-efficient (Autier and Boniol, 2018). Polygenic profiles could also be combined with information about rare variants to improve prediction. For example, high PRS for breast cancer in BRCA1/2 carriers is associated with younger age of cancer diagnosis (Kuchenbaecker *et al.*, 2017) (Figure 8.1B). Similarly, polygenic risk for Huntington's has been shown to accelerate disease onset (Lee *et al.*, 2015).

**Figure 8.1** Examples of PRS Applications in Heart Disease and Breast Cancer. Reproduced with permission from Wray NR, Lin T, Austin J, et al. From Basic Science to Clinical Application of Polygenic Risk Scores: A Primer. JAMA Psychiatry. Published online September 30, 2020.



- A) Conventional and polygenic risk factors for coronary heart disease. Increasing prediction accuracy is shown on the Y axis (Inouye *et al.*, 2018).
- B) Breast cancer risk predicted using percentile of breast cancer polygenic risk and age in *BRCA1* mutation carriers (Kuchenbaecker *et al.*, 2017).

The principles of screening have been reviewed by many organizations, particularly the World Health Organization (Wilson JMG, 1968), and the European Council (*Council of Europe. Recommendation NR (94) 11 on screening as a tool of preventive medicine*, 1994). These codes are designed to ensure that the benefits of screening programmes are greater than the potential harms, at the level of the population and the individual. A summary of the four key principles outlined by the Council of Europe is shown in Table 8.1. Screening is often an attractive idea, as it offers the possibility of reducing morbidity and mortality by early intervention. However, the potential for harm is often underestimated (Hoffmann and Del Mar, 2017). Screening tests will always produce some false positives, which can lead to overdiagnosis and inappropriate medical treatment, and cause significant anxiety. Similarly, harm can result from negative tests if patients are falsely reassured and treatment is delayed (Harris, 2011).

**Table 8.1** Council of Europe, Committee of Ministers, Recommendation No. R (94) 11 on Screening as a Tool of Preventive Medicine (Oct. 10, 1994) (*Council of Europe. Recommendation N R (94) 11 on screening as a tool of preventive medicine, 1994*)

---

<b>Council of Europe criteria for selecting diseases suitable for screening</b>	
1	The disease should be an obvious burden for the individual and/or the community in terms of death, suffering, economic or social costs.
2	The natural course of the disease should be well known and the disease should go through an initial latent stage or be determined by risk factors, which can be detected by appropriate tests. An appropriate test is highly sensitive and specific for the disease as well as being acceptable to the person screened.
3	Adequate treatment or other intervention possibilities are indispensable. Adequacy is determined both by proven medical effect and ethical and legal acceptability.
4	Screening followed by diagnosis and intervention in an early stage of the disease should provide a better prognosis than intervention after spontaneously sought treatment.

---

Irrespective of the accuracy of AD polygenic prediction, including or excluding other risk factors, the clinical application of AD PRS is limited until disease modifying treatments are identified. Even when therapies are available, there will still be a number of crucial questions to answer. For example, it is not clear if a given therapy would have the same effects on the disease course for those at high and low PRS. A drug may target a pathway that is not responsible for neurodegeneration in all patients. Pathway-specific polygenic profiling, as implemented in this thesis, will therefore be needed to facilitate personalised medicine. Randomized controlled trials, the gold standard assessment, are costly, need large samples, and require a long period of implementation and follow-up. It has been suggested that quasi-experimental, observational or comparative effectiveness designs might be used to assess population stratification in addition to RCTs (Goddard *et al.*, 2012; Khoury, Janssens and Ransohoff, 2013).

### **8.2.2 The role of AD biomarkers in translational research and clinical practice**

In this thesis, a number of potential biomarkers were investigated. A biomarker is any biological metric that can be used to measure physiological states or disease (Atkinson *et al.*, 2001). Biomarkers, or tests, as they are more commonly referred to in clinical practice, are used for diagnosis, to measure disease progression, or to monitor

treatment response (Strimbu and Tavel, 2010). They must be sufficiently accurate, sensitive and specific, with good inter-assessment and test-retest reliability (Hooper, Lovestone and Sainz-Fuertes, 2008).

Biomarkers may also be used as a 'surrogate endpoint' during clinical trials, in lieu of a 'clinical endpoint' (Atkinson *et al.*, 2001). A clinical endpoint is a defined patient outcome, such as morbidity or mortality. Surrogate endpoints are used to evaluate the effect of an intervention over a shorter period. An example of a surrogate endpoint is tumour shrinkage in chemotherapy trials. This should be strongly associated with clinical endpoints, e.g., survival and quality of life (Atkinson *et al.*, 2001).

Cognitive assessments can be considered an AD biomarker. There are many psychometric tests available that are used for diagnosis and staging of AD (Behl, Stefurak and Black, 2005). Such tools are reliable and low cost. However, they cannot discriminate between dementias and are unable to detect pre-symptomatic AD. Neuroimaging techniques are more sensitive to pathology and early-stage disease, as demonstrated in this thesis. As discussed above, a number of advanced MRI techniques and nuclear imaging methods can be employed in the assessment of AD pathology. However, all such methods are expensive, and some are invasive, which make them unsuitable for use at scale in pre-symptomatic populations.

The cerebrospinal fluid (CSF) allows access to the central nervous system. Total tau and phosphorylated are elevated in the CSF in AD. Levels of A $\beta$ 1–42 are also reduced (Jack Jr. *et al.*, 2010). A combination of CSF tau and A $\beta$  measurements is considered the gold standard biomarker of AD to date, (Hooper, Lovestone and Sainz-Fuertes, 2008). However, CSF sampling, by lumbar puncture, is also too invasive for widespread use in cognitively healthy individuals and can be unsafe to perform in those with advanced cognitive impairment. As a substitute for CSF, peripheral blood is easily accessible and provides abundant samples for testing. There is some evidence to suggest that the integrity of the blood brain barrier is impaired in diseases like AD, therefore metabolic changes associated with AD might be evident in peripheral blood (Hawkins and Davis, 2005). For example, blood plasma A $\beta$ 1–42 is up-regulated in carriers of *APP* and *PS1/2* (Scheuner *et al.*, 1996), but not sporadic AD cases. A number of other blood-based measures have been proposed, including:

the glycogen synthase kinase 3 (GSK3) enzyme in peripheral white blood cells (Hye *et al.*, 2004); the lipid oxidation products isoprostanes (Pratico *et al.*, 2000); the metabolic intermediate homocysteine (Seshadri *et al.* 2002); an iron transport protein p97 (Feldman *et al.*, 2001); cytokines interleukin 1 and 6; the acute phase protein/protease inhibitors  $\alpha$ -1 antichymotrypsin (Licastro *et al.*, 2000) and  $\alpha$ -2-macroglobulin; and complement factor H (Hye *et al.*, 2006). However, the only blood marker that can reasonably separate cases from controls is plasma T-tau (Olsson *et al.*, 2016), and this still requires verification in larger samples. The experiments presented in this thesis found little evidence for associations between AD PRS and blood and inflammatory markers beyond what can be explained by the function of *APOE* in the periphery. This supports the hypothesis that plasma lipid and inflammatory marker levels may reflect peripheral physiology more than AD pathology.

Chapters 5 and 6 demonstrated that increased PRS for AD was associated with changes in brain structure even in very young adults. Given the lack of other suitable non-invasive biomarkers, advanced neuroimaging techniques have the potential to help identify those at risk of developing AD before significant pathology develops. Further research would be required to identify those neuroimaging measures which are the most sensitive to very early alterations. Longitudinal studies will be needed to establish how well they correlate with other established biomarkers.

Current clinical trials rely on CSF and PET biomarkers markers for amyloid and tau to identify those with detectable pre-clinical disease. However, this assumes that the stage where there is detectable amyloid and tau load is the optimum time to intervene. Given the failure of drug trials targeting amyloid and tau, discussed in Chapter 1, they may not be driving the disease process. It is possible that neurodegeneration results from earlier pathological events, which would be in keeping with the findings of this thesis; some changes relating to AD genetic risk were evident even in very young adults. An added challenge is how to assess the impact of experimental treatments in trial participants who are pre-symptomatic. Further studies are required to investigate the most appropriate biomarkers to monitor disease progression very early in the AD prodrome. This is being assessed by proof-of-concept biomarker studies such as the Deep and Frequent Phenotyping study (Koychev *et al.*, 2019).

### **8.2.3 Value of the pathway PRS approach in AD**

One important implication of this thesis is the viability of the pathway specific PRS approach. Although one previous study reported evidence of associations between the different disease pathway groups and different patterns of cortical thinning (Caspers *et al.*, 2020), this thesis finds no evidence of distinct patterns of changes with different pathway groups. In addition, the systematic review of AD genetic risks and white matter microstructure identified similar patterns of changes in diffusion measures associated with all the known genetic risks for AD. This suggests that further down the pathological cascade, the implicated biological pathways converge to produce the same neurodegenerative biomarker and clinical phenotypes. This is in accordance with studies of AD pathology (Naj and Schellenberg, 2017).

At the outset, it was uncertain whether subdividing the PRS signal by disease pathway groups, thereby reducing the number of loci included in each score, would simply reduce the variance explained. However, the pathway-specific PRS generally showed more evidence of association with phenotypes and explained greater variance than the genome-wide PRS. This suggests that in focusing on SNPs involved in disease pathways, we reduce the noise inherent in the PRS signal or enhance statistical power. This is concordant with the findings of Desikan and colleagues, who found that triangulating information from AD, lipid and inflammatory marker GWAS increased their statistical power for gene discovery (Desikan *et al.*, 2015). Although the pathway specific effects often attenuated when the *APOE* region was excluded, the pathway PRS generally explained more variance than *APOE* alone. For some phenotypes, notably cortical thickness in older adults, the association with pathway PRS appeared to be independent of *APOE*.

## **8.3 Methodological considerations**

### **8.3.1 Participant selection and sample size**

The data used for experiments in this thesis came from two distinct samples. Both were large population cohorts with rich phenotypic data. Both have strengths and limitations. ALSPAC is a longitudinal cohort study, with the participants and their

offspring followed up for decades. UK Biobank is a cross-sectional sample which allows for follow-up of participants through their medical records.

As described in Chapter 4, there is evidence that the population of mothers and children in ALSPAC does not reflect the typical characteristics of the population of the Avon region or the wider British population (Abigail Fraser *et al.*, 2013). Similarly, UK Biobank also shows evidence of selection bias towards healthy volunteers. In particular they appear to be wealthier and have healthier lifestyles than the general population (Fry *et al.*, 2017). As ALSPAC is a longitudinal cohort, it is affected by attrition bias. Whilst much of UK Biobank's phenotyping was conducted at the point of recruitment, participants were recalled for the imaging study. This introduced another opportunity for selection bias in responses to this invitation. These biases would favour the inclusion of participants without significant disease, making it more difficult for this study to find significant effects. Although higher genetic burden for neuropsychiatric conditions such as schizophrenia and depression are associated with participant drop out in ALSPAC, there is no evidence that polygenic risk for AD affects participation or dropout (Taylor *et al.*, 2018).

The ALSPAC imaging sub-studies, described in Chapter 4, recalled participants on the basis of specific inclusion criteria. The largest sub-study recruited only healthy males who had attended sufficient research clinics to have serial testosterone measurements (Sharp *et al.*, 2020). The cohort analysed in this thesis had unbalanced gender ratios as a result. The smaller study recruited male and female participants. In addition to healthy controls, they specifically included some participants who reported psychotic experiences, a small number of which may have met criteria for a neuropsychiatric disorder. This thesis aimed to study the effect of AD polygenic risk in healthy individuals. Whilst 'healthy volunteer' bias and attrition bias operating in ALSPAC will tend to overrepresent those who are well, it is possible that a small number of individuals with emergent psychosis could have been included, which is known to affect brain structure (Lawrie *et al.*, 2001).

### 8.3.2 Imaging considerations

Grey matter volumetric measurements are reliable and reproducible (Fischl, 2012). However, artifacts can result from a number of factors including intensity inhomogeneity, head movement, reduced signal to noise ratio, or partial volume effects (McCarthy *et al.*, 2015). These can all reduce image quality, resulting in altered intensity values and segmentation errors. Manual quality control of these issues could have introduced some error, although this was not likely to have affected the results (McCarthy *et al.*, 2015).

As discussed in Chapter 3, assessing white matter using dMRI is much less straightforward. Unlike grey matter volumetric measurements, dMRI is not a measure of neuroanatomy. As mentioned in Chapters 3 and 6, there are some significant limitations (Jones and Cercignani, 2010; Jones, Knösche and Turner, 2013). Specifically, dMRI is inherently noise-sensitive and low-resolution (Jones, Knösche and Turner, 2013). dMRI signals also show degeneracy. Decreased FA can represent fibres crossing within voxels, axonal loss, axonal growth, oedema or demyelination (Harrison *et al.*, 2020). This lack of specificity leads some to describe signal changes as altered ‘white matter integrity’ (Wheeler-Kingshott and Cercignani, 2009). As discussed in previous chapters, this is inappropriate.

Most studies of white matter microstructure in those at high genetic risk of AD have reported more marked changes closer to the expected age of onset (Harrison *et al.*, 2020). Therefore, it is not surprising that younger adults showed less evidence of changes compared to the older adults. As discussed in Chapter 6, different diffusion MRI analysis methods, such as tract skeleton-based analyses and region-of-interest analyses, can lead to distinctly different results (Seo *et al.*, 2013; Ji *et al.*, 2015). As a region-of-interest analysis was completed for ALSPAC and a tract skeleton-based analysis was conducted by UK Biobank, it is difficult to determine whether differences seen between the two cohorts reflect their respective white matter microstructure or are the result of different analysis frameworks.

### 8.3.3 Genetic considerations

The genetic analyses in this thesis have focused on additive effects of common AD susceptibility loci. Rare variants were not investigated. The role of rare genes in early onset AD is well established. It is likely that some rare variants of moderate effect size also play a role in the development of late-onset AD (Escott-Price, Sims, Bannister, *et al.*, 2015).

As described in Chapters 5, 6, and 7, GWAS for AD has identified a number of individual SNPs that are significantly associated with AD (Lambert *et al.*, 2013; Kunkle *et al.*, 2019), and PRS analyses appear to detect further weakly-associated risk alleles that explain a greater amount of variance cumulatively (Escott-Price, Sims, Bannister, *et al.*, 2015; Escott-Price *et al.*, 2017). Notwithstanding the power of large AD GWAS for detecting true risk loci, the variance explained by the PRS and the effect sizes remain low.

There are a number of important issues around PRS methodology. As described in Chapter 2, polygenic score analyses have three key steps: 1) selection of SNPs within linkage disequilibrium (LD) blocks; 2) selection of SNPs a p-value selection threshold; 3) weighting each SNPs by its effect size (the risk allele odds ratio in the discovery GWAS) and summing the risk alleles for each participant in the target dataset (Wray *et al.*, 2014). First, there are different approaches to SNPs in LD blocks. For example, linkage-disequilibrium pruning (LD-pruning) involves randomly removing (or pruning) those SNPs that are in high LD with others within a sliding window of 200kb. The method used in this thesis, known as clumping, selects SNPs within LD blocks that are more strongly associated with case control status (Wray *et al.*, 2014). A study comparing LD-pruning and clumping in Attention Deficit Hyperactivity data found that LD-pruning was associated with greater explained variance than clumping (Groen-Blokhuis *et al.*, 2014). However, clumping may increase the chance of including true susceptibility loci in the set of SNPs used for polygenic analysis (Wray *et al.*, 2014). Second, a considerable proportion of the SNPs reaching the most liberal p-value threshold for polygenic risk analysis ( $p < 0.5$ ) are probably false positives. Consequently, the risk scores have a high degree of noise. It is standard practice to use several different thresholds to compute polygenic scores (Purcell *et al.*, 2009) to

address this. This allows investigators to capture true risk loci that are weakly-associated, and including a significant number of false positives, and then use more conservative threshold to check the sensitivity of the results. By repeating analyses at different p value thresholds, a robust pattern can be observed, as seen in Chapters 5, 6 and 7. This strengthens the conclusions that can be drawn from them (Wray *et al.*, 2014).

It is not possible to identify causal relationships using PRS because there is no way to formally test for pleiotropic effects. Therefore, associations between the AD PRS with lipids, for example, could reflect: i) changes in lipids resulting from AD pathology, preceding or downstream processes; ii) loci associated with AD with an independent effect on increasing lipids, i.e., pleiotropic effects; iii) detection of genetic loci associated with lipids in the AD GWAS if they are strong risk factors for AD (Davey Smith and Hemani, 2014). The relationship between these factors could be tested with Mendelian Randomisation (MR) and associated sensitivity analyses to identify pleiotropic effects.

This thesis attempted to combine the standard approach to selecting SNPs based on p-value threshold with also selecting sets of SNPs based on functional significance. The pathway analysis that informed the scores used a genome-wide approach, allowing all available genomic data to be used with no a priori hypotheses (Kunkle *et al.*, 2019). Genome-wide pathway analyses also benefit from systemic follow-up to address the high degree of overlap often present across pathways (Ramanan *et al.*, 2012). In this thesis, it was demonstrated that narrowing the set of SNPs to loci which are involved with specific biological pathways may have improved the proportion of alleles in the polygenic score that were truly associated with the disease. Although the number of SNPs selected in this way was smaller, compared to the genome-wide polygenic score, it often explained more of the variance in phenotypes. Of note, a pathway analysis can only be as good as the functional information used for its pathway definitions. There are several different pathway annotation databases, all with different characteristics (Ramanan *et al.*, 2012). Methods of pathway curation can also affect analyses. Whilst most databases use expert reviews for pathway curation, they may not be updated regularly, and databases may apply different criteria to determine

what is sufficient evidence for a gene to be included in a pathway (Ramanan *et al.*, 2012).

A further consideration with polygenic score analysis methods are the nature of control participants in the discovery AD GWAS. The prevalence of AD is high, affecting one in ten people over the age of 65 (Alzheimer's Association, 2019). Even those who have not yet manifested symptoms could still have a significant degree of pathology (Jack Jr. *et al.*, 2010). If even 5% of controls actually have incipient disease, this would have a detrimental effect statistical power akin to reducing the GWAS sample size by approximately 10% (The Wellcome Trust Case Control Consortium, 2007). Therefore this could have reduced the power of the genetic discovery sample (Kunkle *et al.*, 2019) used for the polygenic analyses in Chapters 5, 6 and 7 of this thesis.

#### **8.3.4 Summary of strengths and limitations**

The main strength of the analyses in this thesis is the use of the two large populations cohorts. A further key advantage was the use of a large AD GWAS as our discovery data for polygenic analysis (Kunkle *et al.*, 2019). This provided the most accurate estimates of SNP effects on disease risk. These factors combined to make this the most powerful AD genetic imaging study risk to date. The samples included complementary ages, allowing us to identify some of the earliest changes in the disease process. The samples are both well-phenotyped, with clearly described imaging and serum measures. The chief limitations of the methodology have already been described above and in detail in each results chapter. The main limitations of the analyses are summarised below.

As discussed above, there were some disadvantages to the cohorts included in this study. As described above, both ALSPAC and UK Biobank analyses have shown participants to be generally healthier and from higher socio-economic backgrounds (Abigail Fraser *et al.*, 2013; Fry *et al.*, 2017). This may have served to underestimate the observed effect sizes and may affect the generalisability of the results. Males were over-represented in the ALSPAC imaging cohort, although sex was controlled for in the analyses, and a minority of participants reported psychotic experiences which might have represented incipient psychiatric disorders.

As mentioned above, the use of different analysis frameworks for diffusion MRI data between ALSPAC and UK Biobank made it more difficult to compare findings between the cohorts. Although the results showed some similar trends in increasing diffusivity, it is not possible to determine whether divergent results reflected actual differences in white matter microstructure or were simply due to differences in measurement. A further limitation of the thesis is that the use of lipid lowering drugs, socioeconomic and lifestyle factors were not taken into account in the analyses in Chapter 7. Given that these factors are likely to affect levels of the markers measured, particularly cholesterol, this is a limitation of the analyses.

A number of statistical tests were conducted, requiring correction for multiple testing. This was done using the False Discovery Rate (FDR) in the R statistical computing package (R Development Core Team 3.0.1., 2013). Correction was applied for 21 scores (nine pathway polygenic scores and the genome-wide polygenic score including *APOE*, nine pathway polygenic scores excluding *APOE* and the genome-wide score excluding *APOE* plus the *APOE* SNPs score) and for the number of phenotypes tested in each analysis. The PRS were closely correlated as they contained a significant number of overlapping SNPs. The phenotypes (such as cortical thickness in adjacent brain regions) are also likely to be correlated. Therefore, this approach to adjusting for multiple comparisons was probably too stringent, and some true associations may have been overlooked. Despite these limitations, the findings of this thesis have valuable implications for the understanding of how polygenic risk for AD is manifest in early adulthood and mid-life.

## **8.4 Future research directions**

There are a number of possible analyses linked to those described in this thesis which could further our understanding of how genetic susceptibility for AD affects brain function, as outlined below.

### **8.4.1 AD polygenic risk and brain function**

This thesis presented experiments that focussed on the associations between AD polygenic risk in disease pathways and brain structure. No assessments were made

of how AD polygenic risk manifests in brain function. There are a number of possible approaches to this, which are outlined below.

Functional MRI (fMRI) interprets blood oxygen level dependence (BOLD) signal to estimate brain activity in specific brain regions (Logothetis, 2003). Activity in a brain region is indicated by an increase in the ratio of oxygenated to deoxygenated blood, which have different magnetic properties. Magnetoencephalography (MEG) also detects changes in neuronal activity. It uses superconducting quantum interference devices (SQUIDs) to detect small magnetic fields produced by synchronous postsynaptic currents from groups of pyramidal neurons. It is most sensitive to those currents that are perpendicular to the cortical surface (Hari and Salmelin, 2012). Diffusion MRI, fMRI and MEG signals can be used to study brain network organisation. Complex maps of brain connectivity can be constructed, and techniques such as graph theory can be used to provide a representation of the elements and interactions within the system (E. T. Bullmore and Sporns, 2009). fMRI (Xu *et al.*, 2009) and MEG (Cuesta *et al.*, 2015) have already been applied to study the effect of *APOE* in healthy participants. Similarly, some studies have already explored the effect of *APOE* on brain networks derived using functional (J. Wang *et al.*, 2015) and structural (Ma *et al.*, 2017) data. The relationship between polygenic risk for AD and brain function assessed in these ways has yet to be investigated.

Other imaging techniques provide more direct methods of assessing neurobiological activity. Magnetic resonance spectroscopy (MRS) is a non-invasive technique that measures endogenous brain metabolites. Hydrogen nuclear spins emit specific frequencies depending on the chemical environment of the nuclei. MRS detects the radiofrequency signals that arise from these (Agarwal and Renshaw, 2012). Nuclear imaging techniques such as positron emission tomography (PET) and single photon emission computed tomography (SPECT) use radioactive tracers joined to biologically active molecules, which are given intravenously. Nuclear imaging methods can be used to investigate brain metabolism (such as [<sup>18</sup>F] fluorodeoxyglucose) (Mosconi *et al.*, 2008) and neurotransmitters (such as [<sup>11</sup>C]-flumazenil which binds benzodiazepine receptors) (Pascual *et al.*, 2012). A number of radioligands have also been developed for amyloid and tau, the abnormal proteins that accumulate in AD

(Femminella *et al.*, 2018). As with the other advanced neuroimaging techniques, how polygenic risk for AD affects these markers of neurobiology is unclear.

#### **8.4.2 Longitudinal studies**

This thesis presented evidence that changes in brain structure similar to those seen in early AD neurodegeneration were associated with AD PRS in older and younger cognitively healthy adults. These younger participants would not be expected to show significant amyloid deposition for many years. Therefore, how these alterations in brain structure fit with progressive biomarker abnormalities seen in pre-clinical AD is uncertain. A number of studies have incorporated serial measurements from multi-modal biomarker studies in an effort to map out the sequence of biomarker changes that occur before the onset of symptoms (Jack Jr. *et al.*, 2010; Villain *et al.*, 2010; Chételat *et al.*, 2012; Jack *et al.*, 2013). However, these studies have focused on participants in mid-life or later life. Further studies should seek to replicate and extend the findings of this thesis across the life course and clarify their relationship to other biomarker abnormalities.

A further point that can be addressed by future cohort studies is the relationship between grey matter atrophy and white matter changes. Assuming they form part of a cascade of consecutive pathological events, there are a number of possible mechanisms. Grey matter hypometabolism or atrophy (Braak & Braak, 1997) could cause disruption in distant associated white matter tracts. Alternatively, white matter tract disruption could be responsible for hypometabolism and grey matter atrophy in connected brain regions as a result of retrograde (Reisberg *et al.*, 2002; Bartzokis, 2004) or Wallerian degeneration (Coleman, 2005). Serial imaging is required to investigate dynamic changes in grey matter relative to white matter.

In recent years, some have argued that AD is a disconnection syndrome, with changes preferentially affecting regions of the same brain network (Seeley *et al.*, 2009). fMRI studies have identified changes in functional connectivity in AD (Wang *et al.*, 2007; Zhang *et al.*, 2009). There are also inconsistencies between regions affected by functional and structural changes. For example, early hypometabolism has been

observed in the posterior cingulate cortex but it is not the earliest to atrophy (Chetelat *et al.*, 2009). However, such network alterations could occur in tandem with structural changes as a result of a common disease process, and disruption could result from distant pathology. In a sequential pathological cascade, determining events that drive subsequent neurodegeneration is important as it could help target therapeutic interventions. As discussed in Chapter 3, the neuroimaging changes in autosomal dominant AD parallel those with polygenic risk for AD. Therefore, these groups provide a useful model for longitudinal studies with shorter follow-up periods.

### **8.4.3 Improving and augmenting pathways analyses**

Pathway analysis methods development is a particularly dynamic field, as it applies to a variety of disciplines and subject areas. Future studies would benefit from improved annotation of genes within pathways, consistent pathway names and classifications between databases, and methods for defining pathway overlap. There is also the potential to integrate other types of association signal, using multi-omics data. For example, it may be possible to integrate gene expression data such as expression quantitative trait loci (eQTLs) (Ramanan *et al.*, 2012). Although genetic associations do not always reveal therapeutic targets, pathways and networks indicated by analyses of multiple signals would be key targets for drug therapies. As such, the role of biological networks and pathways as a nucleus for multi-omics integration will be fundamental for future research.

## **8.5 Conclusions**

The work presented in this thesis adds to the emerging body of literature showing evidence of association between AD polygenic risk and evidence of alterations in brain structure in older and younger adults. Results show that pathway specific polygenic scores showed greater evidence of association with brain structure phenotypes than the genome-wide polygenic score, and some brain structure measures were not dependent on *APOE*. There was little evidence of association between AD polygenic risk and peripheral blood biomarkers beyond what *APOE* explained. These results

indicate that neuroimaging changes may be useful biomarkers for the earliest changes associated with AD.

## REFERENCES

- 1000 Genomes Project Consortium *et al.* (2015) 'A global reference for human genetic variation', *Nature*, 526(7571), pp. 68–74.
- Adams, H. H. H. *et al.* (2015) 'Genetic risk of neurodegenerative diseases is associated with mild cognitive impairment and conversion to dementia', *Alzheimer's and Dementia*, 11(11), pp. 1277–1285. doi: 10.1016/j.jalz.2014.12.008.
- Adluru, N. *et al.* (2014) 'White matter microstructure in late middle-age: Effects of apolipoprotein E4 and parental family history of Alzheimer's disease', *Neuroimage-Clinical*, 4, pp. 730–742. doi: 10.1016/j.nicl.2014.04.008.
- Agarwal, N. and Renshaw, P. F. (2012) 'Proton MR spectroscopy - Detectable major neurotransmitters of the brain: Biology and possible clinical applications', *American Journal of Neuroradiology*, pp. 595–602. doi: 10.3174/ajnr.A2587.
- Ahmad, S. *et al.* (2018) 'Disentangling the biological pathways involved in early features of Alzheimer's disease in the Rotterdam Study', *Alzheimer's and Dementia*, 14(7), pp. 848–857. doi: 10.1016/j.jalz.2018.01.005.
- Alexopoulos, P. *et al.* (2011) 'Hippocampal volume differences between healthy young apolipoprotein e  $\epsilon$ 2 and  $\epsilon$ 4 carriers', *Journal of Alzheimer's Disease*, 26(2), pp. 207–210. doi: 10.3233/JAD-2011-110356.
- Alfaro-Almagro, F. *et al.* (2018) 'Image processing and Quality Control for the first 10,000 brain imaging datasets from UK Biobank', *NeuroImage*, 166, pp. 400–424. doi: 10.1016/j.neuroimage.2017.10.034.
- Altmann, A. *et al.* (2020) 'A comprehensive analysis of methods for assessing polygenic burden on Alzheimer's disease pathology and risk beyond APOE', *Brain communications*, 2(1), p. fcz047.
- Alzheimer's association (2019) *Alzheimer's Disease Facts and Figures, Alzheimer's & Dementia Volume 15, Issue 3*.
- Amlien, I. K. *et al.* (2013) 'Mild cognitive impairment: Cerebrospinal fluid tau biomarker pathologic levels and longitudinal changes in white matter integrity', *Radiology*, 266(1), pp. 295–303. doi: 10.1148/radiol.12120319.
- Andersson, J. L. R. and Sotiropoulos, S. N. (2015) 'Non-parametric representation and prediction of single- and multi-shell diffusion-weighted MRI data using Gaussian processes', *NeuroImage*, 122, pp. 166–176. doi: 10.1016/j.neuroimage.2015.07.067.
- Andersson, J. L. R. and Sotiropoulos, S. N. (2016) 'An integrated approach to

correction for off-resonance effects and subject movement in diffusion MR imaging', *NeuroImage*, 125, pp. 1063–1078. doi: 10.1016/j.neuroimage.2015.10.019.

Andrews, S. J. *et al.* (2016) 'Association of genetic risk factors with cognitive decline: The PATH through life project', *Neurobiology of Aging*, 41, pp. 150–158. doi: 10.1016/j.neurobiolaging.2016.02.016.

Andrews, S. J., Das, D., *et al.* (2017) 'Late Onset Alzheimer's Disease Risk Variants in Cognitive Decline: The PATH Through Life Study', *Journal of Alzheimer's disease : JAD*, 57(2), pp. 423–436. doi: 10.3233/JAD-160774.

Andrews, S. J., Eramudugolla, R., *et al.* (2017) 'Validating the role of the Australian National University Alzheimer's Disease Risk Index (ANU-ADRI) and a genetic risk score in progression to cognitive impairment in a population-based cohort of older adults followed for 12 years', *Alzheimer's Research & Therapy*, 9(1), p. 16. doi: 10.1186/s13195-017-0240-3.

Andrews, S. J. *et al.* (2021) 'Causal Associations Between Modifiable Risk Factors and the Alzheimer's Phenome', *Annals of Neurology*, 89(1), pp. 54–65. doi: 10.1002/ana.25918.

Andrews, S. J., Marcora, E. and Goate, A. (2019) 'Causal associations between potentially modifiable risk factors and the Alzheimer's phenome: A Mendelian randomization study', *bioRxiv*. doi: 10.1101/689752.

Apostolova, L. G. *et al.* (2010) 'Subregional hippocampal atrophy predicts Alzheimer's dementia in the cognitively normal', *Neurobiology of Aging*, 31(7), pp. 1077–1088. doi: 10.1016/j.neurobiolaging.2008.08.008.

Ashburner, J. and Friston, K. J. (2000) 'Voxel-based morphometry - The methods', *NeuroImage*, 11(6 l), pp. 805–821. doi: 10.1006/nimg.2000.0582.

Assaf, Y. and Basser, P. J. (2005) 'Composite hindered and restricted model of diffusion (CHARMED) MR imaging of the human brain', *NeuroImage*, 27(1), pp. 48–58. doi: 10.1016/j.neuroimage.2005.03.042.

Atkinson, A. J. *et al.* (2001) 'Biomarkers and surrogate endpoints: Preferred definitions and conceptual framework', *Clinical Pharmacology and Therapeutics*, pp. 89–95. doi: 10.1067/mcp.2001.113989.

Autier, P. and Boniol, M. (2018) 'Mammography screening: A major issue in medicine', *European Journal of Cancer*, 90, pp. 34–62. doi: 10.1016/j.ejca.2017.11.002.

Axelrud, L. K. *et al.* (2018) 'Polygenic risk score for Alzheimer's disease: Implications

for memory performance and hippocampal volumes in early life', *American Journal of Psychiatry*, 175(6), pp. 555–563. doi: 10.1176/appi.ajp.2017.17050529.

Bach, M. *et al.* (2014) 'Methodological considerations on tract-based spatial statistics (TBSS)', *NeuroImage*, 100, pp. 358–369. doi: 10.1016/j.neuroimage.2014.06.021.

Bagepally, B. S. *et al.* (2012) 'Apolipoprotein E4 and brain white matter integrity in Alzheimer's disease: Tract-based spatial statistics study under 3-tesla MRI', *Neurodegenerative Diseases*, 10(1–4), pp. 145–148. doi: 10.1159/000334761.

Bartzokis, G. (2004) 'Age-related myelin breakdown: a developmental model of cognitive decline and Alzheimer's disease.', *Neurobiology of aging*, 25(1), pp. 5–18; author reply 49-62.

Basser, P. J. and Pierpaoli, C. (1996) 'Microstructural and physiological features of tissues elucidated by quantitative-diffusion-tensor MRI', *Journal of Magnetic Resonance - Series B*, 111(3), pp. 209–219. doi: 10.1006/jmrb.1996.0086.

Bastin, M. E. *et al.* (2013) 'Quantitative tractography and tract shape modeling in amyotrophic lateral sclerosis', *Journal of Magnetic Resonance Imaging*, 38(5), pp. 1140–1145. doi: 10.1002/jmri.24073.

Bateman, R. J. *et al.* (2012) 'Clinical and biomarker changes in dominantly inherited Alzheimer's disease.', *New England Journal of Medicine*, 367(9), pp. 795–804.

Beaulieu, C. (2009) 'The Biological Basis of Diffusion Anisotropy', in *Diffusion MRI*, pp. 105–126. doi: 10.1016/B978-0-12-374709-9.00006-7.

Beaulieu, C. and Allen, P. S. (1994) 'Water diffusion in the giant axon of the squid: Implications for diffusion-weighted MRI of the nervous system', *Magnetic Resonance in Medicine*, 32(5), pp. 579–583. doi: 10.1002/mrm.1910320506.

Becker, J. A. *et al.* (2011) 'Amyloid- $\beta$  associated cortical thinning in clinically normal elderly', *Annals of Neurology*, 69(6), pp. 1032–1042. doi: 10.1002/ana.22333.

Behl, P., Stefurak, T. L. and Black, S. E. (2005) 'Progress in clinical neurosciences: Cognitive markers of progression in Alzheimer's disease', *Canadian Journal of Neurological Sciences*, pp. 140–151. doi: 10.1017/S0317167100003917.

Bendlin, B. B. *et al.* (2012) 'CSF T-TAU/A $\beta$  42 predicts white matter microstructure in healthy adults at risk for alzheimer's disease', *PLoS ONE*, 7(6), p. e37720. doi: 10.1371/journal.pone.0037720.

Benitez, A. *et al.* (2014) 'White matter tract integrity metrics reflect the vulnerability of late-myelinating tracts in Alzheimer's disease', *NeuroImage: Clinical*, 4, pp. 64–71. doi: 10.1016/j.nicl.2013.11.001.

- Biffi, A. *et al.* (2010) 'Genetic variation and neuroimaging measures in Alzheimer disease', *Archives of neurology*, 67(6), pp. 677–685.
- Bihan, D. Le (1995) 'Molecular diffusion, tissue microdynamics and microstructure', *NMR in Biomedicine*, 8(7), pp. 375–386. doi: 10.1002/nbm.1940080711.
- Bis, J. C. *et al.* (2018) 'Whole exome sequencing study identifies novel rare and common Alzheimer's-Associated variants involved in immune response and transcriptional regulation', *Molecular Psychiatry*, pp. 1–17. doi: 10.1038/s41380-018-0112-7.
- Björnholm, L. *et al.* (2017) 'Structural properties of the human corpus callosum: Multimodal assessment and sex differences', *Neuroimage*, 152, pp. 108–118.
- Boccaletti, S. *et al.* (2006) 'Complex networks: Structure and dynamics', *Physics Reports*, pp. 175–308. doi: 10.1016/j.physrep.2005.10.009.
- Boyd, A. *et al.* (2013) 'Cohort profile: The 'Children of the 90s'-The index offspring of the avon longitudinal study of parents and children', *International Journal of Epidemiology*, 42(1), pp. 111–127. doi: 10.1093/ije/dys064.
- Braak, H. and Braak, E. (1991) 'Neuropathological staging of Alzheimer-related changes', *Acta neuropathologica*, 82(4), pp. 239–259.
- Braak, H. and Braak, E. (1995) 'Staging of Alzheimer's disease-related neurofibrillary changes', *Neurobiology of aging*, 16(3), pp. 271–278.
- Braak, H. and Braak, E. (1997) 'Diagnostic criteria for neuropathologic assessment of Alzheimer's disease', *Neurobiology of Aging*, 18(4 SUPPL.), pp. S85-8. doi: 10.1016/S0197-4580(97)00062-6.
- Braak, Heiko and Braak, E. (1997) 'Frequency of stages of Alzheimer-related lesions in different age categories', *Neurobiology of aging*, 18(4), pp. 351–357.
- Braak, H. and Del Tredici, K. (2011) 'The pathological process underlying Alzheimer's disease in individuals under thirty', *Acta Neuropathologica*, 121(2), pp. 171–181. doi: 10.1007/s00401-010-0789-4.
- Braskie, M. N. *et al.* (2011) 'Common Alzheimer's Disease Risk Variant Within the CLU Gene Affects white Matter Microstructure in young Adults', *Journal of Neuroscience*, 31(18), pp. 6764–6770. doi: 10.1523/JNEUROSCI.5794-10.2011.
- Bressler, J. *et al.* (2017) 'Genetic variants associated with risk of Alzheimer's disease contribute to cognitive change in midlife: The Atherosclerosis Risk in Communities Study', *American Journal of Medical Genetics, Part B: Neuropsychiatric Genetics*, 174(3), pp. 269–282. doi: 10.1002/ajmg.b.32509.

- Broce, I. J. *et al.* (2018) 'Lipid associated polygenic enrichment in Alzheimer's disease', *bioRxiv*. doi: 10.1101/383844.
- Broce, I. J. *et al.* (2019) 'Dissecting the genetic relationship between cardiovascular risk factors and Alzheimer's disease', *Acta neuropathologica*. 2018/11/09, 137(2), pp. 209–226. doi: 10.1007/s00401-018-1928-6.
- Brown, J. A. *et al.* (2011) 'Brain network local interconnectivity loss in aging APOE-4 allele carriers', *Proceedings of the National Academy of Sciences of the United States of America*, 108(51), pp. 20760–20765. doi: 10.1073/pnas.1109038108.
- Bu, G. (2009) 'Apolipoprotein E and its receptors in Alzheimer's disease: pathways, pathogenesis and therapy', *Nature Reviews Neuroscience*, 10(5), pp. 333–344.
- Büchel, C. *et al.* (2004) 'White Matter Asymmetry in the Human Brain: A Diffusion Tensor MRI Study', *Cerebral Cortex*, 14(9), pp. 945–951. doi: 10.1093/cercor/bhh055.
- Bueller, J. A. *et al.* (2006) 'BDNF Val66Met Allele Is Associated with Reduced Hippocampal Volume in Healthy Subjects', *Biological Psychiatry*, 59(9), pp. 812–815. doi: 10.1016/j.biopsych.2005.09.022.
- Bullmore, E. and Sporns, O. (2009) 'Complex brain networks: graph theoretical analysis of structural and functional systems', *Nature Reviews Neuroscience*, 10(3), pp. 186–198. doi: 10.1038/nrn2575.
- Bullmore, E. T. and Sporns, O. (2009) 'Complex brain networks: Graph theoretical analysis of structural and functional systems Neural Criticality View project neurodevelopment View project'. doi: 10.1038/nrn2575.
- Burggren, A. C. *et al.* (2008) 'Reduced cortical thickness in hippocampal subregions among cognitively normal apolipoprotein E e4 carriers', *NeuroImage*, 41(4), pp. 1177–1183. doi: 10.1016/j.neuroimage.2008.03.039.
- Burggren, A. C. *et al.* (2011) 'The relationship between tomm40 variable-length polymorphism, cortical thickness in the medial temporal lobe, and cognitive performance', *Society for Neuroscience Abstract Viewer and Itinerary Planner*, 41.
- Busatto, G. F., Diniz, B. S. and Zanetti, M. V. (2008) 'Voxel-based morphometry in Alzheimer's disease', *Expert Review of Neurotherapeutics*, pp. 1691–1702. doi: 10.1586/14737175.8.11.1691.
- Caballero, M. A. *et al.* (2018) 'White matter diffusion alterations precede symptom onset in autosomal dominant Alzheimer's disease', *Brain*, 141(10), pp. 3065–3080.
- Cai, S. *et al.* (2017) 'Modulation on brain gray matter activity and white matter

- integrity by APOE  $\epsilon$ 4 risk gene in cognitively intact elderly: A multimodal neuroimaging study', *Behavioural Brain Research*, 322, pp. 100–109. doi: 10.1016/j.bbr.2017.01.027.
- Cardenas, V. A. *et al.* (2012) 'Associations among vascular risk factors, carotid atherosclerosis, and cortical volume and thickness in older adults', *Stroke*, 43(11), pp. 2865–2870. doi: 10.1161/STROKEAHA.112.659722.
- Carrasquillo, M. M. *et al.* (2015) 'Late-onset Alzheimer's risk variants in memory decline, incident mild cognitive impairment, and Alzheimer's disease.', *Neurobiology of aging*, 36(1), pp. 60–7. doi: 10.1016/j.neurobiolaging.2014.07.042.
- Caseras, X. *et al.* (2020) 'Effects of genomic copy number variants penetrant for schizophrenia on cortical thickness and surface area in healthy individuals: analysis of the UK Biobank', *The British Journal of Psychiatry*, pp. 1–8. doi: 10.1192/bjp.2020.139.
- Cash, D. M. *et al.* (2013) 'The pattern of atrophy in familial alzheimer disease: Volumetric MRI results from the DIAN study', *Neurology*, 81(16), pp. 1425–1433. doi: 10.1212/WNL.0b013e3182a841c6.
- Caspers, S. *et al.* (2020) 'Pathway-Specific Genetic Risk for Alzheimer's Disease Differentiates Regional Patterns of Cortical Atrophy in Older Adults', *Cerebral Cortex*, 30(2), pp. 801–811. doi: 10.1093/cercor/bhz127.
- Cavedo, E. *et al.* (2017) 'Disrupted white matter structural networks in healthy older adult APOE  $\epsilon$ 4 carriers – An international multicenter DTI study', *Neuroscience*, 357, pp. 119–133. doi: 10.1016/J.NEUROSCIENCE.2017.05.048.
- Chang, L. *et al.* (2016) 'Gray matter maturation and cognition in children with different APOE  $\epsilon$  genotypes', *Neurology*. 2016/07/13, 87(6), pp. 585–594. doi: 10.1212/WNL.0000000000002939.
- Chang, L. C., Jones, D. K. and Pierpaoli, C. (2005) 'RESTORE: Robust estimation of tensors by outlier rejection', *Magnetic Resonance in Medicine*, 53(5), pp. 1088–1095. doi: 10.1002/mrm.20426.
- Chasman, D. I. *et al.* (2006) 'Qualitative and quantitative effects of APOE genetic variation on plasma C-reactive protein, LDL-cholesterol, and apoE protein', *Genes & Immunity*, 7(3), pp. 211–219. doi: 10.1038/sj.gene.6364289.
- Chaudhury, S. *et al.* (2018) 'Polygenic risk score in postmortem diagnosed sporadic early-onset Alzheimer's disease', *Neurobiology of Aging*, 62, pp. 244.e1-244.e8. doi: 10.1016/j.neurobiolaging.2017.09.035.

- Chen, K. *et al.* (2007) 'Correlations between apolipoprotein E  $\epsilon$ 4 gene dose and whole brain atrophy rates', *American Journal of Psychiatry*, 164(6), pp. 916–921. doi: 10.1176/ajp.2007.164.6.916.
- Chen, Y. *et al.* (2015) 'Disrupted Functional and Structural Networks in Cognitively Normal Elderly Subjects with the APOE epsilon 4 Allele', *Neuropsychopharmacology*, 40(5), pp. 1181–1191. doi: 10.1038/npp.2014.302.
- Chen, Z. Y. *et al.* (2004) 'Variant Brain-Derived Neurotrophic Factor (BDNF) (Met66) Alters the Intracellular Trafficking and Activity-Dependent Secretion of Wild-Type BDNF in Neurosecretory Cells and Cortical Neurons', *Journal of Neuroscience*, 24(18), pp. 4401–4411. doi: 10.1523/JNEUROSCI.0348-04.2004.
- Cherbuin, N. *et al.* (2008) 'Total and regional gray matter volume is not related to APOE\*E4 status in a community sample of middle-aged individuals', *Journals of Gerontology - Series A Biological Sciences and Medical Sciences*, 63(5), pp. 501–504. doi: 10.1093/gerona/63.5.501.
- Cherbuin, N. *et al.* (2009) 'In vivo hippocampal measurement and memory: A comparison of manual tracing and automated segmentation in a large community-based sample', *PLoS ONE*, 4(4). doi: 10.1371/journal.pone.0005265.
- Chételat, G. *et al.* (2009) 'Posterior cingulate hypometabolism in early Alzheimer's disease: what is the contribution of local atrophy versus disconnection?', *Brain*, 132(12), pp. e133–e133. doi: 10.1093/brain/awp253.
- Chételat, G. *et al.* (2012) 'Relationship between memory performance and  $\beta$ -amyloid deposition at different stages of Alzheimer's disease', *Neurodegenerative Diseases*, 10(1–4), pp. 141–144. doi: 10.1159/000334295.
- Chouraki, V. *et al.* (2014) 'A genome-wide association meta-analysis of plasma A $\beta$  peptides concentrations in the elderly', *Molecular Psychiatry*, 19(12), pp. 1326–1335. doi: 10.1038/mp.2013.185.
- Chouraki, V. *et al.* (2016) 'Evaluation of a Genetic Risk Score to Improve Risk Prediction for Alzheimer's Disease', *Journal of Alzheimer's disease : JAD*, 53(3), p. 921. doi: 10.3233/JAD-150749.
- Clerx, L. *et al.* (2012) 'New MRI markers for alzheimer's disease: A meta-analysis of diffusion tensor imaging and a comparison with medial temporal lobe measurements', *Journal of Alzheimer's Disease*, 29(2), pp. 405–429. doi: 10.3233/JAD-2011-110797.
- Coleman, M. (2005) 'Axon degeneration mechanisms: commonality amid diversity.',

*Nature reviews. Neuroscience*, 6(11), pp. 889–98. doi: 10.1038/nrn1788.

Concha, L., Gross, D. W. and Beaulieu, C. (2005) 'Diffusion tensor tractography of the limbic system', *American Journal of Neuroradiology*, 26(9), pp. 2267–2274.

Conturo, T. E. *et al.* (1999) 'Tracking neuronal fiber pathways in the living human brain', *Proceedings of the National Academy of Sciences of the United States of America*, 96(18), pp. 10422–10427. doi: 10.1073/pnas.96.18.10422.

Corder, E. H. *et al.* (1993) 'Gene dose of apolipoprotein E type 4 allele and the risk of Alzheimer's disease in late onset families', *Science*, 261(5123), pp. 921–923. doi: 10.1126/science.8346443.

Corlier, F. *et al.* (2018) 'Systemic inflammation as a predictor of brain aging: Contributions of physical activity, metabolic risk, and genetic risk', *NeuroImage*, 172, pp. 118–129. doi: 10.1016/j.neuroimage.2017.12.027.

*Council of Europe. Recommendation NR (94) 11 on screening as a tool of preventive medicine* (1994). Available at: <http://hrlibrary.umn.edu/instree/coerecr94-11.html> (Accessed: 7 December 2020).

Crivello, F. *et al.* (2010) 'Effects of ApoE- $\epsilon$ 4 allele load and age on the rates of grey matter and hippocampal volumes loss in a longitudinal cohort of 1186 healthy elderly persons', *NeuroImage*, 53(3), pp. 1064–1069. doi: 10.1016/j.neuroimage.2009.12.116.

Cruchaga, C. *et al.* (2018) 'Polygenic risk score of sporadic late-onset Alzheimer's disease reveals a shared architecture with the familial and early-onset forms', *Alzheimer's & Dementia*, 14(2), pp. 205–214. doi: 10.1016/j.jalz.2017.08.013.

Cuesta, P. *et al.* (2015) 'Source Analysis of Spontaneous Magnetoencephalographic Activity in Healthy Aging and Mild Cognitive Impairment: Influence of Apolipoprotein E Polymorphism', *Journal of Alzheimers Disease*, 43(1), pp. 259–273. doi: 10.3233/jad-140633.

D'Agostino, R. B. *et al.* (2008) 'General cardiovascular risk profile for use in primary care: The Framingham heart study', *Circulation*, 117(6), pp. 743–753. doi: 10.1161/CIRCULATIONAHA.107.699579.

Darst, B. F. *et al.* (2017) 'Pathway-Specific Polygenic Risk Scores as Predictors of Amyloid- $\beta$  Deposition and Cognitive Function in a Sample at Increased Risk for Alzheimer's Disease', *Journal of Alzheimer's Disease*, 55(2), pp. 473–484. doi: 10.3233/JAD-160195.

Davey Smith, G. and Ebrahim, S. (2003) "Mendelian randomization": can genetic

epidemiology contribute to understanding environmental determinants of disease?\*', *International Journal of Epidemiology*, 32(1), pp. 1–22. doi: 10.1093/ije/dyg070.

Davey Smith, G. and Hemani, G. (2014) 'Mendelian randomization: genetic anchors for causal inference in epidemiological studies', *Human molecular genetics*. 2014/07/04, 23(R1), pp. R89–R98. doi: 10.1093/hmg/ddu328.

Davis, S. W. *et al.* (2009) 'Assessing the effects of age on long white matter tracts using diffusion tensor tractography', *NeuroImage*, 46(2), pp. 530–541. doi: 10.1016/j.neuroimage.2009.01.068.

Dean, D. C. 3rd *et al.* (2014) 'Brain differences in infants at differential genetic risk for late-onset alzheimer disease: A cross-sectional imaging study', *Jama Neurology*, 71(1), pp. 11–22. doi: 10.1001/jamaneurol.2013.4544.

Dehghan, A. *et al.* (2011) 'Meta-analysis of genome-wide association studies in >80 000 subjects identifies multiple loci for C-reactive protein levels', *Circulation*, 123(7), pp. 731–738. doi: 10.1161/CIRCULATIONAHA.110.948570.

Del-Aguila, J. *et al.* (2018) 'Assessment of the genetic architecture of Alzheimer's Disease risk in rate of memory decline', *Journal of Alzheimer's disease : JAD*, 62(2), pp. 745–756. doi: 10.3233/JAD-170834.

Delaneau, O., Marchini, J. and Zagury, J. F. (2012) 'A linear complexity phasing method for thousands of genomes', *Nature Methods*, 9(2), pp. 179–181. doi: 10.1038/nmeth.1785.

Dell'Acqua, F. *et al.* (2010) 'A modified damped Richardson-Lucy algorithm to reduce isotropic background effects in spherical deconvolution', *NeuroImage*, 49(2), pp. 1446–1458. doi: 10.1016/j.neuroimage.2009.09.033.

Dell'Acqua, F. *et al.* (2015) 'Tract Based Spatial Statistic Reveals No Differences in White Matter Microstructural Organization between Carriers and Non-Carriers of the APOE epsilon 4 and epsilon 2 Alleles in Young Healthy Adolescents', *Journal of Alzheimer's Disease*, 47(4), pp. 977–984. doi: 10.3233/jad-140519.

Dell'Acqua, F. and Tournier, J. -Donal. (2019) 'Modelling white matter with spherical deconvolution: How and why?', *NMR in Biomedicine*, 32(4), p. e3945. doi: 10.1002/nbm.3945.

Deoni, S. C. L. *et al.* (2012) 'Investigating white matter development in infancy and early childhood using myelin water fraction and relaxation time mapping', *NeuroImage*, 63(3), pp. 1038–1053. doi: <https://doi.org/10.1016/j.neuroimage.2012.07.037>.

Desikan, R. S. *et al.* (2010) 'Selective disruption of the cerebral neocortex in Alzheimer's disease', *PLoS ONE*, 5(9), pp. 1–9. doi: 10.1371/journal.pone.0012853.

Desikan, R. S. *et al.* (2015) 'Polygenic Overlap Between C-Reactive Protein, Plasma Lipids and Alzheimer's Disease', *Circulation*, 131, pp. 2061–2069.

Dickerson, B. C., Feczko, E., *et al.* (2009) 'Differential effects of aging and Alzheimer's disease on medial temporal lobe cortical thickness and surface area', *Neurobiology of Aging*, 30(3), pp. 432–440. doi: 10.1016/j.neurobiolaging.2007.07.022.

Dickerson, B. C., Bakkour, A., *et al.* (2009) 'The cortical signature of Alzheimer's disease: Regionally specific cortical thinning relates to symptom severity in very mild to mild AD dementia and is detectable in asymptomatic amyloid-positive individuals', *Cerebral Cortex*, 19(3), pp. 497–510. doi: 10.1093/cercor/bhn113.

Dik, M. G. *et al.* (2005) 'Serum inflammatory proteins and cognitive decline in older persons', *Neurology*, 64(8), pp. 1371–1377. doi: 10.1212/01.WNL.0000158281.08946.68.

Diniz, B. S. and Teixeira, A. L. (2011) 'Brain-derived neurotrophic factor and Alzheimer's disease: Physiopathology and beyond', *NeuroMolecular Medicine*, pp. 217–222. doi: 10.1007/s12017-011-8154-x.

Douaud, G. *et al.* (2011) 'DTI measures in crossing-fibre areas: increased diffusion anisotropy reveals early white matter alteration in MCI and mild Alzheimer's disease.', *NeuroImage*, 55(3), pp. 880–90. doi: 10.1016/j.neuroimage.2010.12.008.

Dowell, N. G. *et al.* (2013) 'MRI of carriers of the apolipoprotein E e4 allele-evidence for structural differences in normal-appearing brain tissue in e4+ relative to e4- young adults', *Nmr in Biomedicine*, 26(6), pp. 674–682. doi: 10.1002/nbm.2912.

Dowell, N. G. *et al.* (2016) 'Structural and resting-state MRI detects regional brain differences in young and mid-age healthy APOE-e4 carriers compared with non-APOE-e4 carriers', *NMR in Biomedicine*, 29(5), pp. 614–624. doi: 10.1002/nbm.3502.

Drachman, D. A. (2014) 'The amyloid hypothesis, time to move on: Amyloid is the downstream result, not cause, of Alzheimer's disease', *Alzheimer's & Dementia*, 10(3), pp. 372–380.

Drakesmith, M. *et al.* (2016) 'Volumetric, relaxometric and diffusometric correlates of psychotic experiences in a non-clinical sample of young adults', *NeuroImage: Clinical*, 12, pp. 550–558. doi: <https://doi.org/10.1016/j.nicl.2016.09.002>.

- Dubé, J. B. *et al.* (2013) 'Genetic determinants of "cognitive impairment, no dementia"', *Journal of Alzheimer's Disease*, 33(3), pp. 831–840. doi: 10.3233/JAD-2012-121477.
- Dudbridge, F. (2013) 'Power and predictive accuracy of polygenic risk scores', *PLoS Genet*, 9(3), p. e1003348.
- Dufouil, C. *et al.* (2007) 'Hippocampal volume, apolipoprotein E and rate of cognitive decline in the EVA-MRI study', *Neurology*, 68(12), pp. A167–A167.
- Duong, T., Nikolaeva, M. and Acton, P. J. (1997) 'C-reactive protein-like immunoreactivity in the neurofibrillary tangles of Alzheimer's disease', *Brain research*, 749(1), pp. 152–156.
- Edden, R. A. and Jones, D. K. (2011) 'Spatial and orientational heterogeneity in the statistical sensitivity of skeleton-based analyses of diffusion tensor MR imaging data', *Journal of Neuroscience Methods*, 201(1), pp. 213–219. doi: 10.1016/j.jneumeth.2011.07.025.
- Egan, M. F. *et al.* (2003) 'The BDNF val66met polymorphism affects activity-dependent secretion of BDNF and human memory and hippocampal function', *Cell*, 112(2), pp. 257–269. doi: 10.1016/S0092-8674(03)00035-7.
- Egli, S. C. *et al.* (2015) 'Varying Strength of Cognitive Markers and Biomarkers to Predict Conversion and Cognitive Decline in an Early-Stage-Enriched Mild Cognitive Impairment Sample', *Journal of Alzheimer's Disease*, 44, pp. 625–633. doi: 10.3233/JAD-141716.
- Eichner, J. E. *et al.* (2002) 'Apolipoprotein E polymorphism and cardiovascular disease: A HuGE review', *American Journal of Epidemiology*, 155, pp. 487–495. doi: 10.1093/aje/155.6.487.
- Eikelenboom, P. *et al.* (2012) 'Whether, when and how chronic inflammation increases the risk of developing late-onset Alzheimer's disease', *Alzheimer's Research and Therapy*, 4. doi: 10.1186/alzrt118.
- Elliott, L. T. *et al.* (2018) 'Genome-wide association studies of brain imaging phenotypes in UK Biobank', *Nature*, 562(7726), pp. 210–216. doi: 10.1038/s41586-018-0571-7.
- Englund, E., Brun, A. and Alling, C. (1988) 'White matter changes in dementia of Alzheimer's type', *Brain*, 111(6), pp. 1425–1439. doi: 10.1093/brain/111.6.1425.
- Escott-Price, V., Sims, R., Bannister, C., *et al.* (2015) 'Common polygenic variation enhances risk prediction for Alzheimer's disease', *Brain*, 138(12), pp. 3673–3684.

doi: 10.1093/brain/awv268.

Escott-Price, V., Sims, R., Harold, D., *et al.* (2015) 'Using polygenic risk score to predict Alzheimer's disease', *Alzheimer's & Dementia*, 11(7), p. P872. doi: 10.1016/j.jalz.2015.08.069.

Escott-Price, V. *et al.* (2017) 'Polygenic risk score analysis of pathologically confirmed Alzheimer disease', *Annals of Neurology*, 82(2), pp. 311–314. doi: 10.1002/ana.24999.

Espeseth, T. *et al.* (2008) 'Accelerated age-related cortical thinning in healthy carriers of apolipoprotein E epsilon 64', *Neurobiology of Aging*, 29(3), pp. 329–340. doi: 10.1016/j.neurobiolaging.2006.10.030.

Fan, M. *et al.* (2010) 'Cortical thickness is associated with different apolipoprotein E genotypes in healthy elderly adults', *Neuroscience Letters*, 479(3), pp. 332–336. doi: 10.1016/j.neulet.2010.05.092.

Feldman, H. *et al.* (2001) 'Serum p97 levels as an aid to identifying Alzheimer's disease', *Journal of Alzheimer's Disease*, 3(5), pp. 507–516. doi: 10.3233/JAD-2001-3510.

Felsky, D. *et al.* (2018) 'Polygenic analysis of inflammatory disease variants and effects on microglia in the aging brain', *Molecular Neurodegeneration*, 13(1), p. 38. doi: 10.1186/s13024-018-0272-6.

Femminella, G. D. *et al.* (2018) 'Imaging and molecular mechanisms of Alzheimer's disease: A review', *International Journal of Molecular Sciences*, p. 3702. doi: 10.3390/ijms19123702.

Ferencz, B. *et al.* (2013) 'The influence of APOE and TOMM40 polymorphisms on hippocampal volume and episodic memory in old age', *Frontiers in Human Neuroscience*, 7(May), p. 198. doi: 10.3389/fnhum.2013.00198.

Ferguson, A. C. *et al.* (2020) 'Alzheimer's Disease Susceptibility Gene Apolipoprotein e (APOE) and Blood Biomarkers in UK Biobank (N=395,769)', *Journal of Alzheimer's Disease*, 76(4), pp. 1541–1551. doi: 10.3233/JAD-200338.

Fernández-Pérez, E. J. *et al.* (2020) 'Changes in neuronal excitability and synaptic transmission in nucleus accumbens in a transgenic Alzheimer's disease mouse model', *Scientific Reports*, 10(1). doi: 10.1038/s41598-020-76456-w.

Filippini, N. *et al.* (2009a) 'Distinct patterns of brain activity in young carriers of the APOE-epsilon 4 allele', *Proceedings of the National Academy of Sciences of the United States of America*, 106(17), pp. 7209–7214. doi: 10.1073/pnas.0811879106.

- Filippini, N. *et al.* (2009b) 'Distinct patterns of brain activity in young carriers of the APOE- $\epsilon$ 4 allele', *Proceedings of the National Academy of Sciences*, 106(17), pp. 7209–7214.
- Fischl, B. (2012) 'FreeSurfer', *NeuroImage*, pp. 774–781. doi: 10.1016/j.neuroimage.2012.01.021.
- Fleisher, A. S. *et al.* (2012) 'Florbetapir PET analysis of amyloid- $\beta$  deposition in the presenilin 1 E280A autosomal dominant Alzheimer's disease kindred: a cross-sectional study', *The Lancet Neurology*, 11(12), pp. 1057–1065.
- Fleisher, A. S. *et al.* (2015) 'Associations between biomarkers and age in the presenilin 1 E280A autosomal dominant Alzheimer disease kindred: A cross-sectional study', *JAMA Neurology*, 72(3), pp. 316–324. doi: 10.1001/jamaneurol.2014.3314.
- Fletcher, E. *et al.* (2013) 'Loss of fornix white matter volume as a predictor of cognitive impairment in cognitively normal elderly individuals', *JAMA Neurology*, 70(11), pp. 1389–1395. doi: 10.1001/jamaneurol.2013.3263.
- Foley, S. F. *et al.* (2016) 'Multimodal brain imaging reveals structural differences in Alzheimer's disease polygenic risk carriers: A study in healthy young adults', *Biological Psychiatry*. doi: 10.1016/j.biopsych.2016.02.033.
- Foley, S. F. *et al.* (2018) 'Fractional anisotropy of the uncinate fasciculus and cingulum in bipolar disorder type I, type II, unaffected siblings and healthy controls', *British Journal of Psychiatry*, 213(3), pp. 548–554. doi: 10.1192/bjp.2018.101.
- Fortea, J. *et al.* (2010) 'Increased cortical thickness and caudate volume precede atrophy in PSEN1 mutation carriers.', *Journal of Alzheimer's disease : JAD*, 22(3), pp. 909–922.
- Fox, N. C. *et al.* (1996) 'Presymptomatic hippocampal atrophy in Alzheimer's disease A longitudinal MRI study', *Brain*, 119(6), pp. 2001–2007. doi: 10.1093/brain/119.6.2001.
- Fox, N. C. *et al.* (2001) 'Imaging of onset and progression of Alzheimer's disease with voxel-compression mapping of serial magnetic resonance images', *Lancet*, 358(9277), pp. 201–205. doi: 10.1016/S0140-6736(01)05408-3.
- Fraser, Abigail *et al.* (2013) 'Cohort profile: The avon longitudinal study of parents and children: ALSPAC mothers cohort', *International Journal of Epidemiology*, 42(1), pp. 97–110. doi: 10.1093/ije/dys066.
- Fraser, A. *et al.* (2013) 'Cohort Profile: The Avon Longitudinal Study of Parents and

Children: ALSPAC mothers cohort', *International Journal of Epidemiology*, 42(1), pp. 97–110. doi: 10.1093/ije/dys066.

Friedewald, W. T., Levy, R. I. and Fredrickson, D. S. (1972) 'Estimation of the concentration of low-density lipoprotein cholesterol in plasma, without use of the preparative ultracentrifuge.', *Clinical chemistry*, 18(6), pp. 499–502. doi: 10.1093/clinchem/18.6.499.

Frisoni, G. B. *et al.* (2010) 'The clinical use of structural MRI in Alzheimer disease', *Nature Reviews Neurology*, pp. 67–77. doi: 10.1038/nrneurol.2009.215.

Fry, A. *et al.* (2017) 'Comparison of Sociodemographic and Health-Related Characteristics of UK Biobank Participants with Those of the General Population', *American Journal of Epidemiology*, 186(9), pp. 1026–1034. doi: 10.1093/aje/kwx246.

Futema, M. *et al.* (2017) 'Screening for familial hypercholesterolaemia in childhood: Avon Longitudinal Study of Parents and Children (ALSPAC)', *Atherosclerosis*, 260, pp. 47–55. doi: 10.1016/j.atherosclerosis.2017.03.007.

Gatz, M. *et al.* (1997) 'Heritability for Alzheimer's disease: the study of dementia in Swedish twins.', *The journals of gerontology. Series A, Biological sciences and medical sciences*, 52(2), pp. M117-25.

Gibson, J. *et al.* (2017) 'Assessing the presence of shared genetic architecture between Alzheimer's disease and major depressive disorder using genome-wide association data', *Translational Psychiatry*, 7(4), p. e1094. doi: 10.1038/tp.2017.49.

Giulietti, G. *et al.* (2018) 'Whole brain white matter histogram analysis of diffusion tensor imaging data detects microstructural damage in mild cognitive impairment and alzheimer's disease patients', *Journal of Magnetic Resonance Imaging*. doi: 10.1002/jmri.25947.

Goddard, K. A. B. *et al.* (2012) 'Building the evidence base for decision making in cancer genomic medicine using comparative effectiveness research', *Genetics in Medicine*, pp. 633–642. doi: 10.1038/gim.2012.16.

Gold, B. T. *et al.* (2014) 'White matter integrity is associated with cerebrospinal fluid markers of Alzheimer's disease in normal adults', *Neurobiology of Aging*, 35(10), pp. 2263–2271. doi: 10.1016/j.neurobiolaging.2014.04.030.

Good, C. D. *et al.* (2001) 'A Voxel-Based Morphometric Study of Ageing in 465 Normal Adult Human Brains', *NeuroImage*, 14(1), pp. 21–36. doi: <https://doi.org/10.1006/nimg.2001.0786>.

Greve, D. N. (2011) 'An Absolute Beginner's Guide to Surface- and Voxel-based

- Morphometric Analysis', *Proceedings of the International Society for Magnetic Resonance in Medicine*, i, pp. 1–7.
- Groen-Blokhuis, M. M. *et al.* (2014) 'Attention-deficit/hyperactivity disorder polygenic risk scores predict attention problems in a population-based sample of children', *Journal of the American Academy of Child and Adolescent Psychiatry*, 53(10), pp. 1123–1129. doi: 10.1016/j.jaac.2014.06.014.
- De Groot, M. *et al.* (2013) 'Improving alignment in Tract-based spatial statistics: Evaluation and optimization of image registration', *NeuroImage*, 76, pp. 400–411. doi: 10.1016/j.neuroimage.2013.03.015.
- Guerreiro, R., Wojtas, A., Bras, J., Carrasquillo, M., Rogaeva, E., Majounie, E., Cruchaga, C., Sassi, C., Kauwe, John S K, *et al.* (2013) 'TREM2 variants in Alzheimer's disease.', *The New England journal of medicine*, 368(2), pp. 117–27. doi: 10.1056/NEJMoa1211851.
- Guerreiro, R., Wojtas, A., Bras, J., Carrasquillo, M., Rogaeva, E., Majounie, E., Cruchaga, C., Sassi, C., Kauwe, John S.K., *et al.* (2013) 'TREM2 variants in Alzheimer's disease', *New England Journal of Medicine*, 368(2), pp. 117–127. doi: 10.1056/NEJMoa1211851.
- Haan, M. N. *et al.* (2008) 'C-reactive protein and rate of dementia in carriers and non carriers of Apolipoprotein APOE4 genotype', *Neurobiology of aging*, 29(12), pp. 1774–1782.
- Habes, M. *et al.* (2016) 'Advanced brain aging: Relationship with epidemiologic and genetic risk factors, and overlap with Alzheimer disease atrophy patterns', *Translational Psychiatry*, 6(4), pp. e775–e775. doi: 10.1038/tp.2016.39.
- Hagenaars, S. P., Harris, S. E., Davies, G., Marioni, R. E., *et al.* (2016) 'Genome-wide association study of cognitive functions and educational attainment in UK Biobank (N=112 151)', *Molecular Psychiatry*, 21, p. 758.
- Hagenaars, S. P., Harris, S. E., Davies, G., Hill, W. D., *et al.* (2016) 'Shared genetic aetiology between cognitive functions and physical and mental health in UK Biobank (N=112 151) and 24 GWAS consortia', *Molecular Psychiatry*, 21, p. 1624.
- Hardy, J. and Allsop, D. (1991) 'Amyloid deposition as the central event in the aetiology of Alzheimer's disease', *Trends in pharmacological sciences*, 12, pp. 383–388.
- Hari, R. and Salmelin, R. (2012) 'Magnetoencephalography: From SQUIDs to neuroscience. Neuroimage 20th Anniversary Special Edition.', *NeuroImage*, pp.

386–396. doi: 10.1016/j.neuroimage.2011.11.074.

Harold, D. *et al.* (2009) 'Genome-wide association study identifies variants at CLU and PICALM associated with Alzheimer's disease', *Nature genetics*, 41(10), pp. 1088–1093.

Harris, R. (2011) 'Epidemiologic Reviews Overview of Screening: Where We Are and Where We May Be Headed', *academic.oup.com*. doi: 10.1093/epirev/mxr006.

Harris, S. E. *et al.* (2014) 'Polygenic risk for alzheimer's disease is not associated with cognitive ability or cognitive aging in non-demented older people', *Journal of Alzheimer's Disease*, 39(3), pp. 565–574. doi: 10.3233/JAD-131058.

Harrison, J. R. *et al.* (2020) 'Imaging Alzheimer's genetic risk using diffusion MRI: A systematic review', *NeuroImage: Clinical*, p. 102359. doi: 10.1016/j.nicl.2020.102359.

Harrison, J. R. and Owen, M. J. (2016) 'Alzheimer's disease: the amyloid hypothesis on trial.', *The British journal of psychiatry: the journal of mental science*, 208(1), pp. 1–3. doi: 10.1192/bjp.bp.115.167569.

Harrison, T. M. *et al.* (2016) 'An Alzheimer's disease genetic risk score predicts longitudinal thinning of hippocampal complex subregions in healthy older adults', *eNeuro*, 3(3), pp. 795–804. doi: 10.1523/ENEURO.0098-16.2016.

Harrison, T. M. and Bookheimer, S. Y. (2016) 'Neuroimaging Genetic Risk for Alzheimer's Disease in Preclinical Individuals: From Candidate Genes to Polygenic Approaches', *Biological Psychiatry: Cognitive Neuroscience and Neuroimaging*, 1(1), pp. 14–23. doi: 10.1016/j.bpsc.2015.09.003.

Hashimoto, R. *et al.* (2009) 'Effect of the brain-derived neurotrophic factor and the apolipoprotein E polymorphisms on disease progression in preclinical Alzheimer's disease.', *Genes, Brain and Behavior*, 8(1), pp. 43–52.

Hawkins, B. T. and Davis, T. P. (2005) 'The blood-brain barrier/neurovascular unit in health and disease', *Pharmacological Reviews*, pp. 173–185. doi: 10.1124/pr.57.2.4.

Hayden, K. M. *et al.* (2015) 'Effect of APOE and CD33 on Cognitive Decline', *PLOS ONE*. Edited by J.-L. Fuh, 10(6), p. e0130419. doi: 10.1371/journal.pone.0130419.

Hayes, J. P. *et al.* (2017) 'Mild traumatic brain injury is associated with reduced cortical thickness in those at risk for Alzheimer's disease', *Brain*, 140(3), pp. 813–825. doi: 10.1093/brain/aww344.

Van Hecke, W. *et al.* (2009) 'Comparing isotropic and anisotropic smoothing for voxel-based DTI analyses: A simulation study', *Human Brain Mapping*, p. NA-NA.

doi: 10.1002/hbm.20848.

Den Heijer, T. *et al.* (2006) 'Use of hippocampal and amygdalar volumes on magnetic resonance imaging to predict dementia in cognitively intact elderly people', *Archives of General Psychiatry*, 63(1), pp. 57–62. doi: 10.1001/archpsyc.63.1.57.

Heise, V. *et al.* (2011) 'The APOE 4 allele modulates brain white matter integrity in healthy adults', *Molecular Psychiatry*, 16(9), pp. 908–916. doi: 10.1038/mp.2010.90.

Hoffmann, T. C. and Del Mar, C. (2017) 'Clinicians' expectations of the benefits and harms of treatments, screening, and tests: A systematic review', *JAMA Internal Medicine*, pp. 407–419. doi: 10.1001/jamainternmed.2016.8254.

Hofman, A. *et al.* (1997) 'Atherosclerosis, apolipoprotein E, and prevalence of dementia and Alzheimer's disease in the Rotterdam Study', *Lancet*, 349, pp. 151–154. doi: 10.1016/S0140-6736(96)09328-2.

Hohman, T. J. *et al.* (2017) 'APOE allele frequencies in suspected non-amyloid pathophysiology (SNAP) and the prodromal stages of Alzheimer's Disease', *PLOS ONE*. Edited by S. D. Ginsberg, 12(11), p. e0188501. doi: 10.1371/journal.pone.0188501.

10.1371/journal.pone.0188501.

Hohman, T. J., Koran, M. E. I. and Thornton-Wells, T. A. (2014) 'Genetic variation modifies risk for neurodegeneration based on biomarker status.', *Frontiers in aging neuroscience*, 6, p. 183. doi: 10.3389/fnagi.2014.00183.

Holmans, P. and Jones, L. (2012) 'Pathway analysis of IGAP GWAS data implicates endocytosis in the aetiology of late-onset Alzheimer's disease', *Alzheimer's & Dementia*, 8(4), p. P102. doi: 10.1016/j.jalz.2012.05.256.

Honea, R. A. *et al.* (2009) 'Impact of APOE on the healthy aging brain: A voxel-based MRI and DTI study', *Journal of Alzheimer's Disease*, 18(3), pp. 553–564. doi: 10.3233/JAD-2009-1163.

Hooper, C., Lovestone, S. and Sainz-Fuertes, R. (2008) 'Alzheimer's disease, diagnosis and the need for biomarkers', *Biomarker Insights*, 2008(3), pp. 317–323. doi: 10.4137/BMI.S682.

Howie, B., Marchini, J. and Stephens, M. (2011) 'Genotype imputation with thousands of genomes', *G3: Genes, Genomes, Genetics*, 1(6), pp. 457–470.

Hu, W. T. *et al.* (2012) 'Plasma multianalyte profiling in mild cognitive impairment and Alzheimer disease.', *Neurology*. Edited by A. Adrian Apostolova, Chen-Plotkin, Clark, Damholt, Deng, Dubois, Ellis, Fagan, Gerardin, Gunstad, Hu, Hu, Hu, Hunt, Inui, Jack, Jack, Kerola, Kondziella, McKeith, McKhann, Morris, Neary, O'Bryant,

Perrin, Petersen, Petersen, Poste, Quan, Ray, Reddy, Shaw, pp. 897–905.

Hye, A. *et al.* (2004) 'Glycogen synthase kinase-3 is increased in white cells early in Alzheimer's disease', *Neuroscience Letters*, 373(1), pp. 1–4. doi: 10.1016/j.neulet.2004.10.031.

Hye, A. *et al.* (2006) 'Proteome-based plasma biomarkers for Alzheimer's disease', *Brain*, 129(11), pp. 3042–3050. doi: 10.1093/brain/awl279.

Imbimbo, B., Solfrizzi, V. and Panza, F. (2010) 'Are NSAIDs useful to treat Alzheimer's disease or mild cognitive impairment?', *Frontiers in Aging Neuroscience*, p. 19.

Inouye, M. *et al.* (2018) 'Genomic Risk Prediction of Coronary Artery Disease in 480,000 Adults: Implications for Primary Prevention', *Journal of the American College of Cardiology*, 72(16), pp. 1883–1893. doi: 10.1016/j.jacc.2018.07.079.

Iwamoto, N. *et al.* (1994) 'Demonstration of CRP immunoreactivity in brains of Alzheimer's disease: immunohistochemical study using formic acid pretreatment of tissue sections', *Neuroscience letters*, 177(1–2), pp. 23–26.

Jack Jr., C. R. *et al.* (2010) 'Hypothetical model of dynamic biomarkers of the Alzheimer's pathological cascade', *Lancet Neurology*, 9(1), pp. 119–128.

Jack, C. R. *et al.* (2005) 'Brain atrophy rates predict subsequent clinical conversion in normal elderly and amnesic MCI', *Neurology*, 65(8), pp. 1227–1231. doi: 10.1212/01.wnl.0000180958.22678.91.

Jack, C. R. *et al.* (2013) 'Tracking pathophysiological processes in Alzheimer's disease: An updated hypothetical model of dynamic biomarkers', *The Lancet Neurology*, pp. 207–216. doi: 10.1016/S1474-4422(12)70291-0.

Jansen, I. E. *et al.* (2019) 'Genome-wide meta-analysis identifies new loci and functional pathways influencing Alzheimer's disease risk', *Nature Genetics*, 51(3), pp. 404–413. doi: 10.1038/s41588-018-0311-9.

Jefferson, A. L. *et al.* (2015) 'Adverse vascular risk is related to cognitive decline in older adults', *Journal of Alzheimer's Disease*, 44(4), pp. 1361–1373. doi: 10.3233/JAD-141812.

Jelescu, I. O., Veraart, J., *et al.* (2016) 'Degeneracy in model parameter estimation for multi-compartmental diffusion in neuronal tissue', *NMR in Biomedicine*, 29(1), pp. 33–47. doi: 10.1002/nbm.3450.

Jelescu, I. O., Zurek, M., *et al.* (2016) 'In vivo quantification of demyelination and recovery using compartment-specific diffusion MRI metrics validated by electron

- microscopy', *NeuroImage*, 132, pp. 104–114. doi: 10.1016/j.neuroimage.2016.02.004.
- Jeurissen, B. *et al.* (2013) 'Investigating the prevalence of complex fiber configurations in white matter tissue with diffusion magnetic resonance imaging', *Human Brain Mapping*, 34(11), pp. 2747–2766. doi: 10.1002/hbm.22099.
- Jeurissen, B. *et al.* (2019) 'Diffusion MRI fiber tractography of the brain', *NMR in Biomedicine*, 32(4), p. e3785. doi: 10.1002/nbm.3785.
- Ji, L. *et al.* (2015) 'White matter differences between multiple system atrophy (parkinsonian type) and parkinson's disease: A diffusion tensor image study', *Neuroscience*, 305, pp. 109–116. doi: 10.1016/j.neuroscience.2015.07.060.
- Jick, H. *et al.* (2000) 'Statins and the risk of dementia', *The Lancet*, 356(9242), pp. 1627–1631.
- Johansen-Berg, H. and Behrens, T. E. J. (2013) *Diffusion MRI: From Quantitative Measurement to In vivo Neuroanatomy: Second Edition*, *Diffusion MRI: From Quantitative Measurement to In vivo Neuroanatomy: Second Edition*. Elsevier Inc. doi: 10.1016/C2011-0-07047-3.
- Johnson, S. C. *et al.* (2011) 'The effect of TOMM40 poly-T length on gray matter volume and cognition in middle-aged persons with APOE  $\epsilon 3/\epsilon 3$  genotype', *Alzheimer's and Dementia*, 7(4), pp. 456–465. doi: 10.1016/j.jalz.2010.11.012.
- Jones, D. K. *et al.* (2005) 'The effect of filter size on VBM analyses of DT-MRI data', *NeuroImage*, 26(2), pp. 546–554. doi: 10.1016/j.neuroimage.2005.02.013.
- Jones, D. K. (2011) *Diffusion MRI : theory, methods, and applications*. Oxford University Press.
- Jones, D. K. *et al.* (2013) 'Distinct subdivisions of the cingulum bundle revealed by diffusion MRI fibre tracking: implications for neuropsychological investigations', *Neuropsychologia*, 51(1), pp. 67–78.
- Jones, D. K. *et al.* (2018) 'Microstructural imaging of the human brain with a "super-scanner": 10 key advantages of ultra-strong gradients for diffusion MRI', *NeuroImage*, pp. 8–38. doi: 10.1016/j.neuroimage.2018.05.047.
- Jones, D. K. and Cercignani, M. (2010) 'Twenty-five pitfalls in the analysis of diffusion MRI data', *NMR in Biomedicine*, 23(7), pp. 803–820. doi: 10.1002/nbm.1543.
- Jones, D. K., Knösche, T. R. and Turner, R. (2013) 'White matter integrity, fiber count, and other fallacies: The do's and don'ts of diffusion MRI', *NeuroImage*, pp.

239–254. doi: 10.1016/j.neuroimage.2012.06.081.

Jones, D. K. and Pierpaoli, C. (2005) 'Confidence mapping in diffusion tensor magnetic resonance imaging tractography using a bootstrap approach', *Magnetic Resonance in Medicine*, 53(5), pp. 1143–1149. doi: 10.1002/mrm.20466.

Jones, L. *et al.* (2010) 'Genetic evidence implicates the immune system and cholesterol metabolism in the aetiology of Alzheimer's disease.', *PloS one*, 5(11), p. e13950. doi: 10.1371/journal.pone.0013950.

Jonsson, T. *et al.* (2013) 'Variant of TREM2 Associated with the Risk of Alzheimer's Disease', *New England Journal of Medicine*, 368(2), pp. 107–116. doi: 10.1056/nejmoa1211103.

JW Gibbs (1898) 'Fourier's series', *nature.com*, 59(200).

Kaden, E., Knösche, T. R. and Anwander, A. (2007) 'Parametric spherical deconvolution: Inferring anatomical connectivity using diffusion MR imaging', *NeuroImage*, 37(2), pp. 474–488. doi: 10.1016/J.NEUROIMAGE.2007.05.012.

Kalaria, R. N., Akinyemi, R. and Ihara, M. (2012) 'Does vascular pathology contribute to Alzheimer changes?', *Journal of the Neurological Sciences*, 322, pp. 141–147. doi: 10.1016/j.jns.2012.07.032.

Kantarci, K. *et al.* (2014) 'White matter integrity determined with diffusion tensor imaging in older adults without dementia: Influence of amyloid load and neurodegeneration', *JAMA Neurology*, 71(12), pp. 1547–1554. doi: 10.1001/jamaneurol.2014.1482.

Karch, C. M., Cruchaga, C. and Goate, A. M. (2014) 'Alzheimer's disease genetics: From the bench to the clinic', *Neuron*, 83, pp. 11–26. doi: 10.1016/j.neuron.2014.05.041.

Karran, E., Mercken, M. and De Strooper, B. (2011) 'The amyloid cascade hypothesis for Alzheimer's disease: an appraisal for the development of therapeutics', *Nature Reviews Drug Discovery*, 10(9), pp. 698–712.

Kaye, J. A. *et al.* (1997) 'Volume loss of the hippocampus and temporal lobe in healthy elderly persons destined to develop dementia', *Neurology*, 48(5), pp. 1297–1304. doi: 10.1212/WNL.48.5.1297.

Kazemifar, S. *et al.* (2017) 'Spontaneous low frequency BOLD signal variations from resting-state fMRI are decreased in Alzheimer disease', *PLOS ONE*. Edited by K. Chen, 12(6), p. e0178529. doi: 10.1371/journal.pone.0178529.

Khan, W. *et al.* (2013) 'No differences in hippocampal volume between carriers and

non-carriers of the ApoE  $\epsilon$ 4 and  $\epsilon$ 2 alleles in young healthy adolescents', *Journal of Alzheimer's disease: JAD*, 40(1), pp. 37–43.

Khoury, M. J., Janssens, A. C. J. W. and Ransohoff, D. F. (2013) 'How can polygenic inheritance be used in population screening for common diseases?', *Genetics in Medicine*, 15(6), pp. 437–443. doi: 10.1038/gim.2012.182.

Killiany, R. J. *et al.* (2002) 'MRI measures of entorhinal cortex vs hippocampus in preclinical AD', *Neurology*, 58(8), pp. 1188–1196. doi: 10.1212/WNL.58.8.1188.

Kline, R. P. and Cuadrado, F. F. (2014) 'Cortical risk factors related to surgery from ADNI database blood and imaging biomarkers', *Anesthesia and Analgesia*, p. S151.

Kljajevic, V. *et al.* (2014) 'The  $\epsilon$ 4 genotype of apolipoprotein e and white matter integrity in Alzheimer's disease', *Alzheimer's and Dementia*, 10(3), pp. 401–404. doi: 10.1016/j.jalz.2013.02.008.

Knickmeyer, R. C. *et al.* (2014) 'Common variants in psychiatric risk genes predict brain structure at birth', *Cerebral Cortex*, 24(5), pp. 1230–1246. doi: 10.1093/cercor/bhs401.

Knight, W. D. *et al.* (2009) 'Acceleration of cortical thinning in familial Alzheimer's disease', *NBA*, 32, pp. 1765–1773. doi: 10.1016/j.neurobiolaging.2009.11.013.

Koal, T. *et al.* (2015) 'Sphingomyelin SM(d18:1/18:0) is significantly enhanced in cerebrospinal fluid samples dichotomized by pathological amyloid- $\beta$ 42, tau, and phospho-tau-181 levels', *Journal of Alzheimer's disease : JAD*, 44(4), pp. 1193–1201. doi: 10.3233/JAD-142319.

Koay, C. G. *et al.* (2006) 'A unifying theoretical and algorithmic framework for least squares methods of estimation in diffusion tensor imaging', *Journal of Magnetic Resonance*, 182(1), pp. 115–125. doi: 10.1016/j.jmr.2006.06.020.

Köhler, S. *et al.* (1998) 'Memory impairments associated with hippocampal versus parahippocampal-gyrus atrophy: an MR volumetry study in Alzheimer's disease', *Neuropsychologia*, 36(9), pp. 901–914.

Korf, E. S. C. *et al.* (2004) 'Medial temporal lobe atrophy on MRI predicts dementia in patients with mild cognitive impairment', *Neurology*, 63(1), pp. 94–100. doi: 10.1212/01.WNL.0000133114.92694.93.

Korologou-Linden, R., O'Keeffe, L., *et al.* (2019) 'Polygenic risk score for Alzheimer's disease and trajectories of cardiometabolic risk factors in children', *Wellcome open research*, 4, p. 125. doi: 10.12688/wellcomeopenres.15359.1.

Korologou-Linden, R., Anderson, E., *et al.* (2019) 'The causes and consequences of

Alzheimer's disease: phenome-wide evidence from Mendelian randomization'. doi: 10.1101/2019.12.18.19013847.

Koudinov, A. R. *et al.* (1998) 'Alzheimer's amyloid  $\beta$  interaction with normal human plasma high density lipoprotein: association with apolipoprotein and lipids', *Clinica chimica acta*, 270(2), pp. 75–84.

Koudinov, A. R. and Koudinova, N. V. (2001) 'Essential role for cholesterol in synaptic plasticity and neuronal degeneration', *The FASEB Journal*, 15, pp. 1858–1860. doi: 10.1096/fj.00-0815fje.

Koychev, I. *et al.* (2019) 'Deep and Frequent Phenotyping study protocol: an observational study in prodromal Alzheimer's disease', *BMJ Open*, 9, p. 24498. doi: 10.1136/bmjopen-2018-024498.

Kuchenbaecker, K. B. *et al.* (2017) 'Evaluation of polygenic risk scores for breast and ovarian cancer risk prediction in BRCA1 and BRCA2 mutation carriers', *Journal of the National Cancer Institute*, 109(7). doi: 10.1093/jnci/djw302.

Kunkle, B. W. *et al.* (2019) 'Genetic meta-analysis of diagnosed Alzheimer's disease identifies new risk loci and implicates A $\beta$ , tau, immunity and lipid processing', *Nature Genetics*, 51(3), pp. 414–430. doi: 10.1038/s41588-019-0358-2.

Lacour, A. *et al.* (2017) 'Genome-wide significant risk factors for Alzheimer's disease: Role in progression to dementia due to Alzheimer's disease among subjects with mild cognitive impairment', *Molecular Psychiatry*, 22(1), pp. 153–160. doi: 10.1038/mp.2016.18.

Lahoz, C. *et al.* (2001) 'Apolipoprotein E genotype and cardiovascular disease in the Framingham Heart Study', *Atherosclerosis*, 154(3), pp. 529–537. doi: 10.1016/S0021-9150(00)00570-0.

Laiterä, T. *et al.* (2016) 'Effects of Alzheimer's Disease-Associated Risk Loci on Amyloid- $\beta$  Accumulation in the Brain of Idiopathic Normal Pressure Hydrocephalus Patients', *Journal of Alzheimer's Disease*, 55(3), pp. 995–1003. doi: 10.3233/JAD-160554.

Lambert, J.-C. *et al.* (2013) 'Meta-analysis of 74,046 individuals identifies 11 new susceptibility loci for Alzheimer's disease', *Nature genetics*, 45(12), pp. 1452–1458.

Laukka, E. J. *et al.* (2015) 'Microstructural white matter properties mediate the association between APOE and perceptual speed in very old persons without dementia', *PLoS ONE*, 10(8), p. e0134766. doi: 10.1371/journal.pone.0134766.

Lawrie, S. M. *et al.* (2001) 'Brain structure, genetic liability, and psychotic symptoms

in subjects at high risk of developing schizophrenia', *Biological Psychiatry*, 49(10), pp. 811–823. doi: 10.1016/S0006-3223(00)01117-3.

Lee, J. M. *et al.* (2015) 'Identification of Genetic Factors that Modify Clinical Onset of Huntington's Disease', *Cell*, 162(3), pp. 516–526. doi: 10.1016/j.cell.2015.07.003.

Leemans, A. *et al.* (2009) 'ExploreDTI: a graphical toolbox for processing, analyzing, and visualizing diffusion MR data', in *Proceedings of the International Society for Magnetic Resonance in Medicine*, p. 3537.

Leemans, A. and Jones, D. K. (2009) 'The B-matrix must be rotated when correcting for subject motion in DTI data', *Magnetic Resonance in Medicine*, 61(6), pp. 1336–1349. doi: 10.1002/mrm.21890.

de Leeuw, C. A. *et al.* (2015) 'MAGMA: Generalized Gene-Set Analysis of GWAS Data', *PLoS Computational Biology*, 11(4). doi: 10.1371/journal.pcbi.1004219.

Lehmann, M. *et al.* (2010) 'Reduced cortical thickness in the posterior cingulate gyrus is characteristic of both typical and atypical Alzheimer's disease', *J Alzheimers Dis*, 20(2), pp. 587–598.

Lemaître, H. *et al.* (2005) 'No  $\epsilon 4$  gene dose effect on hippocampal atrophy in a large MRI database of healthy elderly subjects', *NeuroImage*, 24(4), pp. 1205–1213. doi: 10.1016/j.neuroimage.2004.10.016.

Li, G. *et al.* (2005) 'Serum cholesterol and risk of Alzheimer disease: A community-based cohort study', *Neurology*, 65(7), pp. 1045–1050. doi: 10.1212/01.wnl.0000178989.87072.11.

Li, J. *et al.* (2018) 'Polygenic risk for Alzheimer's disease influences precuneal volume in two independent general populations', *Neurobiology of Aging*, 64. doi: 10.1016/j.neurobiolaging.2017.12.022.

Li, L. H. *et al.* (2019) 'Analytical methods for cholesterol quantification', *Journal of Food and Drug Analysis*, 27(2), pp. 375–386. doi: 10.1016/j.jfda.2018.09.001.

Li, X *et al.* (2015) 'White matter changes in familial Alzheimer's disease.', *Journal of internal medicine*, 278(2), pp. 211–218.

Li, X. *et al.* (2015) 'White matter changes in familial Alzheimer's disease', *Journal of Internal Medicine*, 278(2), pp. 211–218. doi: 10.1111/joim.12352.

Licastro, F. *et al.* (2000) 'Increased plasma levels of interleukin-1, interleukin-6 and  $\alpha$ -1-antichymotrypsin in patients with Alzheimer's disease: peripheral inflammation or signals from the brain?', *Journal of Neuroimmunology*, 103(1), pp. 97–102. doi: 10.1016/S0165-5728(99)00226-X.

- Lind, J. *et al.* (2006) 'Reduced hippocampal volume in non-demented carriers of the apolipoprotein E epsilon4: relation to chronological age and recognition memory.', *Neuroscience letters*, 396(1), pp. 23–27. doi: 10.1016/j.neulet.2005.11.070.
- Liu, C. C. *et al.* (2013) 'Apolipoprotein E and Alzheimer disease: Risk, mechanisms and therapy', *Nature Reviews Neurology*, pp. 106–118. doi: 10.1038/nrneurol.2012.263.
- Logothetis, N. K. (2003) 'The underpinnings of the BOLD functional magnetic resonance imaging signal', *Journal of Neuroscience*, pp. 3963–3971. doi: 10.1523/jneurosci.23-10-03963.2003.
- Logue, M. W. *et al.* (2019) 'Use of an Alzheimer's disease polygenic risk score to identify mild cognitive impairment in adults in their 50s', *Molecular Psychiatry*, 24(3), pp. 421–430. doi: 10.1038/s41380-018-0030-8.
- Louwersheimer, E. *et al.* (2016) 'Alzheimer's disease risk variants modulate endophenotypes in mild cognitive impairment', *Alzheimer's & Dementia*, 12(8), pp. 872–881. doi: 10.1016/J.JALZ.2016.01.006.
- Lupton, M. K. *et al.* (2016) 'The effect of increased genetic risk for Alzheimer's disease on hippocampal and amygdala volume', *Neurobiology of Aging*, 40, pp. 68–77. doi: 10.1016/j.neurobiolaging.2015.12.023.
- Lyall, D. M. *et al.* (2014) 'Alzheimer's disease susceptibility genes APOE and TOMM40, and brain white matter integrity in the Lothian Birth Cohort 1936', *Neurobiology of Aging*, 35(6), pp. 1513–1513. doi: 10.1016/j.neurobiolaging.2014.01.006.
- Ma, C. *et al.* (2017) 'Disrupted Brain Structural Connectivity: Pathological Interactions Between Genetic APOE ε4 Status and Developed MCI Condition', *Molecular Neurobiology*, 54(9), pp. 6999–7007. doi: 10.1007/s12035-016-0224-5.
- Mak, E. *et al.* (2017) 'Structural neuroimaging in preclinical dementia: From microstructural deficits and grey matter atrophy to macroscale connectomic changes', *Ageing Research Reviews*, pp. 250–264. doi: 10.1016/j.arr.2016.10.001.
- Mapstone, M. *et al.* (2014) 'Plasma phospholipids identify antecedent memory impairment in older adults', *Nature Medicine*, 20, pp. 415–418. doi: 10.1038/nm.3466.
- Marcus, D. S. *et al.* (2011) 'Informatics and data mining tools and strategies for the human connectome project', *Frontiers in Neuroinformatics*, 27(5), p. 4. doi: 10.3389/fninf.2011.00004.

- Marden, J. R. *et al.* (2014) 'Validation of a polygenic risk score for dementia in black and white individuals', *Brain and behavior*, 4(5), pp. 687–697.
- Marden, J. R. *et al.* (2016) 'Using an Alzheimer Disease Polygenic Risk Score to Predict Memory Decline in Black and White Americans Over 14 Years of Follow-up', *Alzheimer Disease & Associated Disorders*, 30(3), pp. 195–202. doi: 10.1097/WAD.000000000000137.
- Marioni, R. E. *et al.* (2017) 'Genetic Stratification to Identify Risk Groups for Alzheimer's Disease', *Journal of Alzheimer's Disease*. Edited by M. A. Ikram, 57(1), pp. 275–283. doi: 10.3233/JAD-161070.
- Marioni, R. E. *et al.* (2018) 'GWAS on family history of Alzheimer's disease', *Translational Psychiatry*, 8(1), p. 99. doi: 10.1038/s41398-018-0150-6.
- Marks, D. *et al.* (2003) 'A review on the diagnosis, natural history, and treatment of familial hypercholesterolaemia', *Atherosclerosis*, pp. 1–14. doi: 10.1016/S0021-9150(02)00330-1.
- Martin, S. B. *et al.* (2010) 'Evidence that volume of anterior medial temporal lobe is reduced in seniors destined for mild cognitive impairment', *Neurobiology of Aging*, 31(7), pp. 1099–1106. doi: 10.1016/j.neurobiolaging.2008.08.010.
- Martiskainen, H. *et al.* (2015) 'Effects of Alzheimer's disease-associated risk loci on cerebrospinal fluid biomarkers and disease progression: A polygenic risk score approach', *Journal of Alzheimer's Disease*. doi: 10.3233/JAD-140777.
- Mauch, D. H. *et al.* (2001) 'CNS synaptogenesis promoted by glia-derived cholesterol', *Science*, 294, pp. 1354–1357. doi: 10.1126/science.294.5545.1354.
- Mayo, C. D. *et al.* (2017) 'Longitudinal changes in microstructural white matter metrics in Alzheimer's disease', *NeuroImage: Clinical*. doi: 10.1016/j.nicl.2016.12.012.
- McCarthy, C. S. *et al.* (2015) 'A comparison of FreeSurfer-generated data with and without manual intervention', *Frontiers in Neuroscience*, 9(OCT), p. 379. doi: 10.3389/fnins.2015.00379.
- McCarthy, S. *et al.* (2016) 'A reference panel of 64,976 haplotypes for genotype imputation', *Nature Genetics*, 48(10), pp. 1279–1283. doi: 10.1038/ng.3643.
- McGuinness, B. *et al.* (2009) 'Statins for the prevention of dementia', *Cochrane Database of Systematic Reviews*, (2).
- McKhann, G. *et al.* (1984) 'Clinical diagnosis of alzheimer's disease: Report of the NINCDS-ADRDA work group\* under the auspices of department of health and

human services task force on alzheimer's disease', *Neurology*, 34(7), pp. 939–944. doi: 10.1212/wnl.34.7.939.

McNab, J. A. *et al.* (2013) 'The Human Connectome Project and beyond: Initial applications of 300mT/m gradients', *NeuroImage*, 80, pp. 234–245. doi: 10.1016/j.neuroimage.2013.05.074.

Metzler-Baddeley, C. *et al.* (2011) 'Frontotemporal connections in episodic memory and aging: a diffusion MRI tractography study', *The Journal of Neuroscience*, 31(37), pp. 13236–13245.

Mielke, M. M. *et al.* (2012) 'Fornix integrity and hippocampal volume predict memory decline and progression to Alzheimer's disease', *Alzheimer's & Dementia*, 8(2), pp. 105–113. doi: 10.1016/J.JALZ.2011.05.2416.

Mistry, S. *et al.* (2017) 'The use of polygenic risk scores to identify phenotypes associated with genetic risk of schizophrenia: Systematic review', *Schizophrenia Research*. doi: 10.1016/j.schres.2017.10.037.

Miwa, K. *et al.* (2016) 'Interleukin-6, interleukin-6 receptor gene variant, small-vessel disease and incident dementia', *European Journal of Neurology*, 23(3), pp. 656–663. doi: 10.1111/ene.12921.

Moher, D. *et al.* (2009) 'Preferred Reporting Items for Systematic Reviews and Meta-Analyses: The PRISMA Statement', *Annals of Internal Medicine*, 151(4), p. 264. doi: 10.7326/0003-4819-151-4-200908180-00135.

Morgan, A. R. *et al.* (2017) 'The correlation between inflammatory biomarkers and polygenic risk score in Alzheimer's disease', *Journal of Alzheimer's Disease*, 56(1), pp. 25–36. doi: 10.3233/JAD-160889.

Mori, S. *et al.* (2005) *MRI Atlas of Human White Matter*.

Mormino, E. C. *et al.* (2016) 'Polygenic risk of Alzheimer disease is associated with early- and late-life processes.', *Neurology*, 87(5), pp. 481–8. doi: 10.1212/WNL.0000000000002922.

Mosconi, L. *et al.* (2008) 'Multicenter standardized 18F-FDG PET diagnosis of mild cognitive impairment, Alzheimer's disease, and other dementias', *Journal of Nuclear Medicine*, 49(3), pp. 390–398. doi: 10.2967/jnumed.107.045385.

Moskvina, V. *et al.* (2010) 'Genetic differences between five european populations', *Human Heredity*, 70(2), pp. 141–149. doi: 10.1159/000313854.

Naj, A. C. and Schellenberg, G. D. (2017) 'Genomic variants, genes, and pathways of Alzheimer's disease: An overview', *American Journal of Medical Genetics Part B*:

- Neuropsychiatric Genetics*, 174(1), pp. 5–26. doi: 10.1002/ajmg.b.32499.
- NCBI Genetic Testing Registry (2020). Available at: <https://www.ncbi.nlm.nih.gov/gtr/> (Accessed: 7 December 2020).
- Nevo, U. *et al.* (2001) 'Diffusion anisotropy MRI for quantitative assessment of recovery in injured rat spinal cord.', *Magnetic resonance in medicine*, 45(1), pp. 1–9.
- Newlander, S. M. *et al.* (2014) 'Methodological improvements in voxel-based analysis of diffusion tensor images: Applications to study the impact of apolipoprotein e on white matter integrity', *Journal of Magnetic Resonance Imaging*, 39(2), pp. 387–397. doi: 10.1002/jmri.24157.
- Ng, A. *et al.* (2018) 'IL-1 $\beta$ , IL-6, TNF-  $\alpha$  and CRP in Elderly Patients with Depression or Alzheimer's disease: Systematic Review and Meta-Analysis', *Scientific Reports*, 8(1), p. 12050. doi: 10.1038/s41598-018-30487-6.
- Nie, X. *et al.* (2017) 'Subregional structural alterations in hippocampus and nucleus accumbens correlate with the clinical impairment in patients with Alzheimer's Disease clinical spectrum: Parallel combining volume and vertex-based approach', *Frontiers in Neurology*, 8(AUG), p. 15. doi: 10.3389/fneur.2017.00399.
- Nierenberg, J. *et al.* (2005) 'Abnormal white matter integrity in healthy apolipoprotein E epsilon4 carriers', *NeuroReport*, 16(12), pp. 1369–1372. doi: 10.1097/01.wnr.0000174058.49521.16.
- Nordestgaard, B. G. *et al.* (2013) 'Familial hypercholesterolaemia is underdiagnosed and undertreated in the general population: Guidance for clinicians to prevent coronary heart disease', *European Heart Journal*, 34(45). doi: 10.1093/eurheartj/eh273.
- Novikov, D. S., Kiselev, V. G. and Jespersen, S. N. (2018) 'On modeling', *Magnetic Resonance in Medicine*, pp. 3172–3193. doi: 10.1002/mrm.27101.
- Nyberg, L. and Salami, A. (2014) 'The APOE  $\epsilon$ 4 allele in relation to brain white-matter microstructure in adulthood and aging', *Scandinavian Journal of Psychology*, 55(3), pp. 263–267. doi: 10.1111/sjop.12099.
- O'Bryant, S. E. *et al.* (2013) 'The link between C-reactive protein and Alzheimer's disease among Mexican Americans', *Journal of Alzheimer's disease : JAD*, 34(3), pp. 701–706. doi: 10.3233/JAD-122071.
- O'Dwyer, L., Lamberton, F., Matura, S., Tanner, C., *et al.* (2012) 'Reduced Hippocampal Volume in Healthy Young ApoE4 Carriers: An MRI Study', *Plos One*, 7(11). doi: 10.1371/journal.pone.0048895.

- O'Dwyer, L., Lamberton, F., Matura, S., Scheibe, M., *et al.* (2012) 'White matter differences between healthy young ApoE4 carriers and non-carriers identified with tractography and support vector machines.', *PloS one*, 7(4). doi: 10.1371/journal.pone.0036024.
- Oishi, K. *et al.* (2012) 'The fornix sign: A potential sign for alzheimer's disease based on diffusion tensor imaging', *Journal of Neuroimaging*, 22(4), pp. 365–374. doi: 10.1111/j.1552-6569.2011.00633.x.
- Olsson, B. *et al.* (2016) 'CSF and blood biomarkers for the diagnosis of Alzheimer's disease: a systematic review and meta-analysis', *The Lancet Neurology*, 15(7), pp. 673–684. doi: 10.1016/S1474-4422(16)00070-3.
- Operto, G. *et al.* (2018) 'White matter microstructure is altered in cognitively normal middle-aged APOE-ε4 homozygotes', *Alzheimer's Research & Therapy*, 10(1), p. 48. doi: 10.1186/s13195-018-0375-x.
- Osei-Bimpong, A., Meek, J. H. and Lewis, S. M. (2007) 'ESR or CRP? A comparison of their clinical utility', *Hematology*, pp. 353–357. doi: 10.1080/10245330701340734.
- Pagani, M. *et al.* (2017) 'Early identification of MCI converting to AD: a FDG PET study', *European Journal of Nuclear Medicine and Molecular Imaging*, 44(12), pp. 2042–2052. doi: 10.1007/s00259-017-3761-x.
- Pan, X. *et al.* (2017) 'Metabolomic profiling of bile acids in clinical and experimental samples of Alzheimer's disease', *Metabolites*, 7(2). doi: 10.3390/metabo7020028.
- Panagiotaki, E. *et al.* (2012) 'Compartment models of the diffusion MR signal in brain white matter: A taxonomy and comparison', *NeuroImage*, 59(3), pp. 2241–2254. doi: 10.1016/j.neuroimage.2011.09.081.
- Di Paolo, G. and Kim, T. W. (2011) 'Linking lipids to Alzheimer's disease: Cholesterol and beyond', *Nature Reviews Neuroscience*, pp. 284–296. doi: 10.1038/nrn3012.
- Papenberg, G. *et al.* (2015) 'Genetics and Functional Imaging: Effects of APOE, BDNF, COMT, and KIBRA in Aging', *Neuropsychology Review*, 25(1), pp. 47–62. doi: 10.1007/s11065-015-9279-8.
- Papenberg, G. *et al.* (2017) 'Dopamine Receptor Genes Modulate Associative Memory in Old Age', *Journal of Cognitive Neuroscience*, 29(2), pp. 245–253. doi: 10.1162/jocn\_a\_01048.
- Parker, G.D., Marshall, D., Rosin, P.L., Drage, N., Richmond, S. Jones, D. K. (2013) 'Fast and fully automated clustering of whole brain tractography results using shape-space analysis.', in *Proceedings of the International Society for Magnetic Resonance*

*in Medicine.*

- Parker, G. D. *et al.* (2013) 'RESDORE: Robust Estimation in Spherical Deconvolution by Outlier Rejection', in *Proceedings of the International Society for Magnetic Resonance in Medicine*, p. 3148.
- Parra, M. A. *et al.* (2015) 'Memory binding and white matter integrity in familial Alzheimer's disease', *Brain*, 138(5), pp. 1355–1369. doi: 10.1093/brain/awv048.
- Pascual, B. *et al.* (2012) 'Decreased carbon-11-flumazenil binding in early Alzheimer's disease', *Brain*, 135(9), pp. 2817–2825. doi: 10.1093/brain/aws210.
- Pasqualetti, P. *et al.* (2009) 'A randomized controlled study on effects of ibuprofen on cognitive progression of Alzheimer's disease', *Aging Clinical and Experimental Research*, 21(2), pp. 102–110. doi: 10.1007/BF03325217.
- Pasternak, O. *et al.* (2009) 'Free water elimination and mapping from diffusion MRI', *Magnetic Resonance in Medicine*, 62(3), pp. 717–730. doi: 10.1002/mrm.22055.
- Patel, T. *et al.* (2018) 'Whole-exome sequencing of the BDR cohort: evidence to support the role of the *PILRA* gene in Alzheimer's disease', *Neuropathology and Applied Neurobiology*, 44(5), pp. 506–521. doi: 10.1111/nan.12452.
- Paus, T. (2010) 'Growth of white matter in the adolescent brain: Myelin or axon?', *Brain and Cognition*, pp. 26–35. doi: 10.1016/j.bandc.2009.06.002.
- Perea, R. D. *et al.* (2018) 'Connectome-derived diffusion characteristics of the fornix in Alzheimer's disease', *NeuroImage: Clinical*, 19, pp. 331–342. doi: 10.1016/J.NICL.2018.04.029.
- Persson, J. *et al.* (2006) 'Altered brain white matter integrity in healthy carriers of the APOE  $\epsilon$ 4 allele A risk for AD?', *Neurology*, 66(7), pp. 1029–1033.
- Persson, N. *et al.* (2014) 'Regional brain shrinkage over two years: Individual differences and effects of pro-inflammatory genetic polymorphisms', *Neuroimage*, 103, pp. 334–348. doi: 10.1016/j.neuroimage.2014.09.042.
- Petersen, R. C. and Morris, J. C. (2005) 'Mild cognitive impairment as a clinical entity and treatment target', *Archives of neurology*, 62(7), pp. 1160–1163.
- Pierpaoli, C. and Basser, P. J. (1996) 'Toward a quantitative assessment of diffusion anisotropy', *Magnetic Resonance in Medicine*, 36(6), pp. 893–906. doi: 10.1002/mrm.1910360612.
- Pievani, M. *et al.* (2013) 'Striatal morphology in early-onset and late-onset Alzheimer's disease: A preliminary study', *Neurobiology of Aging*, 34(7), pp. 1728–1739. doi: 10.1016/j.neurobiolaging.2013.01.016.

Pilling, L. C. *et al.* (2016) 'Human longevity is influenced by many genetic variants: Evidence from 75,000 UK Biobank participants', *Aging*, 8(3), pp. 547–560. doi: 10.18632/aging.100930.

Pilling, L. C. *et al.* (2017) 'Red blood cell distribution width: Genetic evidence for aging pathways in 116,666 volunteers.', *PloS one*. Edited by D. E. Arking, 12(9), p. e0185083. doi: 10.1371/journal.pone.0185083.

Polimanti, R. *et al.* (2017) 'Cross-Phenotype Polygenic Risk Score Analysis of Persistent Post-Concussive Symptoms in U.S. Army Soldiers with Deployment-Acquired Traumatic Brain Injury', *Journal of Neurotrauma*, 34(4), pp. 781–789. doi: 10.1089/neu.2016.4550.

Pratico, D. *et al.* (2000) 'Increased 8,12-iso-iPF2a-VI in Alzheimer's disease: Correlation of a noninvasive index of lipid peroxidation with disease severity', *Annals of Neurology*, 48(5), pp. 809–812. doi: 10.1002/1531-8249(200011)48:5<809::aid-ana19>3.0.co;2-9.

Price, A. L. *et al.* (2006) 'Principal components analysis corrects for stratification in genome-wide association studies', *Nature Genetics*, 38(8), pp. 904–909. doi: 10.1038/ng1847.

Price, C. P. *et al.* (1987) 'Development and validation of a particle-enhanced turbidimetric immunoassay for C-reactive protein', *Journal of Immunological Methods*, 99(2), pp. 205–211. doi: 10.1016/0022-1759(87)90129-3.

Proitsi, P. *et al.* (2017) 'Association of blood lipids with Alzheimer's disease: A comprehensive lipidomics analysis', *Alzheimer's & Dementia*, 13(2), pp. 140–151. doi: <https://doi.org/10.1016/j.jalz.2016.08.003>.

Purcell, S. *et al.* (2007) 'PLINK: a tool set for whole-genome association and population-based linkage analyses.', *American journal of human genetics*, 81(3), pp. 559–75. doi: 10.1086/519795.

Purcell, S. M. *et al.* (2009) 'Common polygenic variation contributes to risk of schizophrenia and bipolar disorder', *Nature*, 460(7256), pp. 748–752.

Quiroz, Y. T. *et al.* (2013) 'Cortical atrophy in presymptomatic Alzheimer's disease presenilin 1 mutation carriers', *Journal of Neurology, Neurosurgery and Psychiatry*, 84(5), pp. 556–561. doi: 10.1136/jnnp-2012-303299.

Quiroz, Y. T. *et al.* (2015) 'Brain imaging and blood biomarker abnormalities in children with autosomal dominant Alzheimer disease a cross-sectional study', *JAMA neurology*, 72(8), pp. 912–919.

- R Development Core Team 3.0.1. (2013) 'A Language and Environment for Statistical Computing', *R Foundation for Statistical Computing*.
- Ramanan, V. K. *et al.* (2012) 'Pathway analysis of genomic data: concepts, methods, and prospects for future development.', *Trends in genetics : TIG*, 28(7), pp. 323–32. doi: 10.1016/j.tig.2012.03.004.
- Reiman, E. M. *et al.* (2012) 'Brain imaging and fluid biomarker analysis in young adults at genetic risk for autosomal dominant Alzheimer's disease in the presenilin 1 E280A kindred: A case-control study', *The Lancet Neurology*, 11(12), pp. 1048–1056. doi: 10.1016/S1474-4422(12)70228-4.
- Reisberg, B. *et al.* (2002) 'Evidence and mechanisms of retrogenesis in Alzheimer's and other dementias: management and treatment import.', *American journal of Alzheimer's disease and other dementias*, 17(4), pp. 202–12. doi: 10.1177/153331750201700411.
- Reitz, C. *et al.* (2010) 'Association of higher levels of high-density lipoprotein cholesterol in elderly individuals and lower risk of late-onset Alzheimer disease', *Archives of Neurology*, 67(12), pp. 1491–1497. doi: 10.1001/archneurol.2010.297.
- Remer, J. *et al.* (2020) 'Longitudinal white matter and cognitive development in pediatric carriers of the apolipoprotein  $\epsilon$ 4 allele', *NeuroImage*, 222, p. 117243. doi: 10.1016/j.neuroimage.2020.117243.
- Ries, M. *et al.* (2000) 'Diffusion tensor MRI of the spinal cord', *Magnetic Resonance in Medicine*, 44(6), pp. 884–892. doi: 10.1002/1522-2594(200012)44:6<884::AID-MRM9>3.0.CO;2-Q.
- Ringman, J. M. *et al.* (2007) 'Diffusion tensor imaging in preclinical and presymptomatic carriers of familial Alzheimer's disease mutations', *Brain*, 130(7), pp. 1767–1776. doi: 10.1093/brain/awm102.
- Rodrigue, K. M. *et al.* (2012) ' $\beta$ -Amyloid burden in healthy aging Regional distribution and cognitive consequences', *Neurology*, 78(6), pp. 387–395.
- Rodríguez-Rodríguez, E. *et al.* (2013) 'Genetic risk score predicting accelerated progression from mild cognitive impairment to Alzheimer's disease.', *Journal of neural transmission (Vienna, Austria : 1996)*, 120(5), pp. 807–12. doi: 10.1007/s00702-012-0920-x.
- Roses, A. D. *et al.* (2010) 'A TOMM40 variable-length polymorphism predicts the age of late-onset Alzheimer's disease', *Pharmacogenomics Journal*, 10(5), pp. 375–384. doi: 10.1038/tpj.2009.69.

- Rushworth, J. V and Hooper, N. M. (2011) 'Lipid Rafts: Linking Alzheimer's Amyloid- $\beta$  Production, Aggregation, and Toxicity at Neuronal Membranes', *International Journal of Alzheimer's Disease*. Edited by K. Yanagisawa, p. 14. doi: 10.4061/2011/603052.
- Ryan, L. *et al.* (2011) 'Age-related differences in white matter integrity and cognitive function are related to APOE status', *Neuroimage*, 54(2), pp. 1565–1577. doi: 10.1016/j.neuroimage.2010.08.052.
- Ryan, N. S. *et al.* (2013) 'Magnetic resonance imaging evidence for presymptomatic change in thalamus and caudate in familial Alzheimer's disease', *Brain*, 136(5), pp. 1399–1414. doi: 10.1093/brain/awt065.
- Sabuncu, M. R. *et al.* (2011) 'The Dynamics of Cortical and Hippocampal Atrophy in Alzheimer Disease', *Archives of Neurology*, 68(8), pp. 1040–1048. doi: 10.1001/archneurol.2011.167.
- Sabuncu, M. R. *et al.* (2012) 'The association between a polygenic Alzheimer score and cortical thickness in clinically normal subjects', *Cerebral cortex*, 22(11), pp. 2653–2661.
- Salat, D. H. *et al.* (2004) 'Thinning of the cerebral cortex in aging', *Cerebral Cortex*, 14(7), pp. 721–730. doi: 10.1093/cercor/bhh032.
- Salminen, L. E. *et al.* (2013) 'Neuronal fiber bundle lengths in healthy adult carriers of the ApoE4 allele: A quantitative tractography DTI study', *Brain Imaging and Behavior*, 7(3), pp. 274–281. doi: 10.1007/s11682-013-9225-4.
- Sambamurti, K. *et al.* (2012) 'Can the Failure of Alzheimer's Disease Clinical Trials be Stepping Stones to Ultimate Success: Is the Amyloid Hypothesis Discredited by Animal Models', *J Alzheimers Dis Parkinsonism*, 2, p. e115.
- Sanchez-Valle, R. *et al.* (2016) 'White Matter Abnormalities Track Disease Progression in PSEN1 Autosomal Dominant Alzheimer's Disease', *Journal of Alzheimer's disease : JAD*, 51(3), pp. 827–835. doi: 10.3233/jad-150899.
- Santos, C. Y. *et al.* (2017) 'Pathophysiologic relationship between Alzheimer's disease, cerebrovascular disease, and cardiovascular risk: a review and synthesis', *Alzheimer's & Dementia: Diagnosis, Assessment & Disease Monitoring*, 7, pp. 69–87.
- Sapkota, S. and Dixon, R. A. (2018) 'A Network of Genetic Effects on Non-Demented Cognitive Aging: Alzheimer's Genetic Risk (CLU + CR1+PICALM) Intensifies Cognitive Aging Genetic Risk (COMT + BDNF) Selectively for APOE  $\epsilon$ 4

Carriers', *Journal of Alzheimer's Disease*, 62(2), pp. 887–900. doi: 10.3233/JAD-170909.

Saura, C. A. *et al.* (2004) 'Loss of presenilin function causes impairments of memory and synaptic plasticity followed by age-dependent neurodegeneration', *Neuron*, 42(1), pp. 23–36. doi: 10.1016/S0896-6273(04)00182-5.

Scheuner, D. *et al.* (1996) *Secreted amyloid  $\beta$ -protein similar to that in the senile plaques of Alzheimer's disease is increased in vivo by the presenilin 1 and 2 and APP mutations linked to, nature.com.*

Schizophrenia Working Group of the Psychiatric Genomics, C. (2014) 'Biological insights from 108 schizophrenia-associated genetic loci', *Nature*, 511(7510), pp. 421–427.

Schmidt, R. *et al.* (2002) 'Early inflammation and dementia: a 25-year follow-up of the Honolulu-Asia Aging Study', *Annals of neurology*, 52(2), pp. 168–174.

Schott, J. M. *et al.* (2003) 'Assessing the onset of structural change in familial Alzheimer's disease.', *Annals of neurology*, 53(2), pp. 181–8. doi: 10.1002/ana.10424.

Schultz, S. A. *et al.* (2017) 'Cardiorespiratory fitness alters the influence of a polygenic risk score on biomarkers of AD.', *Neurology*, 88(17), pp. 1650–1658. doi: 10.1212/WNL.0000000000003862.

Seeley, W. W. *et al.* (2009) 'Neurodegenerative Diseases Target Large-Scale Human Brain Networks', *Neuron*, 62(1), pp. 42–52. doi: 10.1016/j.neuron.2009.03.024.

Selkoe, D. J. (1991) 'The molecular pathology of Alzheimer's disease', *Neuron*, 6(4), pp. 487–498.

Seo, Y. *et al.* (2013) 'Diffusion tensor imaging metrics in neonates - A comparison of manual region-of-interest analysis vs. tract-based spatial statistics', in *Pediatric Radiology*, pp. 69–79. doi: 10.1007/s00247-012-2527-7.

Serra, L. *et al.* (2009) 'Grey and white matter changes at different stages of Alzheimer's disease', *Journal of Alzheimer's disease: JAD*, 19(1), pp. 147–159.

Sexton, C. E. *et al.* (2011) 'A meta-analysis of diffusion tensor imaging in mild cognitive impairment and Alzheimer's disease', *Neurobiology of Aging*, 32(12), pp. 2322.e5-2322.e18. doi: 10.1016/J.NEUROBIOLAGING.2010.05.019.

Sharp, T. H. *et al.* (2020) 'Population neuroimaging: Generation of a comprehensive data resource within the ALSPAC pregnancy and birth cohort', *Wellcome Open*

*Research*, 5. doi: 10.12688/wellcomeopenres.16060.1.

Shaw, P. *et al.* (2007) 'Cortical morphology in children and adolescents with different apolipoprotein E gene polymorphisms: an observational study', *Lancet Neurology*, 6(6), pp. 494–500. doi: 10.1016/S1474-4422(07)70106-0.

Shi, F. *et al.* (2009) 'Hippocampal volume and asymmetry in mild cognitive impairment and Alzheimer's disease: Meta-analyses of MRI studies.', *Hippocampus*, 19(11), pp. 1055–64. doi: 10.1002/hipo.20573.

Slattery, C. F. *et al.* (2017) 'ApoE influences regional white-matter axonal density loss in Alzheimer's disease', *Neurobiology of Aging*, 57, pp. 8–17. doi: 10.1016/j.neurobiolaging.2017.04.021.

Sleegers, K. *et al.* (2015) 'A 22-single nucleotide polymorphism Alzheimer's disease risk score correlates with family history, onset age, and cerebrospinal fluid A $\beta$ 42', *Alzheimer's and Dementia*, 11(12), pp. 1452–1460. doi: 10.1016/j.jalz.2015.02.013.

Smith, C. D. *et al.* (2007) 'Brain structural alterations before mild cognitive impairment', *Neurology*, 68(16), pp. 1268–1273. doi: 10.1212/01.wnl.0000259542.54830.34.

Smith, J. C. *et al.* (2016) 'Interactive effects of physical activity and APOE- $\epsilon$ 4 on white matter tract diffusivity in healthy elders', *NeuroImage*, 131, pp. 102–112. doi: 10.1016/j.neuroimage.2015.08.007.

Smith, S., Alfaro-Almagro, F. and Miller, K. (2015) 'UK Biobank Brain Imaging Documentation', (October), pp. 1–31.

Smith, S. M. *et al.* (2006) 'Tract-based spatial statistics: Voxelwise analysis of multi-subject diffusion data', *NeuroImage*, 31(4), pp. 1487–1505. doi: 10.1016/j.neuroimage.2006.02.024.

Smith, S. M. *et al.* (2007) 'Acquisition and voxelwise analysis of multi-subject diffusion data with tract-based spatial statistics', *Nature Protocols*, 2(3), pp. 499–503. doi: 10.1038/nprot.2007.45.

Soares, H. D. *et al.* (2012) 'Plasma biomarkers associated with the apolipoprotein E genotype and Alzheimer disease.', *Archives of Neurology*, pp. 1310–1317.

Soares, J. M. *et al.* (2013) 'A hitchhiker's guide to diffusion tensor imaging', *Frontiers in Neuroscience*, (7 MAR). doi: 10.3389/fnins.2013.00031.

Song, I.-U. *et al.* (2015) 'Relationship between the hs-CRP as non-specific biomarker and Alzheimer's disease according to aging process', *International journal of medical sciences*, 12(8), pp. 613–617. doi: 10.7150/ijms.12742.

- Song, S.-K. *et al.* (2002) 'Dysmyelination revealed through MRI as increased radial (but unchanged axial) diffusion of water.', *NeuroImage*, 17(3), pp. 1429–36.
- Stampfer, M. J. (2006) 'Cardiovascular disease and Alzheimer's disease: Common links', *Journal of Internal Medicine*, 260(3), pp. 211–23. doi: 10.1111/j.1365-2796.2006.01687.x.
- Stang, A. (2010) 'Critical evaluation of the Newcastle-Ottawa scale for the assessment of the quality of nonrandomized studies in meta-analyses', *European Journal of Epidemiology*, 25(9), pp. 603–605. doi: 10.1007/s10654-010-9491-z.
- Stejskal, E. O. and Tanner, J. E. (1965) 'Spin Diffusion Measurements: Spin Echoes in the Presence of a Time-Dependent Field Gradient', *J. Chem. Phys.*, 42, p. 288. doi: 10.1063/1.1695690.
- Stocker, H. *et al.* (2018) 'The genetic risk of Alzheimer's disease beyond APOE  $\epsilon$ 4: systematic review of Alzheimer's genetic risk scores', *Translational Psychiatry*, 8(1), p. 166. doi: 10.1038/s41398-018-0221-8.
- Striepens, N. *et al.* (2011) 'Interaction effects of subjective memory impairment and ApoE4 genotype on episodic memory and hippocampal volume', *Psychological Medicine*, 41(9), pp. 1997–2006. doi: 10.1017/S0033291711000067.
- Strijkers, G. J., Drost, M. R. and Nicolay, K. (2011) 'Diffusion MRI: Theory, methods, and applications', pp. 672–689.
- Strimbu, K. and Tavel, J. A. (2010) 'What are biomarkers?', *Current opinion in HIV and AIDS*, 5(6), pp. 463–466. doi: 10.1097/COH.0b013e32833ed177.
- Su, F. *et al.* (2017) 'Integration of Multilocus Genetic Risk into the Default Mode Network Longitudinal Trajectory during the Alzheimer's Disease Process', *Journal of Alzheimer's Disease*, 56(2), pp. 491–507. doi: 10.3233/JAD-160787.
- Sudlow, C. *et al.* (2015) 'UK Biobank: An Open Access Resource for Identifying the Causes of a Wide Range of Complex Diseases of Middle and Old Age', *PLOS Medicine*, 12(3), p. e1001779. doi: 10.1371/journal.pmed.1001779.
- Swardfager, W. *et al.* (2010) 'A meta-analysis of cytokines in Alzheimer's disease.', *Biological psychiatry*, 68(10), pp. 930–41. doi: 10.1016/j.biopsych.2010.06.012.
- Szekely, C. A. *et al.* (2004) 'Nonsteroidal anti-inflammatory drugs for the prevention of Alzheimer's disease: a systematic review', *Neuroepidemiology*, 23(4), pp. 159–169.
- Takao, H. *et al.* (2011) 'Effect of head size on diffusion tensor imaging', *NeuroImage*, 57(3), pp. 958–967. doi: <https://doi.org/10.1016/j.neuroimage.2011.05.019>.

- Tan, C. H. *et al.* (2018) 'Polygenic hazard score: an enrichment marker for Alzheimer's associated amyloid and tau deposition', *Acta Neuropathologica*, 135(1), pp. 85–93. doi: 10.1007/s00401-017-1789-4.
- Tan, Z. S. *et al.* (2007) 'Inflammatory markers and the risk of Alzheimer disease: The Framingham study', *Neurology*, 68(22), pp. 1902–1908. doi: 10.1212/01.wnl.0000263217.36439.da.
- Tang, S. X. *et al.* (2017) 'Diffusion characteristics of the fornix in patients with Alzheimer's disease', *Psychiatry Research: Neuroimaging*, 265, pp. 72–76. doi: 10.1016/J.PSCYCHRESNS.2016.09.012.
- Tanzi, R. E. (2012) 'The genetics of Alzheimer disease', *Cold Spring Harbor perspectives in medicine*, 2(10), pp. 2157–1422.
- Taylor, A. E. *et al.* (2018) 'Exploring the association of genetic factors with participation in the Avon Longitudinal Study of Parents and Children', *International Journal of Epidemiology*, 47(4), pp. 1207–1216. doi: 10.1093/ije/dyy060.
- Teslovic (2013) 'Biological, clinical and population relevance of 95 loci for blood lipids', *Journal of Chemical Information and Modeling*, 53, pp. 1689–1699.
- The Metabolomics Innovation Centre (2020). Available at: <https://www.metabolomicscentre.ca/> (Accessed: 2 September 2020).
- The Wellcome Trust Case Control Consortium (2007) 'Genome-wide association study of 14,000 cases of seven common diseases and 3,000 shared controls.', *Nature*, 447, pp. 661–678.
- Thomason, M. E. and Thompson, P. M. (2011) 'Diffusion Imaging, White Matter, and Psychopathology', *Annual Review of Clinical Psychology*, 7(1), pp. 63–85. doi: 10.1146/annurev-clinpsy-032210-104507.
- Toledo, J. B. *et al.* (2017) 'Metabolic network failures in Alzheimer's disease: A biochemical road map', *Alzheimer's & Dementia*, 13(9), pp. 965–984. doi: 10.1016/j.jalz.2017.01.020.
- Tosto, G. *et al.* (2017) 'Polygenic risk scores in familial Alzheimer disease', *Neurology*, 88(12), pp. 1180–1186. doi: 10.1212/WNL.0000000000003734.
- Tournier, J.-D., Mori, S. and Leemans, A. (2011) 'Diffusion tensor imaging and beyond.', *Magnetic resonance in medicine*, 65(6), pp. 1532–56. doi: 10.1002/mrm.22924.
- Trushina, E. *et al.* (2012) 'Defects in Mitochondrial Dynamics and Metabolomic Signatures of Evolving Energetic Stress in Mouse Models of Familial Alzheimer's

Disease', *PLoS ONE*. Edited by D. I. Finkelstein, 7(2), p. e32737. doi: 10.1371/journal.pone.0032737.

Tynkkynen, J. *et al.* (2018) 'Association of branched-chain amino acids and other circulating metabolites with risk of incident dementia and Alzheimer's disease: A prospective study in eight cohorts', *Alzheimer's and Dementia*, 14(6), pp. 723–733. doi: 10.1016/j.jalz.2018.01.003.

UK Biobank (2007) *UK Biobank ethics and governance framework version 3.0*.

Verhaaren, B. F. J. *et al.* (2013) 'Alzheimer's Disease Genes and Cognition in the Nondemented General Population', *Biological Psychiatry*, 73(5), pp. 429–434. doi: 10.1016/j.biopsych.2012.04.009.

Villain, N. *et al.* (2010) 'Sequential relationships between grey matter and white matter atrophy and brain metabolic abnormalities in early Alzheimer's disease', *Brain*, 133(11), pp. 3301–3314. doi: 10.1093/brain/awq203.

Viticchi, G. *et al.* (2015) 'Framingham risk score can predict cognitive decline progression in Alzheimer's disease', *Neurobiology of Aging*, 36(11), pp. 2940–2945. doi: 10.1016/j.neurobiolaging.2015.07.023.

Vollmar, C. *et al.* (2010) 'Identical, but not the same: Intra-site and inter-site reproducibility of fractional anisotropy measures on two 3.0T scanners', *NeuroImage*, 51(4), pp. 1384–1394. doi: 10.1016/j.neuroimage.2010.03.046.

Voyle, N. *et al.* (2017) 'Genetic Risk as a Marker of Amyloid- $\beta$  and Tau Burden in Cerebrospinal Fluid', *Journal of Alzheimer's Disease*, 55(4), pp. 1417–1427. doi: 10.3233/JAD-160707.

Vuksanović, V. *et al.* (2019) 'Cortical Thickness and Surface Area Networks in Healthy Aging, Alzheimer's Disease and Behavioral Variant Fronto-Temporal Dementia', *International Journal of Neural Systems*, 29(6), p. 1850055. doi: 10.1142/S0129065718500557.

Wagner, M. *et al.* (2018) 'Evaluation of the Concurrent Trajectories of Cardiometabolic Risk Factors in the 14 Years before Dementia', *JAMA Psychiatry*, 75(10), pp. 1033–1042. doi: 10.1001/jamapsychiatry.2018.2004.

Wai, Y. Y. *et al.* (2014) 'Tract-based spatial statistics: Application to mild cognitive impairment', *BioMed Research International*, 2014. doi: 10.1155/2014/713079.

Wakana, S. *et al.* (2007) 'Reproducibility of quantitative tractography methods applied to cerebral white matter', *NeuroImage*, 36(3), pp. 630–644. doi: 10.1016/j.neuroimage.2007.02.049.

- Walhovd, K. B. *et al.* (2020) 'Genetic risk for Alzheimer disease predicts hippocampal volume through the human lifespan', *Neurology Genetics*, 6(5), p. e506. doi: 10.1212/NXG.0000000000000506.
- Wang, J. *et al.* (2015) 'Apolipoprotein E epsilon4 modulates functional brain connectome in Alzheimer's disease.', *Human Brain Mapping*. Edited by A. Achard Ariza, Bassett, Bialonski, Biswal, Brown, Buchman, Buckner, Buckner, Bullmore, Cao, Corder, Craddock, Dick, Drzezga, Drzezga, Fagundo, Fair, Filippini, Fillenbaum, Fornito, Fox, Ginestet, Goveas, Greicius, He, Hedden, Hermundstad, Honey, Johnson, pp. 1828–1846.
- Wang, K. *et al.* (2007) 'Altered functional connectivity in early Alzheimer's disease: A resting-state fMRI study', *Human Brain Mapping*, 28(10), pp. 967–978. doi: 10.1002/hbm.20324.
- Wang, R. *et al.* (2015) 'Effects of vascular risk factors and APOE  $\epsilon$ 4 on white matter integrity and cognitive decline', *Neurology*, 84(11), pp. 1128–1135. doi: 10.1212/WNL.0000000000001379.
- Wedeen, V. J. *et al.* (2005) 'Mapping complex tissue architecture with diffusion spectrum magnetic resonance imaging', *Magnetic Resonance in Medicine*, 54(6), pp. 1377–1386. doi: 10.1002/mrm.20642.
- Westlye, L. T. *et al.* (2012) 'Effects of APOE on brain white matter microstructure in healthy adults', *Neurology*, 79(19), pp. 1961–1969. doi: 10.1212/WNL.0b013e3182735c9c.
- Wheeler-Kingshott, C. A. M. *et al.* (2012) 'A new approach to structural integrity assessment based on axial and radial diffusivities', *Functional Neurology*, 27(2), pp. 85–90.
- Wheeler-Kingshott, C. A. M. and Cercignani, M. (2009) 'About "axial" and "radial" diffusivities', *Magnetic Resonance in Medicine*, 61(5), pp. 1255–1260. doi: 10.1002/mrm.21965.
- Wilkins, J. M. and Trushina, E. (2018) 'Application of metabolomics in Alzheimer's disease', *Frontiers in Neurology*, p. 1. doi: 10.3389/fneur.2017.00719.
- Wilson JMG, J. G. (1968) 'Principles and Practice of Screening for Disease. WHO Public Paper 34', *Geneva: World Health Bibliography Organization*, p. 168.
- Winston, G. P. (2012) 'The physical and biological basis of quantitative parameters derived from diffusion MRI.', *Quantitative imaging in medicine and surgery*, 2(4), pp. 254–65. doi: 10.3978/j.issn.2223-4292.2012.12.05.

- Wishart, H. A. *et al.* (2006) 'Regional brain atrophy in cognitively intact adults with a single APOE  $\epsilon$ 4 allele', *Neurology*, 67(7), pp. 1221–1224. doi: 10.1212/01.wnl.0000238079.00472.3a.
- Wollam, M. E. *et al.* (2015) 'Genetic Risk Score Predicts Late-Life Cognitive Impairment.', *Journal of aging research*, 2015, p. 267062. doi: 10.1155/2015/267062.
- Wray, N. R. *et al.* (2014) 'Research review: Polygenic methods and their application to psychiatric traits.', *Journal of child psychology and psychiatry, and allied disciplines*, 55(10), pp. 1068–87. doi: 10.1111/jcpp.12295.
- Wray, N. R. *et al.* (2020) 'From Basic Science to Clinical Application of Polygenic Risk Scores', *JAMA Psychiatry*. doi: 10.1001/jamapsychiatry.2020.3049.
- Wu, M. *et al.* (2008) 'Comparison of EPI Distortion Correction Methods in Diffusion Tensor MRI Using a Novel Framework', in, pp. 321–329. doi: 10.1007/978-3-540-85990-1\_39.
- Wurth, C., Guimard, N. K. and Hecht, M. H. (2002) 'Mutations that reduce aggregation of the Alzheimer's A $\beta$ 42 peptide: An unbiased search for the sequence determinants of A $\beta$  amyloidogenesis', *Journal of Molecular Biology*, 319(5), pp. 1279–1290. doi: 10.1016/S0022-2836(02)00399-6.
- Xia, D. *et al.* (2015) 'Presenilin-1 knockin mice reveal loss-of-function mechanism for familial Alzheimer's disease', *Neuron*, 85(5), pp. 967–981. doi: 10.1016/j.neuron.2015.02.010.
- Xiao, E. *et al.* (2017) 'Late-Onset Alzheimer's Disease Polygenic Risk Profile Score Predicts Hippocampal Function', *Biological Psychiatry: Cognitive Neuroscience and Neuroimaging*, 2(8), pp. 673–679. doi: 10.1016/j.bpsc.2017.08.004.
- Xiao, Q. *et al.* (2015) 'Risk prediction for sporadic Alzheimer's disease using genetic risk score in the Han Chinese population', *Oncotarget*, 6(35). doi: 10.18632/oncotarget.6271.
- Xu, G. *et al.* (2009) 'The influence of parental history of Alzheimer's disease and apolipoprotein E epsilon4 on the BOLD signal during recognition memory.', *Brain*. Edited by B. Alexander Bondi, Bookheimer, Borghesani, Braak, Buckner, Chetelat, Corder, Dickerson, Drzezga, Fleisher, Fratiglioni, Ghebremedhin, Greicius, Hao, Harvey, Jack, Janssen, Johnson, Johnson, Johnson, Kao, Kemppainen, Lind, Logothetis, Lundqvist, L, 132(2), pp. 383–391. doi: 10.1093/brain/awn254.
- Yarchoan, M. *et al.* (2013) 'Association of plasma C-reactive protein levels with the diagnosis of Alzheimer's disease', *Journal of the Neurological Sciences*, 333(1–2),

pp. 9–12. doi: 10.1016/j.jns.2013.05.028.

Yeh, C. H. *et al.* (2020) 'Mapping Structural Connectivity Using Diffusion MRI: Challenges and Opportunities', *Journal of Magnetic Resonance Imaging*, p. 88. doi: 10.1002/jmri.27188.

Yeung, C. H. C. and Schooling, C. M. (2020) 'Systemic inflammatory regulators and risk of Alzheimer's disease: a bidirectional Mendelian-randomization study', *International Journal of Epidemiology*. doi: 10.1093/ije/dyaa241.

Yokoyama, J. S., Lee, A. K. L., *et al.* (2015) 'Apolipoprotein epsilon 4 Is Associated with Lower Brain Volume in Cognitively Normal Chinese but Not White Older Adults', *PLoS ONE*, 10(3), p. no pagination. doi: 10.1371/journal.pone.0118338.

Yokoyama, J. S., Bonham, L. W., *et al.* (2015) 'Decision tree analysis of genetic risk for clinically heterogeneous Alzheimer's disease.', *BMC neurology*, 15(1), p. 47. doi: 10.1186/s12883-015-0304-6.

Zhang, H. *et al.* (2012) 'NODDI: Practical in vivo neurite orientation dispersion and density imaging of the human brain', *NeuroImage*, 61(4), pp. 1000–1016. doi: 10.1016/j.neuroimage.2012.03.072.

Zhang, S. *et al.* (2015) 'Association of White Matter Integrity and Cognitive Functions in Chinese Non-Demented Elderly with the APOE  $\epsilon$  4 Allele', *Journal of Alzheimer's Disease*, 48(3), pp. 781–791. doi: 10.3233/JAD-150357.

Zhang, Y. *et al.* (2009) 'White matter damage in frontotemporal dementia and Alzheimer's disease measured by diffusion MRI', *Brain*, 132(9), pp. 2579–2592. doi: 10.1093/brain/awp071.

Zheng, H. *et al.* (2019) 'Tissue-Specific Metabolomics Analysis Identifies the Liver as a Major Organ of Metabolic Disorders in Amyloid Precursor Protein/Presenilin 1 Mice of Alzheimer's Disease', *Journal of Proteome Research*, 18(3), pp. 1218–1227. doi: 10.1021/acs.jproteome.8b00847.

Zhou, X. *et al.* (2019) 'Non-coding variability at the APOE locus contributes to the Alzheimer's risk', *Nature Communications*, 10(1), p. 3310. doi: 10.1038/s41467-019-10945-z.

Zhuang, L. *et al.* (2012) 'Microstructural white matter changes in cognitively normal individuals at risk of amnesic MCI', *Neurology*, 79(8), pp. 748–754. doi: 10.1212/WNL.0b013e3182661f4d.

Zuccato, C. and Cattaneo, E. (2009) 'Brain-derived neurotrophic factor in neurodegenerative diseases', *Nature Reviews Neurology*, pp. 311–322. doi:

10.1038/nrneurol.2009.54.

## APPENDIX A

### Supplementary materials for the AD PRS systematic review

**Table 1.** Search strategy terms used for searching Embase, Medline via Ovid and PsychINFO.

Key word
1. Polygenic risk score.mp
2. Risk profile score.mp
3. Polygenic variation.mp
4. Genome-wide association study/
5. GWAS <sup>a</sup> .mp
6. Gene score.mp
7. Genetic score.mp
8. Allele score.mp
9. Polygenic.mp
10. exp Polymorphism, single nucleotide/
11. SNP <sup>b</sup> score.mp
12. or/1-10
13. exp Alzheimer disease/
14. Alzheimer*.mp
15. or/13-14
16. 12 and 15
17. limit 16 to: <ul style="list-style-type: none"><li>- English language</li><li>- Humans</li><li>- Yr= "2009-3<sup>rd</sup> August 2018"</li></ul>

a. GWAS; Genome Wide Association Studies, b. SNP; Single Nucleotide Polymorphism

**Table 2.** List of data extracted from all studies

Details
• Author
• Year
• Discovery sample
• Target sample
• Outcome measure(s)
• N
• P value thresholds
• Phenotypes/correlates
• $\beta$ , odds ratio or hazard ratio
• Confidence intervals
• P
• R2 (%)

**Table 3.** Studies examining associations with threshold-based PRS, principle results. (Excel file)

<https://www.ncbi.nlm.nih.gov/pmc/articles/PMC7242840/bin/jad-74-jad191233-s002.xlsx>

**Table 4.** Studies examining associations with Bonferroni-significant SNP PRS, principle results. (Excel file)

<https://www.ncbi.nlm.nih.gov/pmc/articles/PMC7242840/bin/jad-74-jad191233-s003.xlsx>

## APPENDIX B

### Supplementary Material for the dMRI Alzheimer's genetics systematic review

**Table 1:** Literature Search Methodology

Search Terms:	Inclusion Criteria:	Exp. Alzheimer* Alzheimer's Disease Mild Cognitive Impairment, MCI Familial Alzheimer's Disease (autosomal-dominant AD) Apolipoprotein E type 4, ApoE4 Presenilin 1 and 2 ( <i>PS1</i> and <i>PS2</i> ) Amyloid beta-Protein Precursor, (APP) Cognitive Performance Cognitive Disorder Cognitive Dysfunction Dementia
	AND	Exp. Diffusion Tensor Imaging* Diffusion Tensor Imaging DTI Diffusion Magnetic Resonance Imaging dMRI White Matter Microstructure White Matter White Matter Integrity Connectome Connectomics
	Selection:	English Language Humans Year: 2000 – 2019
	Exclusion Criteria:	Dementia (unspecified) Vascular dementia Lewy Body dementia Other dementia Huntington's Unspecified memory decline Other Neuropsychiatric disorder Cognitive function – unrelated to Alzheimer's pathology Other Imaging modalities Acquisition method – FMRI, volumetric studies

**Table 2.** List of data extracted

Paper Title
Author
Year
Population Group (i.e. MCI, AD patients, APOE carriers)
Abstract
N
Participant Age
Gene type (e.g. APOE, polygenic, familial, etc)
Study design (e.g. Case-control, etc)
Quality Assessment Score (e.g. Newcastle Ottawa Score)
Country of Origin
Diffusion Method (i.e. ROI, TBSS)
Field Strength (T)
B value (s/mm <sup>2</sup> )
Acquisition Voxel Size
Number of Directions
NEX
Pre-processing
Model Estimation
Anisotropy Measure
Diffusivity Measure
Other Metric Brain Region(s)
AD Associated Symptoms
Key Results
Methods Text

**Table 3. PRISMA Checklist**



**PRISMA 2009 Checklist**

Section/topic	#	Checklist Item	Reported on page #
<b>TITLE</b>			
Title	1	Identify the report as a systematic review, meta-analysis, or both.	1
<b>ABSTRACT</b>			
Structured summary	2	Provide a structured summary including, as applicable: background; objectives; data sources; study eligibility criteria, participants, and interventions; study appraisal and synthesis methods; results; limitations; conclusions and implications of key findings; systematic review registration number.	2
<b>INTRODUCTION</b>			
Rationale	3	Describe the rationale for the review in the context of what is already known.	3-5
Objectives	4	Provide an explicit statement of questions being addressed with reference to participants, interventions, comparisons, outcomes, and study design (PICOS).	6,7
<b>METHODS</b>			
Protocol and registration	5	Indicate if a review protocol exists, if and where it can be accessed (e.g., Web address), and, if available, provide registration information including registration number.	NA
Eligibility criteria	6	Specify study characteristics (e.g., PICOS, length of follow-up) and report characteristics (e.g., years considered, language, publication status) used as criteria for eligibility, giving rationale.	6,7
Information sources	7	Describe all information sources (e.g., databases with dates of coverage, contact with study authors to identify additional studies) in the search and date last searched.	6
Search	8	Present full electronic search strategy for at least one database, including any limits used, such that it could be repeated.	Supplementary Materials
Study selection	9	State the process for selecting studies (i.e., screening, eligibility, included in systematic review, and, if applicable, included in the meta-analysis).	6,7
Data collection process	10	Describe method of data extraction from reports (e.g., piloted forms, independently, in duplicate) and any processes for obtaining and confirming data from investigators.	6,7
Data items	11	List and define all variables for which data were sought (e.g., PICOS, funding sources) and any assumptions and simplifications made.	Supplementary Materials
Risk of bias in individual studies	12	Describe methods used for assessing risk of bias of individual studies (including specification of whether this was done at the study or outcome level), and how this information is to be used in any data synthesis.	7
Summary measures	13	State the principal summary measures (e.g., risk ratio, difference in means).	NA
Synthesis of results	14	Describe the methods of handling data and combining results of studies, if done, including measures of consistency (e.g., $I^2$ ) for each meta-analysis.	NA



**PRISMA 2009 Checklist**

Page 1 of 2

Section/topic	#	Checklist Item	Reported on page #
Risk of bias across studies	15	Specify any assessment of risk of bias that may affect the cumulative evidence (e.g., publication bias, selective reporting within studies).	NA
Additional analyses	16	Describe methods of additional analyses (e.g., sensitivity or subgroup analyses, meta-regression), if done, indicating which were pre-specified.	NA
<b>RESULTS</b>			
Study selection	17	Give numbers of studies screened, assessed for eligibility, and included in the review, with reasons for exclusions at each stage, ideally with a flow diagram.	7-16
Study characteristics	18	For each study, present characteristics for which data were extracted (e.g., study size, PICOS, follow-up period) and provide the citations.	Supplementary Materials
Risk of bias within studies	19	Present data on risk of bias of each study and, if available, any outcome level assessment (see item 12).	21
Results of individual studies	20	For all outcomes considered (benefits or harms), present, for each study: (a) simple summary data for each intervention group (b) effect estimates and confidence intervals, ideally with a forest plot.	NA
Synthesis of results	21	Present results of each meta-analysis done, including confidence intervals and measures of consistency.	NA
Risk of bias across studies	22	Present results of any assessment of risk of bias across studies (see Item 15).	NA
Additional analysis	23	Give results of additional analyses, if done (e.g., sensitivity or subgroup analyses, meta-regression [see Item 16]).	NA
<b>DISCUSSION</b>			
Summary of evidence	24	Summarize the main findings including the strength of evidence for each main outcome; consider their relevance to key groups (e.g., healthcare providers, users, and policy makers).	17-23
Limitations	25	Discuss limitations at study and outcome level (e.g., risk of bias), and at review-level (e.g., incomplete retrieval of identified research, reporting bias).	17-23
Conclusions	26	Provide a general interpretation of the results in the context of other evidence, and implications for future research.	23
<b>FUNDING</b>			
Funding	27	Describe sources of funding for the systematic review and other support (e.g., supply of data); role of funders for the systematic review.	23

Table 4.

Table 3.4 Significant associations (p < 0.05) of AD risk variants and TBSS imaging phenotypes in the UK Biobank GWAS.

Variant	Chr.	Position	Closest gene	ROI FA	P-value	Beta	ROI MD	P-value	Beta				
rs4844610	1	207802552	CR1	Body of corpus callosum	3.30E-04	-0.073	Body of corpus callosum	1.70E-04	0.069				
				Superior corona radiata L	3.30E-04	-0.073	Splenium of corpus callosum	3.90E-04	0.066				
				Posterior thalamic radiation R	5.90E-04	-0.068	Posterior corona radiata R	8.70E-04	0.06				
				Posterior thalamic radiation L	6.80E-04	-0.067	Superior longitudinal fasciculus L	9.10E-04	0.064				
				Posterior corona radiata L	7.00E-04	-0.07	Superior corona radiata L	1.50E-03	0.055				
				Sagittal stratum L	1.90E-03	-0.064	Superior corona radiata R	2.00E-03	0.053				
				Superior corona radiata R	2.50E-03	-0.062	Posterior corona radiata L	2.40E-03	0.056				
				Anterior corona radiata R	2.60E-03	-0.059	Anterior corona radiata R	3.60E-03	0.054				
				Posterior corona radiata R	2.60E-03	-0.063	Sagittal stratum L	5.40E-03	0.053				
				Superior longitudinal fasciculus L	2.60E-03	-0.062	Posterior thalamic radiation R	5.60E-03	0.053				
				Splenium of corpus callosum	3.00E-03	-0.062	Cingulum cingulate gyrus L	5.60E-03	0.049				
				Superior longitudinal fasciculus R	6.80E-03	-0.056	Anterior corona radiata L	7.10E-03	0.049				
				Anterior limb of internal capsule R	9.80E-03	-0.053	Cingulum cingulate gyrus R	8.30E-03	0.045				
				Genu of corpus callosum	1.10E-02	-0.05	Posterior thalamic radiation L	9.30E-03	0.05				
				Anterior corona radiata L	1.50E-02	-0.047	Genu of corpus callosum	1.30E-02	0.044				
				Anterior limb of internal capsule L	4.20E-02	-0.041	Cingulum hippocampus R	1.30E-02	0.049				
				Middle cerebellar peduncle	4.70E-02	-0.039	Fornix cres+Stria terminalis L	1.60E-02	0.046				
							Sagittal stratum R	1.80E-02	0.045				
							Anterior limb of internal capsule L	2.00E-02	0.041				
							Fornix cres+Stria terminalis R	2.00E-02	0.044				
							Superior longitudinal fasciculus R	2.00E-02	0.043				
							Retrolenticular part of internal capsule L	2.40E-02	0.044				
							Middle cerebellar peduncle	2.50E-02	0.042				
							Anterior limb of internal capsule R	2.80E-02	0.038				
							Superior fronto-occipital fasciculus R	4.70E-02	0.034				
							Retrolenticular part of internal capsule R	4.80E-02	0.039				
				rs6733839	2	127892810	BIN1	Uncinate fasciculus L	4.60E-03	0.046	<i>No significant associations</i>		
								Uncinate fasciculus R	4.80E-03	0.046			
								Cingulum cingulate gyrus R	9.20E-03	0.042			
								Anterior corona radiata L	9.50E-03	0.039			
Cingulum cingulate gyrus L	9.70E-03	0.041											
External capsule R	1.10E-02	0.04											
Anterior limb of internal capsule R	3.70E-02	0.033											
Anterior corona radiata R	4.80E-02	0.031											
Uncinate fasciculus L	3.60E-02	0.04											
rs10933431	2	233981912	INPP5D	<i>No significant associations</i>									
rs9271058	6	32575406	HLA -DRB1	<i>Not included in analysis</i>									
rs75932628	6	41129252	TREM2	Cerebral peduncle L	2.40E-02	0.35	Cerebral peduncle L	3.30E-02	-0.32				
				Posterior limb of internal capsule R	2.70E-02	0.37	Retrolenticular part of internal capsule R	4.30E-02	-0.33				
				Posterior limb of internal capsule L	2.70E-02	0.36							
rs9473117	6	47431284	CD2AP	Cingulum cingulate gyrus L	6.30E-03	-0.047	<i>No significant associations</i>						
				Cingulum cingulate gyrus R	2.70E-02	-0.038							
rs12539172	7	100091795	NYAP1	Fornix cres+Stria terminalis R	2.30E-04	0.054	Fornix cres+Stria terminalis R	4.60E-03	-0.043				
				Retrolenticular part of internal capsule L	2.90E-04	0.059	Fornix cres+Stria terminalis L	5.30E-03	-0.044				
				Fornix cres+Stria terminalis L	1.00E-03	0.048							
				Medial lemniscus L	8.00E-03	0.043							
				Superior cerebellar peduncle L	9.10E-03	0.042							
				Superior fronto-occipital fasciculus L	1.30E-02	0.041							
				Genu of corpus callosum	1.40E-02	0.039							
				Retrolenticular part of internal capsule R	1.70E-02	0.04							
				Anterior limb of internal capsule L	2.30E-02	0.038							
				Cingulum cingulate gyrus L	2.70E-02	0.036							
				Inferior cerebellar peduncle L	2.80E-02	0.036							
				Posterior limb of internal capsule R	3.90E-02	0.034							
				Posterior thalamic radiation R	4.70E-02	0.032							
rs10808026	7	143099133	EPHA1	<i>No significant associations</i>									
rs73223431	8	27219987	PTK2B	Fornix	7.90E-04	0.047	Fornix	5.50E-04	-0.048				
				Cingulum cingulate gyrus R	1.20E-02	0.04	Cingulum cingulate gyrus R	1.00E-02	0.034				
rs9331896	8	27467686	CLU	Superior cerebellar peduncle R	2.40E-02	0.035	<i>No significant associations</i>						
				Retrolenticular part of internal capsule L	3.40E-02	0.033							

Continued >>

rs3740688	11	47380340	SPI1	Sagittal stratum L	3.00E-03	0.047	Genu of corpus callosum	6.00E-03	-0.038				
				External capsule L	2.30E-02	0.034	Medial lemniscus R	4.20E-02	-0.031				
				Uncinate fasciculus L	2.60E-02	0.036							
				Inferior cerebellar peduncle R	3.20E-02	0.033							
				Sagittal stratum R	3.30E-02	0.034							
				Uncinate fasciculus R	3.40E-02	0.034							
				Medial lemniscus R	3.60E-02	0.032							
rs7933202	11	59936926	MS4A2	Posterior corona radiata L	4.60E-02	0.032							
				Cingulum cingulate gyrus R	7.20E-03	-0.043	Cingulum cingulate gyrus L	4.80E-03	0.039				
				Middle cerebellar peduncle	7.70E-03	-0.041	Superior corona radiata L	6.10E-03	0.037				
				Cerebral peduncle R	1.40E-02	-0.037	Posterior corona radiata L	1.10E-02	0.037				
				Cingulum cingulate gyrus L	2.20E-02	-0.036	Tapetum L	1.10E-02	0.04				
				Anterior corona radiata R	2.50E-02	-0.035	Genu of corpus callosum	1.80E-02	0.034				
				Cerebral peduncle L	2.90E-02	-0.032	Body of corpus callosum	1.80E-02	0.034				
rs3851179	11	85868640	PICALM	Superior corona radiata R			Superior corona radiata R	2.10E-02	0.031				
				Posterior thalamic radiation R			Posterior thalamic radiation R	3.10E-02	0.032				
				Posterior corona radiata R			Posterior corona radiata R	3.20E-02	0.031				
				Sagittal stratum L			Sagittal stratum L	3.30E-02	0.032				
				Posterior thalamic radiation L			Posterior thalamic radiation L	4.30E-02	0.031				
				Sagittal stratum R			Sagittal stratum R	5.20E-03	-0.042				
				External capsule R			External capsule R	3.70E-02	-0.03				
rs11218343	11	121435587	SORL1	Fornix	2.00E-02	0.083	Fornix	7.80E-03	-0.093				
				External capsule L	3.90E-02	0.08	Uncinate fasciculus R	2.40E-02	-0.083				
rs17125924	14	53391680	FERMT2	No significant associations		Superior fronto-occipital fasciculus R		3.50E-02	-0.072				
				No significant associations		Tapetum R		2.10E-02	-0.06				
rs12881735	14	92932828	SLC24A4	Uncinate fasciculus R	1.90E-03	-0.058	Cingulum cingulate gyrus R	1.20E-02	0.038				
				Splenium of corpus callosum	1.60E-02	-0.045	Splenium of corpus callosum	1.60E-02	0.04				
rs3752246	19	1056492	ABCA7	No significant associations		No significant associations							
				No significant associations		No significant associations							
rs429358	19	45411941	APOE	Middle cerebellar peduncle	9.60E-04	-0.069	Cingulum hippocampus R	6.50E-05	0.084				
				Cingulum hippocampus R	1.40E-03	-0.07	Posterior thalamic radiation R	3.20E-04	0.074				
				Cerebral peduncle L	7.50E-03	-0.054	Posterior thalamic radiation L	1.30E-03	0.066				
				Splenium of corpus callosum	1.60E-02	-0.054	Cingulum hippocampus L	1.80E-03	0.068				
				Superior longitudinal fasciculus R	1.80E-02	-0.052	Sagittal stratum L	3.60E-03	0.059				
				Cingulum hippocampus L	2.10E-02	-0.05	Superior longitudinal fasciculus L	4.40E-03	0.058				
				Corticospinal tract R	2.50E-02	-0.048	Sagittal stratum R	5.80E-03	0.056				
				Genu of corpus callosum	4.10E-02	-0.043	Superior longitudinal fasciculus R	1.00E-02	0.051				
				Posterior thalamic radiation R	4.50E-02	-0.042	Body of corpus callosum	2.20E-02	0.045				
				Body of corpus callosum	4.90E-02	-0.043	Cingulum cingulate gyrus L	2.60E-02	0.042				
				Genu of corpus callosum	4.10E-02	-0.043	Splenium of corpus callosum	2.70E-02	0.044				
				Posterior thalamic radiation R	4.50E-02	-0.042	Anterior corona radiata L	3.50E-02	0.041				
				Body of corpus callosum	4.90E-02	-0.043	Retrolenticular part of internal capsule L	3.90E-02	0.043				
				Retrolenticular part of internal capsule R	4.90E-02	-0.043							
				No significant associations		No significant associations							
				rs6024870	20	54997568	CASS4	No significant associations		No significant associations			
								No significant associations		No significant associations			
rs7920721	10	11720308	ECHDC3	Posterior limb of internal capsule L	5.20E-03	0.044	Retrolenticular part of internal capsule R	4.40E-02	-0.031				
				Retrolenticular part of internal capsule R	7.90E-03	0.043							
				Cerebral peduncle R	8.80E-03	0.039							
				Superior corona radiata R	8.80E-03	0.042							
				Cerebral peduncle L	3.50E-02	0.031							
				External capsule L	4.80E-02	0.03							
rs138190086	17	61538148	ACE	Retrolenticular part of internal capsule L	4.30E-02	-0.11	Anterior limb of internal capsule L	1.70E-02	0.12				
				Sagittal stratum L	4.50E-02	-0.11	External capsule L	4.10E-02	0.098				
rs190982	5	88223420	MEF2C	No significant associations		No significant associations							
				No significant associations		No significant associations							
rs190983	7	37844263	NME8	No significant associations		No significant associations							
				No significant associations		No significant associations							
				Uncinate fasciculus R			Uncinate fasciculus R	3.70E-02	-0.14				
							Anterior limb of internal capsule R	4.00E-02	-0.13				
							Anterior limb of internal capsule L	4.50E-02	-0.13				

The associations between AD risk loci identified by Kunkle et al and TBSS imaging phenotypes from the UK Biobank website. These are based on Elliott et al. (2018) Genome-wide association studies of brain imaging phenotypes in UK Biobank and other sources. See <http://big.stats.ox.ac.uk>. Please note: they are not corrected for multiple comparisons. Acronyms: Chr. = Chromosome; TBSS = Tract-Based Spatial Statistics; ROI = Region of Interest; FA = Fractional Anisotropy; MD = Mean Diffusivity.